La collana della Scuola di Alta Formazione Dottorale accoglie le migliori tesi di dottorato dell'Università degli Studi di Bergamo, insignite della dignità di stampa e sottoposte a procedura di *blind peer review*.

This research deals with the "3R-Green Strategy" aimed at improving the sustainability of cementitious materials, focusing on the alternative binders to Portland cement (alkali-activated slags and calcium sulphoaluminate cements) in order to manufacture "green" mixtures for special applications (repair mortars, special concretes and thermal plasters). Moreover, a new sustainability index EASI was developed taking into account environmental impact, performances and durability of mixtures.

Denny Coffetti is a post-doctoral research fellow (STaRs program) at University of Bergamo, Department of Engineering and Applied Sciences. He holds a master's degree cum laude in Building Engineering in 2015 and a PhD degree in Engineering and Applied Sciences (XXXI cycle) in 2019 at University of Bergamo. His research is mainly focused on the sustainability and durability of concrete structures with particular attention to alternative binders to Portland cement. He is co-authors of a technical book and more than 40 scientific papers on concrete properties, durability, sustainability and admixtures. He won the AIMAT 2019 award for the best PhD thesis on Materials Engineering in Italy.

ISBN: 978-88-97413-24-0
DOI: 10.6092/978-88-97413-24-0

Denny Coffetti
THE BEST PATHS TO GREEN CONCRETE

18

Collana della Scuola di Alta Formazione Dottorale
- 18 -

Denny Coffetti

THE BEST PATHS TO GREEN CONCRETE
Discussion on alternative binders to Portland cement for sustainable cementitious materials

UNIVERSITÀ DEGLI STUDI DI BERGAMO

2021

Collana della Scuola di Alta Formazione Dottorale

Diretta da Paolo Cesaretti

Ogni volume è sottoposto a *blind peer review*.

ISSN: 2611-9927

Sito web: https://aisberg.unibg.it/handle/10446/130100

Denny Coffetti

THE BEST PATHS TO GREEN CONCRETE
Discussion on alternative binders to Portland cement for sustainable cementitious materials

Università degli Studi di Bergamo

2021

The Best Paths to Green Concrete. Discussion on alternative binders to Portland cement for sustainable cementitious materials /
Denny Coffetti. – Bergamo :
Università degli Studi di Bergamo, 2021.
(Collana della Scuola di Alta Formazione Dottorale; 18)

ISBN: 978-88-97413-24-0
DOI: 10.6092/978-88-97413-24-0

Progetto grafico: Servizi Editoriali – Università degli Studi di Bergamo
© 2018 Università degli Studi di Bergamo
via Salvecchio, 19
24129 Bergamo
Cod. Fiscale 80004350163
P. IVA 01612800167

https://aisberg.unibg.it/handle/10446/175116

Dedication

To my daughter Beatrice.

Acknowledgements

This PhD thesis is the output of the support of several people to whom I am extremely grateful. First and foremost, I thank my supervisor Luigi Coppola both for his excellent and outstanding professional qualities and, most important, for the great attention personally paid to me.

I am also grateful for the cooperation, the backing and the great piece of advices of my tutor Tommaso Pastore with Marina Cabrini and Sergio Lorenzi.

Thanks to Fortunato Crea and Sebastiano Candamano from University of Calabria for the opportunity of working together to increase the knowledge in the field of alkali activated materials. Similarly, thanks to Milena Marroccoli and Antonio Telesca from University of Basilicata for their support during the experimental tests on calcium sulphoaluminate cement-based blends. To all of them, a further thank you for the warm welcome in their cities and their laboratories.

My sincere thanks to all the colleagues of Engineering Laboratories of University of Bergamo for their active participation in the research presented in this thesis.

I am also profoundly grateful for the hard revision work of my colleague Elena Crotti and her substantial contribution to uplift the studies presented in this thesis. To Elena and Gabriele Gazzaniga also the credit of having always promoted a friendly and pleasant environment to work and have fun.

To Federica, my life partner, my love, thank you very much for being by my side for 15 years and, most important, for being a delightful mum for our daughter Beatrice.

Finally, there is no way to thank my parents and my sister for everything they have done for me. Simply, thanks to be always present and doing the possible for my happiness.

"More effective prevention strategies would save not only tens of billions of dollars, but safe tens of thousands of lives. Funds currently spent on intervention and relief could be devoted to enhancing equitable and sustainable development instead, which would further reduce the risk for war and disaster. While the cost of prevention has to be paid in the present, its benefits lie in a distant future. Moreover, the benefits are not tangible; they are the disaster that did not happen."

Kofi Annan
World Summit on Sustainable Development
2002

Table of contents

Introduction

With a production of more than 10 billion cubic meters, concrete is the most widely used construction material in the world, especially in areas with high economic and demographic growth, such as China and India. Moreover, the world Portland cement production is 4.1 billion tons with an increase rate equal to 50 ÷ 70 million tons per year (4.8 billion tons at 2030). Furthermore, it has been estimated that about 45% of sand and stone mined globally are used as concrete aggregates (Figure 1) [1,2].

Due to these huge volumes, the concrete industry – and in particular the cement sector – has a very strong environmental impact in terms of greenhouse gas (GHG) emissions, energy requirement and consumption of natural resources. In fact, it has been reported that cement manufacturing is responsible for 5 ÷ 7% of anthropogenic CO_2 emissions [3,4], including the CO_2 released in the clinker industrial process (CO_2: 520 kg CO_2/t of clinker) and by fuel combustion related to the energy use in clinker production (CO_2: 350 kg CO_2/t of clinker).

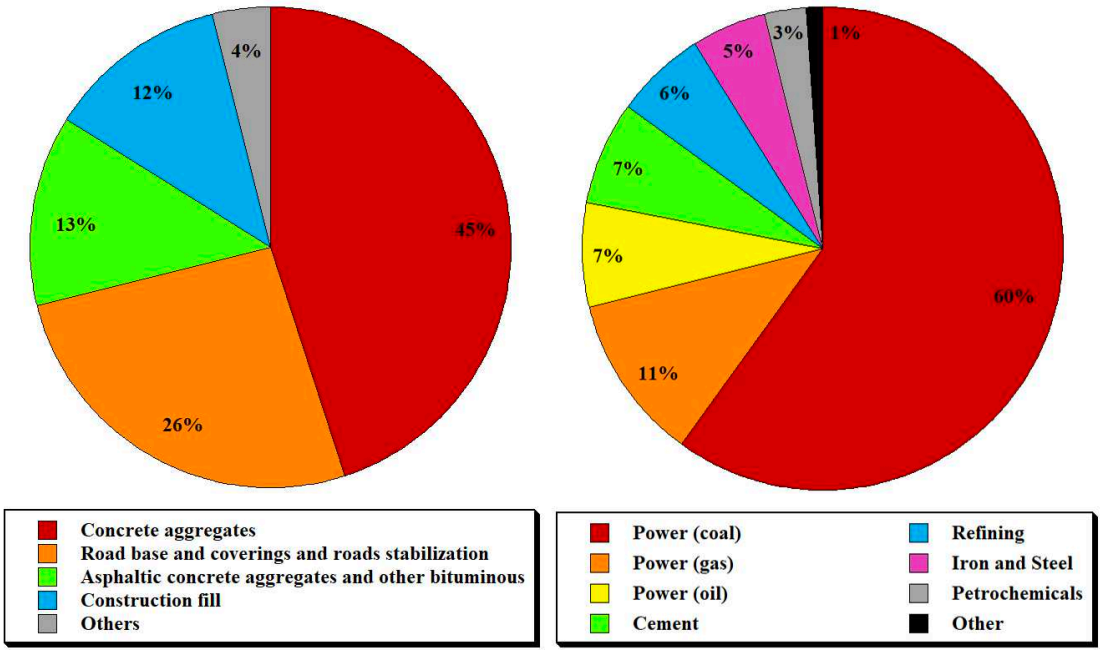

Figure 1 - Utilization of stone (left) and total CO_2 emissions (right) subdivided by sector. Data from [1,3]

Furthermore, despite the fact that energy demand in clinker production has been significantly reduced over the years, a modern cement plant in Europe still requires from 2900 to 3300 MJ of energy for each ton of clinker produced [5]. On the contrary, in the USA and China where minor investments have already been done to enhance the combustion efficiency of the cement kilns, energy consumption is higher. On average, 1.53 ton of raw materials (1.22 ton of limestone, 0.31 ton of clay)

are required to produce 1 ton of ordinary Portland cement [6]. Thus, the cement and concrete industry is under pressure to reduce greenhouse gas emissions as well as both energy and natural resources consumption [7–9], in other words, to be sustainable.

The task is particularly complicated since population is expected to reach ten billion in 2050. As a consequence of this, the main challenge for the concrete industry is how to support the increasing demand of buildings and infrastructures of the growing population being at the same time sustainable. The answer to this hard task is represented by the "3R-Green Strategy": Reduce energy – Reduce pollutant emissions – Reduce consumption of natural resources (Figure 2).

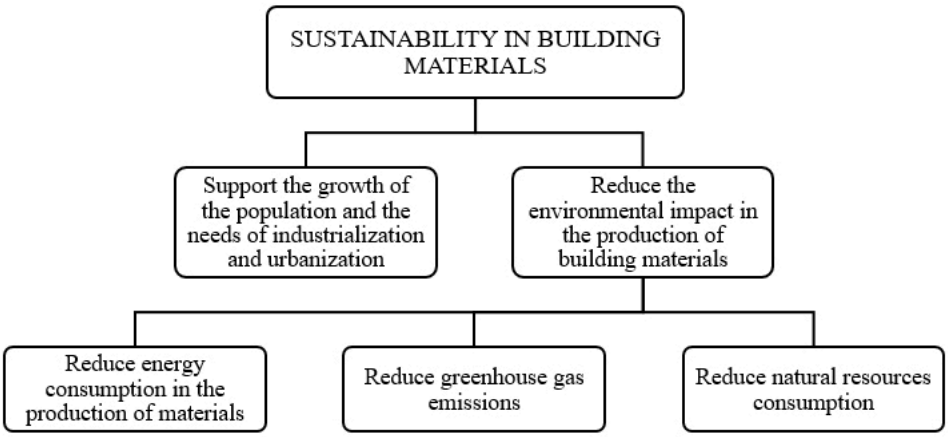

Figure 2 - Main strategies to make concrete sector more environmentally friendly

Reducing in energy consumption and CO_2 emissions

The first two steps of the virtuous path of "3R-Green Strategy" are represented by a strong effort in reducing energy consumption and GHG emissions (Figure 3).

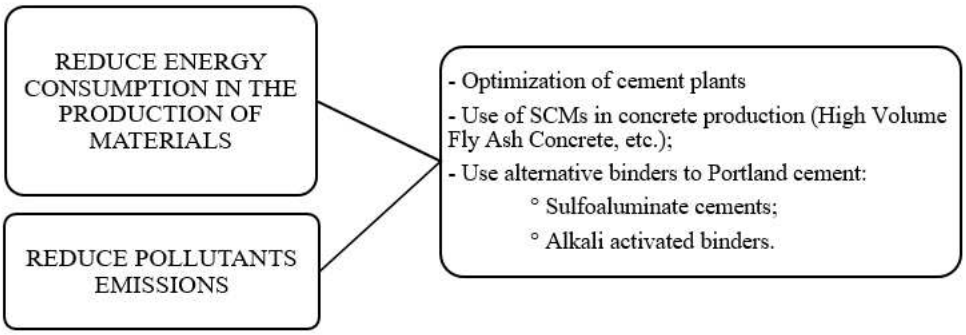

Figure 3 - Strategies to reduce both energy consumption and pollutants emissions in production of construction materials

Optimization of cement plants

The optimization of cement plants can be achieved through a process of revision of both raw materials [8,10,11] and fuels [12,13] used. However, switching from conventional to alternative fuels presents several challenges such as a poor heat distribution, unstable precalciner operation, blockages in the preheater cyclones, build-ups in the kiln riser ducts, higher SO_2, NO_x, and CO emissions. In mid-80's, tires became very popular as alternative fuel to cope with the increasing fossil fuel costs. High carbon content, high heating value of 35.6 MJ/kg and low moisture content make tire-derived fuel one of the most used alternative fuels in cement industry around the world. However, CO, SO_2 and NO_x emissions increase while replacing Tire Derived Fuel (TDF) up to 20% of fossil fuel [14].

Municipal Solid Wastes (MSW) constitute a complex and very variable fuel due to their heterogeneous composition. Indeed, the availability of the MSW makes it one of the most desirable alternative fuels in cement manufacturing. Depending on the composition, MSW can be substituted up to 30% of the fuel mix in cement manufacturing. Overall the substitution of MSW as alternative fuel has a positive effect on greenhouse gas formation over traditional schemes. Unfortunately, during incineration of MSW toxins and heavy metals are produced which can leach into the water supply and soil. With energy recovery in cement manufacturing, these substances are partially transferred to the clinker [11].

Plastic wastes [15] are potential candidates for alternative fuel in cement industry due to their worldwide production and high calorific value 29-40 MJ/kg. Polyethylene and polystyrene plastics as alternative fuel reduced the emission of the CO_2, which is approximately 1.0 ton of CO_2 per ton of coal replacement. However, isolation of materials from plastic waste and retrofitting require additional capital and labor costs. Furthermore, if the chlorine content of plastic waste exceeds 0.7% then it may impact on the quality of the clinker.

In conclusion, on the basis of the above-mentioned items, use of alternative fuels seems to be ineffective in solving environmental problems related to clinker production.

Limitation of clinker factor

The limitation of the clinker factor in cements by blending low-carbon supplementary cementitious materials (SCMs), such as fly ash [16,17], slag cement [18], metakaolin [19] and natural pozzolans [20] can be a suitable solution to improve the sustainability of concrete [21]. These cements are characterized by reduced amounts of Portland cement (OPC) clinker and increasing percentages of secondary raw materials that otherwise would be disposed to landfill. Moreover, SMCs can be used directly in ready-mix concrete plants to manufacture cementitious mixtures for massive structures (dams, foundations, etc.) and elements where a slow strength gain is required. In 2015, about 1000 million tons of fly-ash were generated in the world (Figure 4). However, only about 430 million tons

of fly-ash were consumed in different applications including cement and concrete industry. The remainder of fly-ash was disposed of in landfills, which could be hazardous to the environment and to drinking water resources [22].

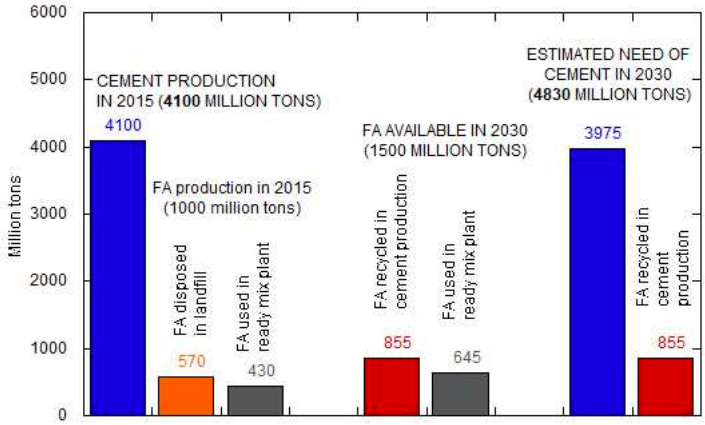

Figure 4 - Cement and fly ash production

Total fly ash production is forecasted to increase about 50% over the next fifteen years (about 1500 million tons of fly-ash available in 2030) [23], because coal use is estimated to rise over 60% to 2030 with developing countries responsible for 97% of this increase primarily to meet improved electrification rates. Moreover, following the Fukushima nuclear accident in April 2011, the future of nuclear plants in industrialized countries (e.g. Germany and Japan) has come under considerably scrutiny resulting in political decisions to reduce nuclear power dependency. For Japan, this results in future increased dependence on coal. Same in India where energy blackouts during 2012 signal more coal power plants will be necessary to serve the growing energy needs. In addition to the increase in fly-ash, cement production is also expected to be 4830 million tons in 2030.

Assuming to recover all the fly ash produced in cement and concrete industry, only about 4000 million tons of clinker will need to be produced. In other words, thanks to the total recycling of fly-ash both in cement plants and in ready-mix concrete it could be possible to feed the demand of buildings and infrastructures in 2030 without increasing ordinary Portland cement production with respect that recorded in 2015 [24].

Alkali activated materials

These materials are raw silico-alumina materials (called precursors) mixed with huge amounts of alkaline activators. Unlike traditional mixtures based on the use of pozzolanic materials in combination with Portland cement, where hardening occurs by reaction with calcium hydroxide made available the hydration of the silicates of OPC clinker, in AAMs and geopolymers the process of hardening is promoted by the dissolution of silica favored by the alkaline activators which generally

consist of sodium or potassium silicate and/or hydroxide. Therefore, alkali-activated materials and geopolymers can be considered “environmentally friendly” since it is not necessary (except for the metakaolin) to burn materials used as precursors.

One of the primary advantages of alkali activated materials relative to Portland cement from an environmental perspective is the lower greenhouse gases (GHG) emissions and energy requirement deriving from AAS manufacture compared to OPC production [25]. In fact, the calcination of Portland cement causes high energy consumption and CO_2 emissions during clinker production phase (i.e. industrial process CO_2 and energy-use CO_2) while the synthesis of AAS cements from slag cement does not require high-temperature calcination steps. However, the carbon dioxide emissions related to the alkaline activators must be taken into account.

The reaction mechanism that governs the setting and hardening of alkaline cements is strongly discussed in the scientific literature, but only partially understood. However, the close correlation between raw materials – both solid precursors [26,27] and alkaline activators [28] – is evident. Similar to the reaction mechanism, the mechanical performances (such as compressive and flexural strength, elastic modulus, etc.) of alkali-activated mortars and concretes are governed by both the nature of the raw materials and the dosage of activators employed.

In general, a properly proportioned mixture makes it possible to produce Portland cement-free mortars and concretes with mechanical properties similar or higher than those of traditional OPC-based mixtures, but with a reduction of GER (Gross Energy Requirement) and GWP (Global Warming Potential) respectively about 80% and 70% compared to traditional mortars. However, before extending the use of alkali-activated binders in construction material it is necessary to solve some critical issue related to autogenous and drying shrinkage, considerably higher than that of OPC. Furthermore, the addition of traditional superplasticizer (such as naphthalene-, melamine-, polycarboxylate- and sulphonate-based admixtures) have limited or no effect on rheological properties of AAS mixtures. Finally, the durability of AAS cements is a subject of strong discussion among researchers due to contradictory results reported in scientific literature [29–31].

Calcium sulphoaluminate cements

The production of calcium sulphoaluminate (CSA) cements requires a lower consumption of primary energy deriving from both lower kiln temperature and grinding of the lower hardness CSA clinker. Consequently, the production of sulphoaluminate cement is also characterized by lower CO_2 emissions, estimated at about 25% less than that of Portland cement clinker. Calcium sulphoaluminate cements are actually used as special binders with rapid setting, shrinkage compensation and high early-age strength. CSA cements can be produced from bauxite, limestone and calcium sulfate (gypsum or anhydrite). Currently, due to the high cost of raw materials, industrial by-products or

waste materials [32,33] such as fly ash, phosphogypsum, blast furnace slag, aluminum anodizing sludge and marble sludge have been analyzed for use in the manufacture of calcium sulphoaluminate-based clinker.

In general, Portland clinker production process can be used in the production of CSA clinker, but at lower kiln temperatures (1250-1300°C) compared to that used in producing OPC clinker (1450°C). The reduced clinkering temperature together with the lower hardness of CSA clinker that facilitates grinding thus lowering energy required, is increasing the attractiveness of CSA cements that provide a low-CO_2 and low-embodied energy alternative to Portland cement. The main phases of CSA are ye'elimite ($C_4A_3\hat{S}$, tetracalcium trialuminate sulfate), whose content in CSA cement varies from 30% to 70%, and belite (C_2S).

Blends of OPC, CSA and gypsum (or anhydrite) can be used to produce mortars and concrete with outstanding properties in terms of setting time, mechanical strength and dimensional stability. The kinetics of ye'elimite hydration and product development are influenced by the addition of calcium sulfate (gypsum or anhydrite) or calcium hydroxide [34–36]. Also, the presence of mineral additions [37,38][112, 186] or admixture [39–42] strongly influences the reaction mechanisms. Finally, Pelletier-Chaignat et al. [43] show that the hydration mechanisms are similar in the presence of gypsum or anhydrite while differences in the kinetics of reactions can be noted due to the slower dissolution of anhydrite compared to gypsum.

Reduction in consumption of non-renewable resources

The problem of environmental sustainability cannot be addressed solely on the basis of primary energy consumption and the amount of CO_2 emitted into the atmosphere. For example, the production of aggregates for concrete requires a very low consumption of primary energy (Table 1), about three orders of magnitude lower than that for the production of cement. Moreover, CO_2 emission are even almost five orders of magnitude lower. In fact, the production of natural aggregates requires only excavation from the rivers and transportation to the concrete mixing plant or, at the most, extraction from the rock quarry bench and subsequent crushing before being used in concrete. On the basis of the GER and GWP, therefore, it should be concluded that the use of aggregates for the production of concrete is an eco-friendly activity. In reality, the production of aggregates must be considered an activity that does not respect the environment as it determines a consistent consumption of non-renewable resources. Therefore, it is possible to state that among the principles of sustainability in the construction sector, reducing the consumption of sand and gravel is one of the basic fundamentals from which one cannot ignore.

	GER [MJ/kg]	GWP [$KgCO_2/kg$]
Portland cement	3.35	0.98
High-range water reducer	16.0	1.8
Natural aggregates	$3.7 \cdot 10^{-3}$	$7.0 \cdot 10^{-5}$

Table 1 - Gross energy requirement (GER) and global warming potential (GWP) of concrete ingredients

The reduction in the consumption of natural aggregates can be pursued through different approaches, all, however, aimed at recovering wastes from various sources, including those produced by the concrete and construction industry itself. This approach also has the advantage of minimizing the number of landfills contributing to a general improvement of the landscape and the livability of our cities. Therefore, the third step of "3R Green Strategy" is represent by a reduction of natural resources consumption by increasing waste utilization [44] in concrete industry.

Waste management

Waste management is one of the most important topics of the Green Economy and has emerged as a main research issue because, every year, only a quarter of the total waste produced is recycled. In this view, in the near future a consistent use is expected of:

- Aggregates arising from demolition of existing concrete structures;
- Sand and limestone filler from waste of marble processing;
- Fresh concrete in excess returned with truck mixers and washing water in ready-mix concrete plants;
- Plastic bottles, glass, tires, automotive shredders, crushed asphalt, foundry sands and biomass ahses.

The sands and calcareous fillers recovered from marble processing waste are already widely used in proprietary pre-packed products for plasters, screeds and repair mortars [45]. There are also numerous studies [46–52] that testify to the possibility of manufacturing cementitious mixtures with excellent performance by using aggregates from demolition of reinforced concrete structures, the ruins of bricks, the recycling of glass and PET bottles, of worn tires, the recovery of car bodies, crushed asphalt, electric arc furnace (EAF) slag and foundry sands. It is not, however, a goal to list the performance improvements that can be achieved by using waste in concrete production. For example, the use of glass in the form of very fine powder, already widespread in Canada, can solve the complicated problem arising from the use of alkali-reactive aggregates [53].

Culture shift

In this paragraph, however, the attention is focused on which virtuous mechanisms should be adopted to encourage the use of waste in place of traditional natural aggregates for concrete production. However, a consistent increase in waste recycling can be achieved only if there is a shift from the "culture" of "not more than" to that of "not less than." In fact, one of the main reasons limiting the use of waste materials in concrete production is the perception that it leads to low quality structures. This perception is perpetuated by standards and norms since that limit ("culture of not more than") the percentage of recycled materials, affirming indirectly that waste materials represent a poor ingredient compared to natural aggregates. This approach has to be changed through regulations that specifically incentivize the use of waste materials in concrete production (bonus or credit in construction tenders) and increasing the taxation for disposal in landfills accompanied by strong penalties for non-compliance. Adopting the approach of "at least – not less than", if someone wants to use an eco-friendly material, he has to introduce a minimum percentage of waste because the concrete can be embellished of the "eco-friendly" title.

A recent survey [54], within the EU, has highlighted how the reduced consumption of recycled aggregates in the production of ready-mix concrete is due to:

- The lack of demand from designers and construction managers;
- The lack of sensitivity of the contracting stations to environmental issues;
- The absence of specific rules on concrete manufactured with recycled aggregates.

In order to modify this "stall" situation, regarding the actual use of wastes in the construction sector, it is necessary to implement an overall strategy as reported in Figure 5.

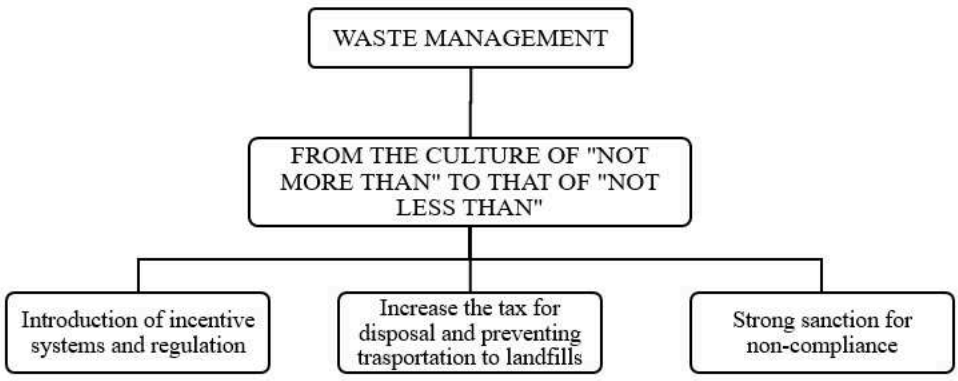

Figure 5 - Switching from the culture of "at most - not more than" to that of "at least - not less than"

The introduction of incentive systems and regulations that allow to increase the percentage of wastes in concrete production can give a great boost to the use of artificial aggregate in concrete. Rules that indicate a minimum percentage of recycled materials to be used to identify concrete as

“environmentally friendly”. Notwithstanding, obviously, the rheological, elasto-mechanical and durability performances for the mixture in relation to the intended use and to the environmental exposure class in which the concrete structure falls. With regard to this aspect, an approach "at least - no less than" is found in the technical document "SIA 2030: 2010 - Recycling Beton", where the legislation requires that, in order to get the “green” title, concrete must be contain at least 25% of recycled aggregates. The same rule - at least for what concerns the aggregates coming from the demolition of the concrete - does not limit the use of recycled aggregates concrete in any environmental exposure class. Furthermore, this technical regulatory tool provides all the information necessary for the structural designer to be able to dimension elements in reinforced recycled concrete.
These regulatory instruments - necessarily of a technical nature - need to be accompanied by administrative tools such as the introduction of reward mechanisms for those projects which, in the context of public works tenders, envisage substantial quantities of reused waste. Obviously, the assessment of how much a concrete is eco-friendly must take place on the basis of certain criteria such as, for example, the "carbon foot print" of the mixtures calculated on the basis of reliable and certified databases (GER and GWP) of the ingredients used.
Finally, the issue of construction licenses - where demolition of existing buildings and/or infrastructures is planned at the construction site - should be subject to the complete recovery of the rubble and of the demolished concrete. With this in mind, the designer of the work must include in the project a plan to recycle the rubble coming from the demolition to which the contractor will have to strictly follow.
It should be noted that in most European countries the construction sector contributes more than two thirds of the overall volume of wastes (urban waste accounts for only about 10% of the total). Therefore, providing both technical and administrative regulatory tools to increase waste consumption in the production of construction materials and making taxing for waste materials in landfills more burdensome could provide the keystone - together with separate collection and recycling urban wastes - to almost completely solve the problem of waste valorization.
Strong penalties for non-compliance complete the actions planned to increase the use of wastes. In fact, it will be necessary to provide fundamentally administrative sanctions for those who do not comply with the rules and which could involve public offices, designers, contractors (for example, providing a period suspension from the register) and the landfill owners themselves.

Increasing durability

Reduction in the consumption of natural resources can also be achieved by a general increase in durability of both masonry and reinforced concrete structures in order to reduce resources for maintenance and refurbishments since repair materials – containing high percentage of both cement

and organic polymers - have a strong impact from the environmental point of view. The options that can be undertaken to achieve this goal are many (Figure 6), but all aimed at preventing the phenomena of degradation and premature deterioration of both reinforcement and concrete, such as improving the models for predicting the onset and propagation of corrosion, optimizing the design of the structures to attain higher robustness, carefully choosing ingredients and mixture composition [55,56] [74, 223], using fiber reinforced plastic (FRP) bars in place of traditional steel, or using non-metallic fibers and nanotubes [72, 73].

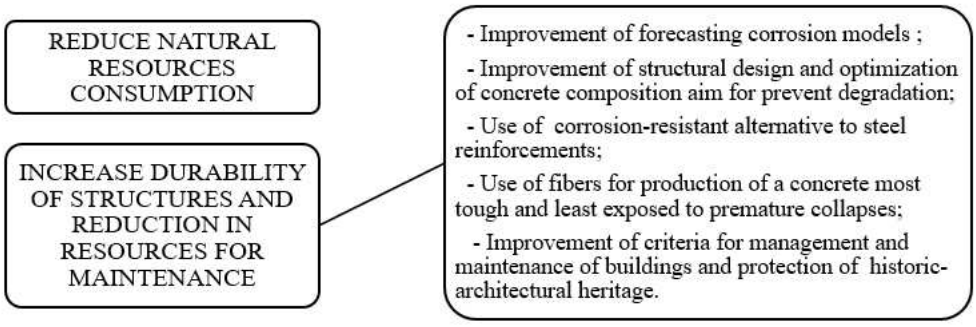

Figure 6 - Further strategies to reduce the consumption of natural resources

Critical issues

For alternative cements, there is a need for extensive testing to establish engineering design properties beyond compressive strength. All of the design properties commonly used for Portland cement concrete must be verified including bond to reinforcing steel, creep, shear properties, etc. The same for all durability issues, recognizing that current test methods may not be appropriate for these materials. For recycled aggregates, the same engineering properties must be established. Additionally, means for ensuring that the concrete produced with alternative aggregates will be consistent must be developed. It is unlikely that the supply of one recycled material aggregate will be exactly the volume required for use in a new structure. For these materials to be accepted, they must be included in a building code. However, life-safety provisions will always take precedence over sustainability issues.

Conclusions

The scientific community is aware the problem of how to make sustainable the construction materials sector appears rather difficult and complicated. The challenge for the concrete industry to sustain growth by reducing the strong environmental impact of "cement"-based materials must necessarily be addressed with a multidisciplinary approach – the “3R Green Strategy” - that takes into consideration the possibility of reducing energy consumption, pollutant emissions together with an

intensive and a generalized use of wastes aimed at drastically reducing the consumption of non-renewable natural resources.

A key stone of "3-R Green Strategy" is represented by alternative binders to Portland cement. Therefore, there is an increasing knowledge about chemistry, reaction mechanisms, elasto-mechanical properties and durability of these sustainable construction materials. However, despite the deep knowledge on this topic, these binders continue to be used only in research laboratories or in niche applications. The reasons for the scarce employment are to be found between costs (often much higher than those of Portland cement), safety (especially for alkaline activators) and the lack of sound background of real-case applications.

CSA-based mixtures combine excellent mechanical properties with both very low shrinkage and limited environmental impact (CO_2 emissions and energy demand) that permits broad use in the field of restoration of concrete structures, seismic retrofitting and flooring. On the other hand, issues related to the durability (i.e. carbonation, chloride permeability) and to the high cost of raw materials (especially bauxite) are still unsolved.

Alkali-activated slag cements offer the possibility to produce binders entirely from waste materials (alkaline activators) or industrial by-products (slag cement). With proper mixture proportioning, it is possible to produce concretes with good mechanical performance and excellent durability. Unfortunately, performance is affected by the variability of raw materials. Finally, there is a need to develop admixtures to manage the rheological properties of AAS- and CSA-based mixtures.

1. Calcium sulphoaluminate cements: literature review

Since the beginning of the 1960s, research on calcium sulphoaluminate ($C_4A_3\hat{S}$) mixed with other minerals in different binding systems has led to the development of different cements potentially able to spread in the concrete industry. Several designations have been proposed for these cements, such as SulphoAluminate Belite (SAB) cement [57,58], SulphoAluminate cement (SAC) [59,60] or FerroAluminate Cement (FAC) [61], modified Portland cement [62], and Calcium SulphoAluminate (CSA) cement [63,64]. Currently, all cements mainly composed of tetracalcium trialuminate sulphate ($C_4A_3\hat{S}$) are called Calcium SulphoAluminate (CSA) cements.

During the 1970s, CSA cements were introduced into the Chinese market as high performance and dimensionally stable binder developed by the China Buildings Materials Academy. In Europe, the use of CSA cements is strongly limited by the lack of norms concerning special binders derived from non-Portland clinkers. However, several cement companies have recently started their production, such as Buzzi Unicem Spa and Italcementi – Heidelberg Spa. Actually, the main use of CSA cements is for quick repairs [65,66], prepacked products [67], self-stressing materials [26], and floor concrete applications. Moreover, ye'elimite-based binders have become highly popular over the last few years for research due to their greater environmental sustainability compared to Portland cement [68] combined with outstanding elasto-mechanical properties and low shrinkage [58]. CSA cements can be used in mixture with a source of calcium sulphate (binary binders), in combination with calcium sulphate and a calcium hydroxide source, generally Portland cement, (ternary binders) or in systems where the OPC is partially or totally replaced by supplementary cementitious materials SCMs (innovative binders), such as fly ash or ground granulated blast furnace slag. Currently, the innovative binders are used only in the research laboratories while binary and ternary are already in use to produce pre-packed mortars. Furthermore, the properties and applications of this type of binder are strongly influenced by many factors:

- Chemical and mineralogical composition of clinker;
- Sulphate source (dosage and type);
- Water/binder ratio;
- Blending with other binders, such as OPC or supplementary cementitious materials (SCMs).

1.1 Production

Raw materials for CSA cements differ from those for Portland cement, especially in terms of sulphate content. Traditionally, the principal raw materials for manufacture calcium sulphoaluminate clinkers are limestone, bauxite, clays, gypsum and iron ores, as source of calcium, silicon/aluminum and

sulfur, respectively, but several industrial by-products or wastes containing high amounts of alumina or sulphates can also be used to produce CSA cement [64,69,70]. In general, there is a great variety of industrial by-products all over the world that could be used as a local source of the main components to manufacture this class of cements in order to reduce the production costs and limit the environmental impact. Guo et al. [71] and Wu el al. [72] investigated the properties of calcium sulphoaluminate cement produced by using municipal solid waste incineration (MSWI) fly ash while Marroccoli et al. [73] and Da Costa et al. [32] showed the possibility of fully replacing the bauxite and natural gypsum with anodization mud and flue gas desulfurization gypsum to manufacture CSA clinker. Furthermore, El-Alfi et al. [33] successfully synthesized the CSA clinker using 25% kaolin, 20% gypsum and 55% marble sludge waste at firing temperature ranging between 1200 and 1250°C. Finally, Shen et al. [74] have highlighted that the use of industrial by-products or wastes, such as phosphogypsum, is a key issue for the economic production of CSA cements. The technological process of the production of CSA cements [75] on an industrial scale can be divided, similarly to Portland cement manufacture, into three stages (Figure 7):

- Preparation of raw materials. The raw materials are coarsely crushed and batched into a closed-circuit dryer-mill for grinding to form raw meal. This is homogenized in a blending tank and stored in a raw meal silo;
- Burning of clinker in kiln. The homogenized raw meal is pumped into a rotary kiln with preheater for initial reaction and, in the kiln at about 1250°C, for clinkerization;
- Cement finishing. After cooling, clinker is crushed and enters a clinker pit for storage. Clinker, gypsum or anhydrite (or, rarely, basanite) and admixtures are proportioned for obtaining different types of cements and enter a closed-circuit grinding mill. Finished cements are homogenized before storage and, if required, packaged.

Another important aspect of CSA cement is that such clinkers can be manufactured in conventional Portland cement kilns, as was demonstrated in full-scale production runs in plants in France.

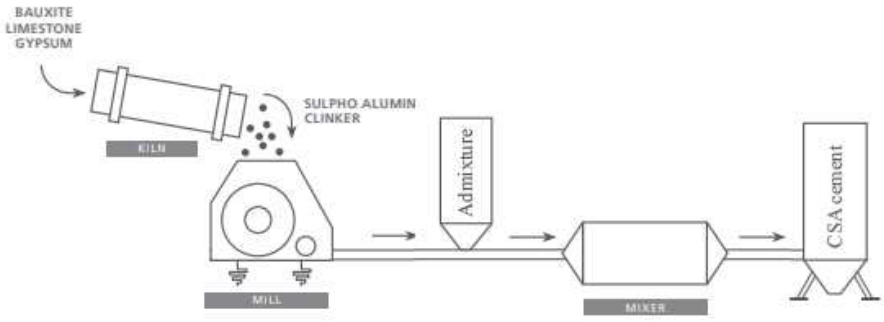

Figure 7 - The production process of CSA cements

1.2 Composition

Calcium sulphoaluminate cements may have quite variable compositions, but all of them contain high amount of ye'elimite, also called Klein's compound or tetracalcium trialuminate sulphate ($C_4A_3\hat{S}$), ranging between 50 and 80 wt.%. As minor constituent, belite (C_2S), tricalcium aluminate (C_3A), calcium sulphosilicates, Al-rich ferrite (C_4AF), calcium-aluminate, and calcium silico-aluminates can also be found in these binders. As reported in Table 2 and Table 3, the chemical and mineralogical composition of CSA cements varies with the composition of raw materials, the raw mix design, and the clinkering processing. In particular, the alumina content varies between 22 wt.% and 45 wt.% and the silica content ranging from 3 wt.% to 9 wt.% while the SO_3 content is about 8 – 22 wt.%. This is reflected in a pronounced variability in the mineralogical constituent that influences both the hydration reactions and the performances of the mixtures manufactured with CSA cements.

Ref.	CaO	Al_2O_3	SiO_2	SO_3	Fe_2O_3	Na_2O	K_2O	MgO
[76]	36.2	44.8	4.1	8.9	1.3	0.07	0.25	1.10
[35]	39.7	31.5	6.2	13.9	1.2	0.70	0.40	3.90
[43]	36.1	45.0	4.5	8.6	1.5	0.07	0.35	0.91
[39,40]	42.0	38.5	5.4	8.8	1.2	0.03	0.14	1.47
[77]	41.6	33.6	6.5	14.0	0.9	0.09	0.39	0.68
[77]	41.9	33.9	8.2	8.8	2.4	<0.08	0.25	2.73
[77]	44.1	27.3	9.0	12.2	2.6	1.40	0.30	1.50
[38]	42.0	33.8	8.2	8.8	2.4	<0.08	0.25	2.73
[78]	45.3	28.9	7.9	11.9	3.7	/	/	1.45
[36]	34.4	35.5	3.2	16.8	0.9	0.05	0.21	0.76
[36]	41.2	26.8	6.9	19.5	0.9	0.13	0.40	0.75
[42]	43.0	22.8	5.7	18.4	2.8	0.10	0.16	0.68
[79]	41.4	27.6	5.1	22.3	1.5	/	/	1.00

Table 2 – Chemical composition in wt% of different CSA cement recently published

Ref.	$C_4A_3\hat{S}$	C_2S	C_3A	$C_{10}S_3\hat{S}_3F_2$	C_4AF	$C_{12}A_7$	CT	Other
[76]	68.1	14.8	3.4	/	/	9.1	3.6	1.1
[35]	65.0	9.1	/	11.3	/	5.1	3.0	7.0
[43]	62.8	18.3	/	/	/	11.2	5.7	2.1
[39,40]	66.8	15.9	/	/	/	9.5	2.9	4.9
[77]	69.5	17.1	/	/	/	/	3.5	9.9
[77]	65.6	16.1	/	/	2.4	/	9.3	6.7
[77]	56.2	31.1	/	/	/	/	3.5	9.2
[80]	66.2	13.5	/	/	/	9.4	2.6	8.5
[81]	52.1	23.8	9.4	0.9	4.7	1.2	/	7.9
[82]	54.7	26.6	9.1	/	1.1	3.1	/	5.5
[82]	70.9	7.2	7.2	/	/	7.6	/	8.3

Table 3 – Mineralogical composition in wt% of different CSA cement recently published

1.3 Environmental issues

In recent years, the attention on CSA cements has grown enormously (Figure 8) due to their low environmental impact compared to the Portland cement. The main advantages related to the sustainability of binders concern both the carbon dioxide emissions and energy requirements during production process.

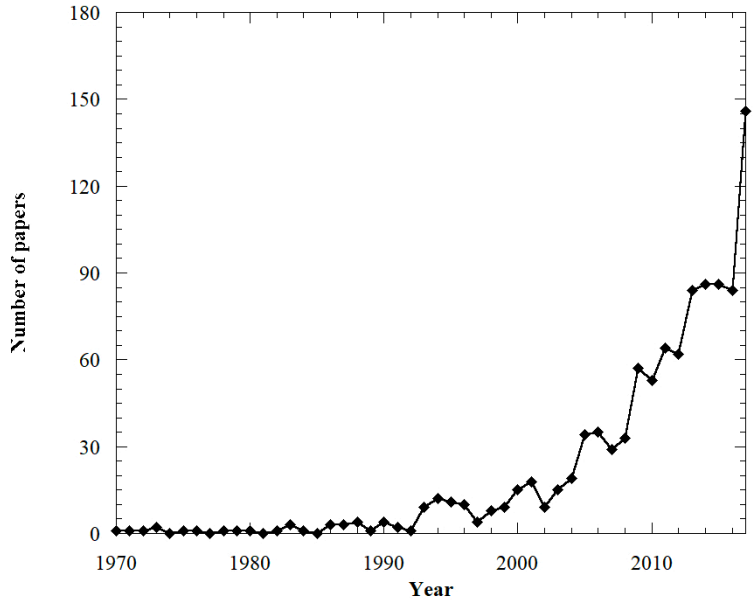

Figure 8 - Number of papers related to CSA cements on Scoups (www.scopus.com)

The carbon dioxide emissions of cement plants can be classified in two main categories: industrial "energy-use CO_2" and industrial "process CO_2". The first one results from combustion of fuels in the manufacturing process while the other refers to chemically-produced CO_2 not directly related to fuel consumption. Given that the majority of the calcium in cements comes from the calcination of limestone (primarily $CaCO_3$), a significant reduction of carbon dioxide emissions of CSA cement compared to OPC arises from the lower weight content of calcium in the major phases (Table 4). In fact, using calcium sulphate ($CaSO_4$) instead of calcium carbonate ($CaCO_3$) as raw materials provides an even lower carbon footprint as the sulphur will be sequestrated in the final product [83]. In particular, Garcia-Matè [84] estimated a 49% reduction in carbon dioxide emissions related to raw materials decomposition with respect to Portland cement. Calcium sulphoaluminate cements also exhibits a significant reduction of energy-use CO_2 due to the reduced energy consumption when compared to Portland cement. This is mainly due to the lower kiln temperature, which is about 200°C lower than that of OPC clinker [3]. According to Phair [85], the saving on CO_2 emissions resulting from the reduction of kiln temperatures is close to 15% (about 40 kg CO_2 per ton of clinker). This also leads to a reduction in energy requirements and fuels consumption, thus increasing environmental and economic sustainability [5]. Furthermore, the heat of formation of ye'elimite (800 kJ/kg) is remarkably lower than the one of alite (1848 kJ/kg) [65].

Phase	**Raw materials**	**g CO_2/g phase**
$C_4A_3\hat{S}$	$CaCO_3 + Al_2O_3 + CaSO_4$	0.216
$C_4A_3\hat{S}$	$CaCO_3 + Al_2O_3 + SO_3$ from combustion	0.288
C_4AF	$CaCO_3 + Al_2O_3 + Fe_2O_3$	0.362
$C_5S_2\hat{S}$	$CaCO_3 + SiO_2 + CaSO_4$	0.366
$C_5S_2\hat{S}$	$CaCO_3 + SiO_2 + CaSO_4$ from combustion	0.457
C_3A	$CaCO_3 + Al_2O_3$	0.489
C_2S	$CaCO_3 + SiO_2$	0.511
C_3S	$CaCO_3 + SiO_2$	0.578

Table 4 – Mineralogical composition in wt% of different CSA cement recently published

During the CSA cement production process, there are several indirect carbon dioxide and energy savings which are not directly associated with the change in clinker chemistry. For example, CSA clinker is easier to grind than OPC clinker [3,65] leading to a reduction in CO_2 emissions through lower electrical energy consumptions. McCaffey [86] published an estimation of 90 kg CO_2 per ton of milled OPC clinker while Garcia-Matè [84] estimated a reduction in emissions related to the

grinding of CSA clinker close to 20 kg CO_2 per ton of clinker. Furthermore, the density of CSA cements is about 7% lower than that of Portland cements, which suggests an additional reduction in the indirect carbon dioxide emissions through transportation of cement on a constant volume basis. Overall, the production of OPC clinker releases approximately 960 kg CO_2 per ton of clinker while by using CSA clinker the carbon dioxide emissions are reduced to about 635 kg CO_2 per ton of clinker, obtaining a 35% reduction in carbon footprint (Figure 9).

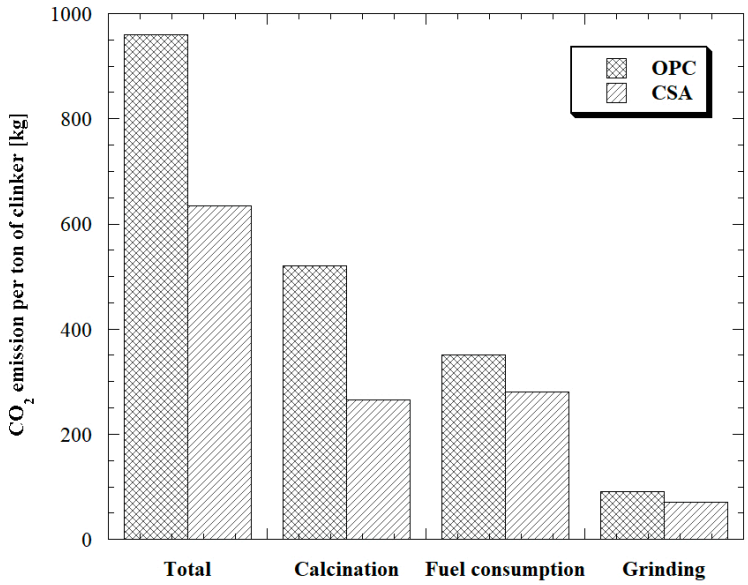

Figure 9 - Carbon dioxide emissions during cement production

1.4 Binary binders

1.4.1 Hydration mechanisms and microstructure

The kinetics of CSA cement hydration and product development are strongly influenced by the addition of calcium sulfate or calcium hydroxide [34,35]. The main phase of CSA clinker, the ye'elimite, reacts very slowly with water alone to form monosulfate ($C_3A{\cdot}C\hat{S}{\cdot}12H$, also known as AFm) and gibbsite (AH_3) as shown in Equation 1.

$$C_4A_3\hat{S} + 18H \Rightarrow C_3A{\cdot}C\hat{S}{\cdot}12H + 2AH_3 \quad (1)$$

On the contrary, when calcium sulfate is present, ye'elimite hydration forms ettringite ($C_3A{\cdot}3C\hat{S}{\cdot}32H$, also known as AFt) and gibbsite (Equation 2).

$$C_4A_3\hat{S} + 2C\hat{S}H_2 + 34H \Rightarrow C_3A{\cdot}3C\hat{S}{\cdot}32H + 2AH_3 \quad (2)$$

The hydration process was clearly demonstrated by Winnefeld et al. [36] by means of XRD analysis (Figure 10) and thermogravimetric measurements (Figure 11) at different ages. The formation of ettringite takes place in the first few hours. In particular, already after 1 hour of hydration, small amount of ye'elimite, calcium aluminate and calcium sulphate have been consumed and ettringite has

formed as new crystalline phase. Between 1 and 5 hours of hydration, the formation of AFt is limited, whereas the hydration accelerates a lot between 5 and 16 hours. After 16 hours of hydration, calcium sulfate is consumed and ye'elimite forms monosulfate. Between 1 and 28 days the hydration kinetics slows down again, displaying only a slight increase of the amount of hydration products. At long ages, the crystalline phases consist of the hydrated phase AFt and AFm, some non-reacted traces of ye'elimite, gypsum and other inert phases, such as gibbsite (aluminum hydroxide).

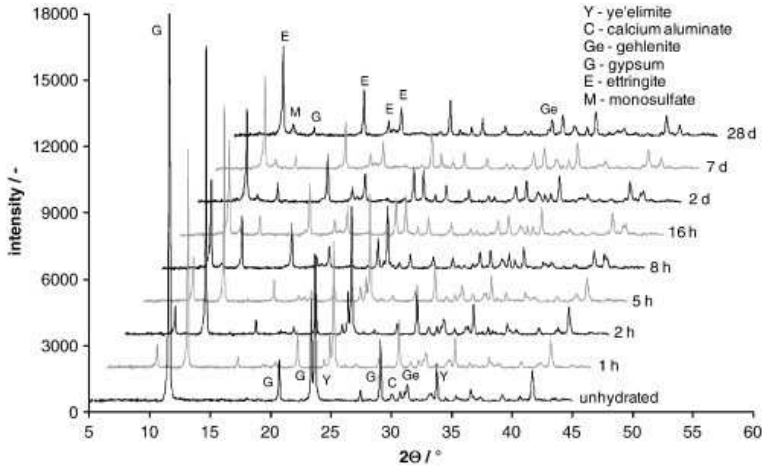

Figure 10 - XRD analysis of CSA cement. Unhydrated sample and hydrated paste at different ages [36]

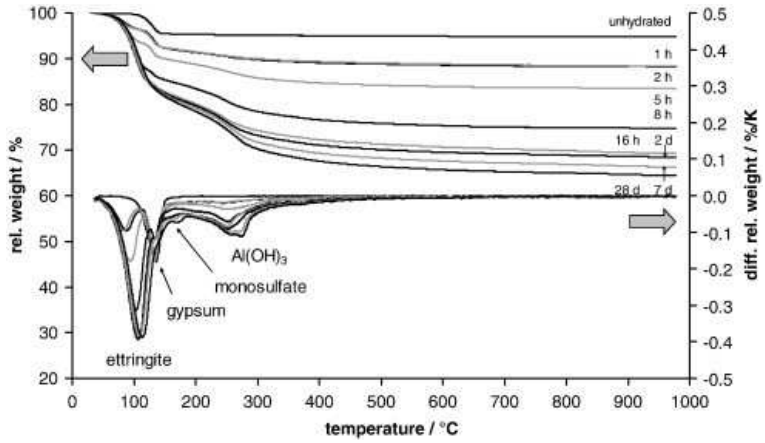

Figure 11 - TG analysis of CSA cement. Unhydrated sample and hydrated paste at different ages [36]

Tang et al. [87] and Gastaldi et al. [82] achieved the same conclusions through calorimetric analysis and near-infrared (NIR) spectroscopy (Figure 12). Moreover, the hydration reaction (Equation 3) of C_2S could be the same as that occurring in OPC independently of the rate of reaction of α and β polymorphs:

$$C_2S + (x+2-y)H \Rightarrow C_ySH_x + (2-y)CH \quad (3)$$

However, in presence of aluminum rich amorphous hydrates, the formation of strätlingite is favored according to the reaction 4 proposed by Alvarez-Pinazo et al. [88]:

$$C_2S + AH_3 + 5H \Rightarrow C_2ASH_8 \quad (4)$$

In CSA cements, which generally contain several secondary phases, similar reactions take place. In particular, according to Meller et al. [89] and Meredith et al. [90], the following reaction may occur during the hydration of CSA cements:

$$C_4AF + 3C\hat{S}H_2 + 30H \Rightarrow C_6A\hat{S}_3H_{32} + FH_3 + CH \quad (5)$$

$$C_{12}A_7 + 12C\hat{S}H_2 + 113H \Rightarrow 4C_6A\hat{S}_3H_{32} + 3AH_3 \quad (6)$$

$$3CA + 3C\hat{S}H_2 + 32H \Rightarrow C_6A\hat{S}_3H_{32} + 2AH_3 \quad (7)$$

$$C_4AF + 16H \Rightarrow 2C_2(A_{0.5}F_{0.5})H_8 \quad (8)$$

$$C_{12}A_7 + 51H \Rightarrow 6C_2AH_8 + AH_3 \quad (9)$$

$$2CA + 11H \Rightarrow 2C_2AH_8 + AH_3 \quad (10)$$

In general, the setting and hardening process of CSA cement-based mixtures can be summarized in a thermodynamic model (Figure 12) that shows the phase volumes during hydration in order to predict the hydration of CSA cements, allowing an easy and fast parameter variation like clinker composition, amount of calcium sulphate or water/binder ratio. In addition to the study of hydration reactions, the analysis of the microstructure is of primary importance for the development of CSA cement-based mixes. Han et al. [91] showed the disordered structure of CSH gel in cement paste, identifying a Ca/Si ratio close to 1.3. Moreover, it was highlighted that the AFt shows intact needle shape with tidy edge while AFm shows layered structure with rough edge, indicating secondary reactions (Figure 13).

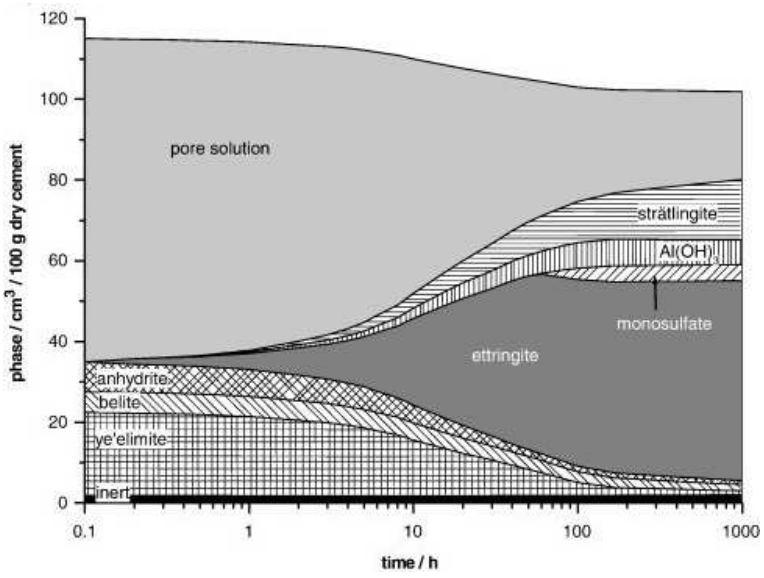

Figure 12 - Modelled changes of phase volume during hydration of CSA cement [36]

Further studies on the hydration products of CSA cement-based compounds were conducted by Telesca et al. [92,93] by means of scanning electron microscopy (Figure 14) that correlated the

ettringite grain size with the expansive behavior of CSA mixtures (expansive CSA pastes are characterized by small AFt grain).

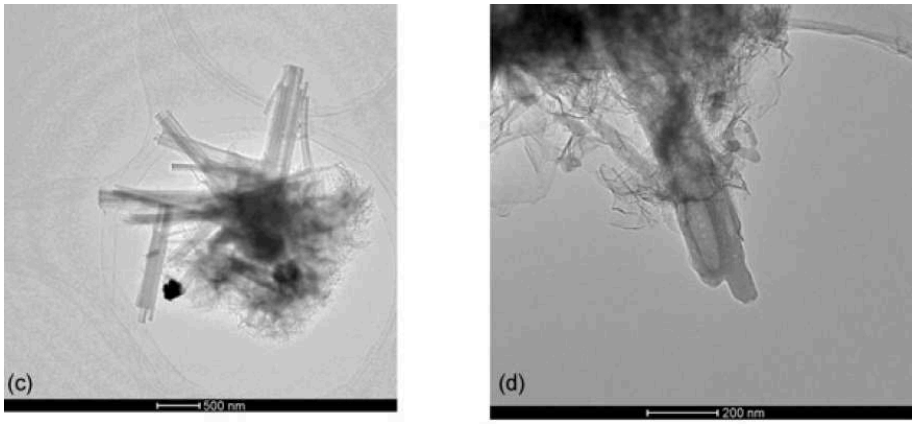

Figure 13 - AFt (left) and AFm (rigth) after hydration for 12h in TEM [91]

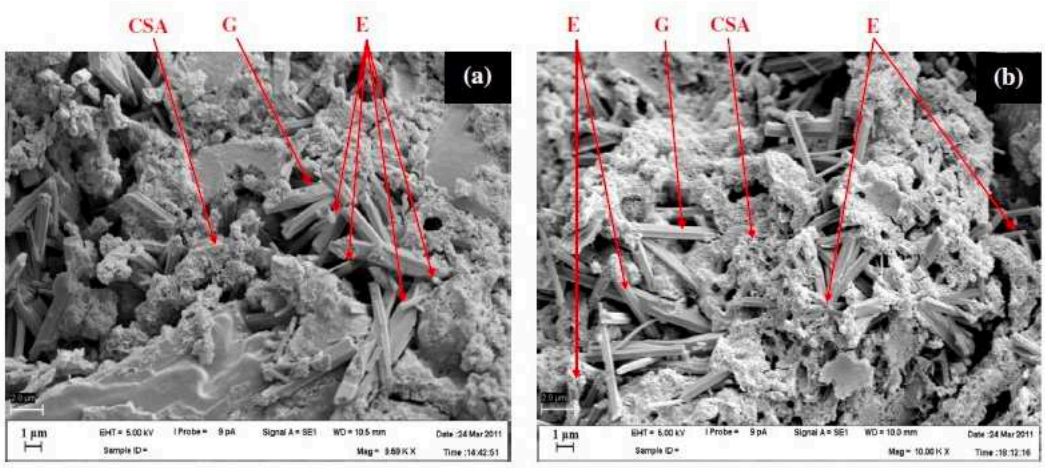

Figure 14 - SEM images of CSA pastes. CSA: clinker grain; G: gypsum; E: ettringite [92]

The hydration of calcium sulphoaluminate cements strongly depends on the amount and reactivity of the calcium sulphate added during the last phase of CSA cement production [43,94–97]. Therefore, the optimum calcium sulphate content is one of the key issues concerning the relevant properties like rapid hardening, high strength and expansive behavior with respect to the application of CSA cements. In the work of Zhang [75], a formula for the calculation of the optimum sulphate level to obtain mixtures with different mechanical and physical properties is reported:

$$C_T = 0.13 \cdot M \cdot A \cdot \frac{A}{S} \qquad (11)$$

Where CT is the ratio gypsum (or anhydrite)/clinker, A is the wt.% of ye'elimite in clinker, S is the wt.% of SO_3 in gypsum or anhydrite, M is the molar ratio gypsum/ye'elimite and 0.13 is a

stoichiometric factor containing all the conversions between mass and molar units. The molar ratio M varies according to the type of mixtures:

- M = 0 – 1.5 with a low calcium sulphate contents yields a rapid hardening or high-strength cement;
- M = 1.5 – 2.5 provides expansive behavior;
- M = 2.5 – 6 is a suitable solution for self-stressing cements.

Winnefeld and Barlag [98] explained this behavior by studying the AFt/AFm ratio (Figure 15). In fact, according to equations 1 and 2, the amount of calcium sulphate added to the clinker influences the ratio of the main hydrate phases, ettringite and monosulphate. In particular, with increasing amounts of calcium sulphate, more ettringite is forming. This may lead to an expansive matrix. On the other hand, low amount of calcium sulphate promotes the formation of AFm phases, resulting in a reduced fluidity and may lead to premature setting.

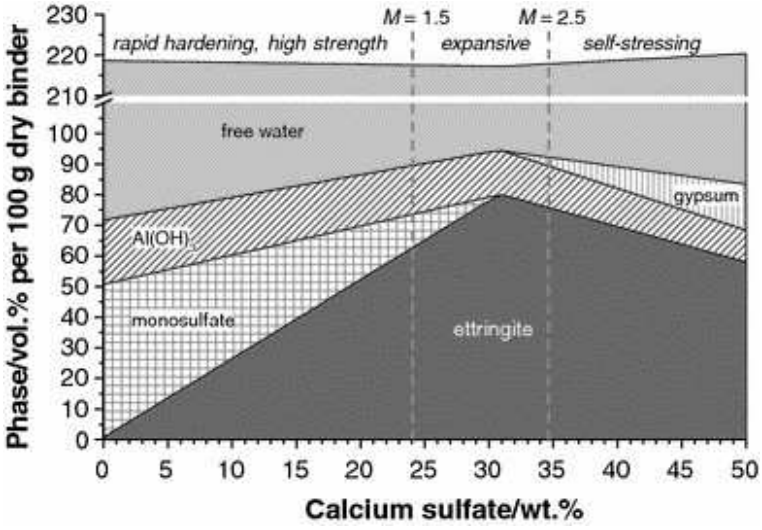

Figure 15 - Phase diagram of the system ye'elimite-calcium sulphate-water at 20°C and water/solid ratio of 2 [98]

As reported by Taczuk et al. [99], the amount of AFt is affected by the reactivity of calcium sulphate (solubility and speed of dissolution) at early ages. If the reactivity of calcium sulphate is too low, AFm might form instead of AFt. Moreover, Pelletier-Chaignat et al. [43] investigated the influence of calcium sulphate source on the hydration of CSA-based mixtures by means of isothermal calorimetry, XRD and TGA analysis. Results shows that the hydration mechanisms are similar in presence of gypsum or anhydrite, the difference being in the kinetics of reactions due to the slower dissolution of anhydrite compared to gypsum. This is clearly visible on the heat flow calorimetric curves reported in Figure 16. The same conclusions can be drawn by analyzing the studies of Winnefeld and Barlag [98]. Furthermore, it seems that a reactive calcium sulphate addition like

gypsum is very suitable to control the hydration and setting of ye'elimite pastes. In contrast to gypsum, the less reactive anhydrite leads to a more complex early hydration kinetics, even if the phases formed are the same as with gypsum (Figure 17).

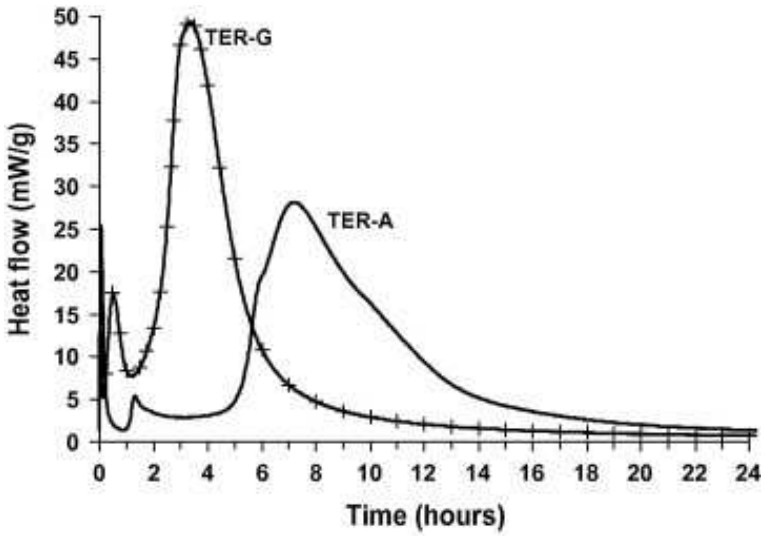

Figure 16 - Heat flow curves obtained by isothermal calorimetry on the gypsum-bearing (TER-G) and on the anhydrite-bearing (TER-A) systems during the first 24h of hydration [43]

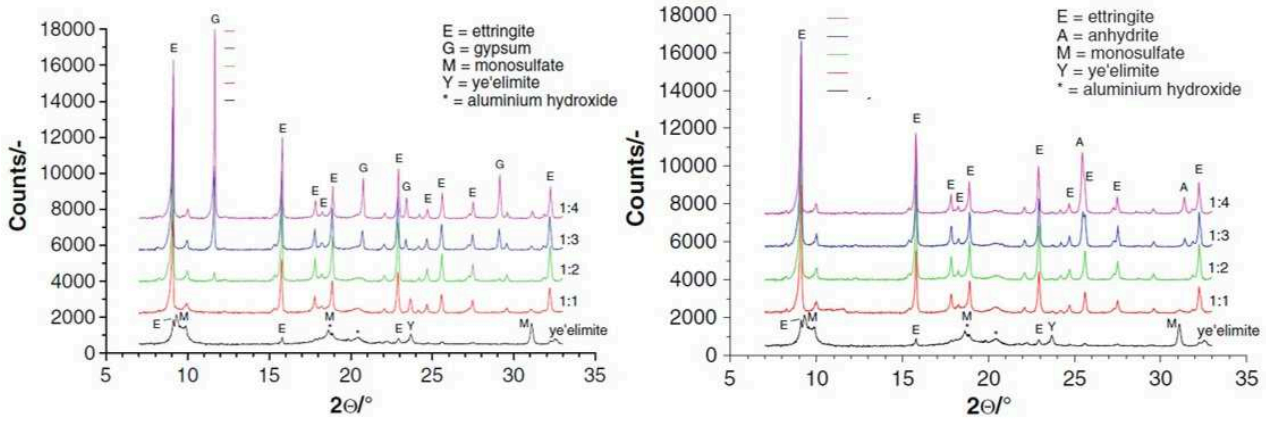

Figure 17 - X-ray diffraction analyses of ye'elimite pastes after 18h of hydration. Influence of gypsum (left) and anhydrite (rigth) addition [98]

It is well known that the water/binder ratio strongly affects the microstructure and the porosity of Portland-based mixtures, providing water to hydrate phases and the porosity where hydration products can precipitate. Moreover, the porosity and hydration degree strongly affect the performance of concretes [100]. The same concepts can also be extended to mixtures based on calcium sulphoaluminate cements. In particular, low w/c ratio results in a denser pore structure, as space available for hydration products formed is smaller, and high-strength mixtures. However, pastes with low water content can suffer from self-desiccation due to the huge amount of water required for AFt formation. This can be critical for expansion properties as large amount of cement grain remain

anhydrate after setting, causing expansion if cement is later exposed to external water from the environment (so-called delayed ettringite attack) [101]. On the contrary, a high w/c ratio ensures high dimensional stability but contributes to the formation of porous microstructures with low mechanical strength [79].

In the literature, the hydration of CSA-based systems has been studied with several water/ cement ratios [65,92,102–104]. The formation reaction of AFt in presence of $C_4A_3\hat{S}$ and $C\hat{S}H_2$ (Equation 2) theoretically requires a w/c ratio of 0.64. However, the presence of second phases in CSA cement strongly influences the w/c ratios needed for full hydration of cement grains. In general, due to the large compositional variability of CSA cements (Table 2 and Table 3), one theoretical water demand for full hydration cannot be established. Anyway, known the mineralogical composition of CSA cement and the sulphate content, a w/b ratio for full hydration can be calculated. Garcia-Matè [84] claims that this value may not be very far from 0.60.

1.4.2 Rheological and physical properties

The setting times of CSA cements depends on their chemical and mineralogical composition (especially in terms of ye'elimite) and the amount and reactivity of calcium sulphate added to the mix. In general, the setting time of CSA-based concretes is more rapid compared with those of traditional concretes manufactured with Portland cement. Typical values are between 30 minutes and 4 hours [63,65,92,105]. Similarly to Portland cement, with high temperatures, initial and final setting time decrease rapidly and the times between initial and final set are also shortened [75]. Moreover, the fresh CSA:C$\hat{S}$ concrete is more workable than OPC at the same w/b ratio and the same water content. This suggest that for the same consistency class and w/b ratio of an OPC concrete, CSA:C$\hat{S}$ concrete requires less cement content.

The workability loss over time of CSA concrete is generally very high. A possible cause for this behavior would be the formation of rich amounts of ettringite in the cement matrix [106]. This sulphoaluminate phase is characterized by a high water demand [65] as 34 H_2O molecules are bound according to equations 2. Upon immediate formation of the needle-like crystals, higher amounts of mixing water were adsorbed, reducing the fluidity of fresh mixture. For these reasons, the rheological properties of CSA cement concretes are tailored by using chemical admixtures, especially citric acid-based retarders, and/or polycarboxylate-based superplasticizers [107].

All authors [35,36,65,76] agree that CSA concrete produces considerably higher strength compared to OPC at the same w/b ratio and cement content due to the ettringite crystal interlocking effect. For this reason, to produce an equal strength class to that of OPC, the w/b ratio must be increased, and to produce the same consistency class, the amount of water must also be reduced [75]. The relationship

between w/b ratio and compressive strength of CSA concrete (Figure 18) was also confirmed (the higher the w/b ratio, the lower the mechanical strength of mixture).

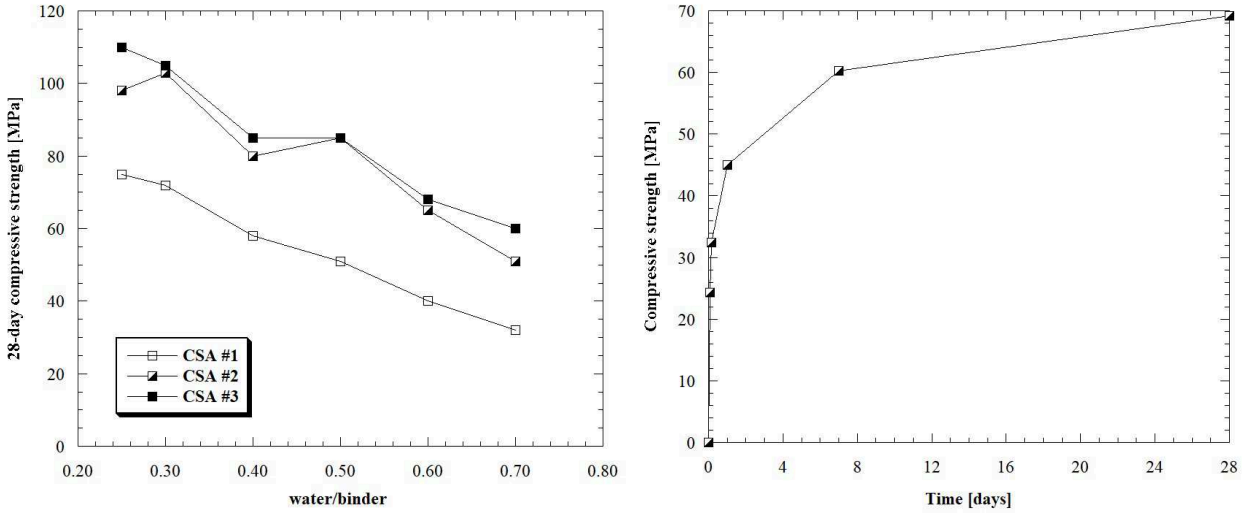

Figure 18 - Relationship between w/b ratio and strength of three different CSA concrete. Data from [75] **(left). Compressive strength over time of CSA concrete. Data from** [108] **(right)**

However, the cause of this behavior is different from what is observed in the OPC system. In fact, the contribution of ettringite to compressive strength is affected by the size of crystals, the void content, and the amounts of anhydrous particles, which influence the distance between Aft crystals. These three factors interact to produce the interlocking and binding ability of ettringite in concrete [100]:

- The size of ettringite crystals increase with the increase of w/b ratio;
- The void content reduces with the reduction of w/b ratio;
- The number of anhydrous particles increases with the reduction of w/b ratio.

The overlap of these three factors caused the relationship between w/b ratio and compressive strength of CSA, as explained by Zhang [75]. The fast-earlier strength development (Figure 18) is another advantage of using calcium sulphoaluminate cement as binder for manufacture flowable mortars and concretes as the formworks can be removed shortly after the casting, improving the efficiency of building yard and, therefore, reducing the construction costs.

Conversely to compression, ettringite crystal interlocking does not work as well under direct and indirect tension. The direct and indirect splitting tension strength is approximately equal to that of Portland concretes manufactured with the same w/b ratio. On the contrary, during the bending test, the CSA concrete can benefit from crystal interlocking. For this reason, the flexural strength of CSA:CŜ concrete is much higher than traditional OPC concrete. Furthermore, CSA concretes cured under water can suffer from a micro-crack induced expansion, responsible for the loss of flexural

strength at long ages. However, in calcium sulphate-rich mixtures, the continuation of ettringite formation was thought to re-heal the micro-crack induced expansion as found by Glasser and Zhang [65]. Sherman et al. [109] noted that, independently of CSA cement composition, concretes had much higher mechanical strength after dry curing (23°C, R.H. 67%) than after wet curing (23°C, R.H. 100%) (Figure 19). The same results, in contrast to what was found for OPC concretes, can be found in the works of Zhang [75]. Nevertheless, none of the researchers identified the reasons for this behavior. The elastic properties of the binary systems have not yet been well investigated. However, Sirtoli [110] has investigated the evolution of the elastic modulus of CSA mortar through three techniques:

- By measuring the strain of mortar samples under compression loads (static method);
- By determining the propagation speed of the ultrasonic waves (dynamic method);
- By using the Ambient Response Method (ARM).

In addition, the Poisson's ratio was also detected. Preliminary results indicated that elastic modulus of CSA mortars is generally lower than that of OPC mortars. Furthermore, the Poisson's ratio seems to be similar to that detected for OPC mixtures at the same strength class (Figure 19).

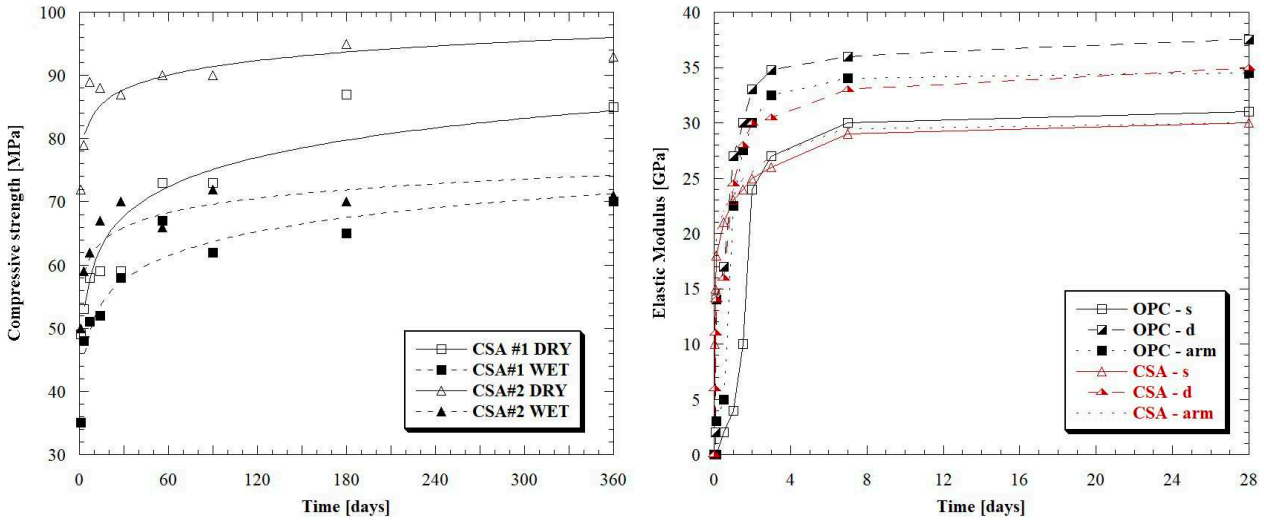

Figure 19 - Compressive strength development of CSA concrete with different curing conditions. Data from [109] **(left). Elastic modulus of OPC and CSA mortars over time measured with different techniques (s-static, d-dynamic, arm-ambient response method). Data from** [110] **(right)**

The most valuable property of CSA-based mixtures is the volume stability over time [103,111,112]. It is well known that these cements are potentially expansive if hydrated:

- In a strong alkaline environment [113];
- In presence of lime [36];
- With a considerable amount of added calcium sulphate (Figure 20) [43,103].

On the contrary, they tend to attain a dimensional stability when hydrated:

- At not elevate pH values;
- In absence of calcium hydroxide;
- Together with relatively moderate calcium sulphate additions.

The expansive behavior mainly concerns the binary compounds with high sulphate content and allows the production of "shrinkage-compensating" or "self-stressing" concretes. Conversely, the generation of non-expansive crystals is related to the reaction 2 or, when calcium sulphate is absent or fully depleted, to the reaction 1.

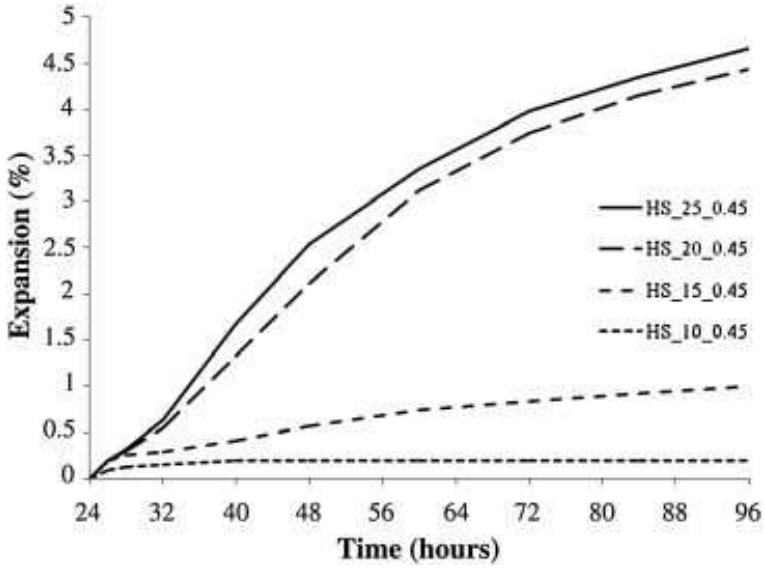

Figure 20 - Expansion of CSA:CŜ cement pastes with different amount of gypsum using w/b of 0.45 [103]

1.5 Ternary binders

1.5.1 Hydration mechanisms and microstructure

In the presence of calcium hydroxide and sulfate, ye'elimite reacts rapidly to form C_4AH_x, whereas the combined presence of CH and CŜ leads to the formation of ettringite as shown in Equation 12.

$$C_4A_3\hat{S} + 8C\hat{S} + 6CH + 90H \Rightarrow 3C_3A{\cdot}C\hat{S}{\cdot}32H \quad (12)$$

The presence of calcium hydroxide, directly added to the mix in form of lime or released during the C_3S hydration from the OPC (portlandite) (Equation 13), makes the reaction 12 more favorable than 2.

$$2C_3S + 6H \Rightarrow C_3S_2H_3 + 3CH \quad (13)$$

Consequently, three moles of AFt are producing instead of one per each unit of ye'elimite, which results in a large potential for expansion. Furthermore, Gastaldi et al. [82] highlighted, through SEM observation, that the presence of CH in the hydrating environment influences the crystal size of

ettringite. In particular, Aft crystals coming from reaction 3 are significantly smaller than those produced by the hydration of $C_4A_3\hat{S}$ with $C\hat{S}H_2$, causing a different microstructure of cement paste.
The hydration of ternary mixtures based on sulphoaluminate cement mixed with Portland cement and calcium sulphate (CSA:OPC:$C\hat{S}$) is not well documented. Pelletier et al. [76] studied the CSA:OPC:$C\hat{S}$ hydration process to determine:

- If the two types of clinkers react simultaneously or consequently;
- Which clinker is responsible for the early and late mechanical properties;
- The influence of CSA/OPC ratio on the hydration process.

The hydration mechanism (Table 5) can be subdivided in three different phases:

- During the first hours from mixing, the main reaction is the AFt formation. However, in mix with low calcium sulphate content, minor quantities of AFm may be produced. Subsequently, minor amount of CA or C3A may participate in the hydration when the calcium sulphates are exhausted, leading to the formation of additional AFm;
- In a second step (1÷7 days of hydration), the main constituents of OPC clinker start to react, producing strätlingite, calcium hydroxide and calcium silicate hydrate. Furthermore, AH_3 can react with CH and $C\hat{C}$ to form monocarbonate. At the same times, secondary reactions may occur between calcium hydroxide and AH_3 produced during AFt formation or C_3A from OPC clinker;
- Lastly, the AFm is produced by the reaction between several pre-existing phases and the main constituent of OPC clinker and CSA cement.

Time		Reaction
< 1 day	Main	$C_4A_3S + 2C\hat{S}H_2 + 34H \Rightarrow C_3A{\cdot}3C\hat{S}{\cdot}32H + 2AH_3$
		$C_4A_3S + 8C\hat{S} + 6CH + 90H \Rightarrow 3C_3A{\cdot}3C\hat{S}{\cdot}32H$
	Secondary	$C_4A_3S + 18H \Rightarrow C_3A{\cdot}C\hat{S}{\cdot}12H$
		From minor phase such as CA or C_3A
1 ÷ 7 days	Main	$C_3S + AH_3 + 6H \Rightarrow C_2ASH_8 + CH$
		$C_3S + 3.7H \Rightarrow CSH_{1.7} + 2CH$
	Secondary	$AH_3 + 3CH + C\hat{C} + 5H \Rightarrow C_4A\hat{C}H_{11}$
	Secondary	$AH_3 + 4CH + 6H \Rightarrow C_4AH_{13}$ from AFt-forming reaction
		$C_3A + CH + 12H \Rightarrow C_4AH_{13}$ from OPC clinker
> 7 days	Main	$3C_4AH_{13} + 2C_3A{\cdot}3C\hat{S}{\cdot}32H + AH_3 \Rightarrow 6C_3A{\cdot}C\hat{S}{\cdot}12H + 34H$
		$C_3A{\cdot}3C\hat{S}{\cdot}32H + 2C_3A + 4H \Rightarrow C_3A{\cdot}C\hat{S}{\cdot}12H$
		$C_3A{\cdot}3C\hat{S}{\cdot}32H + 6CA + 16H \Rightarrow C_3A{\cdot}C\hat{S}{\cdot}12H + 4AH_3$

Table 5 – Hydration mechanism of CSA:OPC:$C\hat{S}$ ternary mixture according to [76,114]

Also in calcium hydroxide-rich systems, the variation of calcium sulphate content has strong impact on the AFt to AFm ratio (Figure 21) and, therefore, on the elasto-mechanical and physical properties of cement paste/mortar/concrete. On the contrary, a small influence seems to have the calcium sulphate dosage on the hydration kinetics [76].

The variation of the OPC content has little impact on the hydration kinetics of cement and almost no effect on the phases which form. However, the CSA/OPC ratio slightly affects the Aft to AFm ratio at later ages, influencing the compressive strength (Figure 21). In particular, low CSA/OPC ratio results in a porous matrix with low mechanical properties while high CSA/OPC ratio allows to obtain high compressive strength. Moreover, Trauchessec et al. [35] showed that both OPC composition and CSA/OPC ratio influence the mechanical strength development as well as ye'elimite hydration rate. High CSA cement percentage increases the hardening speed due to quick ye'elimite hydration that occurs during the first three days. Subsequently, OPC reacts and alite hydration produces strätlingite. On the contrary, for low CSA/OPC ratio, the hardening speed is slower. OPC reacts during the first days and ye'elimite hydration occurs in presence of lime (free lime and portlandite) and form AFt or, in absence of calcium sulphate, AFm. Finally, the importance of OPC composition was emphasized, especially in terms of free lime content.

Currently, no study deals with the hydration of CSA cements in combination with hydrated lime or calcium oxide directly added in the cement mixer.

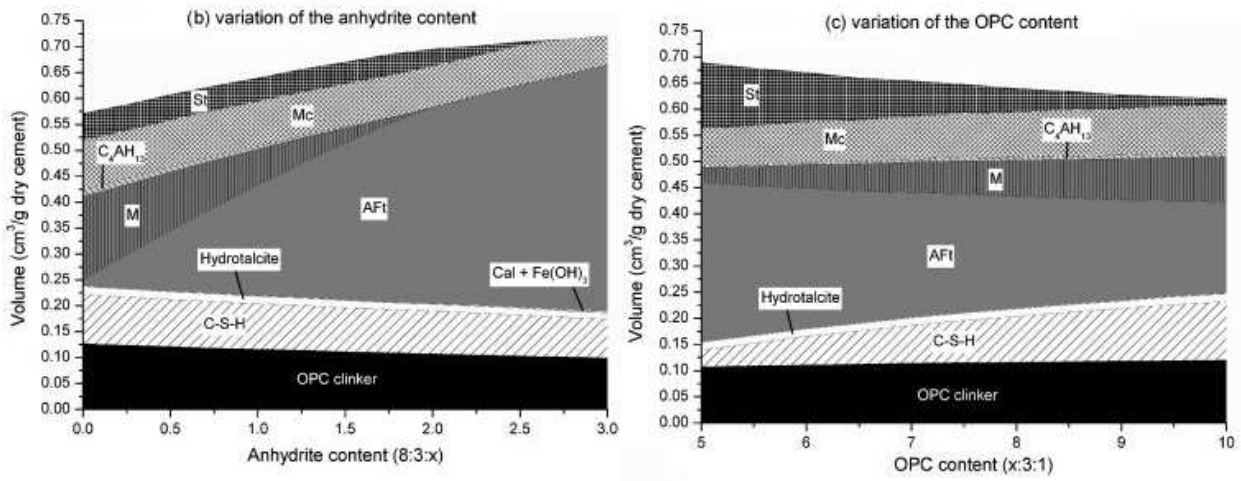

Figure 21 - Modelled hydration of ternary binder. Effect of calcium sulphate content (left) and OPC content (right). Anh:anhydrite, Cal:calcite, M:monosulphoaluminate, Mc:monocarbonate, St:strätlingite, Yee:ye'elimite [76]

1.5.2 Rheological and physical properties

The properties of ternary binders can differ considerably from those of binary binders. In general, the presence of calcium hydroxide as a product of OPC hydration, accelerates the initial setting times and

reduces the initial workability of CSA-based concretes [115]. However, some authors [110,116] have reported an increase in setting times when Portland cement is added to the mixture. The workability retention of ternary binder-based concretes is, in general, similar to that of binary binders-based mixtures, regardless of OPC dosage. The mechanical properties of mixtures manufactured with ternary systems are strongly influenced by both the CSA/CS ratio and the CSA/OPC ratio. In particular, by increasing the calcium sulphate dosage, the mechanical strength increases, while CSA/OPC ratios not minor than 1 allow to attain mixtures whit high compressive strength.

The ternary diagram reported in Figure 22, divided in three different areas, is useful to understand the strong correlation between the ternary mixtures composition and the mechanical strength expected. In particular, by varying the binder composition in the same direction as the arrow, it is possible to attain three different behavior:

- A strength increasing in the green zone;
- A strength plateau or slight decreasing in the yellow zone;
- An excessive expansive behavior in the red zone that does not allow the production of mixtures.

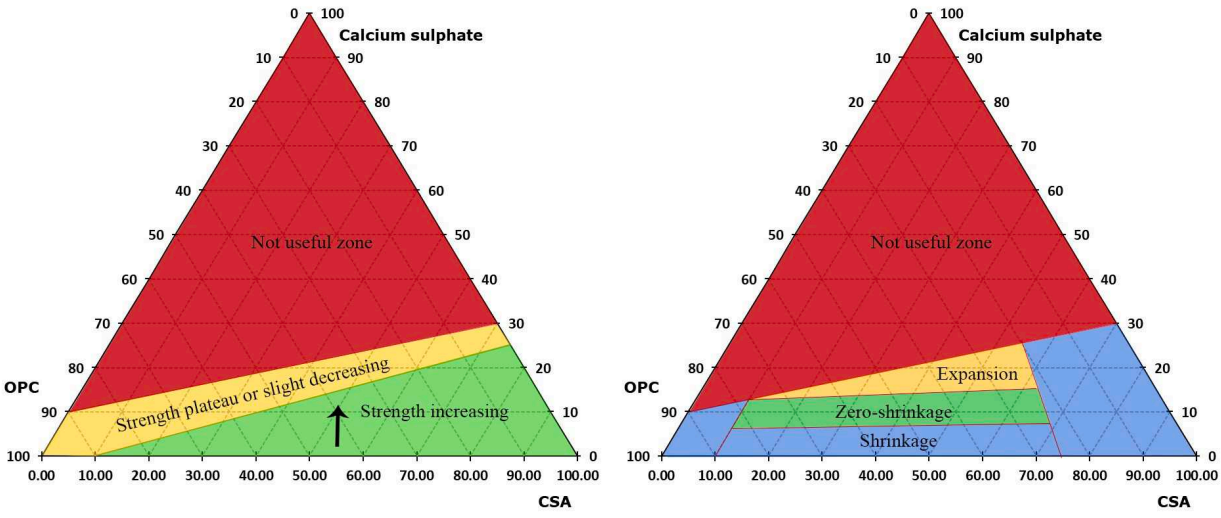

Figure 22 - Ternary diagram of CSA:OPC:CŜ binders and strength evaluation (left) or dimensional stability (right)

In general, the elastic modulus of CSA ternary mixtures is lower than that of CSA binary mixtures, as it is possible to note from Figure 23, while the Poisson's ratio is similar to that of OPC mixtures at the same strength class [61,110]. The composition of the ternary binders strongly influences the dimensional stability of the mixtures. As already seen in Figure 22, a large number of possible binder compositions cannot be used due to excessive expansion (red zone). In the blue zone, on the other hand, are found all those binders that give rise to compounds that shrink over time similarly to Portland cement mixtures. The most interesting zones from an engineering point of view are those

that produce to expansive (yellow zone) or zero-shrinkage (green zone) binders. Traditionally, CSA:OPC:CŜ mortars and concretes have a composition included between these last two areas.

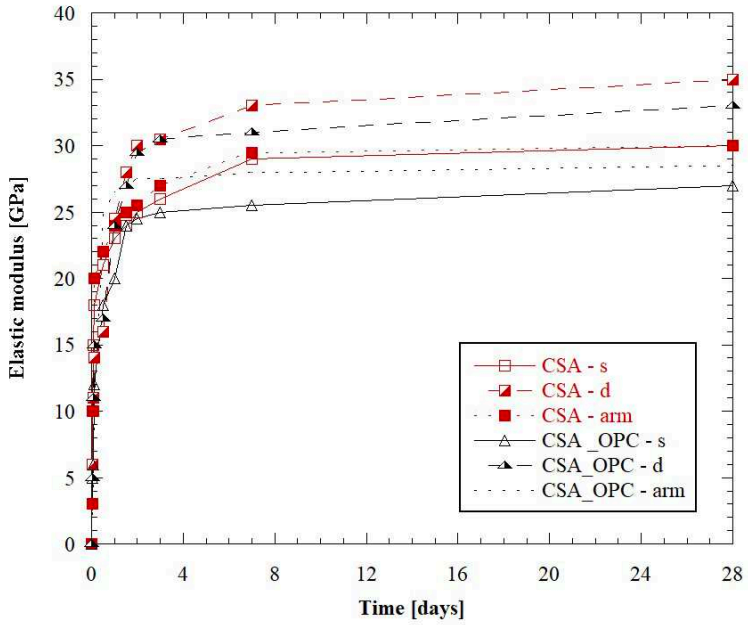

Figure 23 - Elastic modulus of CSA ternary and binary mortars over time measured with different techniques (s-static, d-dynamic, arm-ambient response method). Data from [110]

1.6 Innovative binders

The use of sustainable supplementary cementitious materials, such as fly ash (FA), ground granulated blast furnace slag (GGBFS), and silica fume (SF), in the CSA-based mixtures reduce the environmental impact of concrete and represent an interesting possibility to dispose solid industrial waste.

Currently, only one paper deals with CSA-based mixtures containing GGBFS or silica fume, providing only partial information regarding mechanical strength and setting time [117]. On the contrary, the behavior of mixtures containing fly ash has been mainly investigated. Martin et al. [37] showed that the addition of FA, and the resulting supply of silica from reacted fly ash, results in the formation of additional strätlingite and ettringite according to the following reaction Equation 14:

$$3C_3A{\cdot}C\hat{S}{\cdot}12H + 3S + A + 20H \Rightarrow 3C_2ASH_8 + C_3A{\cdot}3C\hat{S}{\cdot}32H \qquad (14)$$

In particular, the amount of strätlingite is increasing with increasing fly ash replacement, reaching its maximum shortly after all monosulphate is consumed as reported in Figure 24. The same considerations can be drawn analyzing the XRD patterns of mixtures with and without FA proposed by Martin et al. [37] (Figure 25) and Ioannou et al. [118].

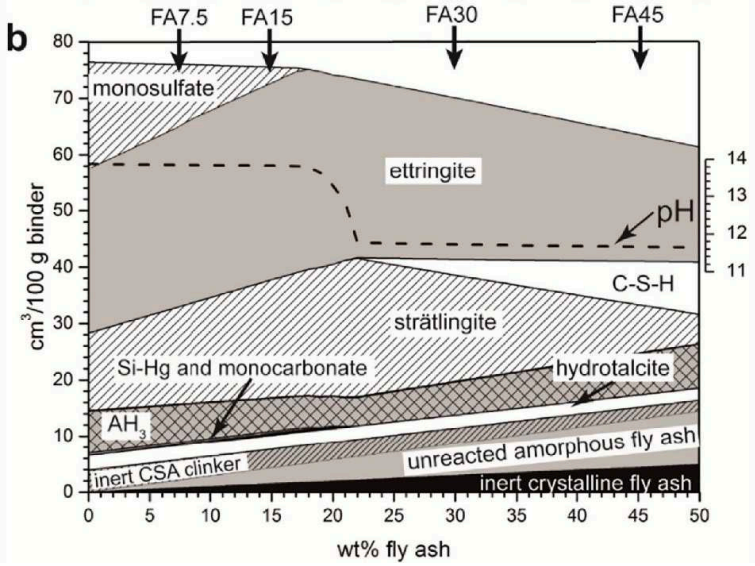

Figure 24 - Calculated hydrated assemblages as a function of FA replacement, assuming a reaction degree of 40% of the fly ash [37]

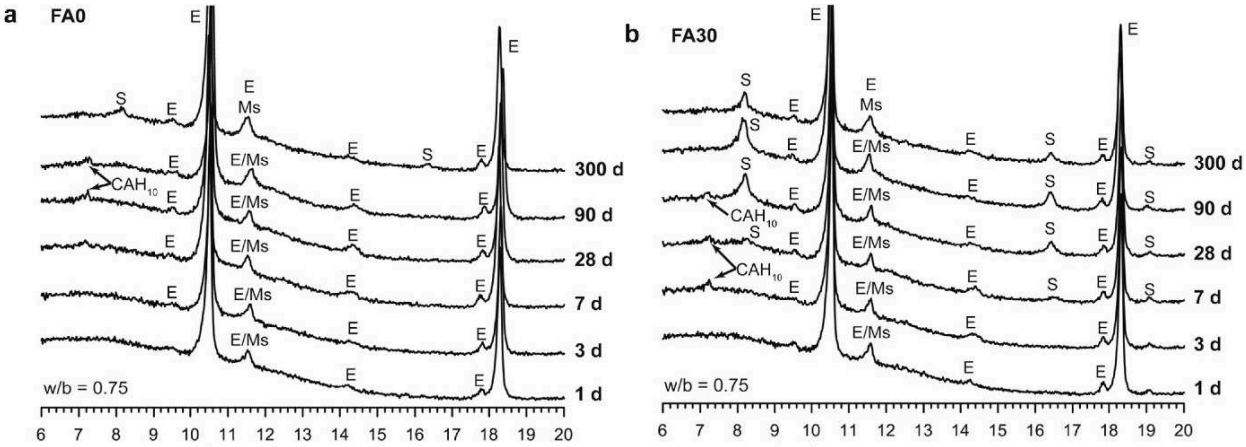

Figure 25 - XRD patterns after 1,3,7,28,90 and 300 days of hydration for mixtures with (right) and without FA (left). E:ettringite, S:strätlingite [37]

Moreover, results from isothermal calorimetry and SEM observations indicate that no or little reaction of the fly ash is observed in the first 28 days. Conversely, after 90 days of hydration, SEM images show that the FA particles have dissolution rims in all blends, which indicates that some reaction of the fly ash occurred (Figure 26). In general, all authors [37,117,118] agree with Garcia-Matè et al. [38] which identified two main effects related to the use of FA in CSA-based system: i) filler effect and ii) dilution effect. The former slightly increases the compressive strength in mortars with up to 15 wt.% of FA while the latter predominates when more than 15 wt.% of FA is added with negative effect in the mechanical strength.

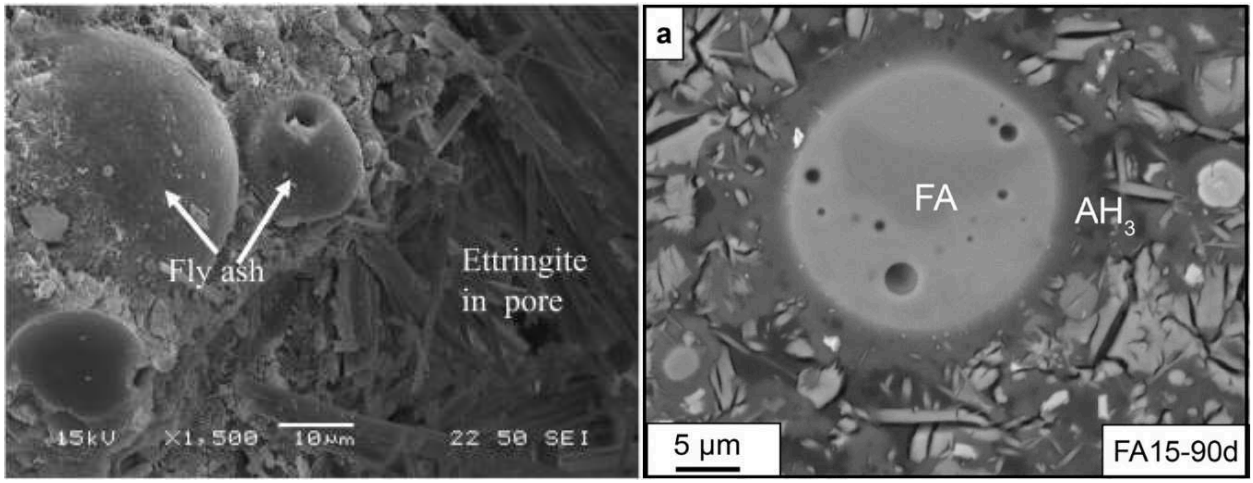

Figure 26 - SEM images of mixture containing FA after 28 days (left) [118] **and 90 days (right)** [37]

1.7 Admixtures

In the previous paragraphs, the effect of calcium sulphate and calcium hydroxide on the hydration kinetics of CSA-based mixtures was widely discussed. However, similarly to Portland cement, it is possible to modify the hydration kinetics of CSA cements by using chemical admixtures. In particular, due to the rapid setting of CSA cements, the use of retarder admixtures is necessary in order to increase their workability, especially for larger scale placements. Currently, citric acid is the primary set retarding admixture recommended by several authors [119–121] for use with CSA cement. The addition of amount between 1 wt.% and 3 wt.% of citric acid strongly retarded the hydration of CSA cement and the total heat released (Figure 27) as reported by Velazco et al. [120] and Burris et al. [119]. Moreover, it was demonstrated that citric acid modified the morphology of AFt needles and changed the microstructural configuration, promoting a general increasing of mechanical strength. For setting time control, also other organic retarders such as polycarboxylate, sodium borate, sodium gluconate, sugars, carbamide, tartaric acid or sodium tartrate have been investigated [40,41,108,121]. Furthermore, compounds containing lithium, aluminum and calcium have been used as hardening accelerator admixtures in CSA-based compounds at low temperature [40,67,108].

Though the performances and hydration behavior of CSA cements have been widely investigated in several works, knowledge on the use of superplasticizers with calcium sulphoaluminate cements has not been established yet. Yuan et al. [42] investigated the influences of two type of superplasticizers (polycarboxylate ether and naphthalene type) on the properties of cement pastes, underlining a remarkable increase in workability without setting time changes. In particular, polycarboxylate-based admixture can retard the early age hydration while naphthalene-based superplasticizer can accelerate the early age hydration and both types of admixtures have no influences on the further hydration of

CSA cement. Guo et al. [122] developed a new amphoteric polycarboxylic acid-based superplasticizer and Zhang et al. [121] showed the presence of competition effect between retarders and β-naphthalenelfonic acid-based or aminosulfonic acid-based superplasticizer.

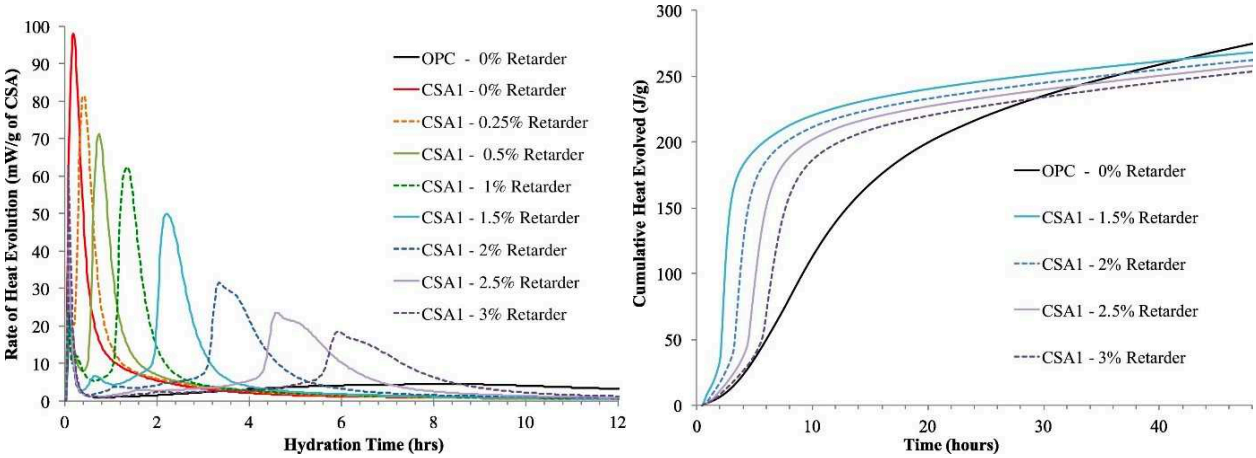

Figure 27 - Rate (left) and cumulative (rigth) heat evolution of CSA cement pastes with dosages of citric acid varying from 0 to 3 wt.% [119]

The effect of shrinkage reducing admixtures (SRA) has been extensively studied in Portland cement concrete, mortars and pastes [123,124]. Conversely, limited information on the pertinence of using SRA in CSA cement mortars and pastes is available. Ambroise et al. [125] proved the efficiency of polyether polyol as SRA on pastes and mortars manufactured with CSA cements. Moreover, it was found that the efficiency of SRA strongly depends on its molecular weight (the higher the molecular weight, the lower the efficiency of the admixture) and the presence of polyether polyol increases the quantity of AFt in hydrated pastes, modifies the morphology of ettringite, leading to the formation of hollow crystals (Figure 28), and reduces the mechanical strength of mortars manufactured with SRA.

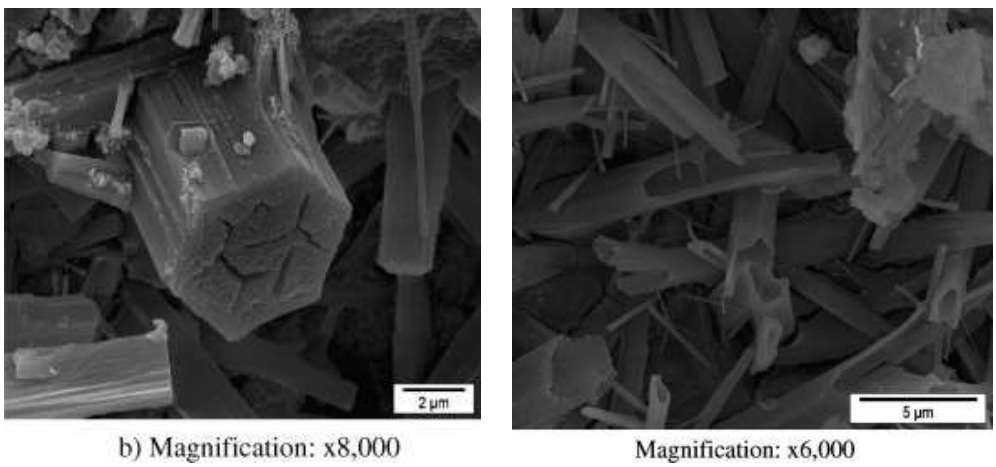

Figure 28 - SEM images of CSA pastes containing polyether polyol-based SRA [125]

1.8 Durability of CSA-based mortars and concretes

To produce a more sustainable binder, it is not sufficient to only produce the binder in a more environmentally friendly way. The cement must also provide the production of a durable mixture. Otherwise, the environmental benefits gained in manufacturing could be offset by shorter service life [126].

The durability of concrete is mainly influenced by the penetration speed of some substances in the cement matrix. In traditional OPC concrete, high strength concrete with low permeability and porosity is mostly more durable against the attack of deteriorating substances, such as chlorides, sulphates, water and carbon dioxide. With a different pore structure and hydration products, the CSA concrete is characterized by a durability different from that of OPC concrete.

There have been relatively few durability studies investigating CSA mixtures compared to OPC mixtures. In particular, no papers deal with the topic of the AAR resistance, fire and high temperature resistance of CSA-based mixtures while valuable studies on resistance against chemical attack are few.

The durability of buildings materials made from CSA cements, both derived from laboratory test and in-situ test, seems to be at least comparable to traditional OPC-based materials, however more data concerning long-term behavior are needed. Binary binder concretes can exhibit a high resistance to freeze-thaw and against sulphates, chlorides and seawater [61,65,75,127] due to its dense pore structure developed by CSA cement. This aspect was confirmed by Bernardo et al. [79] by mercury intrusion porosimetry that have revealed that hydrated CSA cements exhibits mainly pores of a threshold radius below 25 nm (Figure 29) and only a minor content of larger pores forming an interconnected pore network, leading to high impermeability.

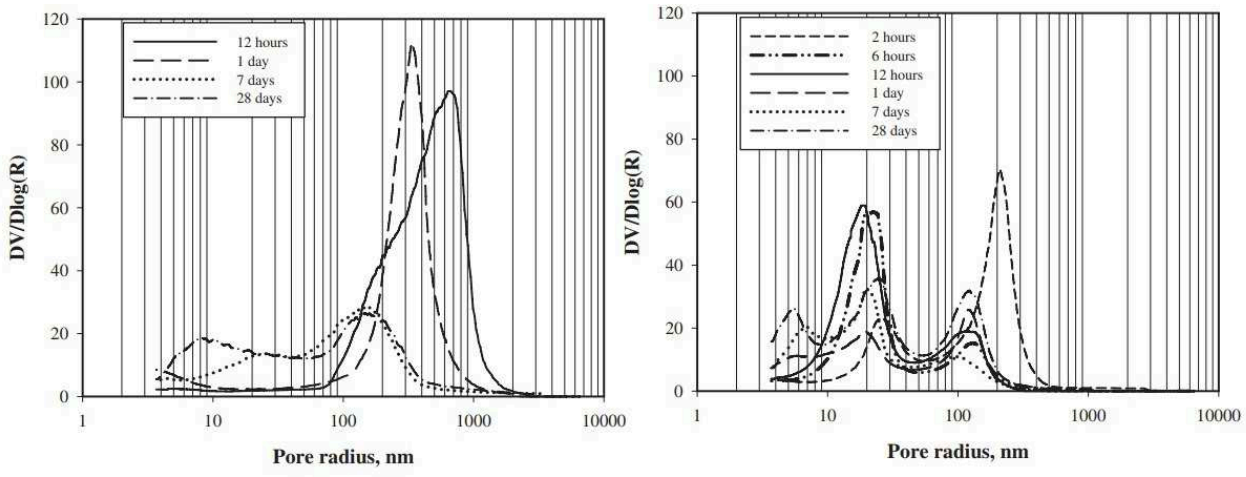

Figure 29 - Intruded Hg volume vs pore radius for OPC- (left) and CSA-based (rigth) pastes cured at various ages [79]

In regards to carbonation of binary mixtures, several researches present conflicting results. Quillin [66] report that CSA carbonates faster than OPC due to the large amount of ettringite produced on hydration (Figure 30), as already reported by Zhang and Glasser [128]. Guo et al. [71] and Zhang et al. [129] found that CSA concrete has similar carbonation rates to OPC concrete, while Duan et al. [78] concluded that CSA mixtures perform better than Portland cement-concretes. Nevertheless, all authors agree on the inversely proportionality between carbonation rate and water to binder ratio. Recently, Hargis et al. [126] performed a wide study on carbonation of CSA-based binary mortars, concluding that the carbonation resistance of CSA mortars is lower than that of OPC mortars and increases with increasing calcium sulphate content. Moreover, the carbonation strongly modifies the porosity of mortars and clearly affects the compressive strength of mixtures. Finally, the authors claimed that the CO_2 binding capacity of CSA hydrated products is lower than that of OPC hydrated products, reducing the total CSA CO_2 binding capacity by half respect to OPC.

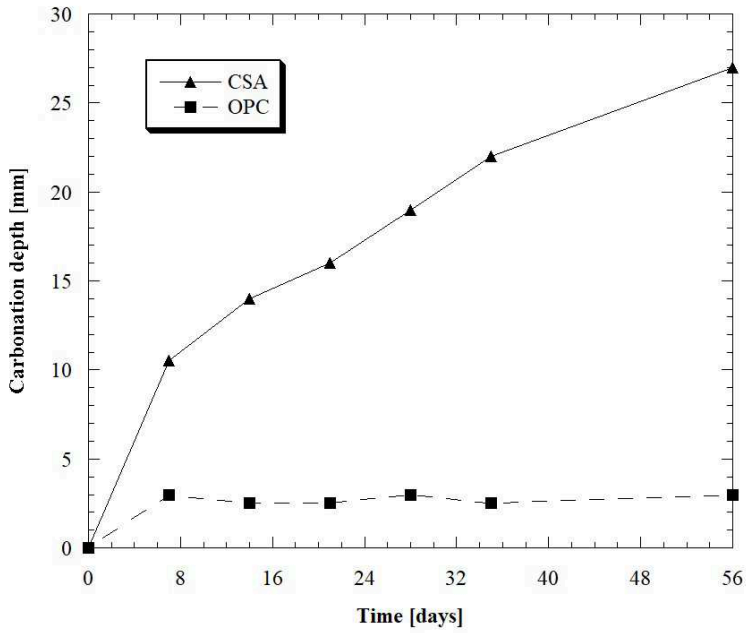

Figure 30 - Accelerated carbonation depths vs time. Data from [66]

Moreover, Zhang [75] highlighted that the incorporation of OPC in ternary binders determines contradictory results in durability of CSA concretes. In particular, the addition of OPC generally reduce the oxygen permeability coefficient of concrete at values equal to that of OPC concrete manufactured with the same w/b ratio. Conversely, the CSA:CŜ concretes absorb less water after 24 hours immersion compared to the CSA:OPC:CŜ concrete and traditional OPC concrete. Finally, the CSA concrete is, regardless of OPC employment, much less permeable compared to the OPC concrete in the chloride permeability test.

Only one paper dealing with the durability of innovative CSA-based mixtures is available [107]. Ioannou et al. investigated the resistance of ternary CSA-based mixtures containing low calcium fly ashes in different environments. Results indicated that, for all w/b ratios, concretes manufactured with FA exhibited very low expansion compared to CEM III/A concretes when exposed to 5 wt.% Na_2SO_3 solution (Figure 31). This is a result of aluminate-bearing phases being bound in the ettringite phase and unavailable for reacting with external sulphates to form expansive sulphoaluminates in the hardened paste.

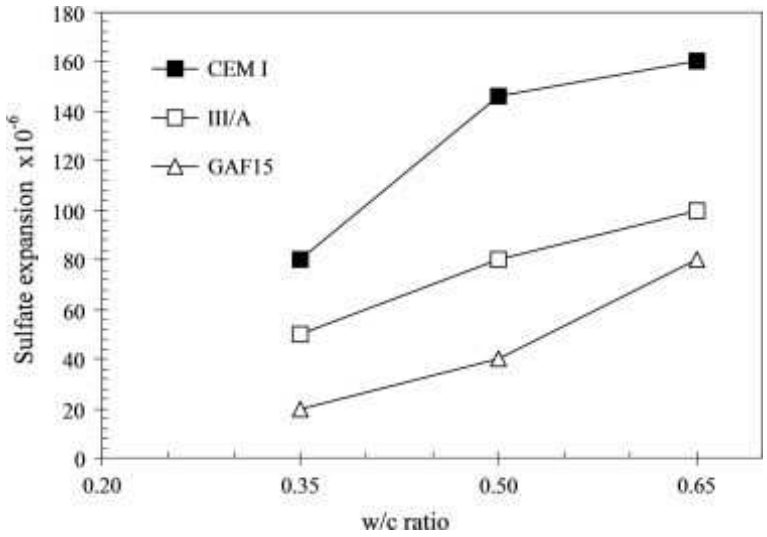

Figure 31 - Relationship between 40-week expansion strains and w/b ratio of concretes. GAF15 is a CSA:FA:CŜ mixture [107]

The results of tests in chloride-rich environment showed a diffusion coefficient D of CSA:FA:CŜ concretes 1.7-6.8·10^{-12} m^2/s higher than those obtained from CEM III/A concretes and approximately 6.8-10.3·10^{-12} m^2/s lower than those of CEM I concretes. Authors indicated that there are probably two main reasons for this behavior. The first would be the beneficial effect form co-existence of ettringite with tightly accommodated unreacted FA particles, responsible for the dense microstructure of the matrix. The second cause would be the absence of calcium monosulphoaluminate. As reported in [107], sufficient amounts of anhydrite were introduced in the mix to prevent conversion of ettringite to monosulphoaluminate thus no additional chemical binding activities were developed to upset the coefficient values (Figure 32).

Finally, the results showed that depths for CSA:FA:CŜ concretes were higher than for both CEM I and CEM III/A concretes at all w/b ratios. Moreover, for a given cube strength, carbonation resistance of FA-based concretes was poorer, indicating that the dense microstructure developed by AFt and firmly accommodated FA particles is not a parameter that significantly improve the resistance to carbonation. Researchers concluded saying that the carbonation resistance of concretes would not

only be strongly defined by the porosity and diffusivity aspects of concretes but also by the presence of alkali hydroxides (Figure 33).

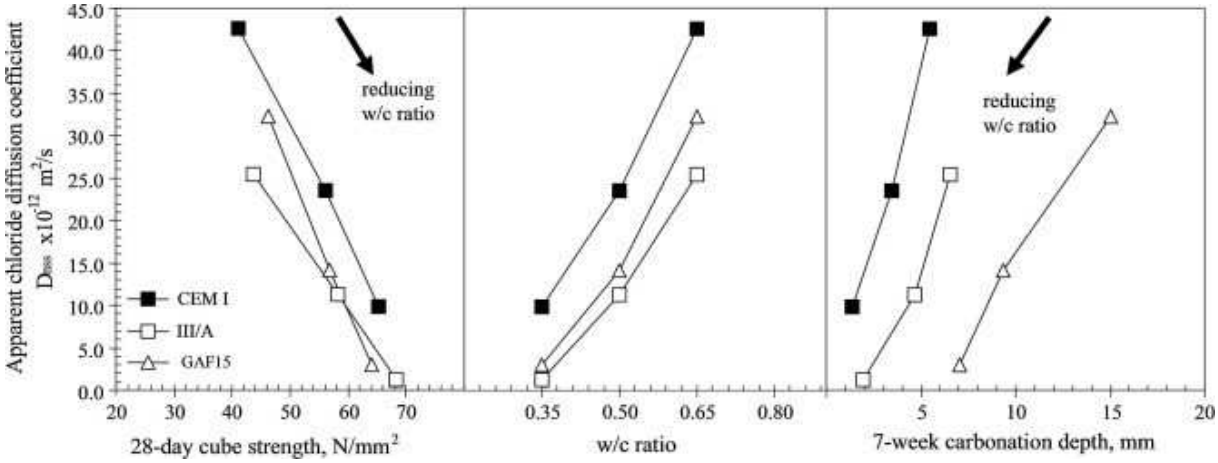

Figure 32 – Non-steady state chloride diffusion coefficients of concretes. GAF15 is a CSA:FA:CŜ mixture [107]

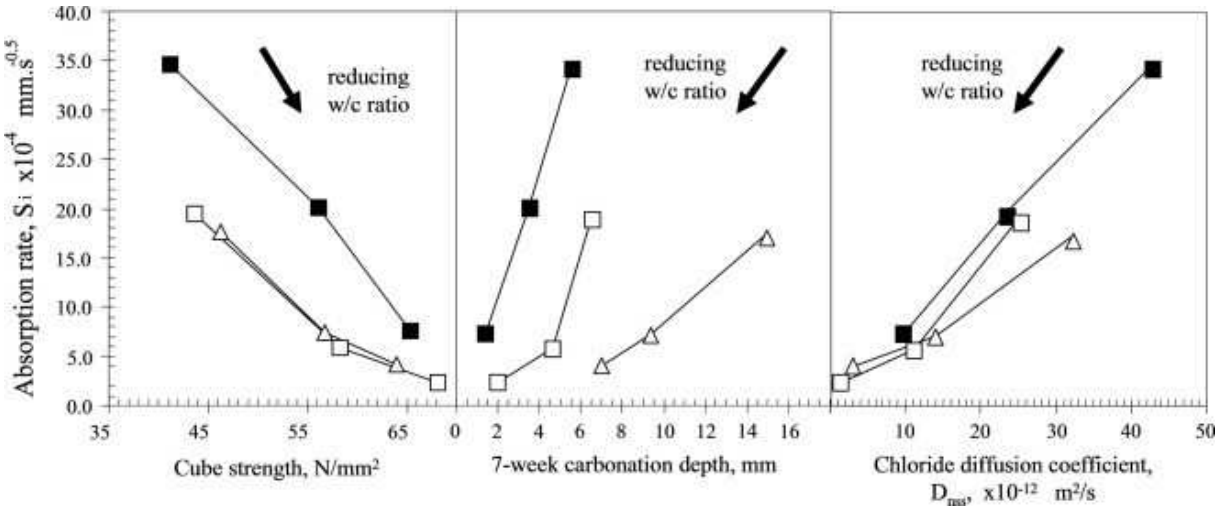

Figure 33 - Water sorptivity rates of tested concretes. GAF15 is a CSA:FA:CŜ mixture [107]

1.9 Applications of CSA cements

The advantages provided by CSA cements already mentioned such as rapid set, high early strength, and low- or zero-shrinkage makes it a very interesting binder for several applications. However, this material is generally used in specific niches but it does not seem probable that CSA may be an alternative to the large-scale uses of OPC due to their unavoidable higher prices. Several CSA-based products such as tile adhesives, repair mortars, grouting mortars, water plug, and self-compacting concretes are already available on the market. Furthermore, CSA cement can be applied in the production of precast concrete where rapid demolding increases productivity and thus profitability. Likewise, it is suitable for acid-treatment, polishing, or blasting even after six hours from casting.

2. Experimental research on CSA based mortars

The aim of this part of the research is to investigate the performance of CSA-based pastes and mortars manufactured with ternary binders CSA:OPC:CŜ in which Portland cement is totally replaced by supplementary cementitious materials (such as fly ash and ground granulated blast furnace slag) and lime. Moreover, the effect of a tartaric acid-based set retarding admixture and curing conditions on rheological, elastic and physical properties of CSA-based mixtures was also evaluated.

2.1 Materials

A ternary binder based on Ordinary Portland cement CEM I 52.5 R (according to EN 197- 1), commercial CSA clinker and technical grade anhydrite (CŜ) was used to manufacture the reference mixture (CSA:OPC:CŜ=40:40:20 by mass). Ground granulated blast furnace slag (S: according to EN 15167-1), V class fly ash (FA: according to EN 450-1 and EN 197-1) and hydrated lime CL90-S class (CH: according to EN 459-1) were employed to replace totally OPC in sustainable mortars (CSA:SCM:CH:CŜ=40:35:5:20 by mass).

CH was used in order to improve the ettringite formation [43] and the pozzolanic reaction of SCM amount not consumed in the reaction with CSA cement. Furthermore, tartaric acid-based set-retarding admixture (TA) was added up to 1.2% with respect to binder mass in order to control the setting time and the workability retention. The physical properties (Table 6) of binders were investigated by means of laser granulometry (Mastersizer 3000 Malven Instruments Ltd). To manufacture CSA-based mortars, 5 different natural siliceous sand with maximum diameter equal to 2.5 mm were combined according to the ASTM C33 limits (Table 7, Figure 34). Moreover, tap water at 20°C was used to produce pastes and mortars.

	CSA	**OPC**	**CŜ**	**CH**	**GGBFS**	**FA**
D_{50} [μm]	8.18	5.19	2.93	3.00	5.48	11.10
Specific surface [cm^2/g]	2722	3175	4837	4678	3049	2283
Specific mass [kg/m^3]	2650	3150	2670	2120	2730	2010

Table 6 – Physical properties of binders

	0/0.25	**0.25/0.50**	**0.50/1.0**	**1.0/1.5**	**1.5/2.5**
Specific mass [kg/m^3]	2410	2700	2580	2630	2620
Water absorption s.s.d. [%]	0.21	0.76	0.77	0.93	1.02
Dosage wt.%	25%	30%	25%	10%	10%

Table 7 – Physical properties of natural siliceous aggregates

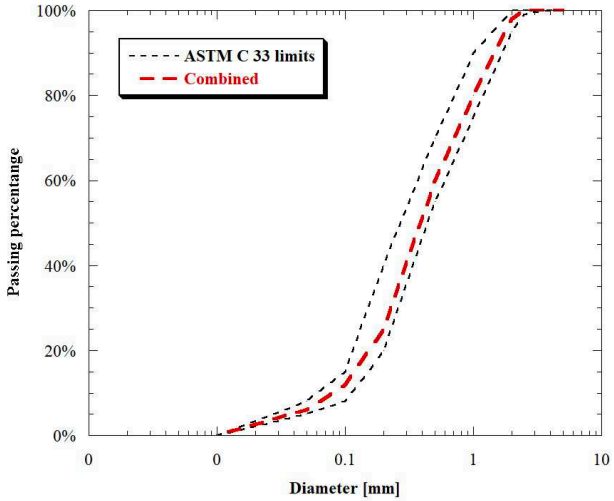

Figure 34 - Granulometry of natural siliceous aggregates

2.2 Mix proportions

12 different CSA-based mixtures were prepared by varying the set-retarding admixture dosage between 0 and 1.2 wt.% with respect to binder and the supplementary cementitious material (SCM) replacing OPC in order to investigate the rheological, microstructural, elasto-mechanical and physical properties of CSA cement-based mixtures. The experimental tests were carried out on pastes or mortars. The water/binder ratio (w/b) of pastes were kept constant at 0.50 while the water/precursor ratio of mortars was adjusted in order to attain, in absence of set retarding admixture, the same workability at the end of the mixing procedure, equal to 160 mm ± 10 mm by means of a flow table. The compositions of pastes and mortars are reported in Table 8 and 9, respectively.

Composition [g]	CSA	OPC	CS̄	CH	GGBFS	FA	Water	TA
REF 40/40	40	40	20				50	
REF 40/40 0.4	40	40	20				50	0.4
REF 40/40 0.8	40	40	20				50	0.8
REF 40/40 1.2	40	40	20				50	1.2
S 40/35/5	40		20	5	35		50	
S 40/35/5 0.4	40		20	5	35		50	0.4
S 40/35/5 0.8	40		20	5	35		50	0.8
S 40/35/5 1.2	40		20	5	35		50	1.2
FA 40/35/5	40		20	5		35	50	
FA 40/35/5 0.4	40		20	5		35	50	0.4
FA 40/35/5 0.8	40		20	5		35	50	0.8
FA 40/35/5 1.2	40		20	5		35	50	1.2

Table 8 – Composition of CSA pastes

Composition [kg/m^3]	CSA	OPC	CS̄	CH	GGBFS	FA	Water	Aggr.	TA
REF 40/40	183	183	91				279	1370	
REF 40/40 0.4	183	183	91				279	1370	1.82
REF 40/40 0.8	183	183	91				279	1370	3.65
REF 40/40 1.2	183	183	91				279	1370	5.48
S 40/35/5	183		90	25	156		275	1355	
S 40/35/5 0.4	183		90	25	156		275	1355	1.81
S 40/35/5 0.8	183		90	25	156		275	1355	3.61
S 40/35/5 1.2	183		90	25	156		275	1355	5.43
FA 40/35/5	170		85	24		147	298	1277	
FA 40/35/5 0.4	170		85	24		147	298	1277	1.70
FA 40/35/5 0.8	170		85	24		147	298	1277	3.41
FA 40/35/5 1.2	170		85	24		147	298	1277	5.11

Table 9 – Composition of CSA mortars

2.3 Experimental methods

CSA pastes and mortars were prepared using a mixer with planetary motion in accordance with EN 196-1. At the end of the mixing procedure, workability was measured on mortars by means of flow

table according to EN 1015-3. In addition, specific mass on fresh mixtures according to EN 1015-6 standard was evaluated. Moreover, the pot-life of the mortars, which corresponds to time during which workability by flow table is higher than 140 mm, was also detected. Specimens 40 x 40 x 160 mm^3 were produced (Table 10) and cured under water at 20°C. In addition, only for mixture containing 0.8% of TA, specimens were cured both under water at 20°C and in a climatic chamber at 20°C and R.H. 60%.

Test	Ages	Format	Number	Note
Strength, specific mass	1-7-28 d	Beam 40x40x160 mm^3	9	3 samples for each age
Shrinkage in hardened phase	Up to 270 d	Beam 40x40x160 mm^3	3	-
Shrinkage in plastic phase	Up to 20 h	Beam 50x100x1000 mm^3	1	-
DTA-TG	4-16-24-48 h 7-14-28-56-84 d	4 ml phial milled	2	2 samples for each age

Table 10 – Specimens manufactured for each mixture

Specific mass, compressive and flexural strength at 1, 7 and 28 days of mortars were also determined (EN 1015-11). Moreover, drying shrinkage was measured over time on specimens stored in dry environment (20°C, R.H. 60%) both in plastic and hardened (according to EN 12617-4) phase.
Simultaneous DTA-TG analysis was carried out on CSA pastes in a Netzsch Tasc 414/3 apparatus operating in the temperature range 20-1000°C, with heating rate of 10°C/min. The technique was able to identify calcium silicate hydrate, ettringite, gypsum, monosulfate, aluminum hydroxide, and calcium hydroxide through the following dehydration endothermal peaks: 97 ± 11°C, 146 ± 18°C, 156 ± 16°C (first gypsum calcination step), 163 ± 17°C (second gypsum calcination step), 201 ± 3°C, 275 ± 7°C and 496 ± 26°C, respectively [130]. A TG analysis was also used for the quantitative determination of ettringite, assuming that 24 water moles were lost by heating 1 mol of ettringite in the narrow temperature range corresponding to its strong endothermal effect.

2.4 Fresh properties

The amount of water to achieve the target workability (160 mm spreading) is, in absence of set retarding admixture, variable due to the different specific surface, texture and shape of binders (Tables 6 and 9). In particular, replacing OPC with GGBFS, no change in terms of mixing water was noticed. On the contrary, the use of FA determines an increase in water demand equal to 7% due to

the high unburnt carbon content (L.O.I = 4.9% according to EN 196-2 and ISO 10694). Furthermore, tartaric acid-based set-retarding admixture acts as a superplasticizer (Figure 35). The super plasticizing effect is more pronounced in fly ash-based mortars (+45% spreading with respect to mixture without set-retarding admixture), while is almost the same for mortars manufactured with OPC and GGBFS (+20%).

TA addition does not produce any abnormal air entrapment. In fact, regardless of set-retarding admixture dosage, specific mass of mortars is substantially the same both in fresh and hardened state (Figure 35). On the contrary, the total substitution of OPC with SCMs modifies density of mortars. In fact, FA-based mixtures showed specific mass (both in fresh and hardened state) lower than that detected on reference (containing OPC) and GGBFS-based mortars as a consequence of the increase of mixing water to achieve the target workability.

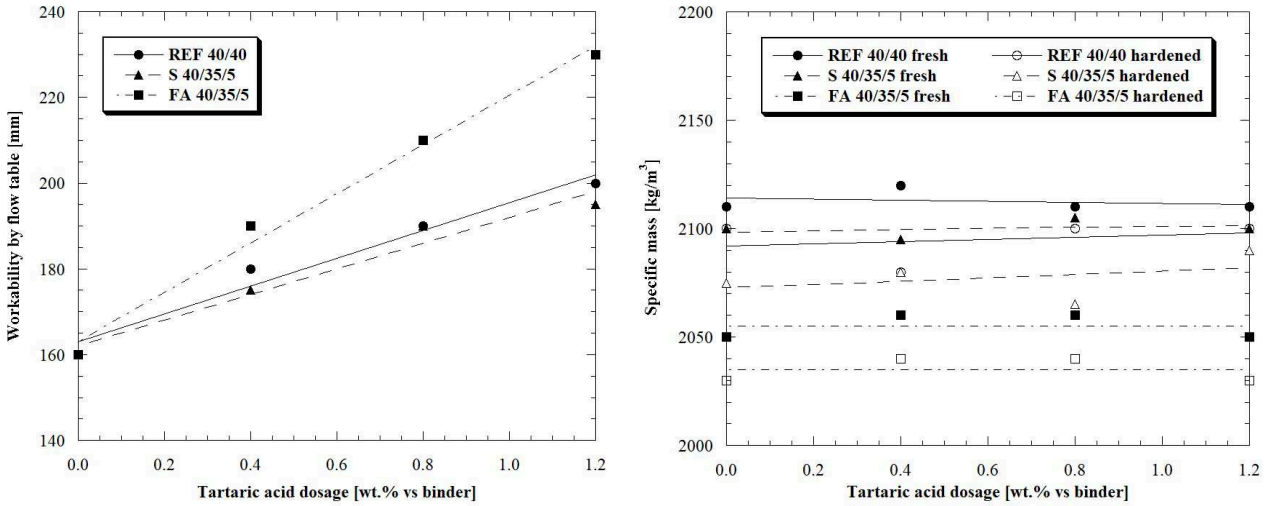

Figure 35 - Workability by flow table (left) and specific mass at fresh state (right) of mortars vs set-retarding admixture dosage

Figure 36 shows that the effectiveness of admixture with different binders is almost the same. Regardless to the binder used, pot-life of mortars without TA is about 20 minutes, which is not suitable for placing in the job-site. The addition of TA-based admixture extends the pot life of mortars up to 2 hours from mixing. The average time between mixing and placing a mortar in the job-site is generally close to 60 minutes. Based on this target, it is possible to conclude that the ideal set-retarding admixture dosage is equal to 0.8 wt.% vs binder.

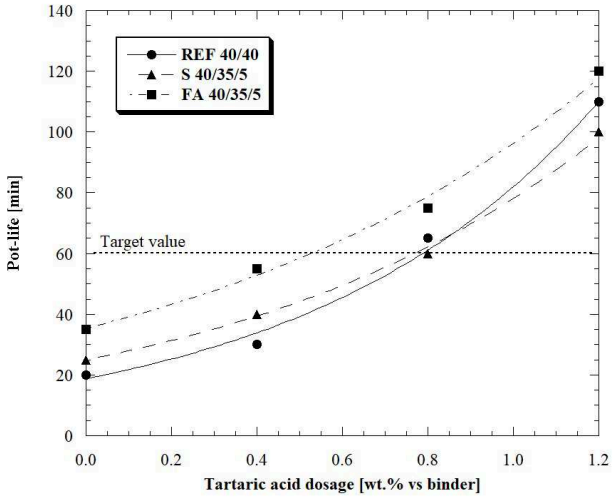

Figure 36 - Pot-life of mortars vs set-retarding admixture dosage

2.5 Hardened properties

Thermogravimetric analyses performed on CSA:OPC:CŜ and CSA:SCM:CH:CŜ pastes reveal that the addition of TA admixture causes a sharp reduction in ettringite formation at early ages (4 and 24 hours). In particular, a mass loss at 1000°C equal to 22% was measured in REF mixtures without retarder while increasing the TA dosage, the mass loss decreases up to 4%, indicating a lower production of AFt, aluminum hydroxide and calcium hydroxide. However, the retarding effect of tartaric acid seems to vanish at long ages (Figures 37 and 38). The same trend is also present in GGBFS- and FA-based pastes (Figures 39 - 42). Mixtures containing slag show mass losses of between 28% and 7% while those based on fly ash between 26% and 8%.

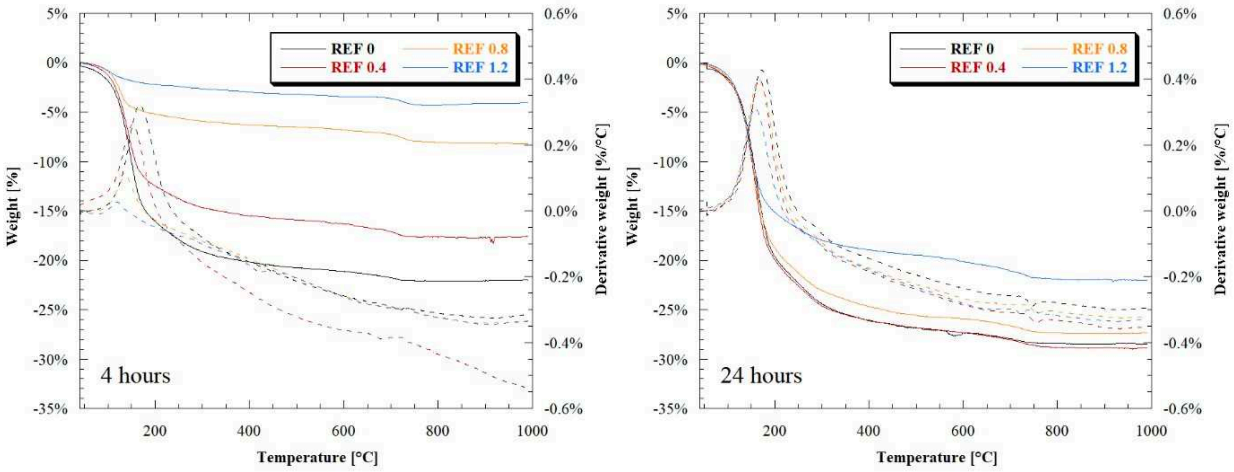

Figure 37 - TG/DTG analyses of REF pastes at different ages (part A)

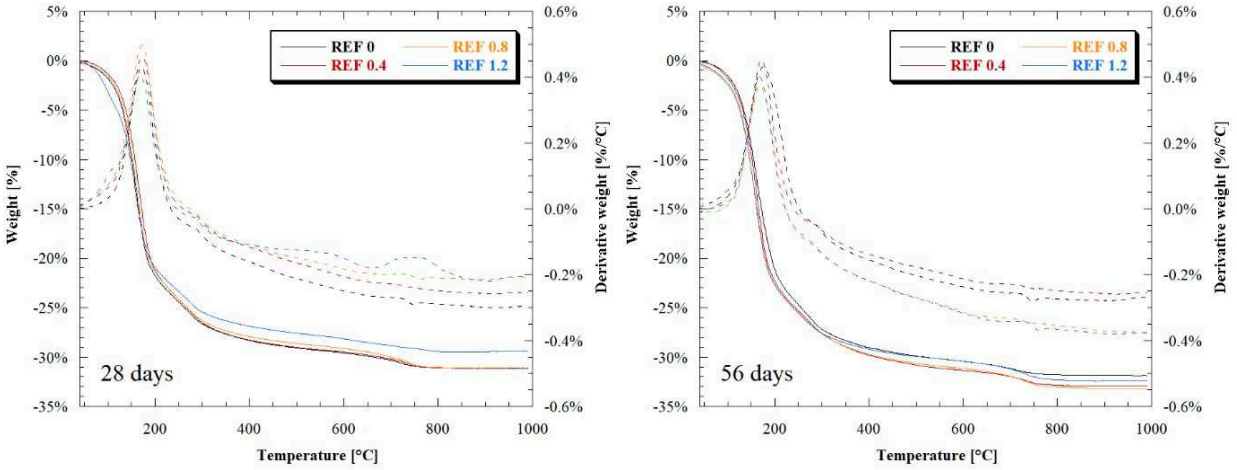

Figure 38 - TG/DTG analyses of REF pastes at different ages (part B)

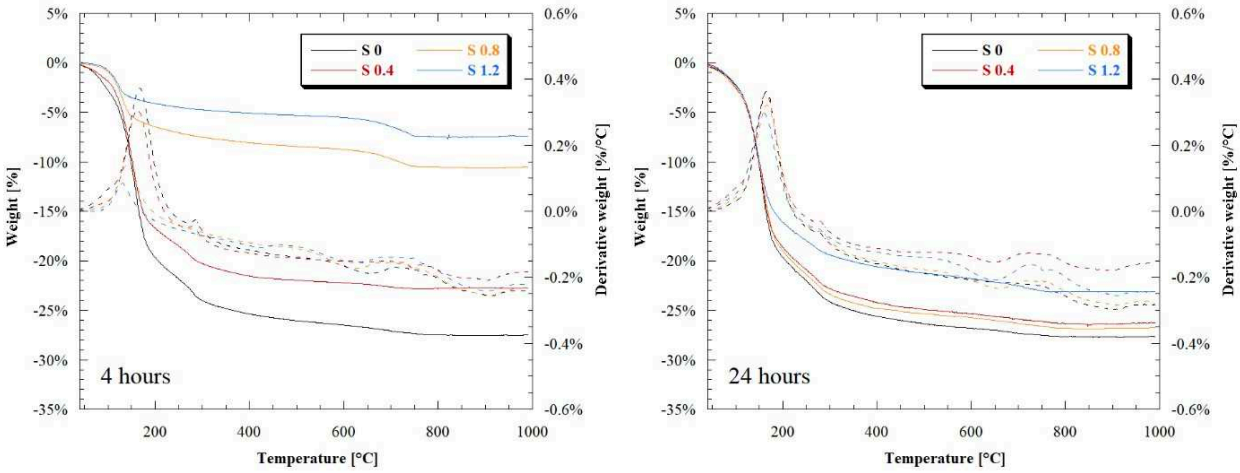

Figure 39 - TG/DTG analyses of slag-based pastes at different ages (part A)

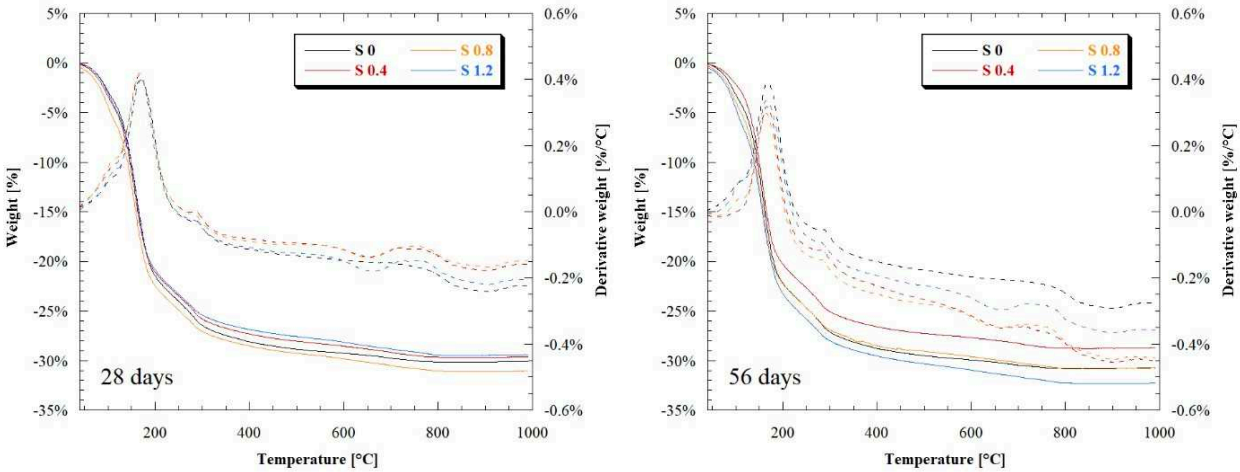

Figure 40 - TG/DTG analyses of slag-based pastes at different ages (part B)

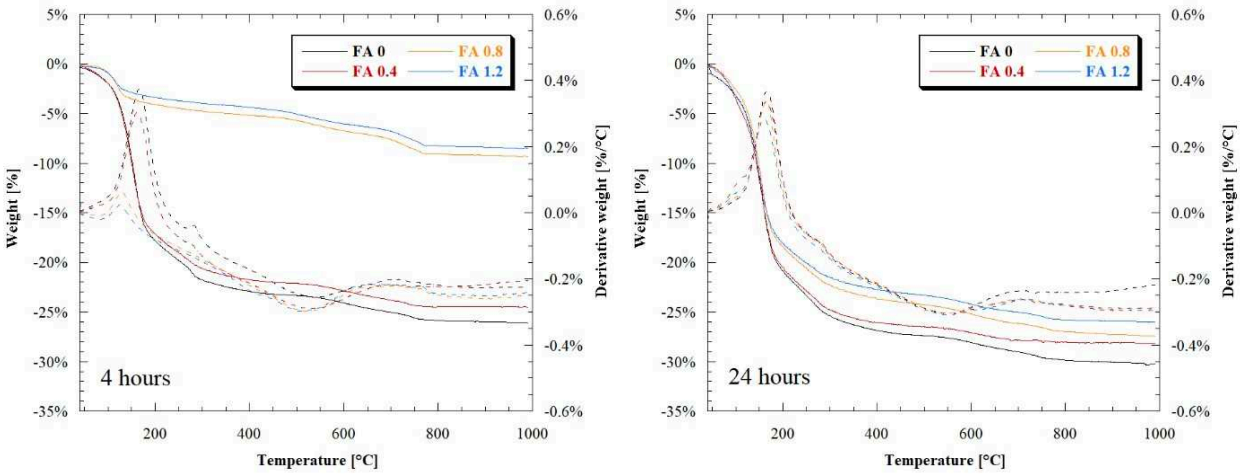

Figure 41 - TG/DTG analyses of fly ash-based pastes at different ages (part A)

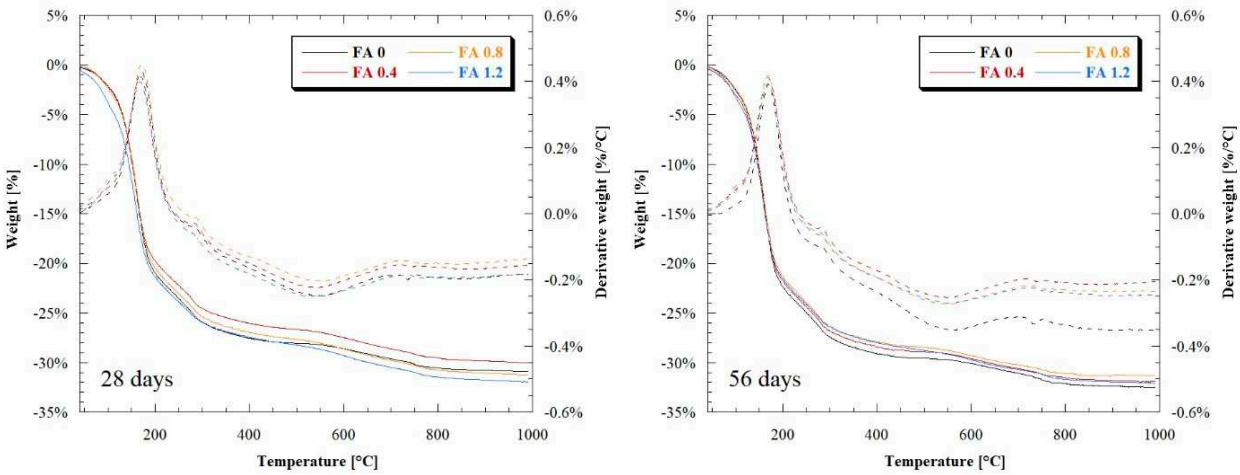

Figure 42 - TG/DTG analyses of fly ash-based pastes at different ages (part B)

This behavior is confirmed by the analysis of compressive strength development over time (Table 11). In particular, results indicate that addition of TA admixture determines a strong retardation of binder hydration and, consequently, a general reduction of 24-hour compressive strength of both OPC- and SCM-based mortars. In particular, the higher the tartaric acid dosage, the stronger the decrease of compressive strength (Figure 43). Since the retarding effect of tartaric acid is more pronounced on OPC [131], the decrease of 24-hour compressive strength in reference mortars, when the dosage of the set-retarding admixture increases, was significantly higher compared to slag and fly ash mortars. Another effect responsible for the lower reduction of compressive strength of SCMs-based mortars should be attributed to a partial absorption of TA by GGBFS and FA. As reported to Bishop and Barron [132], TA adsorbs onto the aluminum surfaces and reacts with calcium ions from binders to deposit a thick calcium tartrate coating on the cement grain. The lower amount of tartaric acid in the aqueous phase could justifies the lower retardation of these mortars. This retarding effect totally disappears at 28 days for all mixtures (Figure 43).

	w/b	R_f [MPa]			R_c [MPa]		
		24h	7d	28d	24h	7d	28d
REF 40/40	0.61	7.27	7.47	7.52	34.69	41.08	47.41
REF 40/40 0.4	0.61	4.69	5.02	6.86	21.53	39.13	44.06
REF 40/40 0.8	0.61	3.28	3.48	7.03	13.03	42.16	52.91
REF 40/40 1.2	0.61	0.82	2.11	7.03	2.22	27.84	47.81
S 40/35/5	0.61	5.09	5.29	5.39	30.50	32.59	35.56
S 40/35/5 0.4	0.61	5.16	5.19	5.25	26.22	31.44	36.69
S 40/35/5 0.8	0.61	4.69	4.69	5.16	21.94	30.22	34.13
S 40/35/5 1.2	0.61	0.96	2.29	4.99	19.98	24.12	34.98
FA 40/35/5	0.70	5.03	5.21	5.32	27.02	33.18	36.02
FA 40/35/5 0.4	0.70	4.92	4.92	5.25	23.50	31.52	35.86
FA 40/35/5 0.8	0.70	4.92	5.01	5.12	18.31	33.00	36.68
FA 40/35/5 1.2	0.70	1.12	2.53	5.33	14.69	22.13	35.82

Table 11 – Composition of CSA mortars

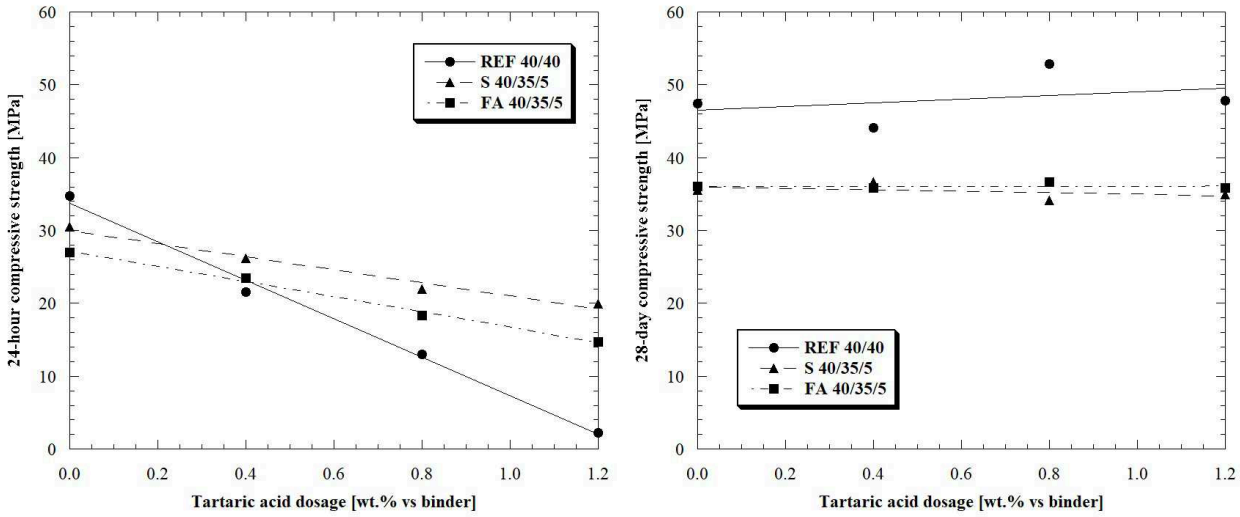

Figure 43 - 24-hour (left) and 28-day (right) compressive strength of CSA-based mortars wet cured

In general, the total replacement of OPC with SCMs causes a reduction in compressive strength of about 30% regardless of ages. However, the thermograms show that the amount of ettringite produced at early ages is lower in mixtures containing OPC than that of mortars based on SCMs while after 28 days from casting, the AFt content is approximately the same for OPC- and SCM-based mixtures (Figure 44). Consequently, it is possible to hypothesize that the variation in the compressive strength is to be ascribed to the quality and not to the quantity of ettringite produced during hydration. The effect of curing conditions was also investigated. Specimens cured at 20°C under water evidenced

compressive strength values about 25% lower than that measured on mortars stored in dry environment (20°C, R.H. 60%), independently of the age and the SCMs used (Figure 45). This results are in accordance with Sherman et al. [109] and Zhang [75].

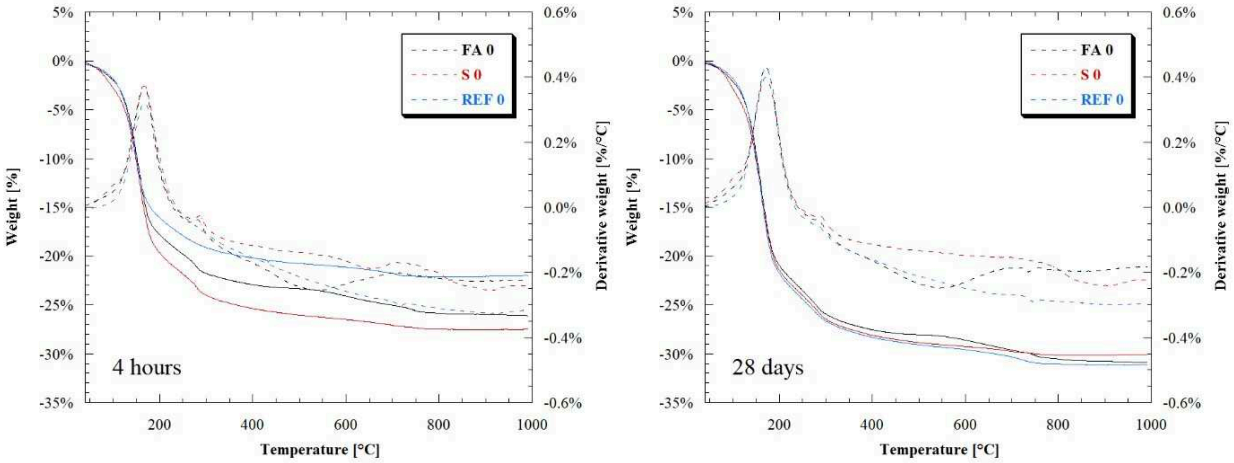

Figure 44 - TG/DTG analyses of mixtures without TA at different ages

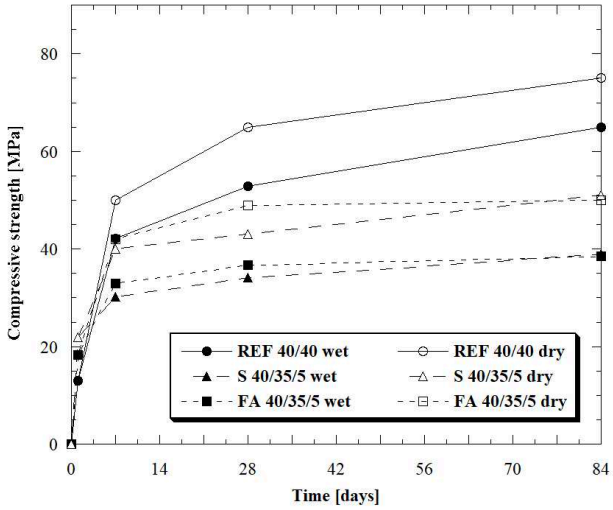

Figure 45 - Development of compressive strength over time under different curing conditions

Shrinkage tests were performed up to 270 days on prismatic 40 x 40 x 160 mm^3 specimens stored at 20°C and R.H. 60% (Figure 46). Reference mortar manufactured without TA shows a marked expansive behavior (up to 0.8 mm/m at 24 hours from casting) followed by shrinkage (-0.4 mm/m at 270 days). Total replacement of OPC with SCMs and hydrated lime determines – in absence of set retarding admixture – a sharp reduction of the initial expansion followed by shrinkage (about -0.5 mm/m after 270 days), independently of the nature of SCM replacing OPC. By using tartaric acid, CSA-based mortars (both that containing OPC and those manufactured with SCMs) did not evidence the initial expansion, but they began to shrink just after the final setting time has occurred. This could

be ascribed to the delay in the development of ettringite when the TA is used as reported in Figures 37 – 42. These mixtures, however, despite the absence of initial expansion, present a quite stable behavior over time, with a free shrinkage lower than -0.5 mm/m after 270 days.

The role of TA is also evident on the expansive behavior in plastic phase (Figure 46). Reference mortar (containing OPC) manufactured without set-retarding admixture achieves an expansion equal to 1 mm/m already after 6 hours from casting while the reference mortar manufactured with 0.4 wt.% TA vs binder is essentially stable over time. In general, use of tartaric acid-based set-retarding admixture, independently of the presence of OPC and the nature of SCM, eliminates the initial expansion typical of reference CSA:OPC:CŜ without admixture. In other words, the "expansive/shrinkage" behavior of the mortar in absence of TA is transformed in an "exclusively shrinkage" behavior.

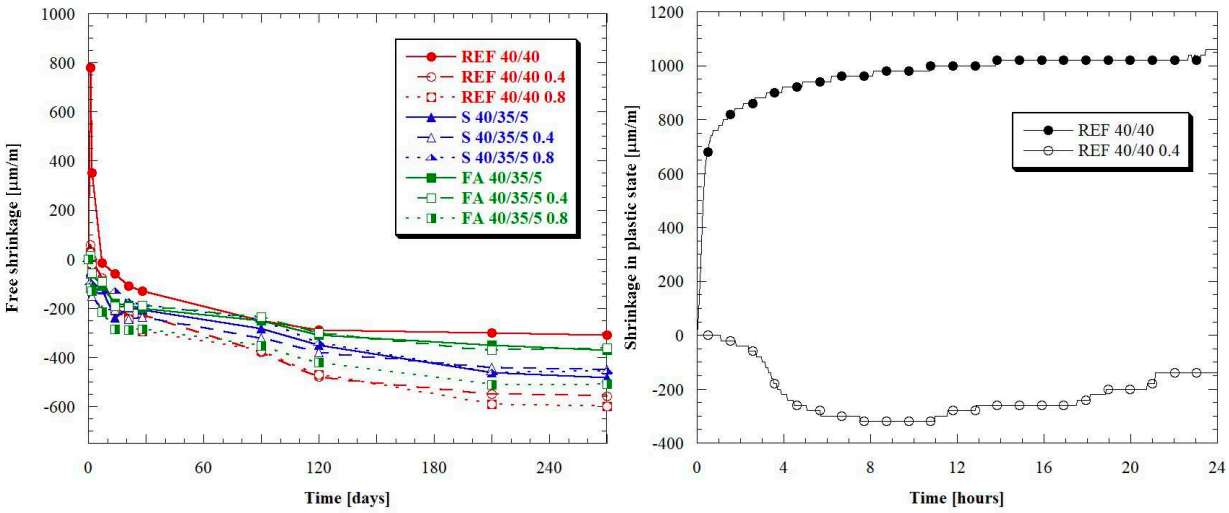

Figure 46 - Free shrinkage (left) and shrinkage in plastic state (right) over time in dry environment (20°C, R.H. 60%)

However, the final contraction detected for mortars containing set-retarding admixture was substantially the same of that measured in reference mortar (containing OPC) without tartaric acid (Figure 47). From a practical point of view, mixture with "exclusively shrinkage" behavior – at the same value of 270-day shrinkage of expansive/shrinkage mortar – seems to be more promising in repair of existing concrete structures since the tensile stress induced by restrained contraction is lower. As a consequence of more stable behavior of SCM mortars manufacture with TA, although the sharp decrease detected for 28-day compressive strength when OPC is replaced by SCMs, FA- and GGBFS-based mortars showed mechanical properties suitable for mixtures devoted to "cosmetic repair" of existing reinforced concrete structures, where shrinkage is the main design parameter. In particular, CSA-Portland free mortar can be classified as R3 strength class (Rc ≥ 25 MPa at 28 days) according

to EN 1504-3 and, hence, suitable for repair of existing concrete structures that present corrosion of rebars and spalling of concrete cover.

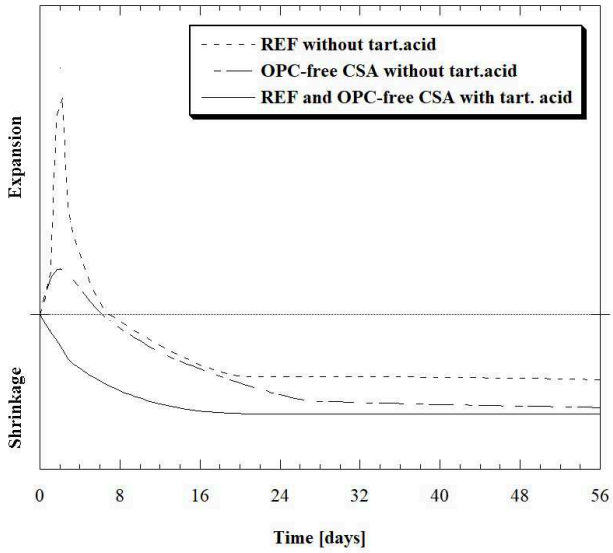

Figure 47 - Expansive-shrinkage behavior of CSA-based mortars without TA compared to stable behavior of mortars manufactured with TA

2.6 Environmental parameters

The worsening in mechanical strength of SCMs mortars is fully offset by a marked improvement in environmental sustainability. Indeed, at equal strength class, gross energy requirement (GER) and global warming potential (GWP) parameters of Portland-free mortars are lower than those of high volume fly ash (HVFA) mortars [133], traditional mortars manufactured with OPC and ternary binders based on CSA. In particular, starting from data on CO_2 emissions and energy production of binders (CEM I, CEM II/A-LL, CSA, CS and CH), supplementary cementitious materials (GGBFS and FA) and aggregates (Table 12), the reduction of GER and GWP deriving from the use of limestone Portland cement, HVFA, CSA:OPC:CŜ ternary mixtures and CSA:SCM:CH:CŜ blends in place of Portland cement or limestone Portland cement was determined.

It is possible to conclude that, at the same strength class, the use of traditional CSA-based ternary mixture in place of Portland cement or limestone Portland cement determines a reduction in terms of GER and CO_2 emissions ranging from 25% to 35% while the total replacement of OPC with SCMs slumps GER and GWP of about 60% (Figure 48).

	GER [MJ/kg]	GWP [Kg CO_2/kg]
CEM I 52.5 R	5.5	$9.8 \cdot 10^{-1}$
CEM II/A-LL 42.5 R	3.6	$8.8 \cdot 10^{-1}$
CSA	2.7	$7.4 \cdot 10^{-1}$
CŜ	1.3	$2.4 \cdot 10^{-1}$
CH	4.5	$4.2 \cdot 10^{-1}$
GGBFS	0.31	$1.7 \cdot 10^{-2}$
FA	0.10	$5.3 \cdot 10^{-3}$
Aggregates	0.13	$2.4 \cdot 10^{-3}$

Table 12 - Environmental parameters of binders and aggregates. Source: Ecoinvent 3.0 Database

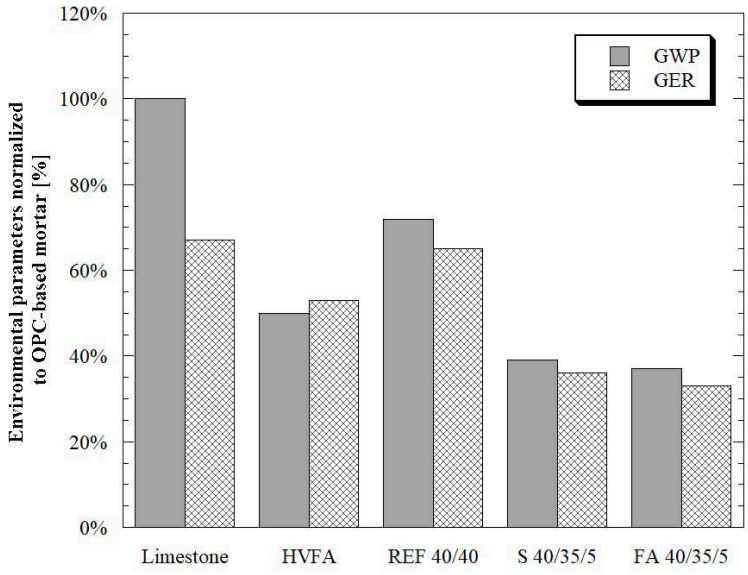

Figure 48 - GER and GWP of mortars at the same strength class normalized by those of CEM I mortar

2.7 Conclusions

In this chapter, the properties of sustainable Portland-free CSA-based mortars manufactured with supplementary cementitious materials and hydrated lime instead of Portland cement were evaluated at different tartaric acid-based set-retarding admixture dosage. Results indicated that the TA, independently of the nature of SCMs replacing OPC, acts as a superplasticizer and it is effective to extend the pot-life of mortars up to about 2 hours. No side-effects were detected on specific mass in fresh and hardened state by increasing the set-retarding admixture dosage. On the other hand, the total substation of OPC with fly ash cause a decrease in specific mass due to the higher water demand to attain the target workability at the end of the mixing procedure.

The use of tartaric acid determines a strong retardation of binder hydration and, consequently, a reduction of compressive strength at early ages, especially in reference mortars containing OPC. No retarding effect was detected at 28 days from casting.

In general, the total replacement of OPC with supplementary cementitious materials and hydrated lime determines a sharp reduction in terms of compressive strength approximately equal to 30%. In addition, as opposed to OPC-based mixtures, mortars containing CSA, SCMs, lime and anhydrite show higher compressive strength values when cured in dry environment respect to that measured on specimens stored under water.

Mortars without TA showed an initial expansion during the first 5-7 days as a consequence of ettringite formation, than the mixture shrink. When set-retarding admixture is used, the free expansion totally disappears and shrinkage begins immediately after final set has occurred. However, after 270 days, shrinkage is substantially the same for mortars with and without TA. In other words, the "expansive/shrinkage" behavior of the mortar in the absence of tartaric acid is transformed in an "exclusively shrinkage" behavior.

Although the compressive strength of CSA:SCM:CH:C$\hat{S}$ mortars is lower than the reference mixtures containing OPC, the more stable behavior evidenced by these Portland-free materials make them suitable for "cosmetic repair" of existing reinforced concrete structures, where shrinkage is the main design parameter. In particular, CSA:SCM:CH:C$\hat{S}$ mortars can be classified as R3 strength class (Rc $\geq$ 25 MPa at 28 days) according to EN 1504-3 and, hence, potentially suitable for repair of existing concrete structures that present corrosion of rebars and spalling of concrete cover. However, several tests on the corrosion behavior of these mixtures must be carried out prior to their use in combination with carbon steel reinforcement.

Finally, OPC-free CSA-based mortars are characterized by a reduction both in energy requirement (GER) and greenhouse gases emissions (GWP) close to 60% and 45% respect to traditional OPC-based and CSA:OPC:C$\hat{S}$ mortars at equal strength class, respectively.

3. Reduction of carbonation rate of CSA mortars

The use of calcium sulphoaluminate cements as a partial or total replacement of Portland cement seems to be the most interesting and easily way to reduce the environmental impact of mortars and concretes [134].

However, some aspects of CSA cements, i.e. carbonation, were not exhaustively investigated. The most of studies about the carbonation of CSA-based systems report a higher carbonation compared with OPC based mixtures [66,126,129,135,136] while someone else found that rate of carbonation are similar in CSA systems and OPC systems [71,128]. Hargis et al. [126] found out that CSA based mortars carbonates faster than OPC based mortars due to a different ability to bind CO_2 among the main phases: $C_4A_3\hat{S}$, the main phase of CSA cement, shows a reduced CO_2 binding capacity compared with OPC's ones (C_3S, C_2S, C_3A and C_4AF). In particular, 100 g of OPC cement are able to bind 50.0 g of CO_2 while the same amount of CSA cement is able to bind only 19.6 g. Moreover, Carsana et al. [137] highlighted that CSA concrete is characterized by a lower resistance to the penetration of carbonation compared to OPC concrete and the pH of the pore solution of the CSA concrete after carbonation was similar to that of the ordinary concrete. Finally, also a very fast strength development seems to improve the carbonation resistance of CSA cements as reported in [66].

The purpose of this chapter is to evaluate the possibility to reduce the carbonation rate by using hardening accelerating admixtures [108] containing lithium carbonate and sodium carbonate.

3.1 Materials

Three different mortars based on calcium sulphoaluminate were investigated as reported in Table 4.1 in accordance with a previous chapter. In particular, a traditional mortar (hereafter referred as TM) containing CSA clinker, Portland cement (OPC, according to EN 197-1) and technical grade anhydrite ($C\hat{S}$) and two sustainable CSA-based mortars (hereafter referred as SM 1 and SM 2, respectively) in which OPC is totally replaced by supplementary cementitious materials (SCMs, ground granulated blast furnace slag (GGBFS) according to EN 1516-7 and low calcium fly ash (FA) according to EN 450-1) and hydrated lime CL-90S class (CH, according to EN 459-1) were manufactured. The physical properties of binders and supplementary cementitious materials were reported in Table 6. A set retarding admixture (0.8 wt.% vs binder) based on tartaric acid (TA) was used to delay the initial set of mortars. Moreover, lithium carbonate (LC) and sodium carbonate (SC) were added to the mix as hardening accelerating admixtures up to 4% by binder mass. Finally, a

natural siliceous sand with maximum diameter equal to 2.5 mm was used. The water/binder ratio and binder/sand ratio were kept constant at 0.53 and 3.0, respectively.

Composition [kg/m^3]	CSA	OPC	CŜ	CH	GGBFS	FA	Water	Aggr.	TA	SC	LC
TM	192	192	96				255	1440	3.8		
SM 1	192		96	24	168		255	1440	3.8		
SM 2	192		96	24		168	255	1440	3.8		
TM-SC	192	192	96				255	1440	3.8	3.8	
SM 1-SC	192		96	24	168		255	1440	3.8	3.8	
SM 2-SC	192		96	24		168	255	1440	3.8	3.8	
TM-LC	192	192	96				255	1440	3.8		3.8
SM 1-LC	192		96	24	168		255	1440	3.8		3.8
SM 2-LC	192		96	24		168	255	1440	3.8		3.8
TM-SC-LC	192	192	96				255	1440	3.8	1.9	1.9
SM 1-SC-LC	192		96	24	168		255	1440	3.8	1.9	1.9
SM 2-SC-LC	192		96	24		168	255	1440	3.8	1.9	1.9

Table 13 – Composition of mortars

3.2 Experimental methods

The workability test by flow table described in EN 1015-3 was conducted on all the fresh mortars over time. In particular, the consistency was detected after the mixing procedure and the pot-life, corresponding the time during which workability by flow table is higher than 140 mm, was also determined. Furthermore, specific mass at fresh state and entrapped air were measured in accordance with EN 1015-6 and EN 1015-7, respectively.

The mixtures were molded into 40 mm x 40 mm x 160 mm specimens, demolded after 24 hours and cured in a climatic chamber at 20°C and 60% R.H. until tests (Table 14). Specific mass and compressive strength were measured at 1, 7, 28, 120 and 150 days according to EN 1015-1 and dry shrinkage was detected in accordance with EN 12617-4 up to 150 days. Furthermore, dynamic modulus of elasticity (Ed) was measured by means of Ultrasonic Digital Indicator Tester at 1, 7, 28, 120 and 150 days (EN 12504-4). Moreover, natural carbonation (specimens stored in air) was measured by a colorimetric test done by using phenolphthalein according to EN 14630 up to 150 days. Finally, the capillary water absorption coefficient (AC) was estimated in accordance with EN 13057.

Test	Ages	Format	Number
Compressive strength, specific mass and elastic modulus	1-7-28-120-150 d	Beam 40x40x160 mm^3	15
Shrinkage	Up to 150 d	Beam 40x40x160 mm^3	3
Carbonation	Up to 150 d	Beam 40x40x160 mm^3	12
Water absorption	150 d	Beam 40x40x160 mm^3	3

Table 14 – Specimens manufactured for each mixture

3.3 Fresh properties

The addition of lithium carbonate and sodium carbonate does not produce any abnormal air entrapment or variation in specific mass at fresh state (Table 15). Moreover, results show that the addition of LC and SC has different effects on consistency of mortars. In particular, a small increase in workability was observed in mortars manufactured with sodium carbonate admixtures or SC-LC blends both TM and SM while no variation were detected on workability by using LC regardless of binders used.

	Air content [%]	Specific mass at fresh state [kg/m^3]	Specific mass at hardened state [kg/m^3]	Workability [mm]
TM	4.9	2195	2175	165
SM 1	4.8	2190	2160	150
SM 2	4.8	2180	2165	160
TM-SC	4.9	2200	2185	180
SM 1-SC	5.0	2190	2170	160
SM 2-SC	4.9	2185	2170	180
TM-LC	5.0	2190	2170	170
SM 1-LC	5.1	2195	2170	150
SM 2-LC	5.0	2175	2165	160
TM-SC-LC	4.8	2190	2170	180
SM 1-SC-LC	4.8	2185	2170	170
SM 2-SC-LC	4.9	2175	2160	175

Table 15 – Properties of mortars with and without admixtures

Lithium carbonate caused a sharp reduction in pot-life of mortars, independently of binder used (Figure 49). In particular, LC seems to completely neutralize the retarding effect promoted by tartaric acid, decreasing the pot-life of mixtures to value close to 30 minutes. On the contrary, mortars containing SC showed a very slight decrease in pot-life. Finally, the combination of SC and LC determined a reduction of pot-life approximately equal to 30%, independently of binder used.

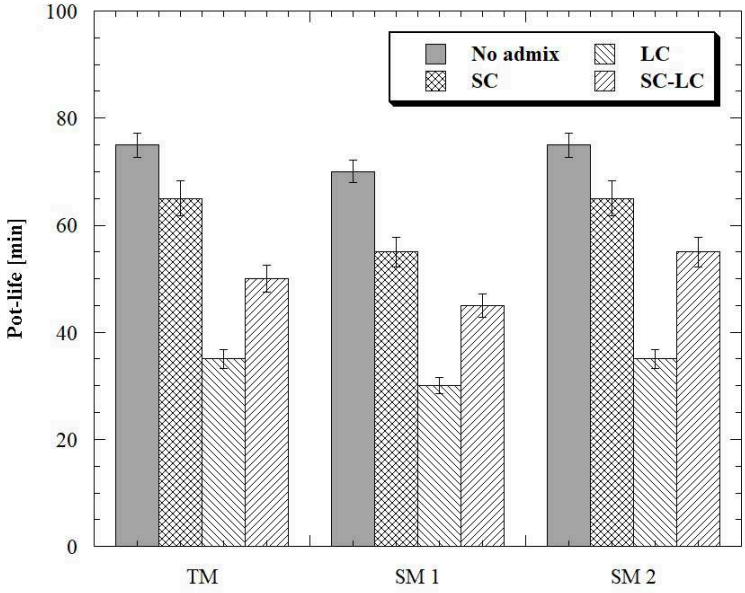

Figure 49 - Pot life of fresh mixtures

3.4 Hardened properties

Results (Figures 50 and 51, Table 16) indicated that lithium carbonate and sodium carbonate affect the elasto-mechanical properties of both TM and SM. The compressive strength at early ages (24 hours) is strongly improved by the addition of SC and LC admixtures. In particular, the compressive strength approximately doubled with respect to reference mortars manufactured without hardening accelerating admixtures, regardless the nature of alkaline ions (Li or Na) present in the admixtures. Sodium carbonate promotes the formation of gyrolite that is responsible for the acceleration of setting times and the improvement of compressive strength at early ages as reported by Reddy et al. [138]. On the other hand, lithium carbonate addition is responsible for the precipitation of lithium aluminate hydrate $LiAl_2(OH)_7 \cdot 2H_2O$ which serves as nucleation site for aluminum hydroxide precipitation that accelerates the whole hydration process and promotes the production of ettringite, the main hydration product of CSA cements [39,40,139].

However, at long ages, compressive strength was similar in mortars manufactured with and without hardening accelerating admixtures, regardless of binder employed. In detail, TM were characterized by strength close to 60-70 MPa after 150 days while SM 1 and SM 2 reached values equal to 40 MPa

in accordance with data reported in the previous chapter. Also the dynamic modulus of elasticity was influenced by the addition of admixtures at early ages. The development of E_d is similar to that of compressive strength.

In general, it is possible to state that the effectiveness of SC is greater than LC or SC-LC blends.

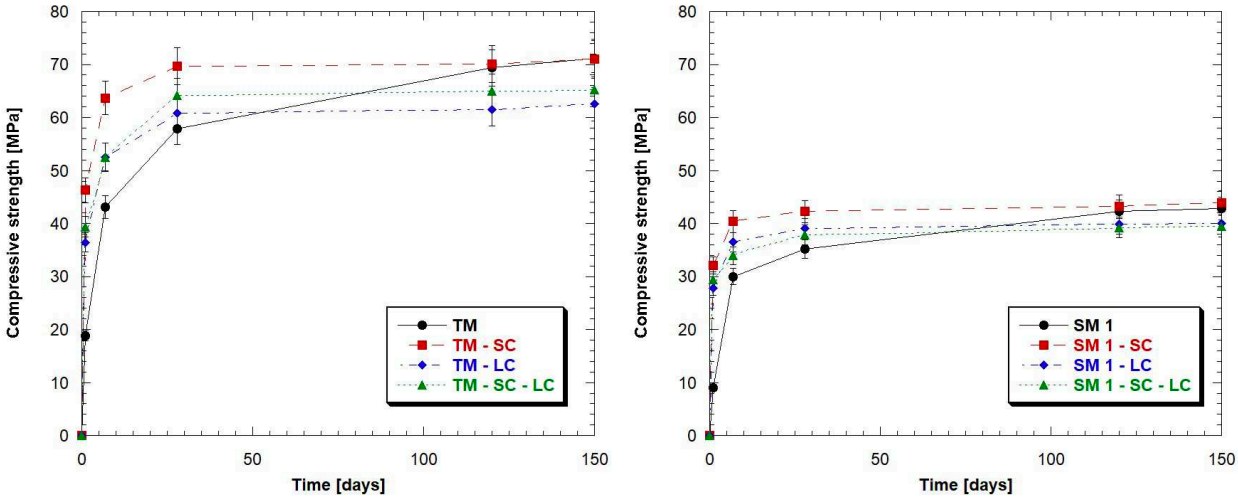

Figure 50 - Compressive strength development of TM (left) and SM 1 (right) mortars with different admixtures

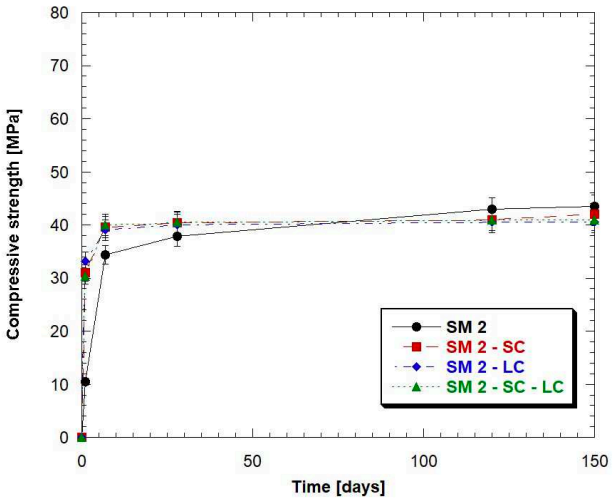

Figure 51 - Compressive strength development of SM 2 mortars with different admixtures

E_d [GPa]	24 h	7 d	28 d	120 d	150 d
TM	22.0	29.6	30.8	34.7	34.8
SM 1	23.0	30.7	36.5	36.6	36.8
SM 2	24.6	31.2	31.8	32.6	33.1
TM-SC	31.8	32.5	33.6	33.8	34.1
SM 1-SC	30.9	32.6	33.8	34.2	34.9
SM 2-SC	30.6	31.9	33.9	34.5	34.8
TM-LC	27.7	29.7	31.2	33.5	34.2
SM 1-LC	29.0	31.1	32.4	33.3	34.1
SM 2-LC	28.9	30.1	32.5	33.7	34.0
TM-SC-LC	30.6	32.0	33.0	33.8	33.9
SM 1-SC-LC	29.9	31.8	32.4	32.9	33.5
SM 2-SC-LC	29.9	30.8	32.7	33.9	34.0

Table 16 – Dynamic modulus of elasticity at different ages

Free shrinkage of traditional and sustainable mortars was shown in Figures 52 and 53. The addition of hardening accelerating admixtures strongly influenced the shrinkage of CSA-based mortars. The use of LC, alone or with SC, increased the free shrinkage of both TM and SMs up to 100%. In particular, traditional mortar without admixtures was characterized by shrinkage equal to 200 μm/m after 150 days while TM–LC and TM–SC–LC reached values close to 380 μm/m and 280 μm/m, respectively. Also the sustainable mortars were influenced by the lithium-based admixtures, reaching shrinkage ranging from 350 μm/m to 450 μm/m.

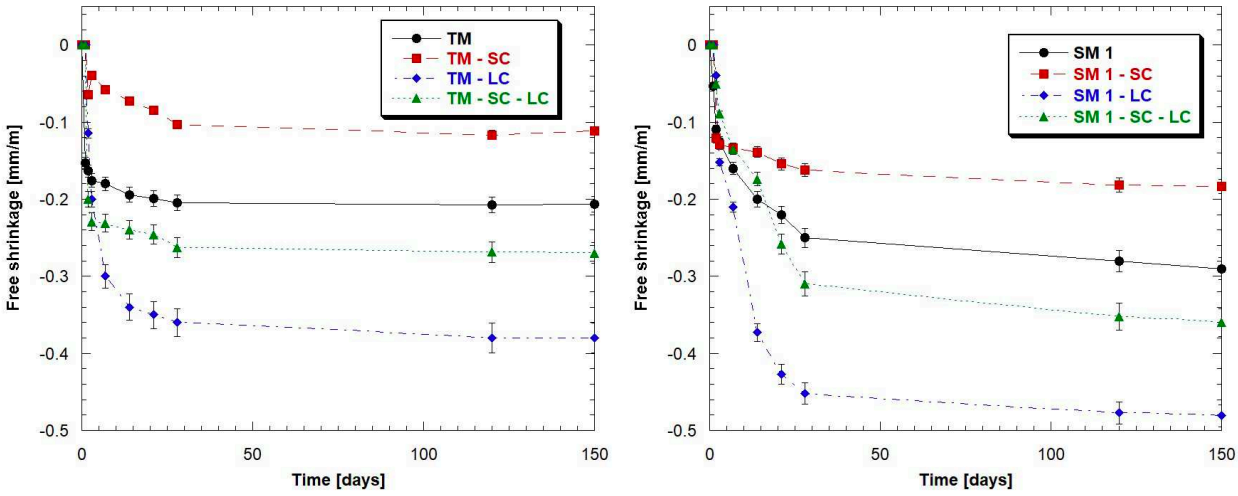

Figure 52 - Free shrinkage of TM (left) and SM 1 (right) mortars with different admixtures

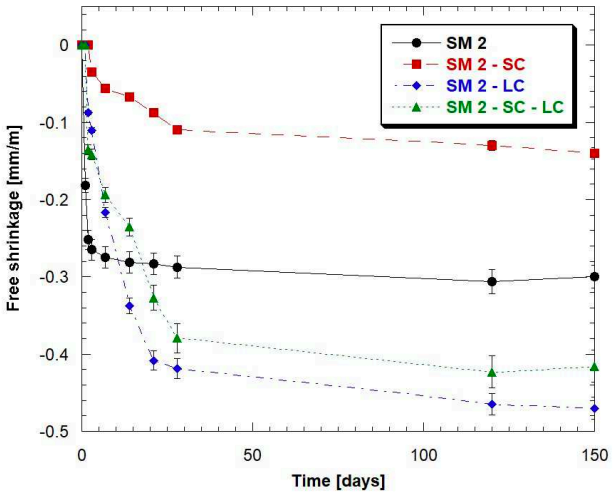

Figure 53 - Free shrinkage of SM 2 mortars with different admixtures

On the contrary, the addition of SC allows to reduce by half the shrinkage of CSA-based mortars, regardless of binder probably due to the greater amount of ettringite produced during hydration as reported by Li et al. [108].

The capillary water absorption coefficient (AC) of mortars was strongly influenced by the addition of sodium carbonate and the binder used (Figures 54 and 55, Table 17). A higher value of AC means a faster water uptake of the specimens, thus a high fraction of pores with large diameters. The total substitution of Portland cement with supplementary cementitious materials and hydrated lime increased the capillary water absorption coefficient by about 220% probably due to the higher porosity of sustainable mixtures SM respect to traditional mortar TM. Moreover, the use of SC admixture allows to obtain a less porous binder matrix characterized by a lower water absorption coefficient (-25%) respect to those of LC-based or no-admixed mortars, regardless of binder used.

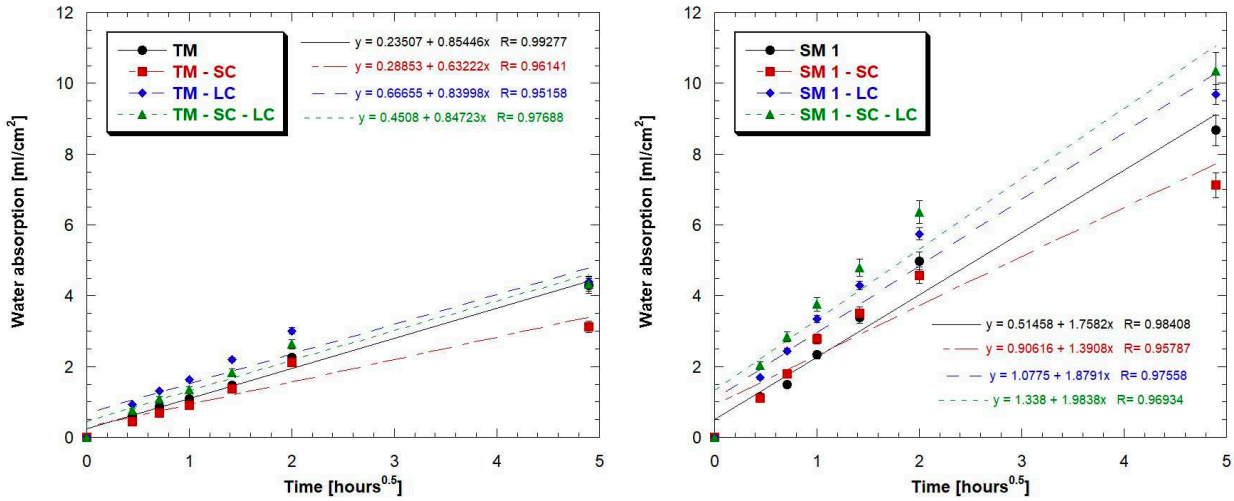

Figure 54 - Water absorption of TM (left) and SM 1 (right) mortars with different admixtures

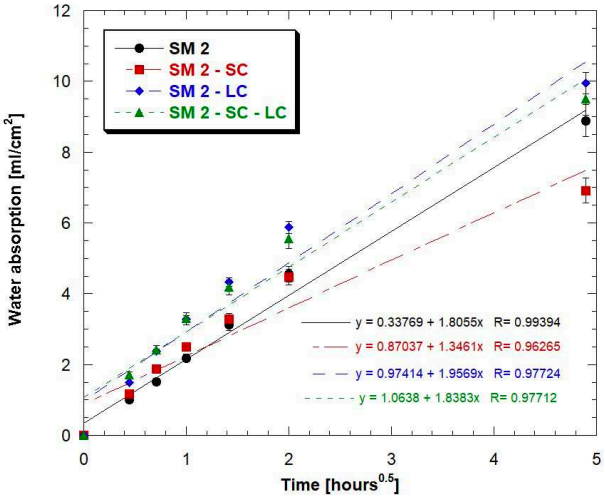

Figure 55 - Water absorption of SM 2 mortars with different admixtures

AC [ml/cm²h^0.5]	-	SC	LC	SC-LC
TM	0.854	0.632	0.840	0.847
SM 1	1.758	1.391	1.879	1.984
SM 2	1.806	1.346	1.957	1.838

Table 17 – Capillary water absorption coefficient (AC) of mortars with different admixtures

3.5 Natural carbonation

Figures 56 and 57 reported the natural carbonation depth of mortars over time. First of all, it was evident that the carbonation rate of this mixtures is more than one order of magnitude higher respect to that of OPC-based mortars at the same strength class as already reported by Hargis et al. [126], Quillin [66] and Zhang et al. [129].

Results show that TM mortars (containing OPC) were characterized by lower carbonation then SM mortars (containing SCMs) due to the lower porosity already shown in the absorption tests. In particular, after 150 days the TM reached carbonation depth close to 11 mm while SM were characterized by a carbonation depth higher than 14 mm.

A beneficial effect against the carbonation is given by the addition of hardening accelerating admixtures. In fact, lithium carbonate and sodium carbonate by improving the hardening phase and consequently by giving a more stable configuration and a lower matrix porosity are able to reduce carbonic dioxide penetration both in case of mortars containing OPC and SCM-based mortars. The most significant reduction in carbonation depth can be observed in mortars containing SC where a reduction of about 60% respect to mortar without admixtures could be found. On the contrary, the addition of LC or blends SC-LC led to lower benefits, in the order of 30-40%. Although the

admixtures of lithium carbonate and sodium carbonate give a beneficial effect on carbonation of CSA-based mortars, these systems are characterized by a very high value of carbonation respect to traditional mortars manufactured with Portland cement.

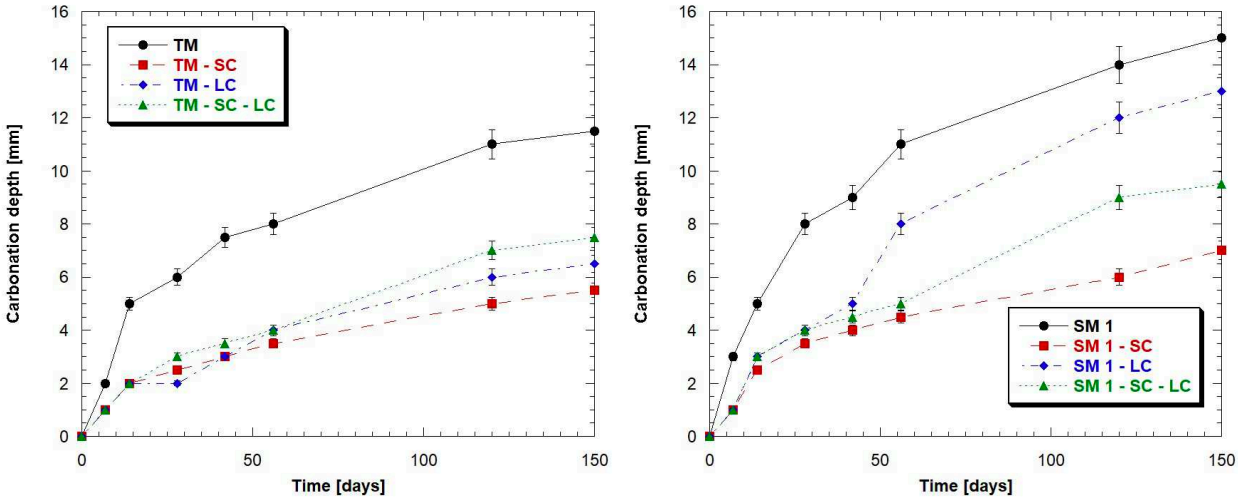

Figure 56 - Carbonation depth of TM (left) and SM 1 (right) mortars with different admixtures

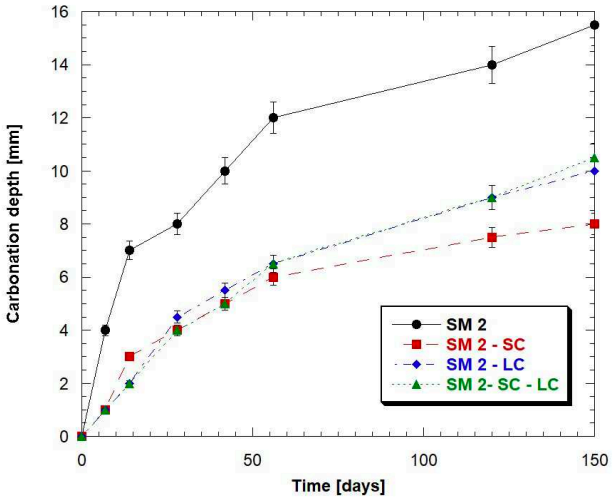

Figure 57 - Carbonation depth of SM 2 mortars with different admixtures

3.6 Conclusions

In this chapter, the influence of lithium carbonate and sodium carbonate in CSA based mortars manufactured with SCMs replacing OPC was investigated in terms of fresh properties, mechanical strength, water absorption, free shrinkage and natural carbonation. The following conclusions were made according to the results of this chapter:

- Lithium carbonate and sodium carbonate act like accelerator admixture in CSA-based mortars independently of nature binder employed;

- Lithium carbonate strongly affects the workability and the pot life of mortars, compromising the possible utilization in building yard. On the contrary, sodium carbonate ensures a workability and a pot life similar to mortars manufactured without hardening accelerating admixtures;
- The compressive strength and the elastic modulus at 24 hours is strongly improved by the addition of SC and LC admixtures. On the other hand, no significant differences were detected on the elasto-mechanical properties of mortars at 28 days;
- The use of LC, alone or with SC, increased the free shrinkage of both TM and SMs up to 100% while the addition of SC reduced the shrinkage up to 50%;
- The SC-based mortars were characterized by a less porous binder matrix and a lower water absorption coefficient (-25%) respect to those of LC-based or no-admixed mortars, regardless of binder used;
- A 60% reduction in carbonation depth can be observed in mortars containing SC respect to mortar without admixtures while the addition of LC or blends SC-LC led to lower benefits, ranging from 30% to 40%.

4. An application: CSA concrete for slabs on ground

Nowadays, reinforced concrete slabs on grade are increasingly present both in infrastructures and in residential or industrial buildings. Unfortunately, in many cases these elements suffer from severe damage due to a poor design, a wrong materials selection and/or an inaccurate concrete casting and curing [140]. Drying shrinkage is one of the common causes of cracking and curling of concrete slabs-on-ground, also because these structures possess a high ratio between the surfaces exposed to the air and the concrete volume [141]. The high shrinkage typical of these slabs, in the presence of internal and external constraints (such as reinforcing bars, floor foundation or other structural elements), determines notable internal tensile stress [142,143]. Cracking can be avoided only if tensile stress induced by shrinkage, reduced by creep, is always lower than the tensile strength of concrete. The cracking risk limitation can be achieved through a proper mix design (reducing the cement factor and increasing both the maximum size of aggregates and the dosage of superplasticizer) [144], adequate placing and curing [145] and by using high stiffness natural or artificial aggregates [146].

Use of expansive or shrinkage-compensating concrete (EC), although more expensive than Portland cement-based mixtures, is valuable in concrete structures where a reduction in cracking is of crucial importance, such as in pavement slabs, bridge decks and liquid storage tanks. This technique is based on the early restrained expansion that occurs between the expansive agents and water [147–149]. Generally, EC are manufactured with expansive agents that lead to the formation of ettringite ($C_3A{\cdot}3C\hat{S}{\cdot}H_{32}$) or calcium hydroxide (CH) according to the following reactions:

$$C_4A_3\hat{S} + 6C + 8CS + 96H \Rightarrow C_3A{\cdot}3C\hat{S}{\cdot}32H \quad (15)$$

$$C + H \Rightarrow CH \quad (16)$$

However, several authors [124,150] and standards show that EC can be advantageously used in reinforced concrete slabs-on grade without control joints only if an adequate wet curing is ensured. In particular, depending on the nature of expansive agent, 2- or 7-day wet curing period is needed. Otherwise, use of expansive agents is totally unsuccessful.

Collepardi et al. [151] and Maltese et al. [123] showed that the combined addition of an ethylene glycol-based shrinkage-reducing admixture (SRA) with a CaO-based expansive agent seems to have beneficial effects on concrete shrinkage even in absence of wet curing. On the other hand, a wrong choice of the type and dosage of expansive agent can lead to an inadequate expansion and, therefore, to crack formation in concrete slabs [152].

Another effective method to produce EC involves the use of expansive binders, alternative to Portland cement, based on a controlled production of ettringite. Between these special binders, ternary

mixtures based on calcium sulphoaluminate cements, Portland cement and gypsum (CSA:OPC:CŜ) are certainly the most widespread.

In previous chapters, results showed the possibility to manufacture shrinkage-compensating mortars using CSA-based ternary mixtures in which OPC is totally replaced by supplementary cementitious materials (SCMs, such as fly ash and ground granulated blast furnace slag) and lime (CH). In particular, the experimental data highlighted the primary role of tartaric acid in the expansive behavior of Portland-free CSA-based mixtures. In fact, dosages between 0.4% and 1.2% of tartaric acid vs binder mass guarantee a quite stable behavior over time (free shrinkage lower than -0.5 mm/m after 270 days at 20°C and R.H. 60%), without affecting negatively mechanical performances. On the other hand, as opposed to OPC-based concretes, Portland-free CSA-based mortars evidenced higher compressive strength values when cured in dry environment respect to those measured on specimens stored under water. This behavior has strong consequences on job-site operations and could make unnecessary wet curing operations (often not done or carried out wrongly). Finally, from an environmental point of view, many authors have shown the beneficial effects deriving from the use of SCMs/lime [153] replacing Portland cement, reaching up to 60% reduction in CO_2 emissions and energy requirements to produce 1 cubic meter of concrete, at equal 28-day strength class.

The purpose of this chapter is the evaluation of rheological, elastic and physical performances of shrinkage-compensating Portland-free concretes for slabs on grade without control joints manufactured with CSA:SCM:CH:CŜ and tartaric acid-based set-retarding admixture at different water/binder ratios.

4.1 Materials

A commercial CSA clinker, ordinary Portland cement (OPC) type I 52.5 R (EN 197-1 compliant) and technical grade anhydrite (CŜ) were used to manufacture the reference shrinkage-compensating concretes (CSA:OPC:CŜ = 40:40:20). Ground granulated blast furnace slag (S: according to EN 15167-1), type V (according to EN 450-1 and EN 197-1) low calcium siliceous fly ash (FA) and hydrated lime (CH) CL90-S (according to EN 459-1) were employed to replace totally OPC in environmentally friendly mixtures (CSA:SCM:CH:CŜ = 40:35:5:20). The physical properties of binders were reported in the previous chapter (Table 6). Furthermore, four different types of natural calcareous aggregates (maximum diameter equal to 32 mm) were combined to meet the Bolomey curve (Figure 58, Table 18).

Tartaric acid-based set-retarding admixture was added up to 0.6% with respect to binder mass in order to control the expansive behavior and the workability loss over time. Finally, the mixing water was fixed equal to about 200 kg/m^3 to achieve the consistency class S4 (EN 12350-5) and the water/binder ratio was varied between 0.55 and 0.70.

	Fine sand	Fine gravel	Coarse gravel	Coarse gravel
Specific mass [kg/m^3]	2550	2660	2680	2650
Water absorption s.s.d. [%]	1.69%	2.12%	1.62%	1.16%
Diameter min/max [mm]	0/6	6/12	10/20	20/32

Table 18 – Properties of natural aggregates

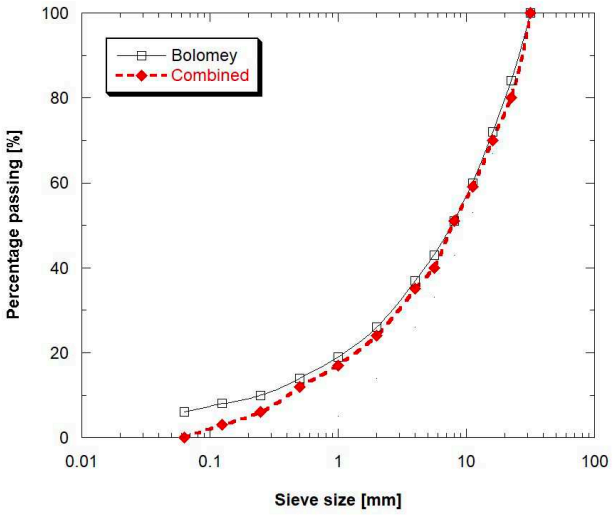

Figure 58 - Bolomey's and combined aggregate grading curves

4.2 Test on concretes

Fifteen concretes were manufactured according to EN 12390-2 (Tables 19 and 20). At the end of the mixing procedure, workability was measured over time (at 0, 30, 60, 90, and 180 minutes from mixing) by means of Abram's cone according to EN 12350-5. In addition, specific mass and entrapped air were evaluated on fresh concretes according to EN 12350-6 and EN 12350-7 standards. Specimens were produced and cured both under water at 20°C (W) and in a climatic chamber at 20°C and R.H. 60% (D). Specific mass and compressive strength at 1, 7 and 28 days were also determined (EN 12390-3). In addition, only for mixture containing 0.6% of tartaric acid, free and restrained shrinkage/expansion were measured up to 56 days on specimens stored both under water at 20°C (W) and in dry environment (D: 20°C, R.H. 60 according to EN 11307 and EN 8148, respectively. Finally, tensile strength on 28-day cured cylindrical specimens (according to EN 12390-6), elastic modulus (in accordance with method B, EN 12390-13) and water penetration under pressure (according to EN 12390-8) were measured.

Composition [kg/m^3]	CSA	OPC	CŜ	CH	GGBFS	FA	Water	Aggr.	TA
RC 0.55-0.4	142	142	72				196	1788	2.20
RC 0.60-0.4	132	132	66				197	1818	2.22
RC 0.65-0.4	122	122	61				199	1845	2.23
RC 0.70-0.4	113	113	57				199	1857	2.23
S 0.55-0.4	142		71	18	123		195	1776	2.18
S 0.60-0.4	131		65	16	115		196	1806	2.20
S 0.65-0.4	121		60	15	105		197	1821	2.21
S 0.70-0.4	113		57	14	98		198	1845	2.22
FA 0.55-0.4	142		71	18		124	195	1780	2.19
FA 0.60-0.4	131		65	16		115	196	1802	2.20
FA 0.65-0.4	121		60	15		106	197	1825	2.21
FA 0.70-0.4	113		57	14		98	198	1849	2.22
RC 0.55-0.6	142	142	72				196	1788	3.35
S 0.55-0.6	143		72	18	125		197	1799	3.37
FA 0.55-0.6	142		71	18		124	195	1780	3.33

Table 19 – Composition of CSA concretes

Test	Ages	Curing conditions	Format	Number
Compressive strength	1-7-28 d	W-D	Cube 100 mm	18
Tensile strength	28 d	W-D	Cylinder h/d:2 d:100 mm	6
Elastic modulus	28 d	W-D	Cylinder h/d:2 d:100 mm	6
Water penetration	28 d	W-D	Cube 150 mm	6
Free shrinkage/exp.	Up to 56 d	W-D	Beam 100x100x500 mm^3	6
Rest. Shrinkage/exp.	Up to 56 d	W-D	Beam 80x80x240 mm^3	6

W: curing under water at 20°C – D: curing in climatic chamber at 20°C, 60% R.H.

Table 20 – Specimens manufactured for each mixture

4.3 Results and discussion

4.3.1 Fresh properties

Workability at the end of the mixing procedure remains almost constant independently of the water/binder ratio by using 0.4% of tartaric acid dosage with respect to binder mass. In particular, reference concretes (RC, Figure 5.2) and mixtures manufactured with slag (S, Figure 5.2) show an initial slump equal to 200 mm, reaching the consistency class S2 (100 mm slump) after about 60

minutes. On the contrary, FA-based concretes (Figures 59 and 60), at the same initial consistency class, evidenced a lower workability loss over time, achieving the consistency class S2 30 minutes later than the references and S concretes (S2 after 90 minutes from casting). According to results reported in the previous chapter, the tartaric acid dosage strongly influences the slump of concretes. A general increase in the initial workability (more marked in FA-based mixtures than those containing OPC and S) and a reduction in workability loss over time are observed by using 0.6% tartaric acid with respect to binder mass. In detail, reference and S concretes reach the consistency class S2 after about 120 and 90 minutes, respectively. On the contrary, mixtures based on fly ash show an excellent maintenance of workability over time, reaching the S2 consistency class after about 180 minutes. It is possible to conclude that, for practical uses, OPC- or S-based concretes require greater set-retarding admixture dosage (0.6% by binder mass) than that (0.4% by binder mass) needed for FA mixtures.

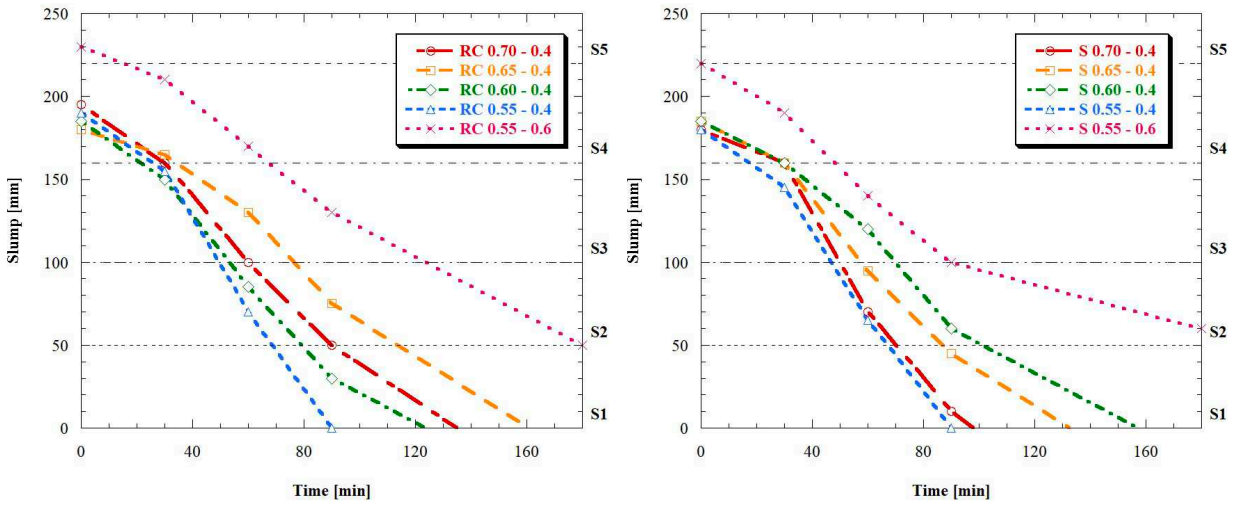

Figure 59 - Workability vs time of OPC- (left) and S-based (right) concretes

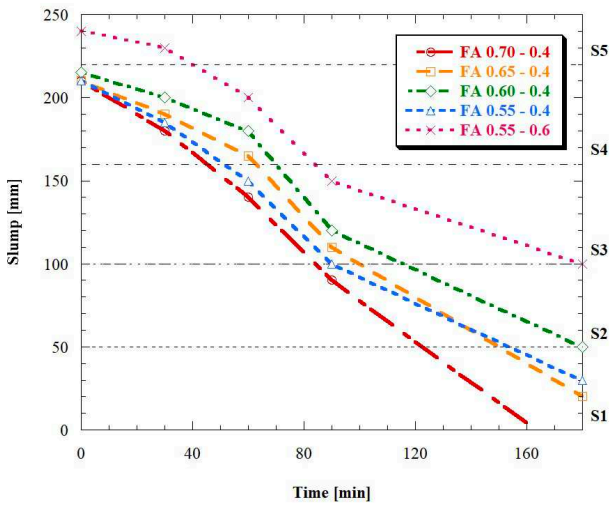

Figure 60 - W Workability vs time of FA-based concretes

Moreover, variation in water/binder and tartaric acid dosage does not determine substantial changes of entrapped air (always between 0.8% and 1.5% by concrete volume) and specific mass in the fresh state. In particular, density is close to 2340 kg/m^3 for reference concretes (RC) while it attains values close to 2325 kg/m^3 for mixtures in which SCMs/lime have totally replaced ordinary Portland cement (Figure 61).

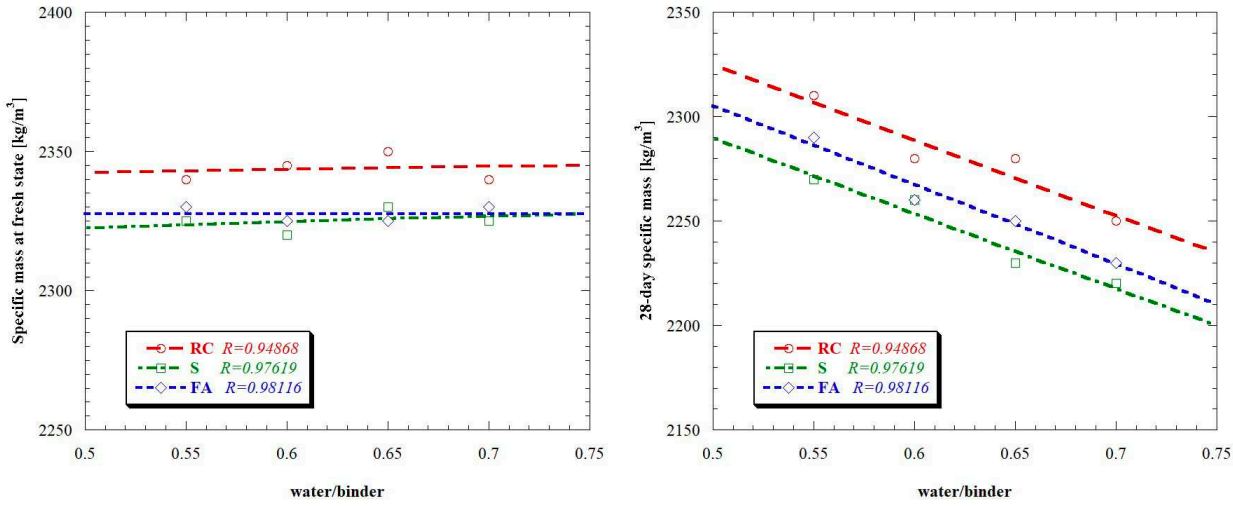

Figure 61 - Specific mass at fresh (left) and hardened (right) state vs water/binder ratio

4.3.2 Hardened properties

Conversely to density at fresh state, the increase in water/binder ratio leads to a linear decrease in 28-day specific mass, independently of tartaric acid dosage and type of binder (Figure 61). Concerning compressive strength measured on cubic specimens cured under water, it is possible to note that the water/binder is a key factor (Figures 62 and 63).

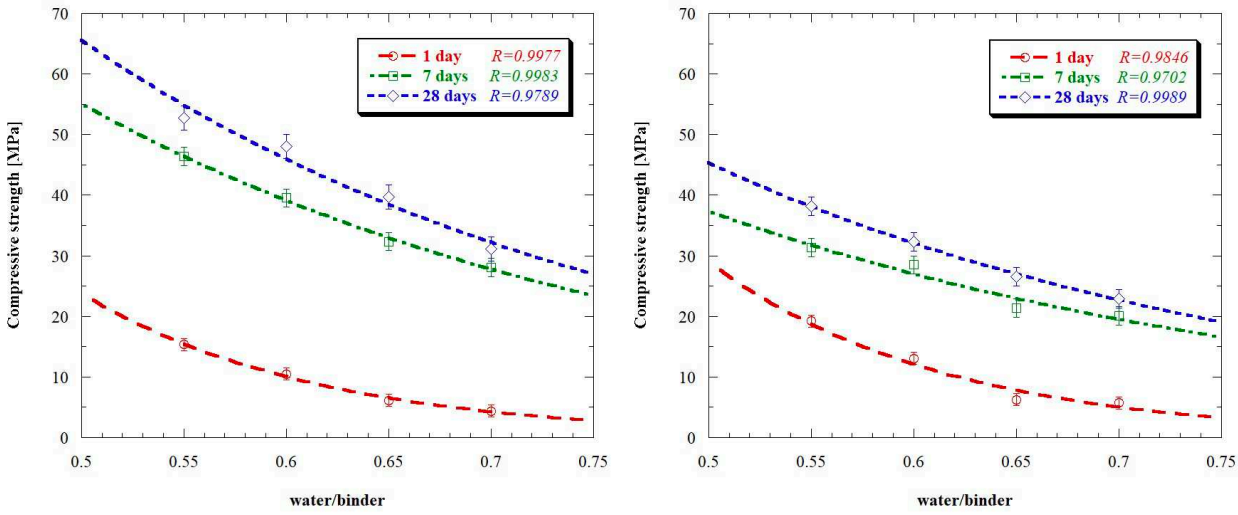

Figure 62 - Compressive strength of OPC- (left) and S-based (right) concretes vs water/binder ratio (wet curing)

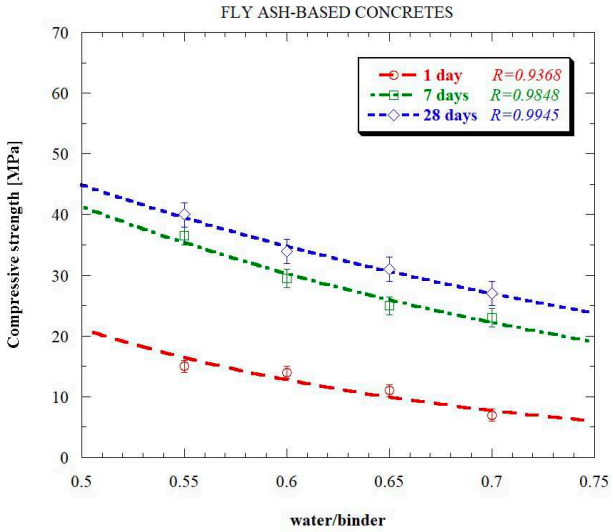

Figure 63 - Compressive strength of FA-based concretes vs water/binder ratio (wet curing)

Indeed, similarly to Portland cement concretes [100], low w/b allows to obtain mixtures of excellent strength properties while increasing this parameter results in a general worsening of mechanical performances, regardless of binders employed and the age of concrete. Moreover, replacing OPC with hydrated lime and SCMs, negligible changes in 24-hour strength are noted. On the contrary, 30% reduction in compressive strength at 7 and 28 days were measured, independently of w/b. However, SCM-based concretes with w/b ratio from 0.55 to 0.70 exhibit 28-day compressive strength (25-40 MPa) suitable for reinforced slabs on grade.

Experimental data were used to determine the parameters A and B of Abram's model to estimate the compressive strength at 28 days of concrete manufactured with 0.4% vs binder mass of tartaric acid and cured underwater at 20°C:

$$f_{c,28} = \frac{A_{28}}{(B_{28})^x} \qquad (17)$$

where ($f_{c,28}$) is the concrete compressive strength at 28 days, (A_{28}) and (B_{28}) are experimental parameters depending on the mixture composition and (x) is the water/binder ratio [154,155]. Results in Table 21and Figure 64 show that concretes based on SCMs and lime have a mechanical behavior similar to that shown by traditional concretes manufactured with CEM I 52.5 R or CEM II/A-LL 42.5 R. On the contrary, compressive strength of reference mixtures CSA:OPC:CŜ is more affected by w/b ratio, even if at equal w/b ratio, compressive strength is significantly higher than that exhibited by CEM I 52.5 R mixtures at low w/c ratios. Finally, it should be noted that, by using sustainable CSA-based mixtures manufactured with FA or S and lime, it is possible to reach similar mechanical strength to those obtainable, at equal w/c ratio, with a traditional limestone Portland cement (CEM II/A-LL 42.5 R).

	RC 0.4	S 0.4	FA 0.4	CEM I	CEM II/A-LL
A_{28}	386.61	255.31	261.47	261.25	263.32
B_{28}	34.78	31.72	33.15	22.00	29.61

Table 21 – Coefficient of Abram's model for different mixtures

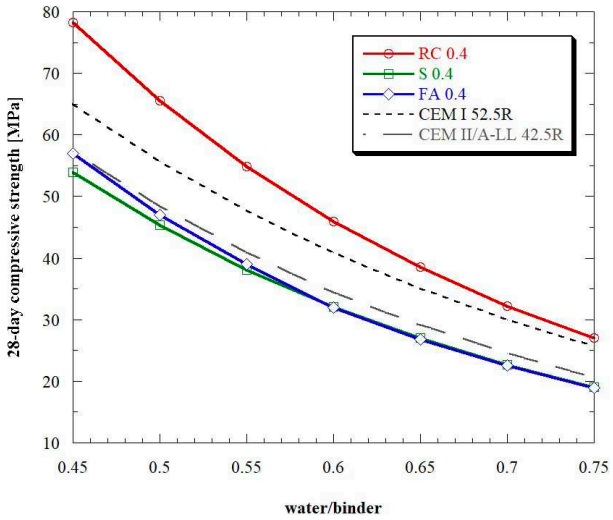

Figure 64 - 28-day compressive strength of concrete manufactured with different binders (Abram's model, wet curing) vs water/binder

Also, the curing conditions strongly influence the mechanical properties of CSA-based concretes (Figure 65). In fact, the reference concrete (RC) cured in dry environment (T = 20°C, R.H. 60%) exhibited compressive strength approximately 15% higher compared to that of the same mixture cured under water. Concrete manufactured with SCMs/lime replacing OPC showed more marked differences, up to 30%, between wet and dry cured specimens. Furthermore, increasing the tartaric acid dosage up to 0.6% vs binder mass, all concretes (both references and those containing SCMs/lime replacing OPC) evidenced a general reduction in mechanical performances up to 25% both at early and long ages (Figure 65).

Total replacement of OPC with supplementary cementitious materials/lime and the underwater curing conditions determine a general worsening of both elasto-mechanical properties and watertightness of concretes. In FA- and S-based concretes, tensile strength decreases up to 40% compared to the reference mixtures (RC), independently of the curing conditions (wet or dry). However, tensile strength of CSA-based concretes (Figure 66) follows the equation proposed by Eurocode 2 (EN 1992-1-1) for ordinary Portland cement concretes (strength class lower than C50/60):

$$f_{ctm} = 0.30 \cdot {f_{ck}}^{2/3} \qquad (18)$$

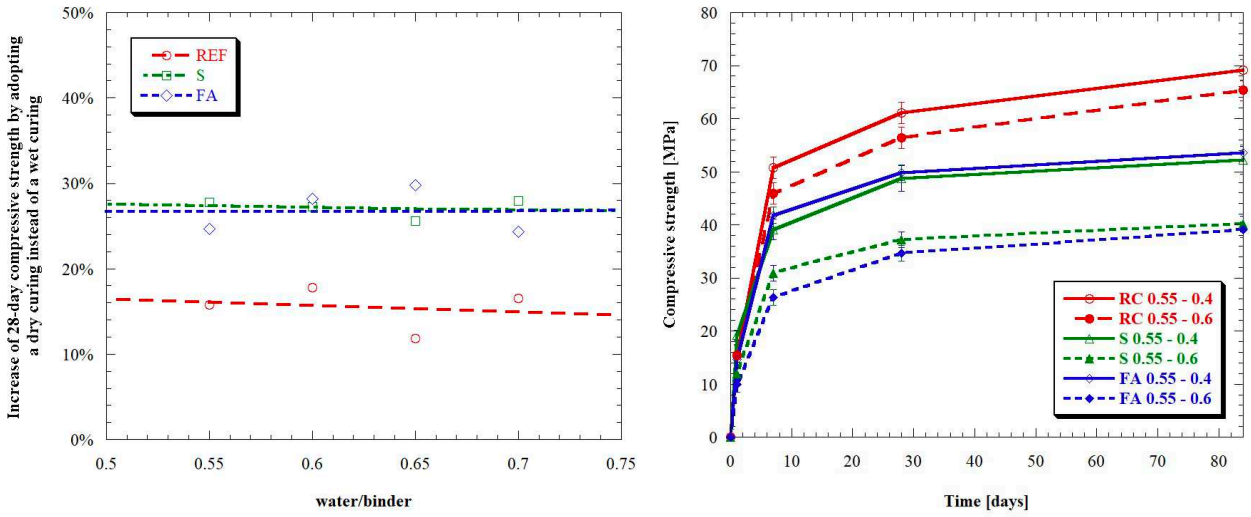

Figure 65 - Difference between wet and dry curing conditions on 28-day compressive strength vs water binder (left). Development of compressive strength over time on concretes (w/b 0.55) manufactured with different tartaric acid dosage (right, dry curing)

Young's modulus decreases, at the same w/b, replacing Portland cement with SCMs/lime due to the reduction of compressive strength caused by using FA or S (Figure 66). Nevertheless, elastic modulus of concrete based on calcium sulphoaluminate cement can be well approximated by the following equation proposed by Eurocode 2:

$$E_{cm} = k \cdot \left(\frac{f_{cm}}{10}\right)^{0.3} \qquad (19)$$

with k depending on the mineralogical nature of aggregates used.

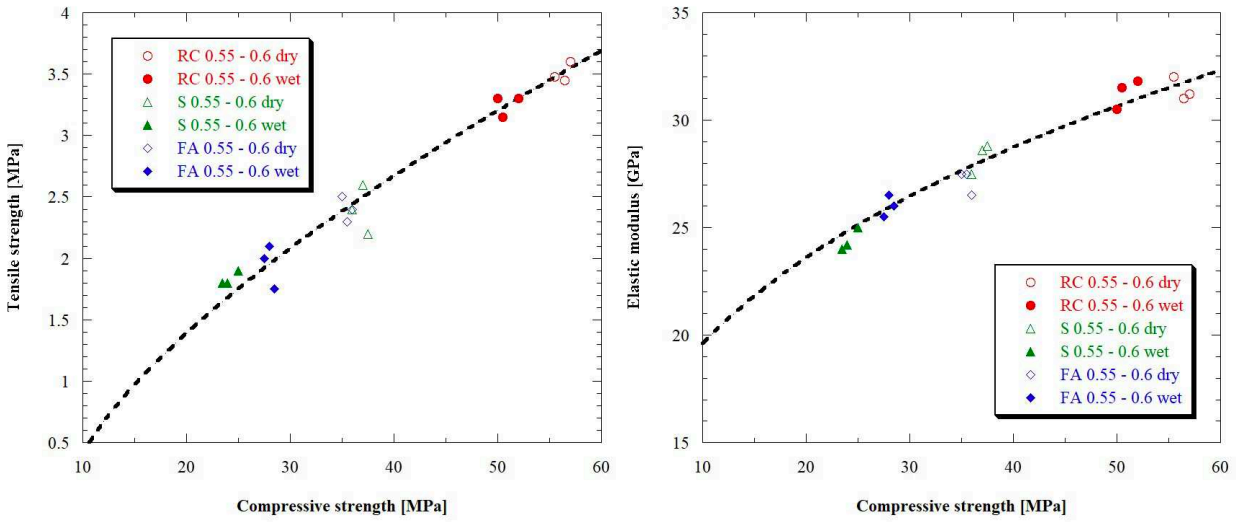

Figure 66 - Tensile strength (left) and elastic modulus (right) of concrete vs 28-day compressive strength. In dash line, the correlation proposed by EC2

Water penetration under pressure is influenced by the curing conditions of specimens. In general, concretes cured in dry environment show a lower water penetration respect to that of the same mixture

stored underwater (Figure 67). This result is in good agreement with compressive strength data. Furthermore, water penetration in Portland-free concretes (S or FA) grows strongly compared to that detected for the reference mix (RC), independently of the curing conditions (wet or dry). In particular, water penetration in dry cured SCMs/lime-based concretes was about 100 mm. This value is double compared to that of the reference mixture cured in the same conditions (D). In wet cured SCMs/lime mixtures water penetration was about 140 mm. This value is about two times and a half higher than the corresponding water penetration (60 mm) measured for the reference concrete containing OPC.

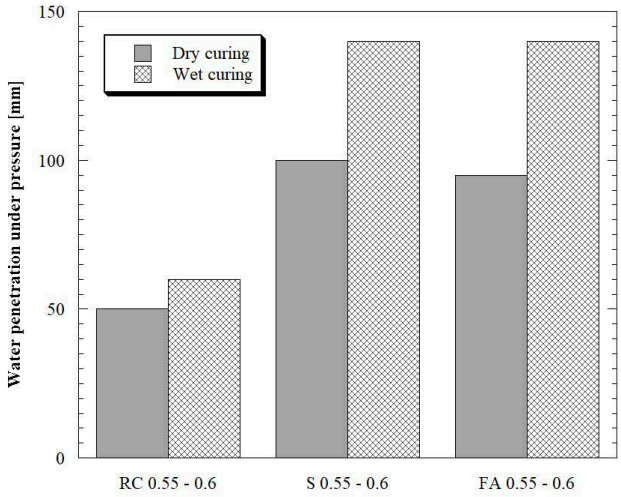

Figure 67 - Water penetration under pressure at different curing conditions (W o D)

Regardless of the binder used, shrinkage of CSA-based concretes (Figure 68) is strongly influenced by curing conditions [103,111]. Indeed, free and restrained shrinkage tests show a stable behavior over time when specimens are stored in a climatic chamber at 20°C and 60% R.H (D).

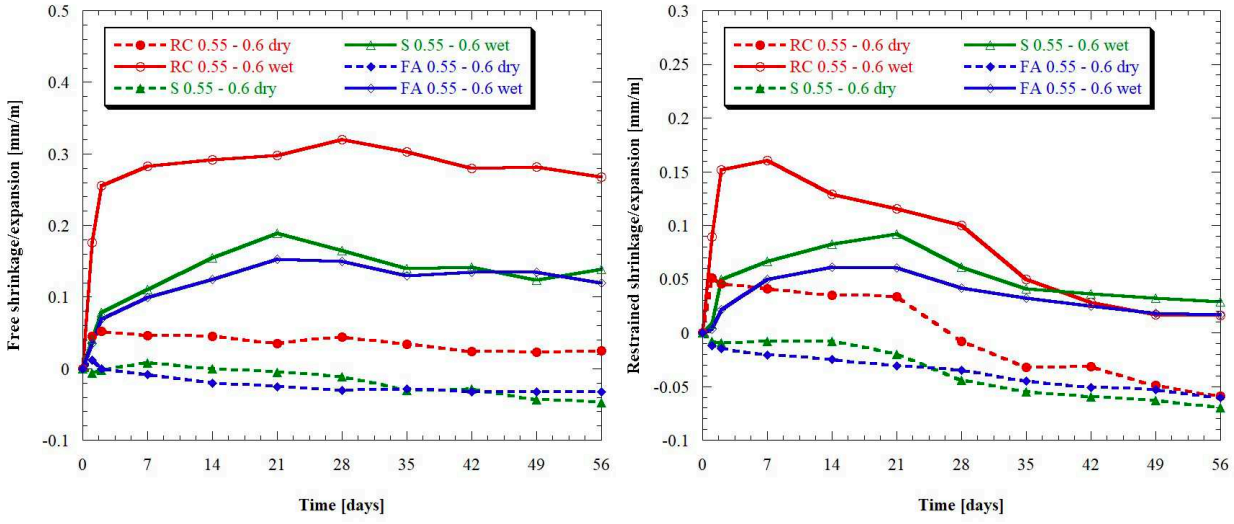

Figure 68 - Free (left) and restrained (right) shrinkage vs time in different curing conditions (positive values indicate expansion of concrete)

On the other hand, in concretes cured under water (W) an initial expansion was followed by a negligible shrinkage. Total replacement of OPC with SCMs/lime modifies the shrinkage behavior of concretes. In fact, reference mixtures (RC) show more marked expansion underwater at early ages with respect to Portland-free concretes (S or FA), both in free and restrained conditions.

4.3.3 Environmental parameters

Figure 69 shows the environmental parameters GER (Gross Energy Requirement that correspond to the total energy necessary to produce 1 m^3 of concrete) and GWP (Global Warming Potential, related to the greenhouse gases emitted for 1 m^3 of cementitious mixture) for class C30/37 concretes manufactured with different type of binders calculated starting from the raw materials data reported in Table 12.

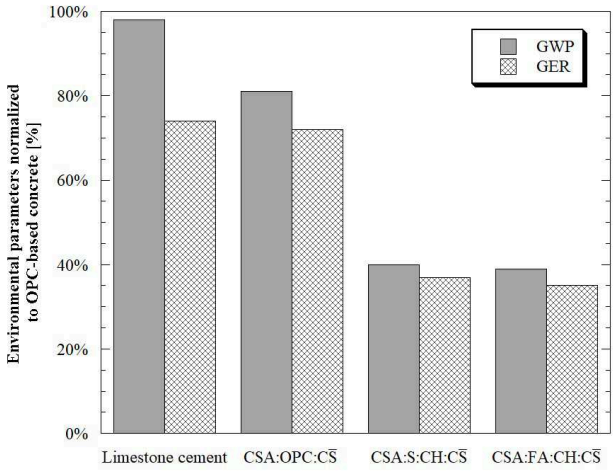

Figure 69 - GWP and GER parameters normalized to those of an OPC-based concrete at equal strength class C30/37

If the aim is to increase sustainability, reducing both the emissions of CO_2 (GWP) and the primary energy required (GER) for the production of one cubic meter of concrete, replacement of Portland cement type I with limestone Portland cement type II or with a ternary mixture, in which OPC and CSA are present in equal parts, is not a suitable solution to obtain a sharp reduction of the environmental impact in concrete production. In fact, improvements are rather limited, since reduction of GER and GWP is generally between 15% and 25%, due to both the high kiln temperatures required during Portland clinker production and the strong environmental impact of the extraction and grinding phase [134]. The best way to achieve a remarkable improvement in terms of sustainability is use of mixtures based on sulphoaluminate cement (CSA) in which OPC has been totally replaced by supplementary cementitious materials (SCMs) and hydrated lime (CH). In this case, it is possible to obtain, both for GHG emissions and consumption of energy, a reduction of about 60% at equal strength class due to the nature of the binders employed (generally wastes deriving from industrial process) that required limited processing before being used in mortars and concretes.

4.4 Conclusions

In this chapter, the influence of water/binder ratio, dosage of tartaric acid set-retarding admixture and curing conditions on rheological, elastic and physical properties of environmentally friendly shrinkage-compensating concretes manufactured with calcium sulphoaluminate cement (CSA), anhydrite (C$\hat{S}$), lime (CH) and two different supplementary cementitious materials (fly ash and ground granulated blast furnace slag) replacing totally ordinary Portland cement was investigated. According to the experimental data, the following conclusions can be drawn:

- At equal mixing water, workability at the end of the mixing procedure is not influenced by type of SCMs employed and the water/binder ratio;
- The tartaric acid-based set-retarding admixture acts as a superplasticizer;
- OPC- or GGBFS-based mixtures require higher amount of tartaric acid (0.6 wt.% vs binder) respect to that needed for concretes manufactured with FA (0.4 wt.% vs binder) in order to ensure a suitable workability retention;
- In general, by using Abram's model, it is possible to note that Portland-free concretes have mechanical behavior close to that shown by traditional concretes manufactured with Portland cement or limestone Portland cement;
- Compressive strength values of reference mixtures CSA:OPC:C$\hat{S}$ are more affected by water/binder ratio than those of CSA:SCM:CH:C$\hat{S}$ concretes. However, reference concretes, independently of w/b, exhibited compressive strength values higher than those obtained for CEM I 52.5 R based mixtures;
- Total replacement of OPC with supplementary cementitious materials and lime in underwater curing conditions determine a general worsening of elastic and mechanical properties (compressive and tensile strength, Young's modulus) and watertightness of concretes;
- Independently of binders employed, CSA-based concretes exhibit a stable behavior over time when specimens were cured at 20°C and 60% R.H. (D) while an underwater curing (W) determines an initial expansion of concretes followed by a negligible shrinkage;
- CSA-based concretes manufactured with SCMs and hydrated lime in place of OPC are very promising from an environmentally point of view since GER and GWP parameters decrease about 60% at equal strength class compared to traditional OPC or CSA:OPC:C$\hat{S}$ mixture.

5. Alkali-activated slag cements: literature review

The reaction of an alkali source with a silica- and alumina-containing solid precursor to form a solid material comparable to hardened Portland cement was first patented by Kühl in 1908 [156]. The scientific basis for these binders was then developed in more detail by Purdon who was able to understand that this method of concrete production is adequate only in ready-mixed and precast applications where activator dosage can be accurately controlled [157]. However, sensitivity of the activation conditions to the amount of mixing water and the difficulties inherent in handling concentrated caustic solution, were noted as critical issues. These weaknesses were identified even half a century later by Wang et al. [158]. After the works of Purdon, alkali activation research in United States and Europe was quite limited until the 1980s. On the contrary, alkali activation was developed in Soviet Union and China in order to reuse metallurgical slags. In particular, work in the former Soviet Union was initiated by Glukhovsky in Kiev [159].

Actually, there are a great number of scientific papers available in the literature which report the chemistry and properties of alkali-activated binders manufactured with different raw materials (Figure 70).

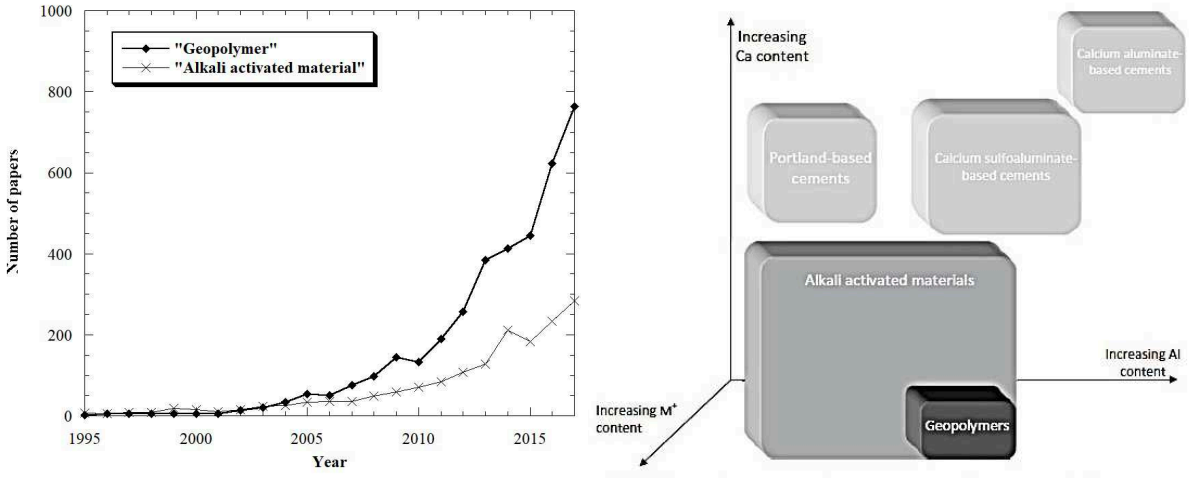

Figure 70 - Number of papers related to AAMs and geopolymers on Scopus (left, www.scopus.com). Classification of AAMs with comparison to OPC and CSA cement chemistry. Shadings indicates the alkali content; darker shadings corresponds to higher concentration of alkalis (right) [5]

Unfortunately, a large number of names have been used to describe the issue of alkali activation such as “mineral polymers”, “soil cements”, “soil silicates”, “SKJ-binders”, “F-concretes”, “hydroceramics”, “zeoceramics”, “zeocements”, “inorganic polymers”, “inorganic polymer glasses” and other. In general, the term “alkali-activated material” (AAM) identifies any binder system derived by the reaction of an alkali metal source (e.g. sodium or potassium) with a solid silicate powder,

generally based on calcium or alumina. Conversely, the term “geopolymers” is related to a subset of AAMs where the binding phase is almost exclusively aluminosilicate and highly coordinated, such as low-calcium fly ashes and calcined clays. The distinction between alkali- activated materials and geopolymers is shown schematically in Figure 70.

In this PhD thesis the attention is focused on the alkali-activated materials based on ground granulated blast furnace slag (GGBFS), simply called alkali-activated slag (AAS) cements.

5.1 Structure and chemistry of AAS cements

The calcium- and silicon-rich material most commonly used to produce alkali-activated concretes and mortars is ground granulated blast furnace slag because its chemical composition and highly amorphous nature favor the formation of reaction products that develop high mechanical strengths within a moderate curing time and low water demand [160]. This vitreous steel industry waste is generally composed by CaO (34-40%), SiO_2 (25-35%), MgO (5-10%) and Al_2O_3 with other minor constituent (Fe_2O_3, MnO, S, TiO_2 and K_2O) as reported by Provis and van Deventer [161]. Slow-cooled slag tends to be crystalline and unreactive, but many rapid-cooled (granulated or pelletized) slags can also contain crystalline inclusions.

The hydraulic activity of GGBFS is measured through parameters such as the basicity coefficient (K_b) and the quality coefficient (K_q):

$$K_b = \frac{CaO + MgO}{SiO_2 + Al_2O_3} \quad (20)$$

$$K_q = \frac{CaO + MgO\ + Al_2O_3}{SiO_2 + TiO_2} \quad (21)$$

As reported by Pal et al. [162], the ideal values for basicity coefficient K_b are between 1.0 and 1.3 while quality coefficient K_q should be higher than 1.0.

In general, the main properties required of GGBFS to be adapt for use in AAS cement are as listed below:

- Vitreous phase content higher than 85% and disordered structure [160];
- CaO/SiO_2 ratio between 0.5 and 2.0 [163];
- Al_2O_3/SiO_2 ratio between 0.1 and 0.6 [160];
- Specific surface equal to 350-550 m^2/kg [160,164,165].

The structural development of AAS cements is a highly heterogeneous reaction process that is mainly governed by four mechanisms: dissolution of the glassy precursor particles, nucleation and growth of the initial solid phases, interactions and mechanical binding at the boundaries of the phases formed, and ongoing reaction via dynamic chemical equilibria and diffusion of reactive species through the reaction products formed at advanced times of curing [166].

The main reaction product is an aluminium-substituted C-S-H type gel [158,167–170], with a disordered tobermorite-like C-S-H (I) type structure (Figure 71) accompanied by the formation of secondary reaction products such as monosulfate (AFm), ettringite (AFt), strätlingite, hydrotalcite, and zeolites such as gismondine and garronite [170–175].

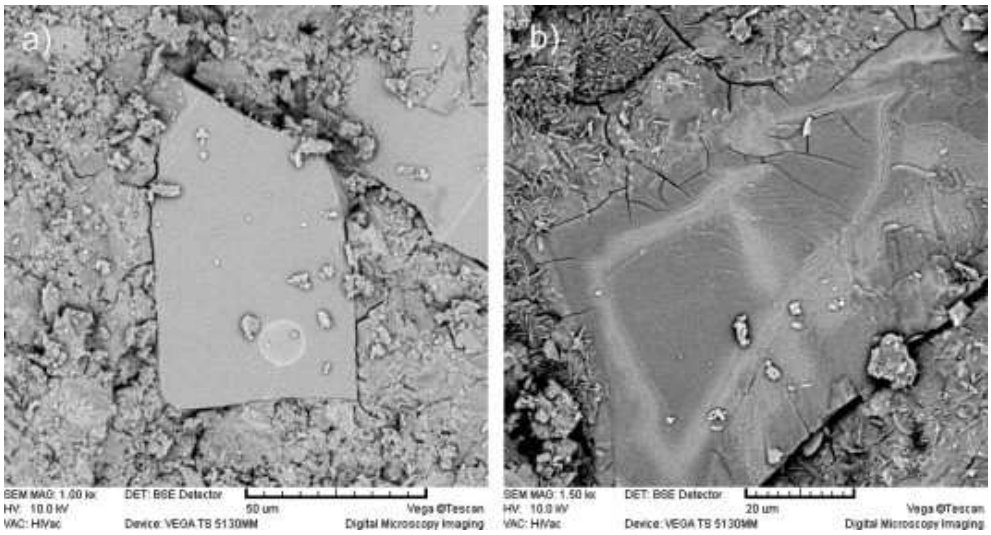

Figure 71 - C-S-H (I) gel and unreacted slag grains in AAS paste [176]

The structure of the C-S-H type product and the secondary reaction products properties are strongly dependent on the nature and the concentration of the activator used [177].

As it is well known, the reaction of GGBFS with water leads to the formation of a hardened binder (Figure 72). The main role of the alkaline activator in AAS cements is therefore to accelerate this reaction to take place within a reasonable timeframe for the production of an engineering materials, and this is most readily achieved by increasing the pH (the higher the pH, the greater the speed of dissolution of the precursor and the condensation reactions). The possible activating solutions include alkaline hydroxide (ROH, $Ca(OH)_2$), weak salts (R_2CO_3, R_2S, RF), strong acid salts (Na_2SO_4, $CaSO_4{\cdot}2H_2O$) and alkali silicate salts ($R_2O{\cdot}rSiO_2$), where R is Na^+, K^+, or less commonly Li^+, Cs^+ or Rb^+. Among these, the commonly used activators for AAS cements are sodium hydroxide (NaOH), sodium silicate (Na2O ¢ rSiO2), potassium hydroxide (KOH) and sodium carbonate (Na2CO3).

Alkali hydroxides and silicates generate the highest pH among these common activators, while carbonates generate moderately alkaline conditions. Moreover, the pH of the activating solution also strongly influences the dissolution of GGBFS constituents. In fact, calcium solubility decreases at higher pH while silica and alumina solubility increases. Therefore, the selection of the most appropriate alkaline activator needs to include consideration of the solubility of calcium species at the pore solution pH in the fresh paste, as well as the interaction involving the cations supplied by the activator, which can promote the formation of specific reaction products [166].

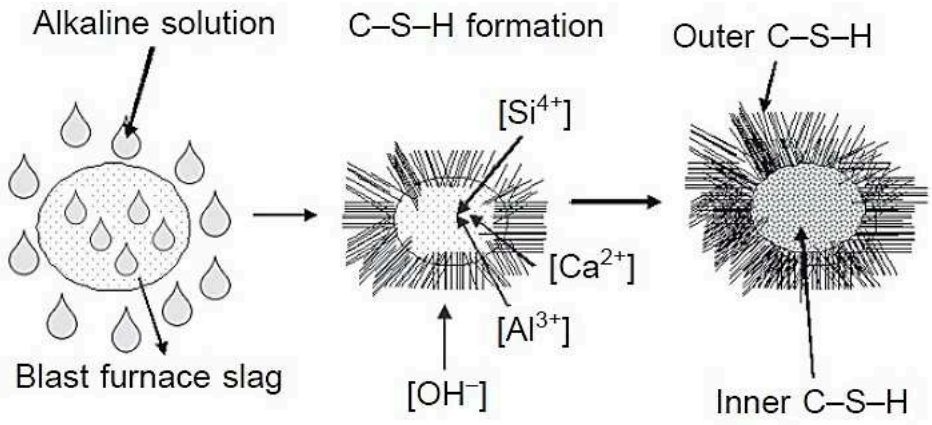

Figure 72 - Theoretical model for the reaction mechanism in AAS [166]

5.1.1 Effect of CaO/SiO_2 ratio

The chemical composition of the GGBFS and its mineralogical characteristics are determinants in the formation of the C-S-H gel which, in turn, strongly conditions both the mechanical properties and the durability of AAS mortars and concretes.

The characteristics of the gel formed can be evaluated and the mixture performance predicted by measuring the CaO/SiO_2 ratio as reported by several authors [26,166]. Slag dissolution after addition of the alkaline activators generates a series of dissolved Si^{4+}, Al^{3+} and Ca^{2+} species that are immediately available to form C-S-H gel. This reaction product is similar to that generated during OPC hydration, although it CaO/SiO_2 ratio is lower than in the latter (C-S-H gel ratios usually range from 0.9 to 1.2). Therefore, the silica content affects the polymerization of C-S-H gel. Taylor [178] showed that the higher the silica content, the longer the silicate chains (Figure 73).

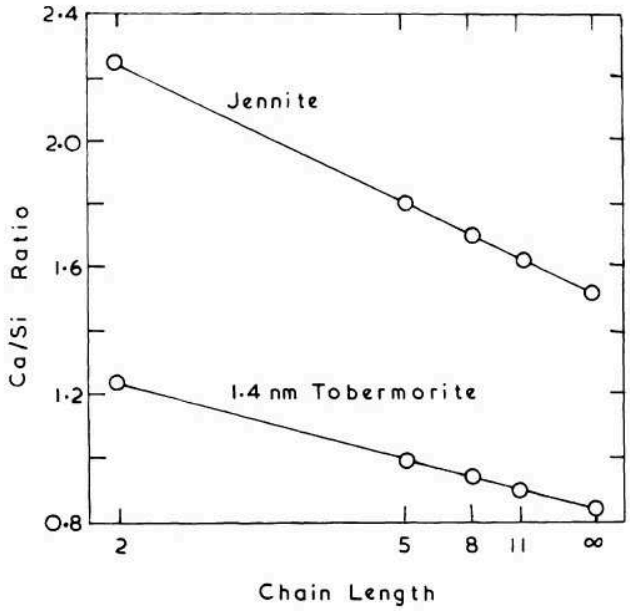

Figure 73 - Calculated CaO/SiO_2 ratio plotted against a function of chain length [178]

Thus, the standard method for modifying the CaO/SiO_2 ratio is by adding soluble silica to the system along with the alkaline activator in form of sodium silicate.

5.1.2 Effect of hydroxides

OH- ions catalyze the dissolution of Si^{4+} and Al^{3+} cations by inducing the hydrolysis of Si-O-Si and Si-O-Al bonds [159]. Furthermore, the presence of OH^- raises the pH to the values required for the initial slag dissolution and the subsequent condensation reactions. Very high pH (derived from very high alkaline hydroxides concentrations) are not favorable when slag is the raw material, however, for unlike silica and alumina, calcium becomes less soluble with rising pH. In general, alkaline hydroxide are effective GGBFS activators at concentration ranging from 2M to 4M.

In hydroxide-activated slag, because there is no extra Si supplied by activators, the CaO/SiO_2 ratio of C-S-H gel is higher than that in silicate-activated binders and the structure tends to have a relatively low degree of crosslinking [177].

Efflorescence (Figure 74) is also a known issue in binders activated with a too high concentration of hydroxide solutions, where the excess of alkali reacts with atmospheric CO_2 to form salts on the mixture surfaces. This is generally more marked in the presence of Na than K in hydroxide-activated binders, as reported by Kani et al. [179].

Figure 74 - Efflorescences in AAS mortars after 28 days from casting

5.1.3 Effect of silicates

The availability of soluble silica is of primary importance in AAS systems because it affects workability, setting, and mechanical strength development, modifying both gel composition and the microstructure of AAS paste. Silicate solutions is generally produced with sodium silicate and can be modified by dilution in deionized water or by adding extra alkalis (in forms of NaOH) to change the silica modulus of the solution Ms = molar ratio SiO_2/Na_2O (also called “moduli of solution”) and to raise the solution pH. The result is known as waterglass ($xSiO_2 \cdot yNa_2O \cdot nH_2O$).

In GGBFS activation, waterglass is responsible to a dual contribution to strength development, as an alkaline activator and an inducer of the formation of a high-silica primary gel. Depending on curing condition and slag nature and fineness, the ideal Na_2O content is approximately equal to 4% by slag weight and the optimal Ms strongly depends on the chemical composition of slag, as reported in Figure 75.

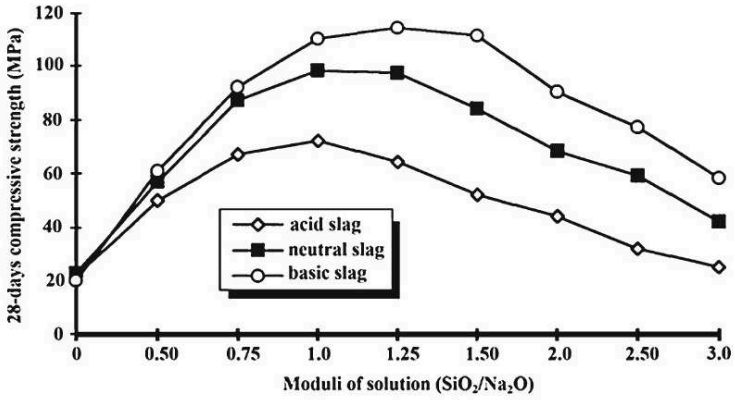

Figure 75 - 28-day compressive strength of AAS mortars vs silica modulus Ms [160]

Finally, viscosity of alkaline solution increases dramatically at higher silica content (Figure 76). Therefore, mixing and finishing freshly placed sodium silicate-activated mortars and concretes could be problematic, because the workability of fresh mixture is generally low and AAS paste tend to stick to building yard equipment, as reported by several authors [180–182]. On the other hand, potassium silicate solutions show a much lower viscosity than sodium silicates of comparable composition.

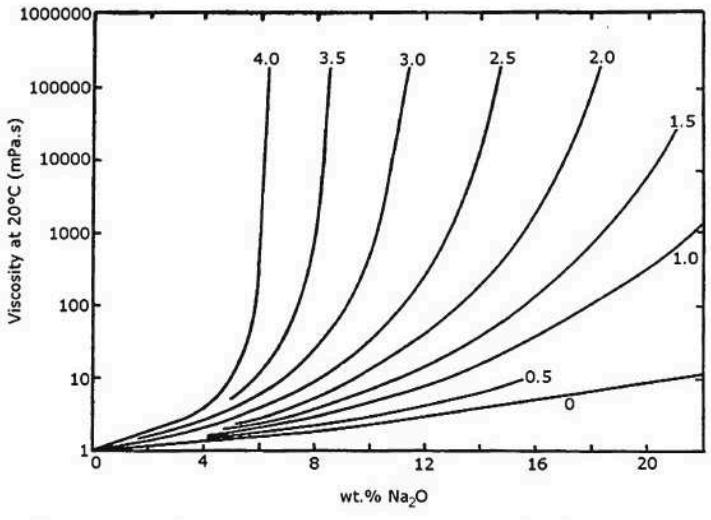

Figure 76 - Viscosity of sodium silicate solutions vs mass ratio SiO_2/Na_2O [166]

5.1.4 Effect of carbonates

The use of carbonates in AAS cements has been researched by several authors due to the lower environmental impact of carbonates respect to silicates or hydroxides. This activator induces a lower pH than found in many AAS systems with potential benefits in terms of occupational health and safety. On the other hand, carbonate-activated binders have attracted less attention from academia and industry than other systems because they generally harden and develop strength much more slowly than sodium hydroxide- or sodium silicate-activated binders.

Fernandez-Jimenez and Puertas [183] showed that in the early stages, activation of GGBFS with Na_2CO_3 leads to formation of calcium carbonates and mixed sodium/calcium carbonate double salts as a result of the interaction between the CO_3^{2-} present in the activator and the Ca^{2+} released form the slag. The formation of these carbonates, together with the lower pH solution, lengthen the induction period and intensify the plasticity loss in the paste. The result is lower initial strength than NaOH- or waterglass-activated materials, although at later ages strength may be higher than in sodium hydroxide-based AAS mixtures (Figure 77).

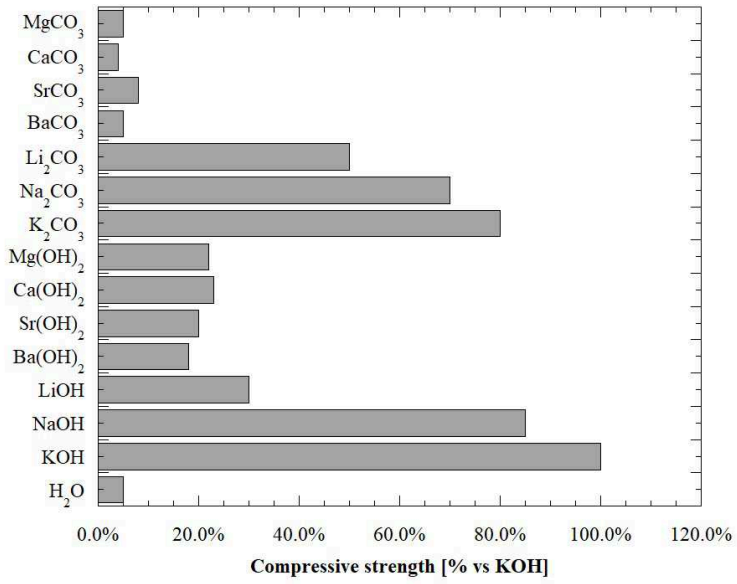

Figure 77 - 1-day compressive strength of AAS manufactured with different activators. Alkali content fixed. Data from [166]

5.2 Properties of AAS mortars and concretes

During the alkali activation process, the vitreous phase of slag dissolves, forming C-S-H gel. This reaction depends on a whole series of parameters such as particle size distribution, chemical composition and amount of vitreous phase in raw materials, as well as the nature, concentration, and pH of activators. Conditions of the reaction (i.e. curing conditions) also show a great influence on the

development of microstructure, and thereafter on the physical and elasto-mechanical properties of AAS mixtures.

5.2.1 Fresh properties

The knowledge of the fresh behavior of AAS mixtures is of primary importance because it allows to optimize the mixing, placing and finishing operations of alkali-activated slag-based concretes and mortars. Several researches have been conducted on these issues, however some fresh properties of AAS mixtures have not yet been fully investigated (e.g. bleeding, segregation, workability retention). Setting time of alkali-activated slag is influenced by the basicity of the slag. In particular, the higher the basicity, the shorter the setting time regardless of activators used. On the contrary, the fineness of slag does not appear to affect the setting time of AAS binders, especially in the range of 350-550 m^2/kg [184]. As reported earlier, waterglass-activated slag cements tend to exhibit shorter setting time than either hydroxide- or carbonate-activated GGBFS. Furthermore, as shown in Figure 78, increasing the activator dosage or the silica modulus Ms, the setting time usually decrease [185]. In general, the combination of two or more activators can drastically change the setting characteristics of AAS cements [183].

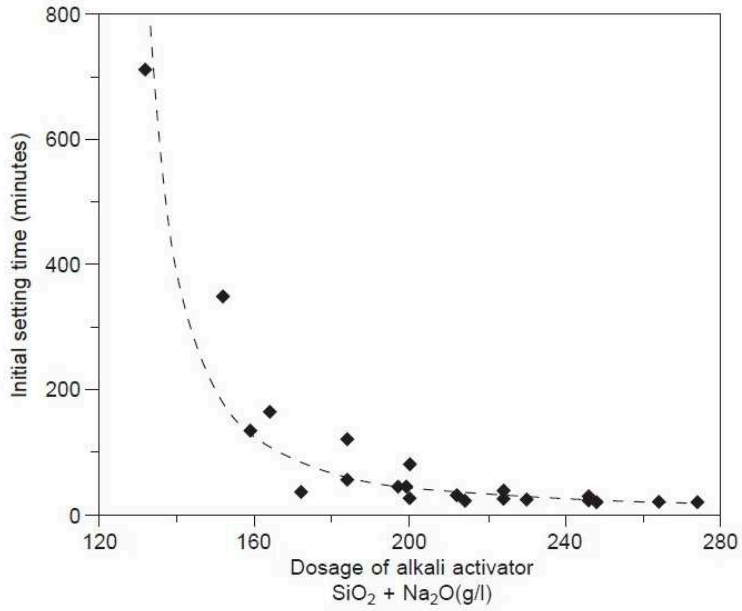

Figure 78 - Influence of activator dosage on initial setting time of AAS cements [185]

For AAS cements, there have not been any reports indicating that mortars or concretes manufactured with this binder are prone to excessive bleed under handling, compaction or vibration.

Collins and Sanjayan [186] reported that workability is sensitive to the dosages of activators (especially silica modulus and NaOH dosage) and the composition and fineness of slag. In most cases, high one-day strengths were accompanied with rapid workability loss beyond 45 minutes from

mixing. However, a suitable mix design can lead to the production of AAS mortars and concretes with workability retention higher than that of OPC-mixtures.

5.2.2 Mechanical properties

The performance of alkali-activated slag mortars and concretes is governed primarily by the nature of the slag and the nature of the activators used (Figure 79). Properly designed AAS mixtures exhibit much higher strength than conventional Portland-based concretes and mortars, as well as improvements in other properties [167].

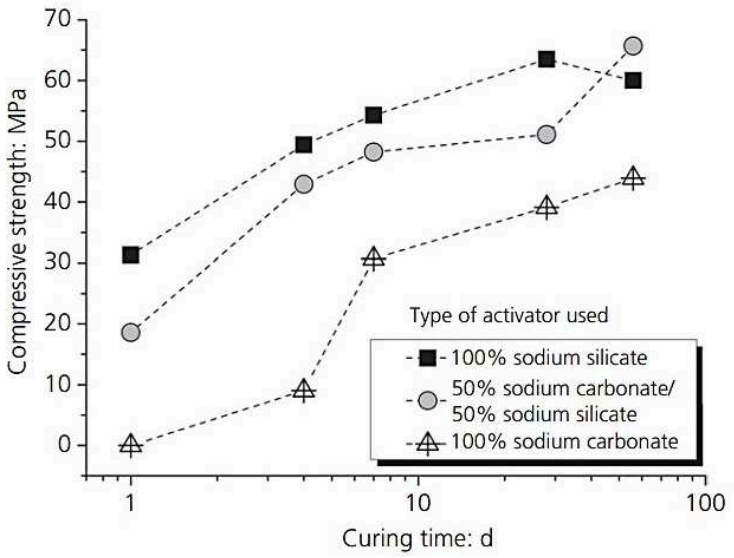

Figure 79 - Compressive strength development of sodium silicate/carbonate activated slag binder [187]

Fernandez-Jimenez et al. [188] have studied the influence of several factors on the development of mechanical performance in AAS cements, concluding that the order of the most significant effects on the development of mechanical strength is: nature of alkaline activator ≫ activator concentration > curing temperature ~ specific surface of slag. Moreover, as a function of the strength obtained, the waterglass seems to promote the development of higher mechanical strength than sodium carbonate or sodium hydroxide.

AAS concrete showed greater tensile strain capacity than OPC concrete due to the greater creep, lower elastic modulus and higher tensile strength of AAS concretes (Figure 80). Moreover, AAS mortars generally exhibit higher splitting tensile strength than the OPC mortar of similar compressive strength [189]. Furthermore, Thomas and Peethamparan found that Poisson's ratio for AAS concrete is about two-thirds that typical of OPC concrete and Young's modulus is generally lower respect to Portland cement-based concrete at equal strength class [190].

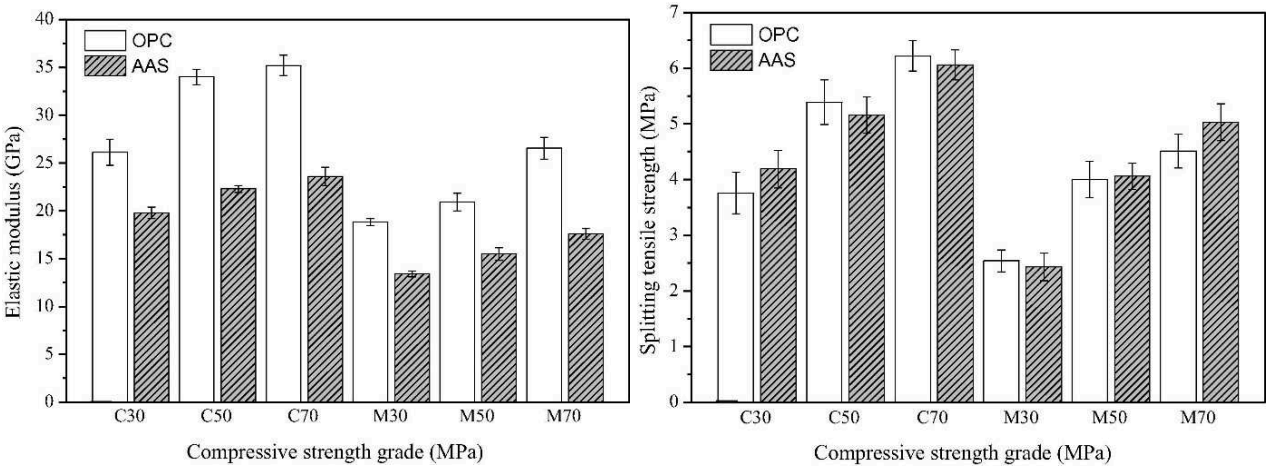

Figure 80 - Elastic modulus (left) and tensile strength (right) of concretes (C) and mortars (M) manufactured with OPC or AAS [191]

5.2.3 Shrinkage

Several studies reported that AAS mixture exhibits large autogenous and drying shrinkage, considerably higher than that of OPC-based materials (Figure 81) [192,193]. Cartwright et al. [194] measured the autogenous and drying shrinkage of AAS mortars manufactured with different types and dosages of activators. Their research evidenced that AAS has up to six times higher shrinkage, finer pore structure, and lower stiffness than OPC.

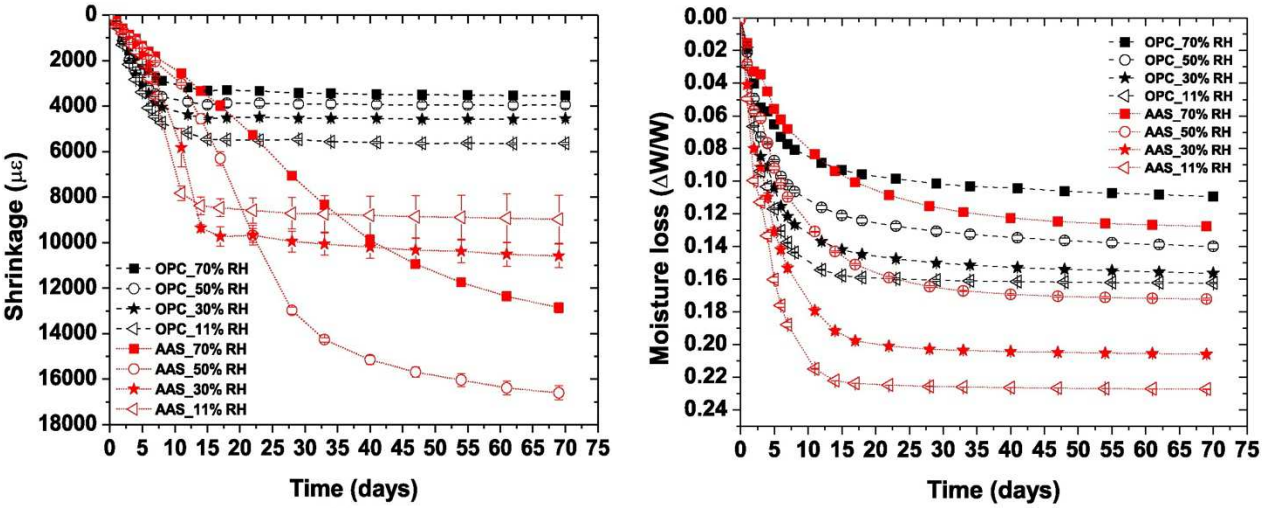

Figure 81 - Shrinkage (left) and moisture loss (right) of OPC and AAS mortars vs time [195]

Collins et al. [196] attributed the high shrinkage of AAS to the higher capillary stress deriving from its pore size distribution. Furthermore, Ye and Radlinska [195] noted that the shrinkage of AAS exhibits a pronounced viscous characteristic upon drying especially at high relative humidity (RH). In addition, the kinetics of shrinkage in AAS seems to be strongly dependent on the experienced RH. They also confirmed that the viscous performance in alkali-activated materials is due to the

rearrangement and reorganization of C-S-H particles under capillary stress. Finally, during drying-induced microstructure rearrangement, considerable chemical and physical modifications occur in AAS.

5.2.4 Curing conditions

There is widespread debate in the scientific community regarding the most appropriate curing conditions to be applied to alkali-activated binders for optimal strength development, low shrinkage and excellent durability. The experimental data show that the ideal curing conditions for Portland cement, such as underwater curing, is not applicable because it leads to premature leaching and unavoidable loss of strength [197]. Curing at high relative humidity (RH > 90%) and room temperature represents a more appropriate option. If the reaction of alkali activation at room temperature is too slow, heat or steam curing is needed. However, it might lead to a halt in strength development if the water present in the system and required for the reaction continuance is irreversibly lost [160,176,198,199].

Similarly to OPC mixtures, there is a strong influence of curing temperature on strength of AAS mortars and concrete, with significant retardation at 5°C and important acceleration at 40°C with respect to a curing temperature equal to 20°C [167]. In general, it is almost universally agreed that an extended period of sealed curing is important in the development of a dense and durable matrix [166].

5.3 Durability issues

The durability of alkali-activated materials is strongly affected by the nano- and micro-structure of the reaction products forming in these systems, as a function of the characteristics of precursor and the nature and the concentration of the activators. Slag-based systems have a structure mainly dominated by a C-S-H gel that is one of the main factors controlling the transport properties of AAS.

5.3.1 Carbonation

In traditional Portland cement mixtures, carbonation is understood as the chemical reaction taking place between the carbonic acid formed through the dissociation, in the pore solution, of the carbon dioxide that diffuses into the material from the external atmosphere, and the hydration products of the binder, producing carbonate deposits within the binder itself [200]. This mechanism of deterioration leads to a significant decrease in the pH of binder paste along with an increase in the total porosity. These combined physicochemical changes in the cement matrix mean that the metallic reinforcements become very prone to suffer corrosion.

It is well known that carbonation is controlled by both diffusional and chemical mechanisms, and is influenced by the RH in the material, the concentration of carbon dioxide in the atmosphere, and the tortuosity of the pore network, along with the chemistry of the binding phases and the pore solution environment [100].

In AAS, the mechanism of carbonation is strongly affected by the chemical composition of raw materials and the nature and concentration of activators employed [201,202]. Bernal et al. [203] claimed that the MgO content of the slag has a significant influence on both the mechanism and rate of carbonation of alkali-activated slag (Figure 82). This is related to the formation of layered double hydroxides with a hydrotalcite type structure as a secondary reaction product, when using slags with higher MgO content. In particular, layered double hydroxides have the capacity to absorb carbon dioxide, and the formation of these Al-rich secondary phases also reduces the degree of Al incorporation in the C-S-H type gel. These combined effects seem to enhance the resistance to carbonation of AAS binders.

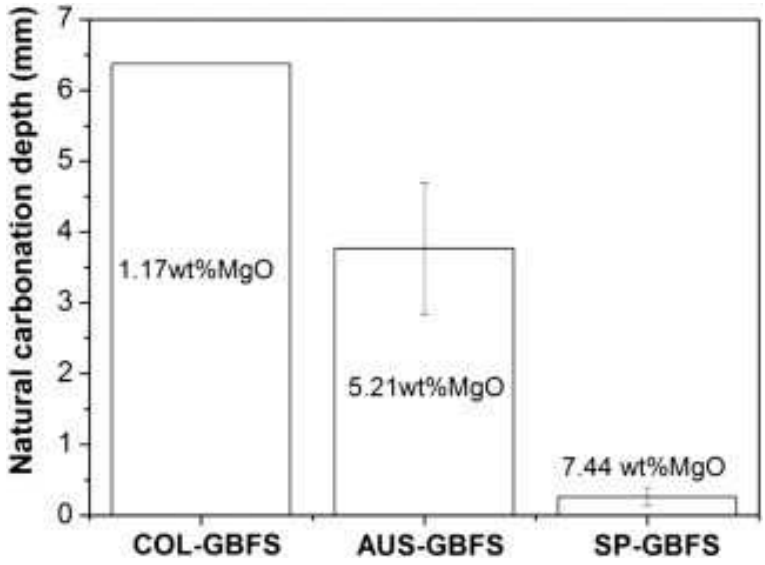

Figure 82 - Natural carbonation depth of three different slag-based mortars [203]

Bernal et al. [204] noted that design parameters of the concrete, such as the content of binder, can influence the rate of carbonation in alkali-activated slag cements. This means that adequate formulation and selection of precursors, aiming to reduce the permeability of binder paste, can strongly reduce the degradation of concrete structures exposed to CO_2.

Carbonation is generally a relative slow process under environmental conditions due to the low carbon dioxide concentration (~ 0.04%) in the atmosphere. For this reason, to predict the performance of binders against carbonation within an experimentally acceptable timescale, accelerated carbonation tests have been developed, using chamber containing high CO_2 concentrations. Nevertheless, the results of the carbonation tests on AAS at different CO_2 concentration seems to be discordant.

Under accelerated carbonation testing conditions (Figure 83), a higher susceptibility to carbonation has been identified in alkali-activated slag compared to Portland cements, which is attributed to the

absence of portlandite as a reaction product in these systems, the low CaO/SiO_2 ratio of the binding gel, and the high alkali content of the pore solution [203–205].

However, it is important to highlight that these observations differ from the trends reported in specimens tested after several decades of service life [206], which are comparable to what can be expected for reasonably good-quality Portland cement-based materials exposed under the same conditions.

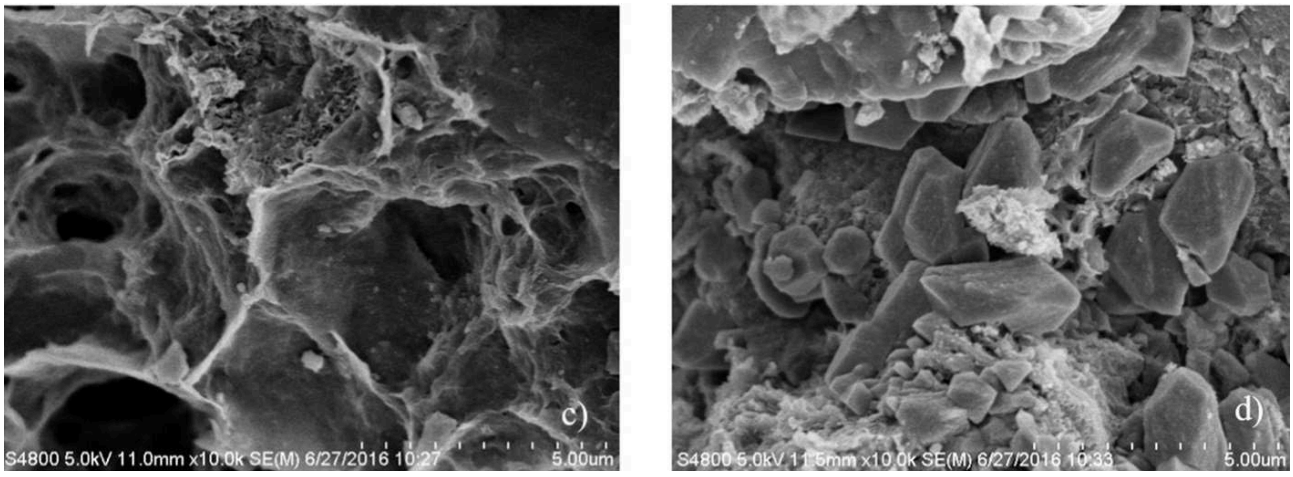

Figure 83 - SEM images of AAS mortars before (left) and after (right) carbonation [207]

5.3.2 Chloride penetration

The rate of chloride penetration into a cementitious material is often used as a key parameter in durability or service life analysis because, under many environmental conditions, the corrosion of embedded steel reinforcing elements by chlorides is the main cause of concrete deterioration.

Chlorides are either applied as de-icing salts in cold climate regions, or enter into the material due to marine water/aerosol in coastal regions. The degree of structural change induced by chloride in the Portland cement is generally low and the main influence of binder characteristics in resisting chloride ingress is that the binder must provide resistance to chloride transport.

There are a limited number of papers focused specifically on the chloride permeability of alkali-activated slag cements, nevertheless there is a general consensus that these materials exhibit a lower permeability to chlorides compared to Portland cements, if cured adequately [207–213]. However, there is not yet an extensive database of chloride diffusion coefficients available for AAS concretes and mortars (Figure 84). Recently, Ismail et al. [207] have demonstrated that the nature of the binder gel strongly influences the chloride permeability in AAS systems. This is a combined effect of the space-filling characteristics of the gels and the capacity of gels to bind chloride ions. In high-Ca mixtures, chloride ions can not only be chemisorbed onto C-S-H products in the layers and interlayer spaces but can also be chemically bound to the C-S-H.

Another important parameter associated to the reinforcement corrosion is the chloride threshold for pitting corrosion initiation. However, this topic has not yet been exhaustively treated in the scientific literature even though it is of primary interest.

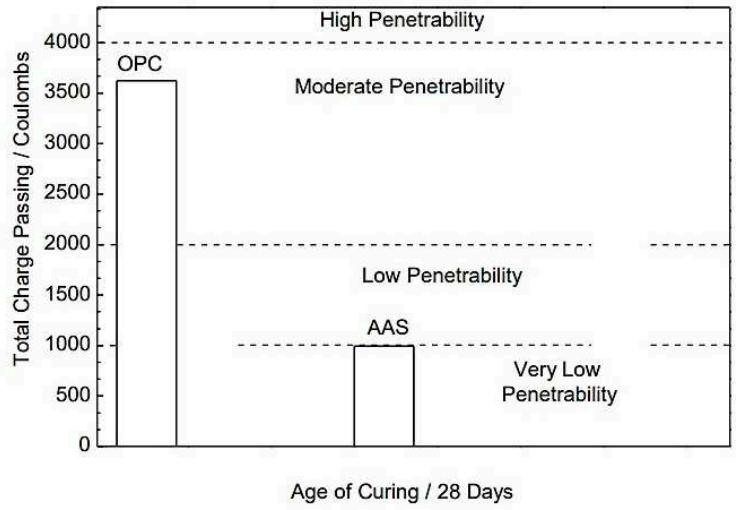

Figure 84 - Values of permeability to chlorides in AAS concretes [212]

5.3.3 Sulphate attack

There is a relatively limited knowledge of the effect of sulphate exposure on the durability of AAS cements. Immersion of alkali-activated slag binders in sodium sulphate solutions according to traditional test method for OPC-based concretes does not promote expansion or cracking of binder paste [214]. On the contrary, Portland cement-based samples show significant expansion and cracking associated with the formation of secondary ettringite and gypsum [100].

Recent results [215] have revealed that the key factor controlling the degradation mechanism of AAS is not the sulphate itself, as tends to be the case in Portland cement mixtures, but rather it is the nature of the cation accompanying the sulphate anions. Exposure to sodium sulphate seems to favor the structural evolution of the binding phases and densification of the system, which is consistent with the known role of Na_2SO_4 as activator. Conversely, the presence of magnesium leads to decalcification of the Ca-rich gel phases in alkali-activated materials, promoting the decay of the main binding phases and leading to formation of low-strength M-S-H type phases.

5.3.4 Acid attack

Several authors [30,216] reported that chemical resistance is one of the main advantages of AAS cements over Portland cements. In particular, Scrivener and Young [217] studied the exposure of AAS mortars during six months in 5% acid solution concentration, reporting that for citric acid changes were low, for nitric and hydrochloric acid alterations were moderate although severe changes

were noticed when sulphuric acid was used. Davidovits et al. [218] reported mass losses of 6% and 7% for AAS immersed in 5% concentration hydrochloric and sulphoric acids during 4 weeks. For the same conditions they also reported that Portland cement-based concretes suffered mass losses between 78% and 95%. Moreover, Bakharev et al. [219] studied OPC and slag concretes activated with NaOH and waterglass, immersed in an acetic acid solution (pH = 4) for one year. They reported a 33% strength loss for the former and 47% for OPC concretes, claiming that the strength loss is influenced by Ca content, 64% for OPC mixtures and 39% for AAS concretes (Figure 85). Besides slag compounds have lower CaO/SiO_2 ratio and are more stable in acid medium.

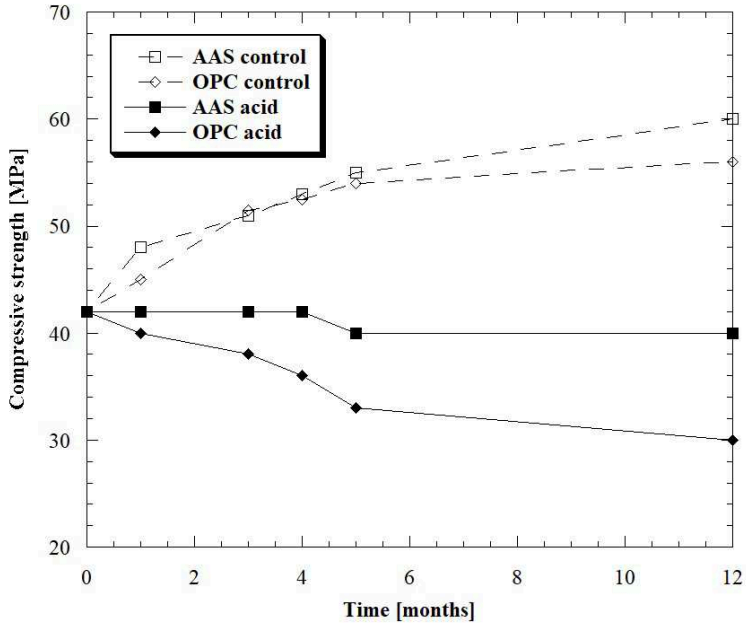

Figure 85 - Compressive strength of AAS and OPC mortars in acid environment. Data from [219]

5.3.5 Alkali-silica reaction

The chance of alkali-silica reaction (ASR) may take place in AAS binders is an unknown issue while, for Porland-based binders, the knowledge of ASR has been intensively investigated. For this reason, some explanations could be also applied to understand the possibility of ASR when alkali-activated binders are used. The ASR needs the simultaneous action of three elements in order to occour [100]:

- Enough amorphous silica in the aggregates;
- Alkaline ions;
- Water.

The alkali-silica reaction begins when the reactive silica from the aggregates is attacked by the alkaline ions from cement forming an alkali-silica gel, which attracts water and starts to expand, leading to internal cracking. Puertas [165] and Davidovits [220] believe ASR could occur for alkali-activated slag binders containing reactive opala aggregates. Moreover, Bakharev et al. [221]

compared the expansion of OPC and alkali-activated binders reporting that the first ones had higher expansion.

5.3.6 Resistance to freeze-thaw cycles

Durability against freeze and thaw cycles is an important factor influencing the durability of concrete structures in cold regions. The freezing and thawing resistance of concretes depends mainly on the structure of its paste (e.g. its porosity, pore size, capillaries, distribution, and type of pores). Proper pore distribution can cause pressure diffusion and improvement in resistance against freezing-thawing cycles. Obviously, utilizing a cementitious material with lower permeability in producing concrete could increase the lifetime of the concrete structures.

Fu et al. [222] studied the durability of AAS concrete in cold regions concluding that the resistance to freeze-thaw cycles is high due to the high compactness of the pastes (Figure 86). Moreover, Cai et al. [223] claimed that the frost-resisting grade of AAS concrete is above F300 and the coefficient of freeze-thaw resistance is about 90%, which can fully meet the requirements of the freeze-thaw resistance of the concrete in colds areas. Similar results were obtained by other authors [224].

Recently, Shahrajbian and Behfarnia [225] produced AAS concrete with the addition of nanoparticles such as nano-silica, nano-alumina and nano-clay. Experimental results indicated that adding nanoparticles up to 3% by mass could reduce the compressive strength loss and the weight reduction of concrete under freezing-thawing cycles.

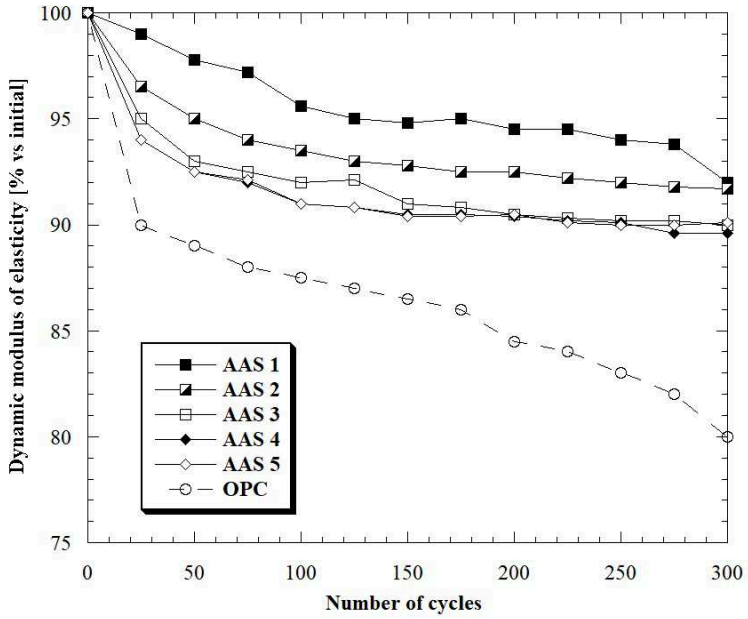

Figure 86 - Dynamic modulus of elasticity attenuation of 5 different AAS mortars under freeze/thaw cycles. Data from [222]

5.3.7 Resistance to high temperature and fire

OPC-based concretes show a weak performance when subjected to a thermal treatment and when the temperature rises above 400°C they begin to disintegrate. In particular, the mechanical properties deteriorate due to chemical and physical changes in the hydrated phases of the binder. The thermal transformations lead to dehydration and loss of chemically bound water, mainly from the dihydroxylation of the portlandite, which induces a reduction in chemical bonding and strength [100]. In addition to strength loss, Portland cement-based mixtures are prone to fire induced spalling which can reduce the section thickness and expose the steel bars to fire.

Mixtures manufactured with AAS contain little $Ca(OH)_2$ following hydration and as a result, their fire performance is not governed by the dihydroxylation of portlandite [226,227]. Above 350°C, there are two competing mechanisms – namely thermal expansion of the aggregates and thermal shrinkage of paste – responsible for the cracking and the strength loss in AAS concrete.

De Gutierrez et al. [228] concluded that the residual strength of alkali-activated slag materials up to 1000°C were similar to the control OPC mixtures. The strength loss was concluded to be the dehydration of the C-S-H gel. Similar results were obtained by Guerrieri et al. [229] that detected that AAS mortars had a rapid strength loss of approximately 60% between 100 and 200°C and a further strength loss in the order of 30% at 800°C (Figure 87). Finally, Rashad et al. [230,231] highlighted that the internal pH was affected by the elevated temperature, with a drop after 600°C for slag-based pastes.

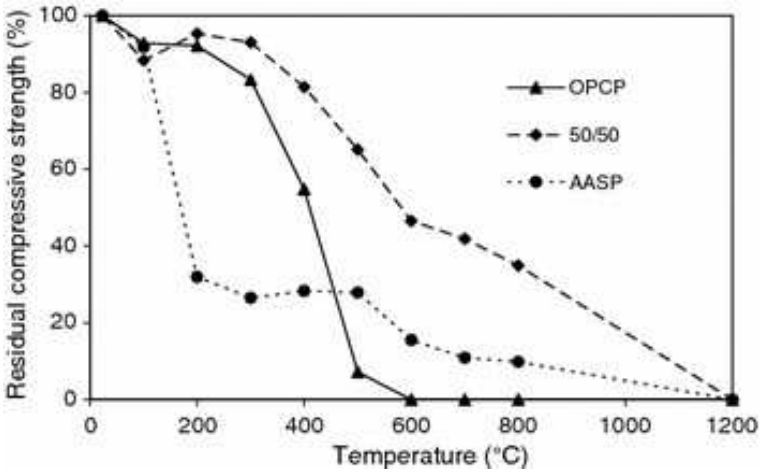

Figure 87 - Residual compressive strength profile [229]

5.4 Admixtures

Nowadays, the use of chemical admixtures aimed at improving the physical and mechanical properties of OPC-based concrete is common during concrete production. In addition, the admixtures

have been developed and optimized for system containing Portland cement. For these reasons, the effect of admixtures on alkali-activated slag pastes and mortars could differ entirely from the effect on OPC mixes. Several papers concerning the use of traditional additives in AAS systems are in disagree, as it is possible to see in Table 22.

Ref.	Admixture	Flow	Water content	Setting time	Strength
[232]	Lignosulphonate	Increase	-	Retard	Reduce
[233]	Lignosulphonate	No var.	-	-	-
[160]	Lignosulphonate	No var.	-	-	Reduce
[232]	Naphtalene	Increase	-	Accelerate	Reduce
[234]	Naphtalene	-	Decrease	*	Increase
[235]	Naphtalene	Increase	-	No var.	-
[233]	Naphtalene	No var.	-	-	-
[160]	Naphtalene	No var.	-	-	Reduce
[236]	Naphtalene	Increase	-	-	-
[234]	Polycarboxylate	-	Decrease	*	No var.
[235]	Polycarboxylate	Increase	-	Retard	Reduce
[8]	Polycarboxylate	No var.	-	No var.	No var.
[237]	Polycarboxylate	No var.	-	-	-
[234]	Melamine	-	Decrease	No var.	Increase
[236]	Melamine	*	-	-	-
[237]	Melamine	No var.	-	-	-
[237]	Melamine	Increase	-	-	-
[234]	Vinyl copolymer	-	No var.	Retard	Increase
[237]	Vinyl copolymer	No var.	-	Retard	Reduce
[236]	Vinyl copolymer	*	-	-	-
[237]	Vinyl copolymer	No var.	-	-	-

* variable results depending on the nature and concentration of alkaline activator

Table 22 – Effect of superplasticizers on properties of AAS systems

From the review of literature on this issue, it can be noted that several superplasticizers are not suitable for alkali-activated slag cements due to the low water-reducing effect and the negative effect on the development of mechanical strength. Naphthalene-based water reducers seems to be the most

promising superplasticizer for AAS cements because the alkaline pH of activators does not alter its molecular architecture [238].

The use of shrinkage reducing admixtures (SRA) to reduce both autogenous and drying shrinkage of OPC-based composites is well established and such admixtures are commercially available. The beneficial effect of SRA is attributed mainly to the decline of the surface tension of the pore water. Only a few studies investigating the influence of these admixtures on properties of AAS mortars and concrete were reported. Palacios and Puertas [234,239] reduced both autogenous (-85%) and drying (-50%) shrinkage of AAS by using polypropylene glycol-based admixture. Higher reduction was detected at R.H. 99% than at R.H. 50% (Figure 88). Better results for wet curing than for dry curing were also reported by Bilim et al. [240]. Moreover, Bakharev et al. [232] significantly reduced shrinkage by using some nonstandard SRA while Bilek et al. [241] investigated the effect of SRA based on 2-methy-2,4-pentanediol, claiming that the SRA greately influences both the shrinkage and the course of hydration of the AAS systems.

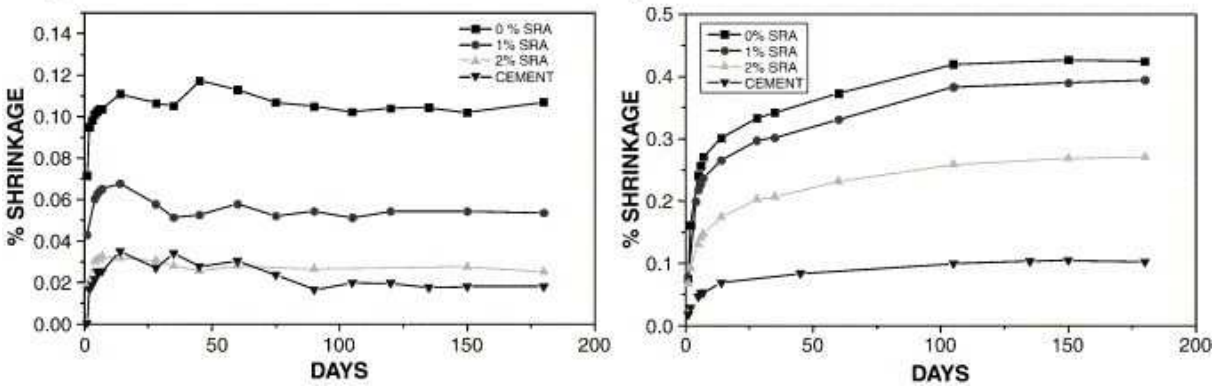

Figure 88 - Shrinkage in waterglass-activated slag mortars, with and without SRA, under different curing conditions: R.H. 99% (left) and R.H. 50% (right) [239]

The shrinkage compensating of AAS concrete with expanding admixtures (EA) is already not well investigated. Yuan et al. [242] used an EA composed of anhydrite and quick lime, establishing that the expansive agent is effective to compensating the shrinkage of AAS concrete. On the other hand, adding EA into alkali-activated slag concrete can increase its early age compressive strength, but lowers slightly the mechanical properties at late ages.

Conversely, Ye and Radlinska [243] concluded that the addition of CaO as expansive agent for shrinkage compensation refines the pore structure of AAS pastes and increase the shrinkage of slag-based mixtures (Figure 89).

In conclusion, it can be seen from a survey on the available literature that the majority of the commonly-available admixtures which are used in Portland cement-based materials, and which have

been developed over several decades, are either ineffective or detrimental when added to AAS mixtures. This is primary due to the very different chemistry of the alkali-activation process when compared with the hydration of OPC, and in particular the high pH conditions prevailing during the synthesis of AAS.

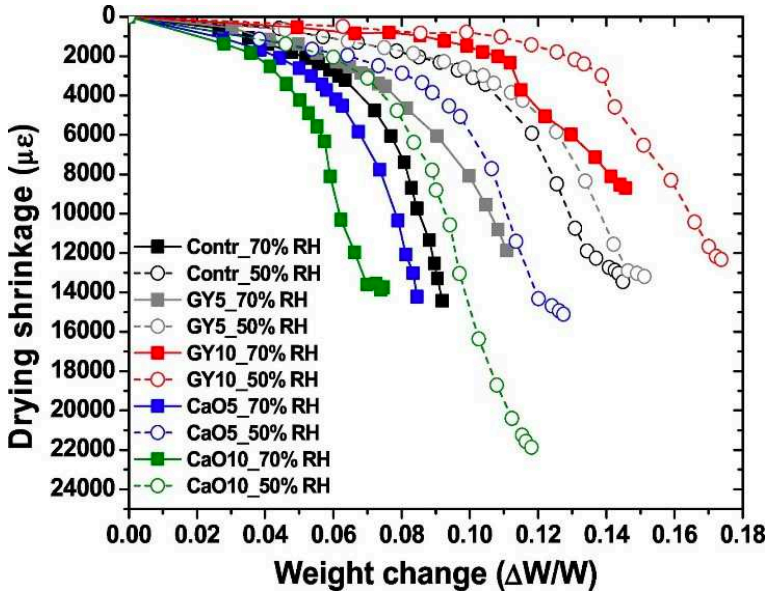

Figure 89 - Correlation between length and weigth changes for AAS with different levels of gypsum or CaO incorporation [243]

5.5 Applications

Several high-rise residential buildings were built in Lipetsk, Russia, using alkali-activated slag concrete between 1986 and 1994. The exterior walls of the buildings were cast in situ, and the floor slabs, stairways and other structural components were pre-cast, all using AAS concrete with water/binder ratio 0.35. Moreover, these concretes, in the form of pre-cast blocks, have been used for the construction of houses, garages, and other structures including two-storey and 15-storey apartment buildings in Mariupol, Ukraine [166].

In 1974 a storehouse was built in Krakow, Poland, using pre-cast steel-reinforced AAS concrete for the floor slabs and wall panels. This building has been monitored for many years. More than 25 years after its construction, cylindrical core samples were taken from the outside wall panels, and tested for compressive strength, carbonation depth and microstructure. Results indicated that there is a very significant increase in strength from 28 days to 27 years in all cases, as well as an average carbonation rate of less than 0.5 mm/year$^{1/2}$ in all samples. Finally, there was no evidence of micro-cracking, alkali-silica reaction problems, or steel corrosion after this extended period of time in service.

Two alkali-activated concrete roads built in Magnitogorsk, Russia, and in Ternopol, Ukraine, in 1984 were inspected in 1999. The road and basin built using AAS concrete were in very good condition, while those built using OPC concrete deteriorated seriously (Figure 90).

Figure 90 - Comparison of cast-in-situ AAS concrete (left) and OPC concrete (right) at Ternopol, Ukraine [166]

Around 40 AAS concrete pipes were prefabricate in 1965 and used to construct a 33 km long underground drainage collector along the sea bank in Odessa, Ukraine. The results on an examination after 34 years of service life confirmed that the AAS concrete pipes exhibited good durability. The compressive strength of the material had increased from 40 MPa to 62 MPa, the pH remained above 11.5, water absorption was less than 5% and there was no visual indication of corrosion of embedded steel bars.

In Orlyanka, Ukraine, several access roads were constructed to serve dairy farms by using precast, steam-cured reinforced AAS concrete panels. Field inspection after 18 years in service indicated that the part of the roads built using AAS concretes did not show any indication of deterioration, while the OPC concrete panels installed and inspected at the same times and serving under the same conditions showed evidently deteriorated concrete and exposed reinforcement.

In addition to applications in the building sector, alkali-activated slag cements are widely used for the production of foamed binders [130,244] and autoclaved aerated concrete for multipurpose applications. Furthermore, the intrinsic thermal resistance of AAS materials had led them to be considered for a range of high temperature applications, and in particular fire-proofing (e.g. coatings, fire resistant structural elements) [245–247].

Finally, AAS binders have been tested, and used in practice, for the soil stabilization [248,249] and the immobilization of a wide variety of wastes. Detailed reviews of the use of AAS materials in the treatment of toxic and radioactive wastes have been published [250–252].

5.6 Environmental issues

The environmental impact of alkali-activated materials remains an open debate, especially since they are presented as an alternative to Portland cement-based concrete as reported in Table 23.

Ref.	Reference OPC	Impact considered	Conclusions
[253]	Freeze-thaw resistant concrete	ADP, GWP, GER	Improvement on GWP, similar impact on ADP and GER
[254]	Equivalent strength class	10 indicators	GWP reduced, Higher impact in another category
[255]	100% OPC, OPC and slag, OPC and fly ash	GER, GWP and cost	Results depend on the transport distance and activators
[256]	100% OPC	GWP	Small improvement
[257]	100% OPC, OPC + SMCs	GWP	Favorable to AAS

Table 23 – Comparison of recent articles on the LCA of alkali-activated materials

Initially, Duxon et al. [25] affirmed that one of the primary advantages of AAS over traditional cements from an environmental point of view is the much lower CO_2 emission rate from alkali-activated binders compared to OPC production. This is mainly due to the absence of high temperature calcination step, whereas the calcination of Portland clinker not only consumes a large amount of fossil fuel-derived energy, but also releases CO_2 as a reaction product. While the use of an alkaline hydroxide or silicate activating solution rather than water for cement hydration does reintroduce some greenhouse gases (GHG) cost, the overall CO_2 saving due to widespread AAS utilization is expected to be highly significant. In particular, the authors estimated up to 80% reduction in CO_2 emission respect to Portland cement-based mixtures at equal strength class.

Other researcher [253] indicated that there is a potential for 25%-70% reduction in GHG emissions. Furthermore, McLellan et al. [255] have focused attention on the strong influence of the transport distances and the different alkaline activators production techniques, indicating that, depending on the source of supply, emissions from AAS concrete can be 97% lower up to 14% higher compared with emissions from OPC concrete.

Habert et al. [254] carried out a detailed environmental evaluation of AAS concrete production using the Life Cycle Assessment (LCA) methodology, highlighted that the production of most standard types of alkali-activated binder concrete has a slightly lower impact on Global Warming Potential (GWP) than traditional concrete (Figure 91).

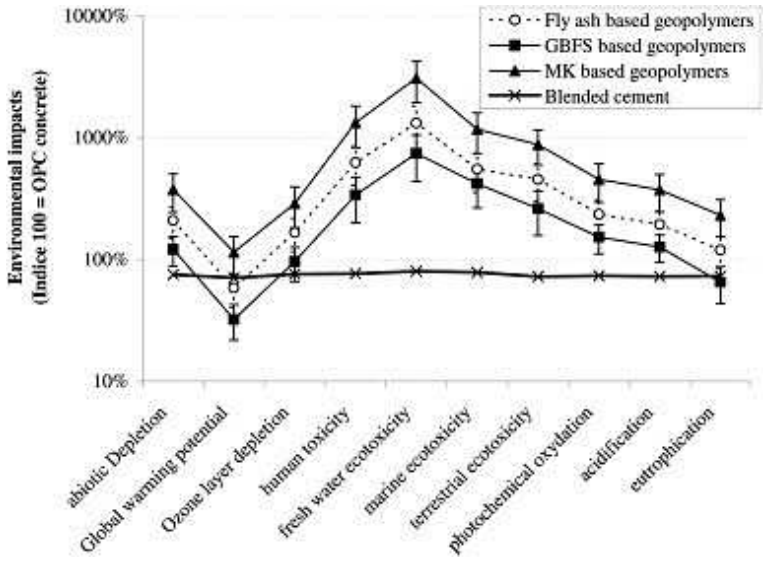

Figure 91 - Eco-profile of different concretes compared to OPC concrete [254]

The efficient use of a binder to reduce GHG emissions has been discussed by Damineli et al. [81]. The authors concluded that concrete efficiency should be defined in terms of the total binder consumption, total cost of concrete production and environmental impact. Considering the interrelation of the compressive strength of concrete, the total amount of binder and the environmental impact including CO_2 emissions, Damineli et al. proposed the use of two parameters (the binder intensity Bi and the CO_2 intensity Ci) in order to assess the binder's influence on CO_2 emissions.

$$Bi = \frac{B}{f'_c} \tag{22}$$

$$Ci = \frac{C_d}{f'_c} \tag{23}$$

where B is the total consumed amount of binder materials (kg/m^3), f_c' is the 28-day compressive strength of concrete (MPa), and C_d is the total CO_2 emissions (kg/m^3) resulting from the concrete production. Based on these coefficients, Yang et al. [257] demonstrated that the binder intensity of AAS concrete is an average of 1.67 times that of OPC concrete with the same compressive strength (Figure 92). This indicates that the AAS concrete requires a greater amount of binder in order to obtain the same strength as OPC concrete.

Conversely, the AAS concrete reveals a CO_2 intensity that is around 3.3 times lower than that of OPC concrete with the same strength class, even though the binder consumption is higher in alkali-

activated slag concrete than in OPC concrete (Figure 92). Authors concluded claiming that replacing Portland cement with alkali-activated slag cement can be regarded as a key approach for producing sustainable concrete.

Finally, Turner and Collins [256] showed different data than those available in the literature, estimating a 9% reduction in CO_2 footprint of AAS concrete respect to a comparable concrete manufactured with traditional Portland cement.

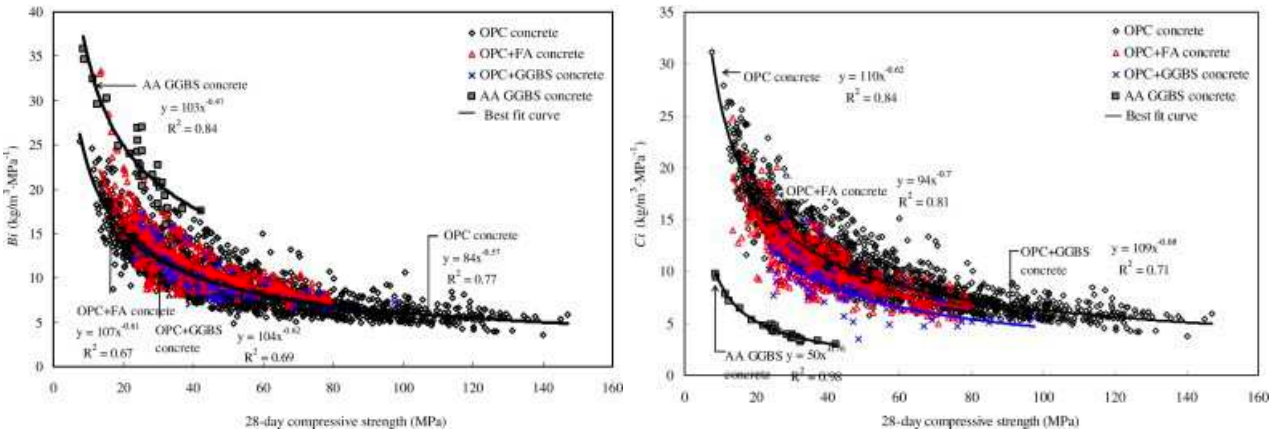

Figure 92 - Relationship between Bi (left) or Ci (right) and compressive strength of concrete [257]

6. Experimental research on AAS mortars

The aim of this part of the research is the production of mortars based on ground granulated blast furnace slag activated by a mixture of sodium metasilicate pentahydrate, potassium hydroxide and sodium carbonate in powder form for multipurpose applications, from plasters and renders to repair mortars for retrofitting and seismic upgrade of reinforced concrete elements.

6.1 Materials

Ground granulated blast furnace slag with 28-day pozzolanic activity index equal to 0.76 (according to UNI EN 15167-1 and EN 196-5) as precursor and alkaline powder as activator were used to produce different pastes and mortars with activator/precursor ratio between 2 wt.% and 32 wt.%. The alkaline agents were blends of sodium metasilicate pentahydrate, potassium hydroxide and sodium carbonate with relative mass ratio equal to 7 : 3 : 1, all of industrial grade. The maximum activator/precursor ratio was limited to ensure both environmental and economic sustainability. Moreover, potassium hydroxide was used instead of sodium hydroxide to reduce efflorescence in pastes and mortars, because potassium is more strongly bound to the aluminosilicate gel frameworks [258], and also because potassium carbonate crystals are usually less visually evident than their sodium counterparts [179].

The physical properties and the chemical and mineralogical composition of slag cement were investigated by means of laser granulometry (Mastersizer 3000 Malven Instruments Ltd), XRD analysis (Rigaku Miniflex 60, X-ray source Cu K-α (0.15418 nm), 40kV 15mA, θ step 0.02, rate 1°/min) and SEM-EDS measurements (Inspect, FEI company). The GGBFS particles have a specific mass equal to 3.13 g/cm^3, an average size of 12.42 μm and a specific surface equal to 345 m^2/kg (Figure 93). Moreover, the XRD pattern shows a typical amorphous hump around 25° and 35° 2θ that reflects the short-range order of CaO-Al_2O_3-MgO-SiO_2 glass structure as reported by Wang and Scrivener [259]. Furthermore, starting from the weight composition (Table 24) of GGBFS, the basicity coefficient Kb and quality coefficient Kq were calculated according to [297]:

$$K_b = \frac{CaO + MgO}{SiO_2 + Al_2O_3} = 1.20 \qquad (24)$$

$$K_q = \frac{CaO + MgO\ + Al_2O_3}{SiO_2 + TiO_2} = 1.77 \qquad (25)$$

Component	CaO	Al_2O_3	SiO_2	SO_3	Fe_2O_3	TiO_2	K_2O	MgO
wt.%	45.56	10.35	32.93	1.58	0.23	2.25	0.72	6.38

Table 24 – Chemical composition of GGBFS

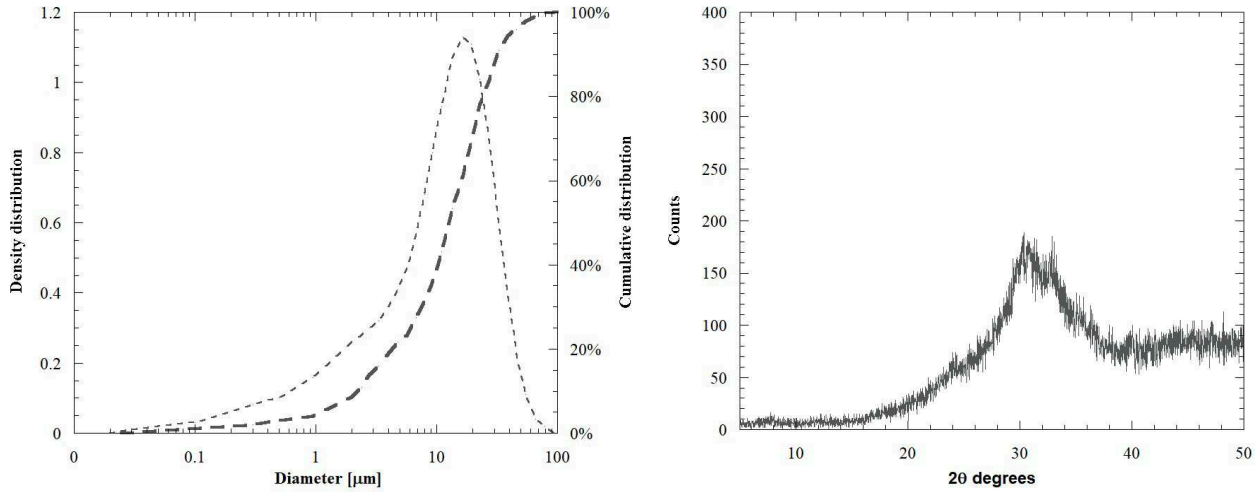

Figure 93 - Laser granulometry (left) and XRD pattern (right) of GGBFS

To manufacture alkali activated slag cement-based mortars, 5 different natural siliceous sand with maximum diameter equal to 2.5 mm were combined according to the ASTM C33 limits (Table 7, Figure 34). Moreover, tap water at 20°C was used to produce pastes and mortars.

6.2 Mix proportions

7 different AAS mixtures were prepared by varying the alkali content (Ac)

$$Ac = \frac{Na_2O + K_2O}{GGBFS} wt.\% \qquad (26)$$

between 0% and 15% (a/p: activator/precursor ratio between 0 and 32%) in order to investigate the rheological, microstructural, elasto-mechanical and physical properties of slag cement-based mixtures. The experimental tests were carried out on pastes (Sp, slag pastes) or mortars (Sm, slag mortars).

6.2.1 AAS pastes

The molar silica modulus (Ms)

$$Ms = \frac{SiO_2}{Na_2O + K_2O} \qquad (27)$$

and the water/precursor ratio (w/p) of pastes were kept constant at 0.48 and 0.30, respectively.

The composition of pastes is reported in Table 25.

6.2.2 AAS mortars

The molar silica modulus (Ms) and the sand/precursor ratio (s/p) of mortars were kept constant at 0.48 and 3, respectively. The water/precursor ratio was adjusted in order to attain the same workability at the end of the mixing procedure, equal to 160 mm ± 10 mm by means of a flow table.

The composition of mortars is reported in Table 26.

Composition [g]	Sp0	Sp2	Sp4	Sp8	Sp16	Sp24	Sp32
GGBFS	100	100	100	100	100	100	100
$Na_2SiO_3 \cdot 5H_2O$	-	1.26	2.52	5.04	10.08	15.12	20.16
KOH	-	0.54	1.08	2.16	4.32	6.48	8.64
Na_2CO_3	-	0.18	0.36	0.72	1.45	2.18	2.90
Water	30	30	30	30	30	30	30
Ms	-	0.48	0.48	0.48	0.48	0.48	0.48
Ac	-	0.0095	0.0190	0.0380	0.0750	0.1120	0.1500
w/p	0.30	0.30	0.30	0.30	0.30	0.30	0.30
a/p	-	0.02	0.04	0.08	0.16	0.24	0.32

Table 25 – Composition of AAS pastes

Composition [kg/m^3]	Sm0	Sm2	Sm4	Sm8	Sm16	Sm24	Sm32
GGBFS	475	475	475	475	475	475	475
$Na_2SiO_3 \cdot 5H_2O$	-	6.05	12.09	24.69	48.87	73.31	96.73
KOH	-	2.59	5.18	10.58	20.95	31.42	41.45
Na_2CO_3	-	0.86	1.73	3.53	6.98	10.47	13.82
Aggregate	1420	1420	1420	1420	1420	1420	1420
Water	280	275	275	255	240	220	205
Ms	-	0.48	0.48	0.48	0.48	0.48	0.48
Ac	-	0.0095	0.0190	0.0380	0.0750	0.1120	0.1500
w/p	0.59	0.58	0.58	0.53	0.50	0.46	0.43
a/p	-	0.02	0.04	0.08	0.16	0.24	0.32

Table 26 – Composition of AAS mortars

6.3 Experimental methods

Alkali activated pastes and mortars were prepared using a mixer with planetary motion in accordance with “Dry mixing method” proposed by Bayuaji et al. [260]. In particular, the mixing procedure followed five steps:

- The slag cement, alkali activators in powder or flakes and water are placed into the bowl;
- The mixer starts mixing at low speed for 30 seconds;
- The aggregates (if present) are added to the compound and mixing proceeds at high speed for 60 seconds;

- The mixing stops for 90 seconds;
- The mixing procedure is completed with a further 60 seconds at high speed.

6.3.1 Tests on AAS pastes

Workability was measured on pastes by means of flow table according to EN 1015-3. In addition, specific mass on fresh mixtures according to EN 1015-6 standard was evaluated. Specimens 40 x 40 x 160 mm^3 and 10 x 10 x 10 mm^3 were produced (Table 27), cured for 24 hours in steel mould covered by plastic films and stored in a climatic chamber at 20°C and R.H. 60%. Specific mass, compressive and flexural strength at 1, 7 and 28 days of pastes were also determined (EN 1015-11). Furthermore, dynamic modulus of elasticity was measured by means of Ultrasonic Digital Indicator Tester at 1, 7 and 28 days from casting (EN 12504-4). The tester gives the time value of the ultrasonic pulse through the specimens (in μs), then the velocity pulse value can be calculated by the following equation:

$$v = \frac{l}{t} \qquad (28)$$

with v: velocity of the ultrasonic pulse (m/s); l: length of specimen (m); and t: time of the sonic wave to go through the specimens (s). Knowing the velocity pulse, the dynamic modulus of elasticity (E_d) can be calculated by equation:

$$E_d = v^2 \rho \frac{(1+\gamma_d)(1-2\gamma_d)}{(1-2\gamma_d)} \qquad (29)$$

with E_d: dynamic modulus of elasticity (GPa); v: velocity of the ultrasonic pulse (m/s); ρ: specific mass at hardened state (kg/m^3) and γ_d: Poisson's modulus. The Poisson's modulus, equal to 0.20, was estimated as the mean value between 0.15 and 0.25, as reported in literature for alkali activated materials [261].

Test	Ages	Format	Number
Flexural and compressive strength	1-7-28 d	Beam 40x40x160 mm^3	9
Specific mass and E_d	1-7-28 d	Beam 40x40x160 mm^3	9
TGA and DSC	28 d	Cube 10 mm milled	2
XRD	1-2-7-28 d	Cube 10 mm milled	8

Table 27 – Paste's specimens manufactured for each mixture

X-ray diffraction (XRD), thermogravimetry (DSC and TGA) were used to determine the mineralogical composition of the solid phase. Prior to analysis, pastes were ground to a grain size < 63 μm.

The thermogravimetric analyses were done with a Netzsch STA 409, where about 10 mg of sample were placed in an open vessel under air, heating at 10°C/min up to 820°C.

XRD data were collected using a Rigaku Miniflex diffractometer in a θ-2θ configuration using an incident beam monocromator employing the Cu Kα radiation (λ = 1.5418 Å) in a range of 5°-50° (2θ) with a step size of 0.02° and a count time of 10 seconds for step.

6.3.2 Tests on AAS mortars

Workability, specific mass at fresh and hardened state, flexural and mechanical strength of AAS mortars were studied as reported in chapter 3. Moreover, the pot-life of the mixtures, corresponding the time during which workability by flow table is higher than 140 mm, was also detected. Dry shrinkage was measured over time on prismatic specimens stored 24 hours after the mixing in a climatic chamber at a controlled temperature and humidity (T = 20°C, R.H. = 60%) according to EN 12617-4. In addition, optical microscopy observations were performed on AAS mortars in order to evaluate the micro-cracking formation in binder paste. Finally, elastic modulus E_s (in accordance with method B, EN 12390-13) on 28-day cured cylindrical specimens was measured (Table 28).

Test	Ages	Format	Number
Flexural and compressive strength	1-7-28 d	Beam 40x40x160 mm^3	9
E_s	28 d	Cylinder, d:100 mm h/d:2	6
Free shrinkage	Up to 150 d	Beam 40x40x160 mm^3	3
Optical microscopy observation	28 d	Cube 10 mm	3

Table 28 – Mortar's specimens manufactured for each mixture

6.4 Microstructure and hydration products

Figure 94 presents the X-ray diffraction data collected from AAS pastes with Ms = 0.48 and Ac = 0.075 for up to 28 days of curing. Peak identification was difficult because of the overlapping of phase reflection. However, after a careful examination, the compounds considered present were included in Table 29.

The major X-ray crystalline phase identified corresponds to a calcium silicate hydrate (C-S-H). An increased intensity of the C-S-H peaks was observed at longer curing ages, probably form an increase in the degree of crystallinity or by an increased formation of such phase as reported in [262]. Moreover, hydrotalcite (Ht), tobermorite (Tb) and gehlenite (G) are also present in AAS pastes already after 2 days from casting. The observed assemblage of phases is in agreement with other articles related to GGBFS activated with sodium silicate [168,259,263]. The XRD patterns also show a relative strong contribution from non-crystalline fraction, as noted by the amorphous hump around

2θ = 25° - 35°, from the glassy unreacted GGBFS and silica gel, as well as from the compounds as the C-S-H gel [262]. In particular, after 1 day of curing, only the characteristic peak at 2θ = 29.7° of C-S-H was identified. On the contrary, already after two days from casting, it is possible to identify all the phases shown in Table 29.

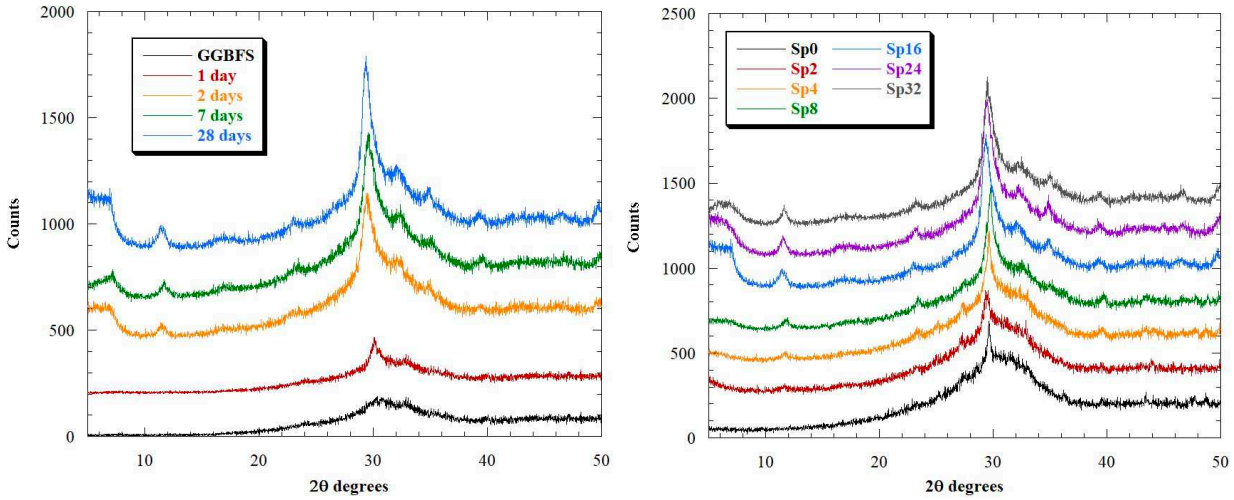

Figure 94 - XRD patterns of Sp16 samples at different ages of curing (left) and AAS pastes at 28 days (right)

2θ	Phase	Symbol	Reference
~ 7.4	C-S-H	CSH	[264]
~ 7.9	Tobermorite	Tb	[265]
~ 11.5	Hydrotalcite	Ht	[266]
~ 23.3	Hydrotalcite	Ht	[266]
~ 29.7	C-S-H	CSH	[264]
~ 31.3	Gehlenite	G	[267]
~ 31.9	C-S-H	CSH	[264]
~ 31.9	Tobermorite	Tb	[265]
~ 34.7	Hydrotalcite	Ht	[266]
~ 39.0	C-S-H	CSH	[264]
~ 39.0	Hydrotalcite	Ht	[266]
~ 49.8	C-S-H	CSH	[264]
~ 49.8	Tobermorite	Tb	[265]

Table 29 – X-ray diffractometry data for identification of main peaks

In general, it is possible to observe that the phases identified by the XRD analysis are perfectly compatible with the models proposed by Haha et al. [173,268]. In particular, by activating with alkali a GGBFS with a content of alumina and magnesium oxide equal to 10.35% and 6.38%, respectively, the thermodynamic models (Figure 95) provide for the formation of high amount of calcium silicate hydrates accompanied by hydrotalcite. On the contrary, the model provides the formation of traces of strätlingite, not identifiable in the XRD patterns.

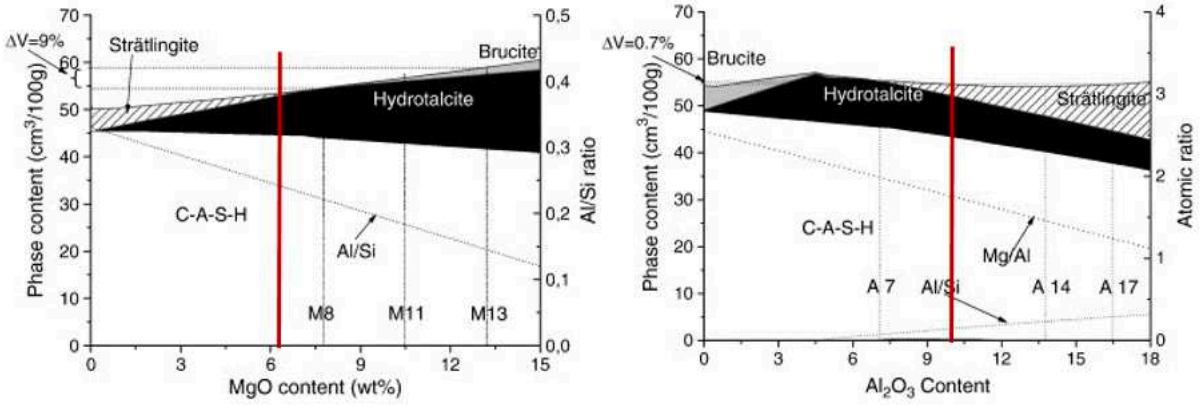

Figure 95 - Influence of MgO content (left) and alumina content (right) on the hydrates present in AAS [173,268]

Figure 94 illustrates X-ray diffractograms of AAS pastes with various alkali content (Ac), after 28 days of curing at 20°C. All the samples show formation of C-S-H, in agreement with previous report for similar systems [263,269]. The C-S-H peak intensity increased with higher alkali content within the system, consistent with the higher degree of reaction identified by termogravimetric analysis and elasto-mechanical tests discussed in the next paragraphs.

Furthermore, peaks of a hydrotalcite-type phase were also identified when Ac is greater than 0.0095 while tobermorite and gehlenite are present in pastes with Ac = 0.0750 ÷ 0.1500. This is in agreement with Song and Jennings [270], who have reported that hydrotalcite apparently forms when a high degree of slag hydration is reached. On the other hands, the mixing of GGBFS with water only determines the formation of small amounts of C-S-H as also reported by Park et al. [271].

The thermograms (TGA and DTA) of alkali activated slag pastes with various Ac at 28 days from casting are shown in Figure 96. A high mass loss between 30°C and 120°C is observed for all the samples, attributed to the release of evaporable water. In particular, the total mass loss up to 120°C increases from 3% for the pastes activated with Ac = 0.0095 to 9% for the pastes with Ac greater than 0.1120. The exception is the paste Sp0 manufactured without activators, which is totally anhydrous.

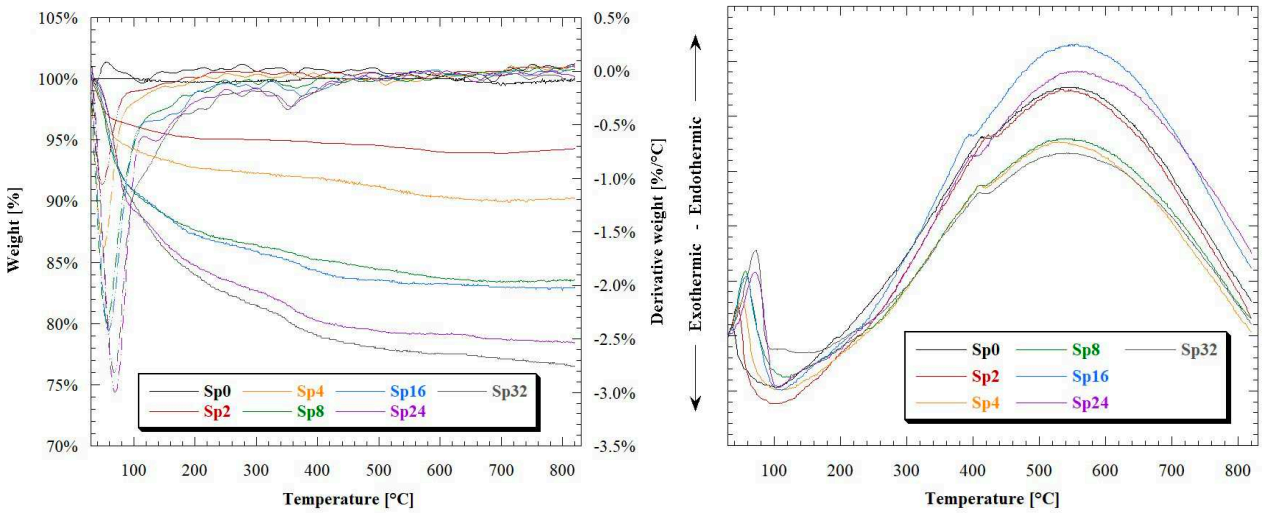

Figure 96 - Thermograms (left) and DSC results (right) of AAS pastes at 28 days from casting

The nonevaporable water (NEW) provides a semiquantitative indicator for the reactivity of the slag as indicated by Escalante-Garcia et al. [168,272]. In particular, NEW was estimated by means of thermal analysis as:

$$NEW = 100 \cdot \frac{(weight_{120°C} - weight_{280°C})}{weight_{280°C}} \qquad (30)$$

Figure 97 presents the results of NEW for AAS pastes at different alkali content (Ac). As reported by Escalante-Garcia et al. [168], the increase in concentration of activators (expressed as an increase in Ac) resulted in higher NEW values and strong activity at 28 days from casting. In particular, the bound water content obtained by measuring the weight loss between 120°C and 180°C using TGA is related with the dehydration of C-S-H [273] while the weight loss between 300°C and 400°C is assigned to the decomposition of hydrotalcite [274].

Similarly to NEW, it is possible to estimate two parameters related to the CSH and HT content of alkali-activated slag pastes according to the following equations:

$$CSH_{content} = 100 \cdot \frac{(weight_{120°C} - weight_{180°C})}{weight_{180°C}} \qquad (31)$$

$$Ht_{content} = 100 \cdot \frac{(weight_{300°C} - weight_{400°C})}{weight_{400°C}} \qquad (32)$$

The increase in mass loss related to decomposition of both C-S-H and hydrotalcite (Figure 97) confirms that a higher concentration of the activator promotes the formation of a larger amount of reaction products, consistent with the escalation of hydrated products formation as observed in the XRD results. However, unlike XRD measurements, termogravimetric analysis seem to show the presence of small amounts of hydrotalcite even in AAS pastes with low alkali content. The DSC analyses reported in Figure 96 show an endothermic peak due to the evaporation of free water at

temperatures below 100°C and an endothermal effect in the range of 380 – 400°C related to the decomposition of hydrotalcite [275] The results obtained are in agreement with the thermogravimetric analyses and X-ray diffractions.

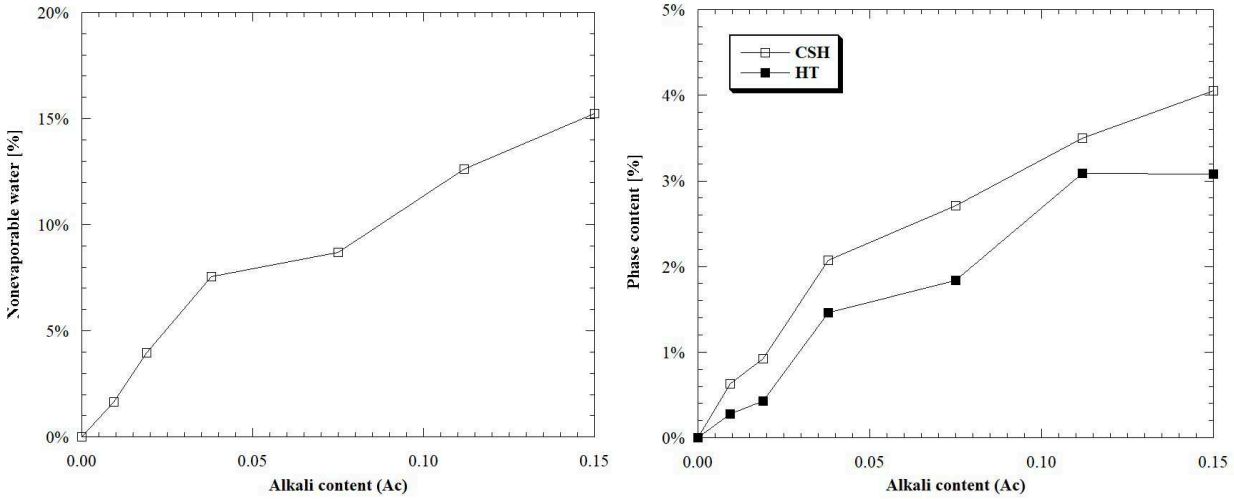

Figure 97 - Non-evaporable water NEW (left) and coefficients related to the phase content (right) vs alkali content (Ac) at 28 days

6.5 Fresh properties

The workability of the AAS pastes is strongly influenced by the alkali content. Figure 98 shows that increasing the alkali content through the addition of growing amounts of activators, the consistency of AAS pastes increases at equal water content. In particular (Table 30), the non-activated or weakly alkali activated pastes exhibits a thixotropic consistency (about 150 mm spreading by flow table) while greater dosages of alkaline powders allow to obtain high flowable pastes (spread higher than 200 mm).

	Sp0	Sp2	Sp4	Sp8	Sp16	Sp24	Sp32
Workability [mm]	140	150	170	180	200	240	250
Specific mass (fresh) [kg/m^3]	2010	2015	2025	2040	2050	2060	2090
Specific mass (hardened) [kg/m^3]	1950	1970	1985	2010	2025	2045	2085

Table 30 – Fresh properties of AAS pastes (w/p: 0.30)

The role of alkaline activators on fresh behavior of AAS mixtures is evident also in mortars (Table 31 and Figure 98). In fact, the amount of mixing water to achieve 160 mm spreading depends on the alkali content. This behavior is in accordance with Kashani et al. [276] that explain the plasticizing and deflocculating effects of sodium silicate on alkali-activated slag-based mixtures with the

increasing of the magnitude of repulsive double layer electric forces, causing the reduction in the yield stress at early ages.

	Sm0	Sm2	Sm4	Sm8	Sm16	Sm24	Sm32
w/p	0.59	0.58	0.58	0.53	0.50	0.46	0.43
Specific mass (fresh) [kg/m^3]	2170	2185	2185	2220	2240	2250	2280
Specific mass (hardened) [kg/m^3]	1940	2040	2070	2165	2195	2240	2275
Pot-life [min]	>360	60	60	45	45	35	30

Table 31 – Fresh properties of AAS mortars (workability: 160 ± 10 mm)

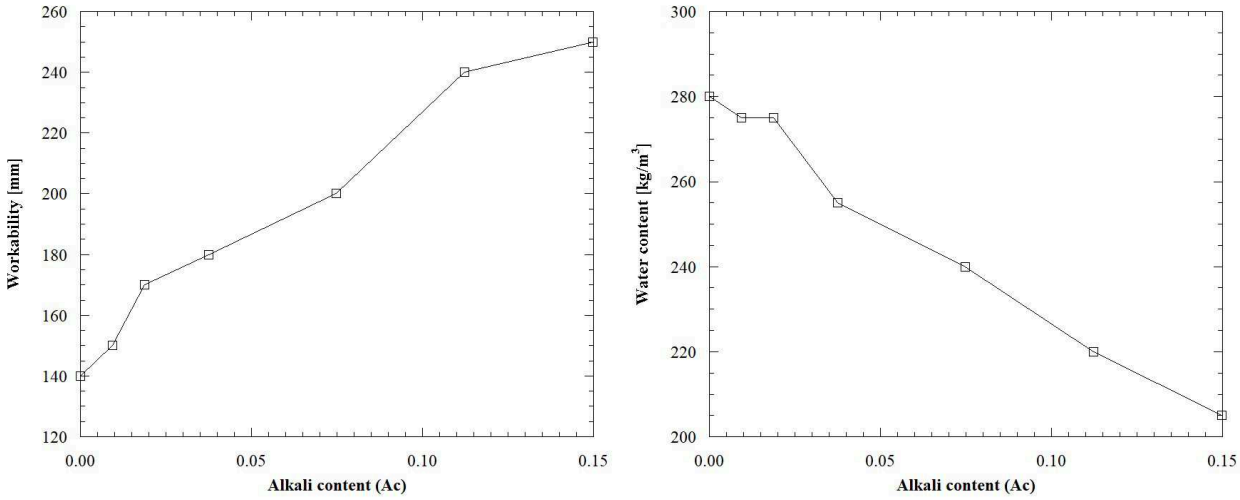

Figure 98 - Workability of AAS pastes (left) and mixing water of AAS mortars (right) vs alkali content (Ac)

Pot-life of non-activated mortar (Sm0) is dramatically shortened to 30 – 60 min from casting when the activator is added (Figure 99). The reduction of setting time is in agreement with Huanhai et al. [169] and Chang [185] that show as increasing the alkali content (Ac) increases the released heat and shortens the peak time. In fact, a higher concentration of activator helps the resolution of calcium ions from the slag grains and consequently increases the reaction rate. In particular, Zivica [277] has shown the crucial role of sodium silicate in the reduction of setting times in AAS-pastes.

The density of AAS-pastes and mortars is also significantly influenced by the alkali content Ac of the solid phase activators (Figure 99). In fact, the specific mass of pastes both at fresh and hardened state grows by increasing the alkali content, growing from 2010 kg/m^3 to 2090 kg/m^3 at fresh state and from 1950 kg/m^3 to 2085 kg/m^3 at hardened state. It is also evident that the water loss during the first 28 days, taken equal to the difference between the fresh and hardened density, decreases with the increase of activator content. This behavior could be ascribed to the nonevaporable water (NEW)

detected by thermogravimetric analyses (Figure 97) that grows by increasing the alkali content of pastes.

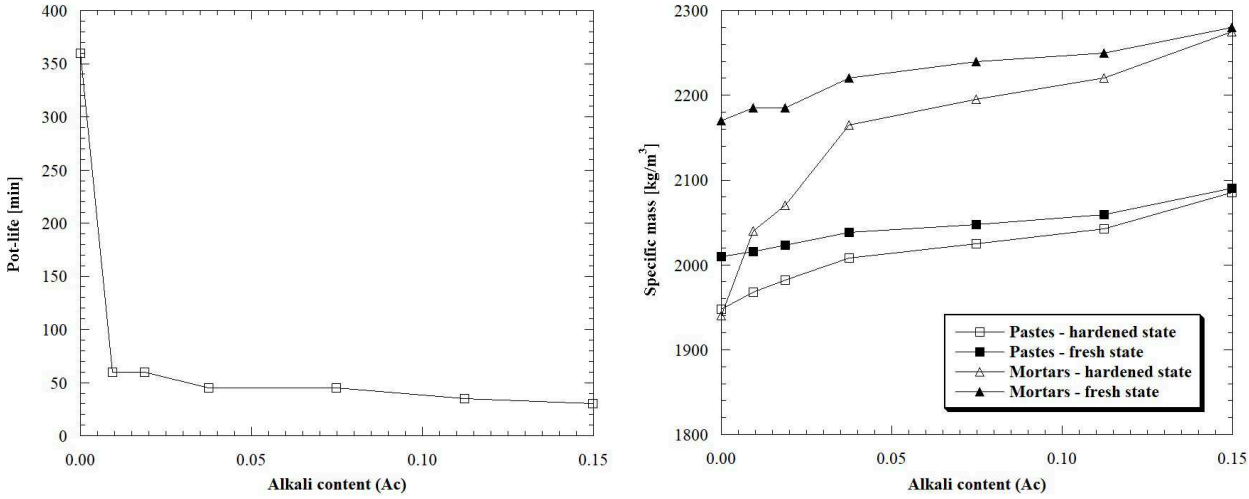

Figure 99 - Pot-life (left) and specific mass at fresh and hardened state (right) of AAS pastes and mortars vs alkali content (Ac)

6.6 Hardened state properties

Compressive and flexural strength are strongly influenced by the alkali content. In particular, after 24 hours, no-activated pastes were not enough hardened to measure mechanical properties (Table 32). On the contrary, the addition of alkaline activators in powder form allows to obtain pastes of excellent mechanical properties, already after 1 day from mixing. In particular, the compressive strength reaches values close to 50 MPa at early ages, achieving 28-day compressive strength up to 100 MPa (Figure 100). Also the modulus of elasticity is strictly related with the dosage of the activators.

		Sp0	Sp2	Sp4	Sp8	Sp16	Sp24	Sp32
Flexural strength [MPa]	1 d	-	0.14	1.45	3.05	4.05	3.38	3.73
	7 d	0.45	1.15	2.18	4.19	5.21	4.88	4.91
	28 d	0.70	1.33	2.92	4.36	5.39	5.03	5.12
Compressive strength [MPa]	1 d	-	0.13	11.43	28.40	42.81	49.59	46.31
	7 d	3.94	15.90	30.59	49.88	64.44	59.28	58.72
	28 d	7.33	26.08	46.24	76.89	102.07	87.58	85.18
Elastic modulus [GPa]	1 d	-	-	13.3	18.0	20.8	20.8	21.1
	7 d	1.9	13.8	18.2	21.7	22. 8	22.3	23.1
	28 d	6.2	17.0	21.3	25.4	26.1	25.1	25.3

Table 32 - Elasto-mechanical properties of AAS pastes

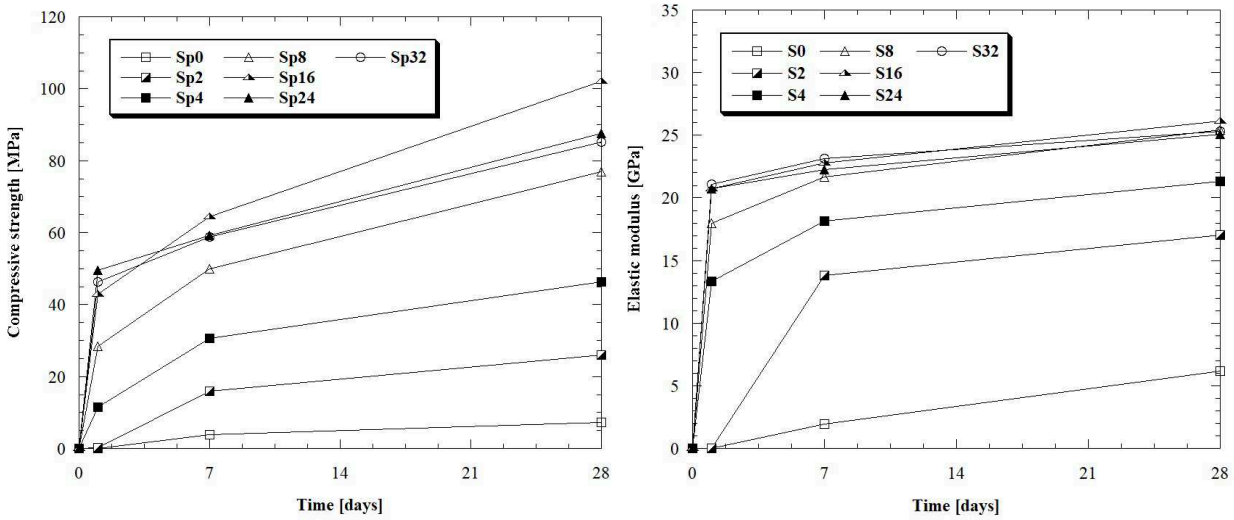

Figure 100 - Compressive strength (left) and dynamic modulus of elasticity (right) of AAS pastes vs time

Figure 101 shows the effect of alkali content Ac on compressive strength and Young's modulus of pastes at different ages. As seen, the strength increases at relatively lower alkali content, i.e. in the range between 0 and 0.075, while is almost constant or slightly decreasing at relatively higher alkali content, i.e. for Ac greater than 0.075. This behavior depends on the action of the different activators used during the production of AAS-pastes.

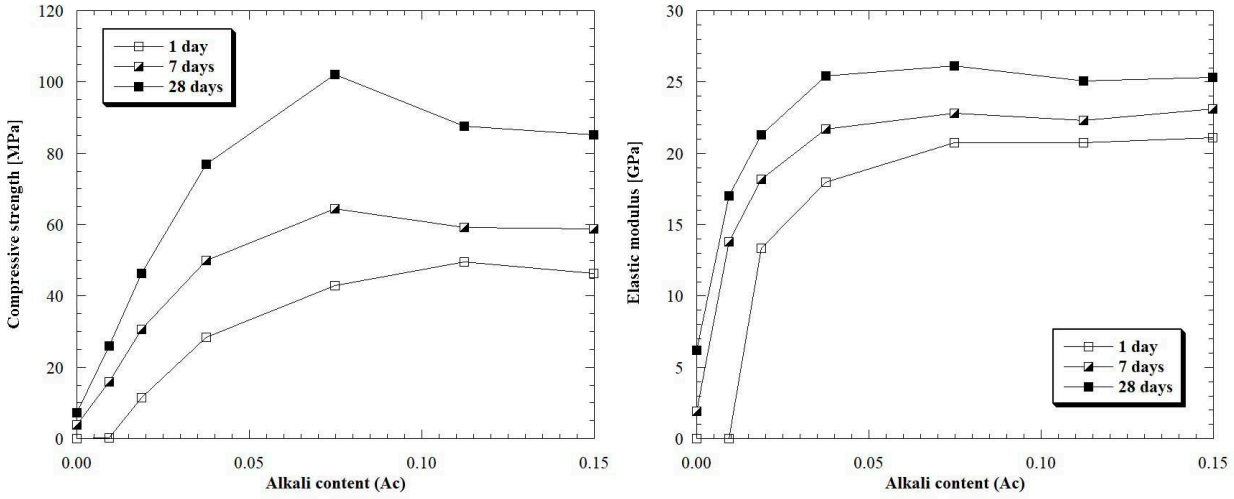

Figure 101 - Compressive strength (left) and dynamic modulus of elasticity (right) of AAS pastes vs alkali content (Ac)

Indeed, all the activators play important roles in geopolymerization reactions. Potassium hydroxide provides both hydroxide anion (OH^-) which is very important for the dissolution of the aluminosilicates in the first stage [278] and alkali cation (K^+) which is important for charge balance of the aluminosilicate network formed in the last stage [269]. As reported by Tang and Su-Fen [279],

solubility of aluminosilicate increases with increasing OH- concentration. Utilization of too much potassium hydroxide in preparation of alkali-activator, however, is not beneficial due to the high alkalinity that hinders the process of dissolution of the GGBFS [262]. Sodium silicate also provides good interparticle bonding and therefore mechanical strength of the material by synthetizing CSH gel as explained by Lecomte et al. [280]. Sodium carbonates promote the development of highly cross-linked structured CSH gel and form precipitates along with carbonate salts [177,281].

Compressive and flexural strength tests were also carried out on mortars (Table 33 and Figure 102). After 24 hours from casting, mortars activated with an activators dosage lower than 8% were not enough hardened to perform the mechanical tests. Similarly to AAS-pastes, flexural and compressive strength are strictly related with the dosage of the activator. Independently of the age (1, 7, 28 days), the higher the alkali content the stronger mechanically is the mortar (Figure 102). 28-day compressive strength was 6.72 MPa and 63.65 MPa for the no-activated mortars and the mixture containing 32% of activator by mass, respectively.

		Sm0	Sm2	Sm4	Sm8	Sm16	Sm24	Sm32
Flexural strength [MPa]	1 d	-	-	-	1.21	2.90	3.18	4.68
	7 d	1.08	3.21	3.98	4.03	6.29	6.45	6.63
	28 d	1.24	3.45	4.04	4.38	6.47	6.61	6.74
Compressive strength [MPa]	1 d	-	-	-	4.41	13.83	21.37	27.93
	7 d	3.74	13.31	18.10	34.18	49.69	52.83	55.84
	28 d	6.72	19.16	26.35	46.17	62.81	61.49	63.65

Table 33 – Mechanical strength of AAS pastes

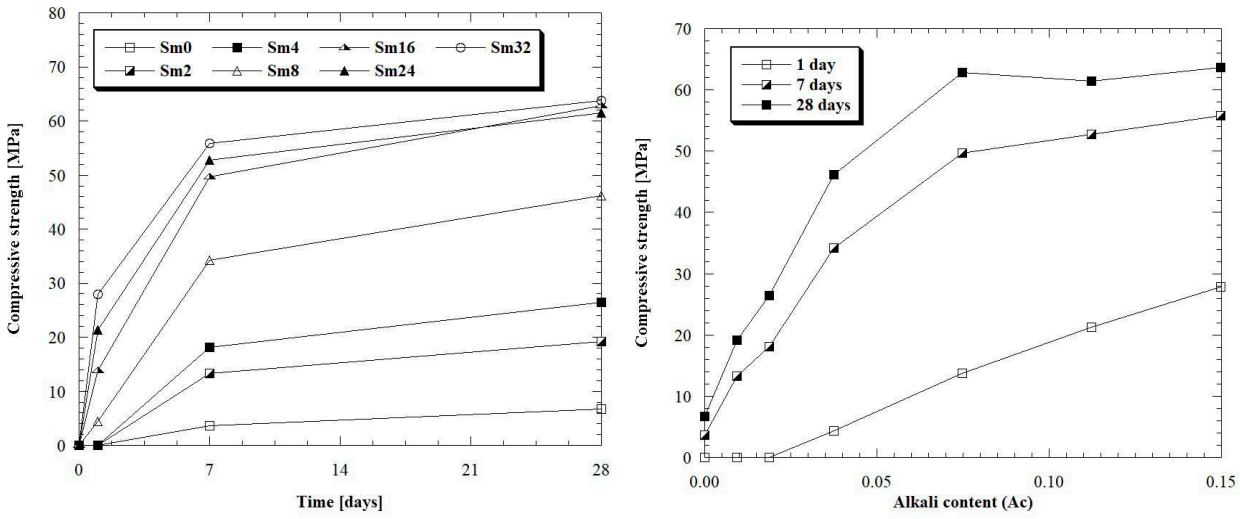

Figure 102 - Compressive strength of AAS mortars vs time (left) and vs alkali content (right)

In other words, it is therefore possible to tailor the compressive strength of AAS-mortars through the dosage of activator. Specifically, no-activated mortar can be used for plasters and renders (28-day compressive strength of about 5 MPa). Weakley AAS mortars (2 – 4%) exhibit compressive strength values specified for seismic retrofitting of masonry buildings (strength between 15 and 25 MPa after 28 days). Higher dosage of the activators (≥ 8% by GGBFS mass) allows to manufacture mixtures devoted to structural and/or "cosmetic" repair of existing reinforced concrete elements (Figure 103).

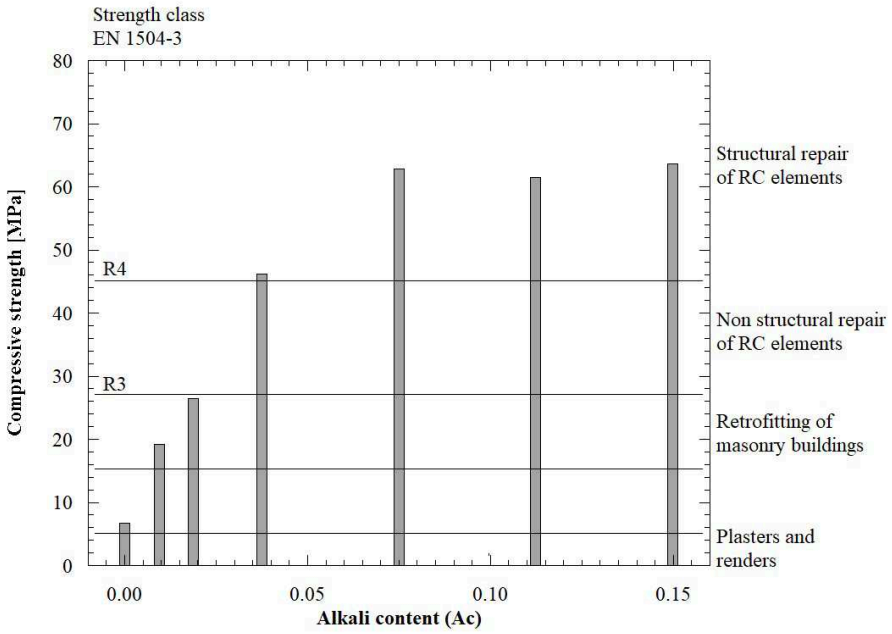

Figure 103 - Applications of AAS mortars

Shrinkage tests were performed up to 150 days on mortar specimens at 20°C and R.H. 60%. Figure 104 shows very high free shrinkage of AAS mortars compared to mixtures manufactured with traditional binders. This phenomenon is due to the different porosity of slag-based mixtures compared to traditional cement pastes [282,283].

Indeed, alkali-activated slag pastes have a much higher proportion of pore size within mesopore region than OPC pastes. Further, the radius of pore where the meniscus forms is smaller for AAS than OPC pastes, in accordance with the theory that capillary tensile forces set up during drying is a very significant factor for the drying shrinkage of alkali-activated slag materials [196].

In addition, it is possible to note that shrinkage is also influenced by the dosage of alkaline activators. Mortar manufactured with 2% of activators by precursor mass shows free shrinkage equal to 2000 μm/m at 150 days from casting while mixtures with 32% of activator by slag mass experienced a contraction equal to 4500 μm/m at 150 days. Given the considerable shrinkage, Jennings [284]

proposed to treat the C-S-H formed in AAS as a gelled colloid or granular material with micro-defects instead of a continuous porous material.

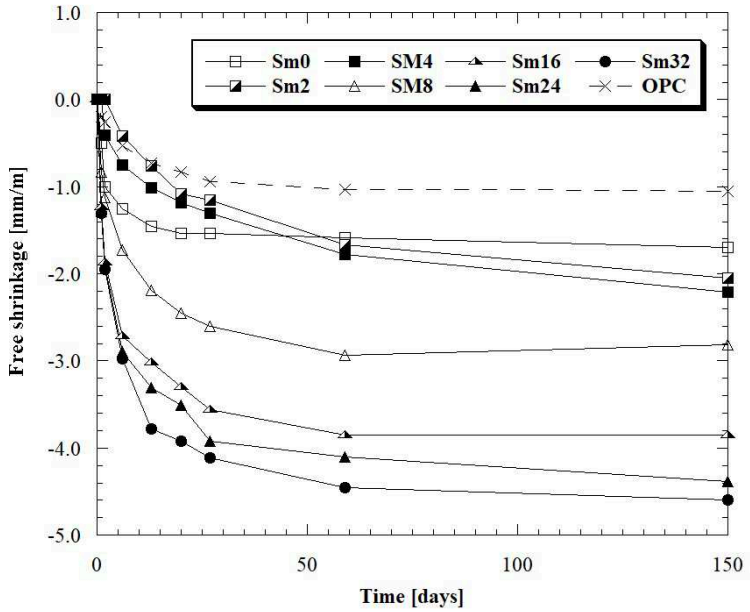

Figure 104 - Free shrinkage over time of AAS mortars

Considering the granular nature, the visco-elastic/visco-plastic shrinkage performance of AAS can be attributed to the time-dependent rearrangement and redistribution of C-S-H nanoparticles under the capillary stress [285]. Therefore, the shrinkage of AAS at R.H. greater than 50% is basically a results of denser nanoparticle packing, which in principal will result in collapse of gel pores and refinement of pore structured as reported by Ye and Radlinska [195]. Moreover, several authors [192,193] showed that during drying-induced microstructural rearrangement, considerable chemical (e.g. silicate polymerization, chain length elongation) and physical (e.g. micropore closure, interlayer formation and sliding) modification occur in alkali activated slag-based materials. In particular, the large shrinkage in AAS may be attributed to the structural incorporation of alkali cations (Na^+ and K^+) in C-S-H, which reduces the stacking regularity of C-S-H layers and make the C-S-H easier to collapse and redistribute upon drying. For these reasons, the use of high alkali activator dosages increases the sodium and potassium content in C-S-H structure and promotes the development of high shrinkage.

On the other hand, Chen et al. [286] demonstrated that the mechanical properties of cementitious materials are strongly associated with the dispersed inclusion (e.g. unhydrated particles, crystals). Previous calculations have shown that the existence of nano-sized portlandite considerably increases the stiffness of OPC pastes. This can partially account for the lower stiffness and enlarged shrinkage in AAS, due to its limited amount of calcium hydroxide [287].

As far as elastic modulus, results indicated that stiffness of AAS-based materials is significantly lower compared to ordinary Portland cement mortars manufactured with the same aggregates, at equal strength class (Figure 105). These results are in agreement with Thomas et al. [190] which explain the reduction of Young's modulus as a consequence of the high shrinkage of AAS mortars which causes micro-crack formation.

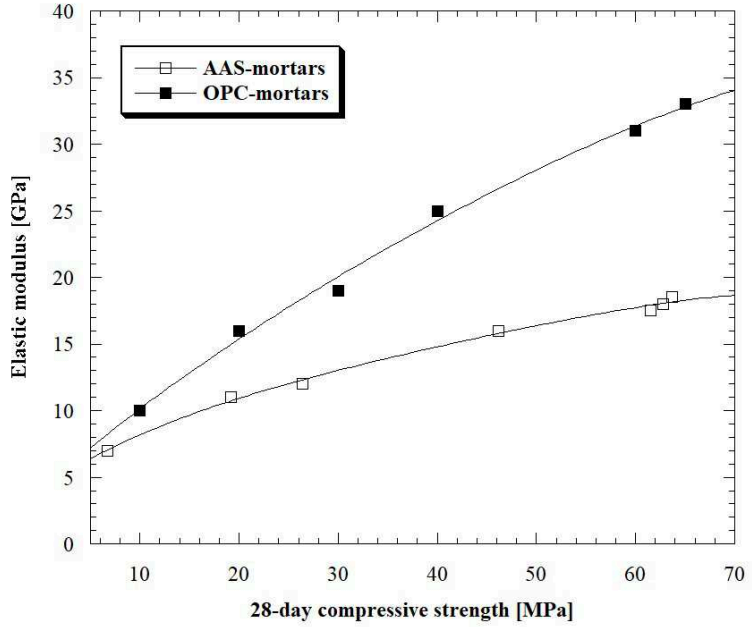

Figure 105 - Elastic modulus as a function of compressive strength

The presence of micro-cracks is confirmed by observation under optical microscope on a thin section. In fact, OPC-based matrix is dense and compact while AAS-mortars show several cracks in binder paste (Figure 106).

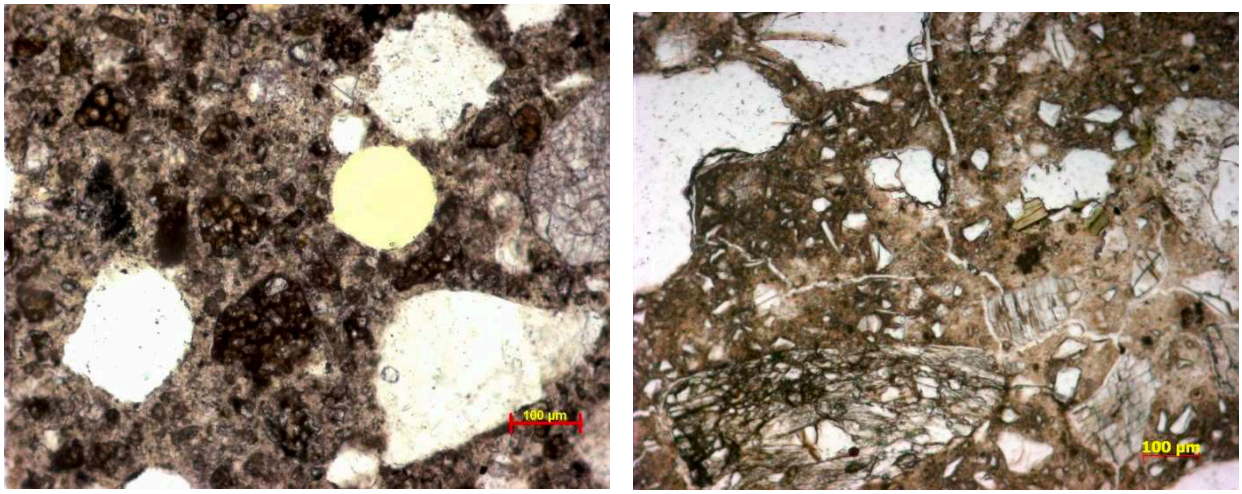

Figure 106 - Optical microscope observation of OPC-based mortars (left) and AAS-based mortar Sm16 (right)

Low alkali content determines a modulus of elasticity ranging from 10 GPa and 15 GPa, while higher alkaline powders dosages cause an increase in compressive strength and, consequently, elastic modulus grows up to 20 GPa (Figure 105). Since, elastic modulus is significantly lower than that of OPC-based mortars, tensile stress induced by restrained shrinkage could still be low, preventing the AAS from cracks and detachments.

6.7 Environmental parameters

Scientific literature condemns that the use of alkali-activated binders gives enormous benefits from the environmental and ecological point of view [244,288,289]. For this reason, two fundamental parameters were analyzed: GWP (Global Warming Potential) and GER (Gross Energy Requirement). In particular, the environmental impact of slag-based mortars was calculated on the basis of the data shown in Table 34 and compared to that of OPC mortars at equal 28-day strength class (Table 35).

	GER [MJ/kg]	**GWP [Kg CO_2/kg]**
CEM I 52.5 R	5.5	$9.8 \cdot 10^{-1}$
GGBFS	0.31	$1.7 \cdot 10^{-2}$
Aggregates	0.13	$2.4 \cdot 10^{-3}$
Sodium metasilicate	10.58	1.24
Potassium hydroxide	20.50	1.94
Sodium carbonate	7.23	2.20

Table 34 - Environmental parameters of raw materials. Source: Ecoinvent 3.0 Database

28-day strength		**GER**		**GWP**	
		[MJ/kg]	**[% vs OPC]**	**[Kg CO_2/kg]**	**[% vs OPC]**
25 MPa	OPC	2374	-	395	-
	Sm4	541	23%	38	10%
45 MPa	OPC	3314	-	566	-
	Sm8	774	23%	66	12%
65 MPa	OPC	3906	-	674	-
	Sm16	1242	32%	120	18%

Table 35 – Parameters GER and GWP of mortars at the same 28-day strength class

It is possible to observe how, at the same compressive strength, 80 – 90% and 70 – 80% reduction in greenhouse gas emission and energy production, respectively, can be achieved compared to mortars produced with Portland cement (Figure 107).

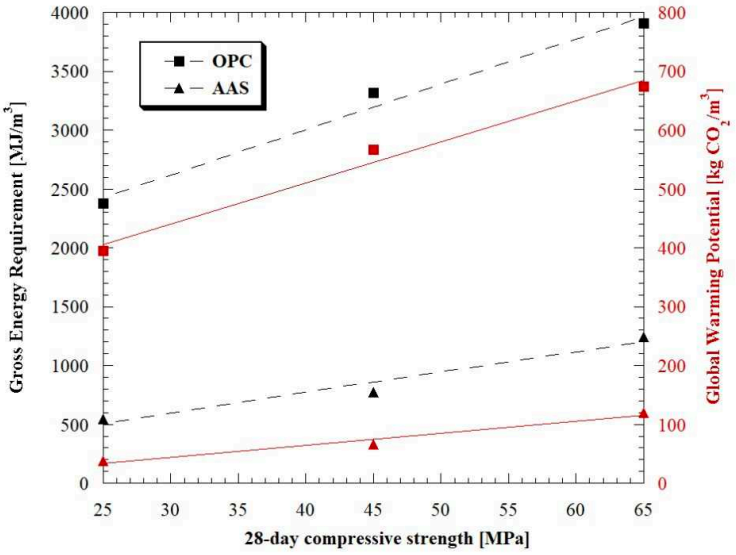

Figure 107 - GER (black line) and GWP (red line) of Portland cement mortars and AAS mortars as a function of compressive strength

6.8 Conclusions

In this chapter, performances of alkali-activated binder based on ground granulated blast furnace slag (GGFBS) were evaluated in terms of rheological and physical properties.

Experimental results indicated that:

- The key parameter that regulates most of the properties both in fresh and hardened state of alkali-activated compounds is the alkali content Ac;
- The main hydration product is a calcium silicate hydrate (C-S-H). Minor amount of hydrotalcite, tobermorite and ghelenite was also identified;
- The C-S-H peak intensity increased with higher alkali content within the system, consistent with the higher degree of reaction identified by termogravimetric analysis and elasto-mechanical tests;
- The higher the alkali content, the lower is the water demand at equal workability class due to the effect of sodium silicate-slag particles interaction;
- A higher concentration of activator increases the reaction rate, sharply reducing the setting time of mortars from 6 hours to 30 minutes;
- Slag without activator evidences compressive strength required for plasters and renders. When the dosage of the activator is in the range 2-4% by precursor mass, mortars exhibit compressive strength values specified for seismic retrofitting of masonry buildings. Alkali content equal to about 0.04 allows to manufacture mixtures specifically indicated for structural and/or “cosmetic” repair of existing reinforced concrete elements. No significant benefits are observed in increasing the alkali content by more than 0.075 due to the high alkalinity that hinders the process of dissolution of the GGBFS;

- Shrinkage values for AAMs are significantly higher (2000 – 4000 μm/m at 150 days from casting) compared to that of a cement-based mortars with the same compressive strength. Moreover, the higher the activator/precursor ratio, the higher the shrinkage due to the different porosity and density of AA slag matrix by varying the activators dosage;
- The modulus of elasticity is about 40% lower than that of a cementitious mortar (at the same strength level) due to the micro-cracking formation caused by shrinkage;
- At the same 28-day compressive strength, AAMs evidence 80 – 90% and 70 – 80% reduction in greenhouse gas emission and energy production, respectively, compared to mortars produced with Portland cement.

In conclusion, from the analysis of the strengths and weaknesses of alkali-activated binders, it turns out that alkali-activated mortars and concretes seem to be a reasonable alternative to natural hydraulic lime-based and/or traditional Portland cement-based mixtures for rehabilitation or restoration of ancient masonry buildings and existing concretes structures.

7. Shrinkage mitigation strategies for AAS mortars

Tests on shrinkage of AAS-based mixtures have been widely carried out in the last years both on pastes and on mortars [31,158,184,194,195]. In general, drying shrinkage of AAS-materials is at least twice as much as for OPC concrete and the difference tends to be higher as the age of concrete increases. Several studies on shrinkage of alkali-activated slag tried to develop an understanding of the mechanism of shrinkage as well as other properties of AAS. The parameters studied include the types, dosage and combination of activators [192], the use of admixtures and additives [204,234,241,243,290], the type of aggregate and the curing conditions.

One possible way to improve the properties of AAS materials is through the use of admixtures and additives. Bakharev et al. [232] showed that the use of air-entraining agent, water reducers and shrinkage reducing admixtures at proper dosage could significantly reduce the shrinkage of AAS concretes. Moreover, also the addition of Portland cement or gypsum can reduce the contraction of slag-based mixtures [243,290]. Finally, also the addition of highly reactive MgO considerably reduces the shrinkage, but more cracks are generated when magnesium oxide dosage is higher than 5% by slag mass [291].

Curing conditions play an important role in the properties of AAS materials. In particular, heat curing or steam curing was found to be effective in reducing the drying shrinkage of slag-based mortars.

The purpose of this chapter is to evaluate the effect of the addition of different admixtures on the properties of AAS pastes and mortars at equal alkali content and silica modulus.

7.1 Materials and methods

Several AAS pastes and mortars were manufactured by using the raw materials and according to the procedure reported in the previous chapter. In order to reduce the shrinkage of alkali-activated slag-based materials, methylcellulose (MC), modified starch (MS), polypropylene fibers (length 6.5 mm, aspect ratio 200), CaO-based expansive agent (EA) and shrinkage reducing admixture (SRA) were added to paste Sp16 and mortar Sm16 (Table 36). The mix design is reported in Table 37 and 38.

Property	MC	MS	EA	SRA	Fibers
Composition	Hydroxy-propyl cellulose	Hydroxy-propylated starch	Calcium oxide (CaO > 93%)	Ethylene glycol	Polypropylene
Specific mass [g/cm^3]	1.39	1.30	3.35	0.95	0.91

Table 36 – Properties of admixtures

Composition [g]	Sp16	Sp16 M	Sp16 ME	Sp16 MS	Sp16 MES
GGBFS	100	100	100	100	100
$Na_2SiO_3 \cdot 5H_2O$	10.08	10.08	10.08	10.08	10.08
KOH	4.32	4.32	4.32	4.32	4.32
Na_2CO_3	1.45	1.45	1.45	1.45	1.45
Water	30	30	30	30	30
MC	-	0.35	0.35	0.35	0.35
MS	-	0.11	0.11	0.11	0.11
EA	-	-	3.50	-	3.50
SRA	-	-	-	1.50	1.50

Table 37 – Composition of AAS pastes with shrinkage reducing admixtures

Composition [kg/m^3]	Sm16	Sm16 M	Sm16 ME	Sm16 MS	Sm16 MES
GGBFS	480	480	480	480	480
$Na_2SiO_3 \cdot 5H_2O$	48.87	48.87	48.87	48.87	48.87
KOH	20.95	20.95	20.95	20.95	20.95
Na_2CO_3	6.98	6.98	6.98	6.98	6.98
Aggregates	1445	1445	1445	1445	1445
Water	240	240	240	240	240
MC	-	0.60	0.60	0.60	0.60
MS	-	0.20	0.20	0.20	0.20
EA	-	-	55.00	-	55.00
SRA	-	-	-	7.00	7.00
Fibers	-	4.00	4.00	4.00	4.00

Table 38 – Composition of AAS mortars with shrinkage reducing admixtures

Workability, specific mass at fresh and hardened state, flexural and mechanical strength of AAS pastes and mortars were studied as reported in the previous chapter. Dry shrinkage was measured over time on prismatic specimens stored 24 hours after the mixing in a climatic chamber at a controlled temperature and humidity (T = 20°C, R.H. = 60%) according to EN 12617-4.

Furthermore, dynamic modulus of elasticity was measured on pastes by means of Ultrasonic Digital Indicator Tester at 1, 7 and 28 days from casting (EN 12504-4). Moreover, X-ray diffraction (XRD)

and thermogravimetry (TGA and DTG) were used to determine the mineralogical composition of the solid phase similarly to the procedure reported in the previous chapter.

7.2 Results and discussion

Figure 108 shows the XRD patterns of AAS pastes at 28 days from casting. Compared to the reference paste (Sp16, black line), it can be observed that in pastes manufactured with admixtures there are no substantial variations in the crystalline phases except for the peak of C-S-H at 2θ ~ 7.4° which seems to be attenuated. Moreover, in pastes containing EA it is evident the peak of portlandite at 2θ ~ 18.0° and 2θ ~ 34.5° [292]. This phase derives from the hydration of calcium oxide-based admixture which turns into calcium hydroxide in presence of water.

The thermograms shown in Figure 108 show negligible variations between the reference paste Sp16 and pastes with admixtures. In particular, from the DTG curves (dash lines), neglecting a different free water loss at T < 100°C, the presence of C-S-H (weight loss between 120°C and 180°C) and HT (thermal decomposition between 300°C and 400°C) is evident.

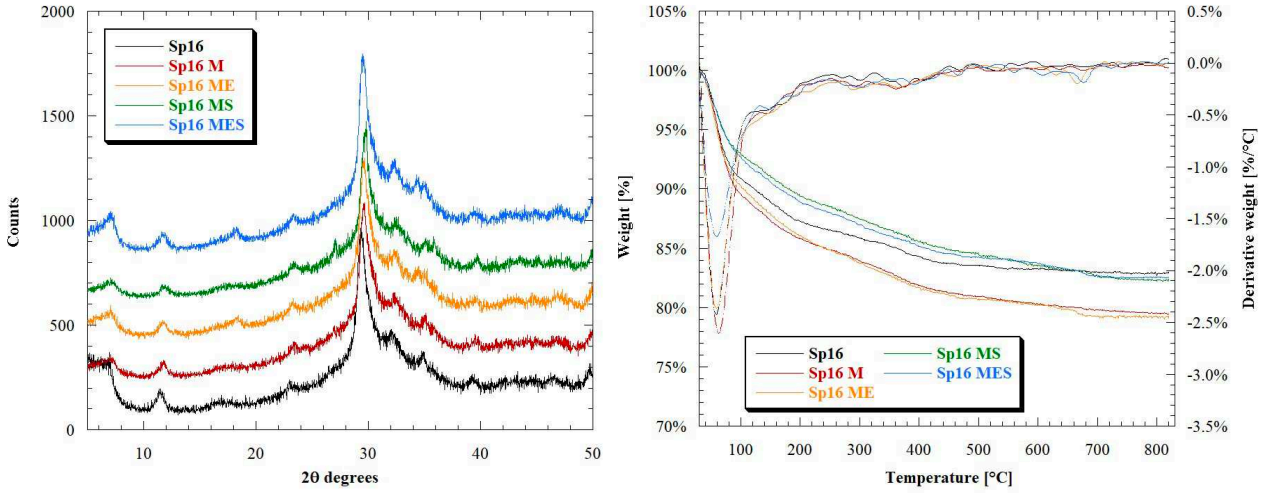

Figure 108 - XRD patterns (left) and thermograms (right) of AAS pastes at 28 days with different admixtures

The specific mass in both fresh and hardened state is not affected by the admixtures. On the other hand, the high fineness of EA (D_{90} equal to 10 μm) reduces the workability of AAS pastes and mortars at the same water content. In particular, mixtures manufactured with CaO-based AE are characterized by a workability reduction of about 15% respect to reference mixture (Table 39 and 40).

	Sp16	Sp16 M	Sp16 ME	Sp16 MS	Sp16 MES
Workability [mm]	200	200	170	200	190
Specific mass (fresh) [kg/m^3]	2050	2045	2055	2050	2055
Specific mass (hardened) [kg/m^3]	2025	2025	2035	2030	2030

Table 39 – Fresh properties of AAS pastes with and without admixtures (w/p: 0.30)

	Sm16	Sm16 M	Sm16 ME	Sm16 MS	Sm16 MES
Workability [mm]	160	160	140	165	150
Specific mass (fresh) [kg/m^3]	2240	2235	2250	2250	2240
Specific mass (hardened) [kg/m^3]	2195	2200	2190	2195	2195
Pot-life [min]	45	45	35	50	40

Table 40 – Fresh properties of AAS mortars with and without admixtures (w/p: 0.50)

The use of admixtures limits the development of the mechanical strength of both AAS pastes and mortars (Table 41 and 42). In analogy with the OPC-based compounds [100], MC and ME have no influence on the elasto-mechanical properties of the mixtures. On the contrary, both EA and SRA reduce compressive strength up to 20% compared to the reference mortars and pastes at early and long ages (Figure 109).

		Sp16	Sp16 M	Sp16 ME	Sp16 MS	Sp16 MES
Flexural strength [MPa]	1 d	4.05	4.08	3.93	3.89	3.66
	7 d	5.21	5.12	4.98	5.15	4.53
	28 d	5.39	5.51	5.12	5.21	4.99
Compressive strength [MPa]	1 d	42.81	42.44	36.75	35.66	31.19
	7 d	64.44	64.66	60.50	56.94	50.13
	28 d	102.07	97.13	92.88	81.76	78.35
Elastic modulus [GPa]	1 d	20.8	20.9	20.9	20.0	19.9
	7 d	22.8	23.9	24.0	23.2	23.1
	28 d	26.14	25.4	26.1	24.9	25.2

Table 41 - Elasto-mechanical properties of AAS pastes with and without admixtures

		Sm16	Sm16 M	Sm16 ME	Sm16 MS	Sm16 MES
Flexural strength [MPa]	1 d	2.90	2.83	2.71	2.69	2.81
	7 d	6.29	6.38	6.33	6.43	6.19
	28 d	6.47	6.51	6.55	6.67	6.41
Compressive strength [MPa]	1 d	13.83	13.53	11.32	11.89	10.87
	7 d	49.69	49.13	41.93	43.12	39.91
	28 d	62.81	61.98	53.81	55.27	51.12

Table 42 - Elasto-mechanical properties of AAS mortars with and without admixtures

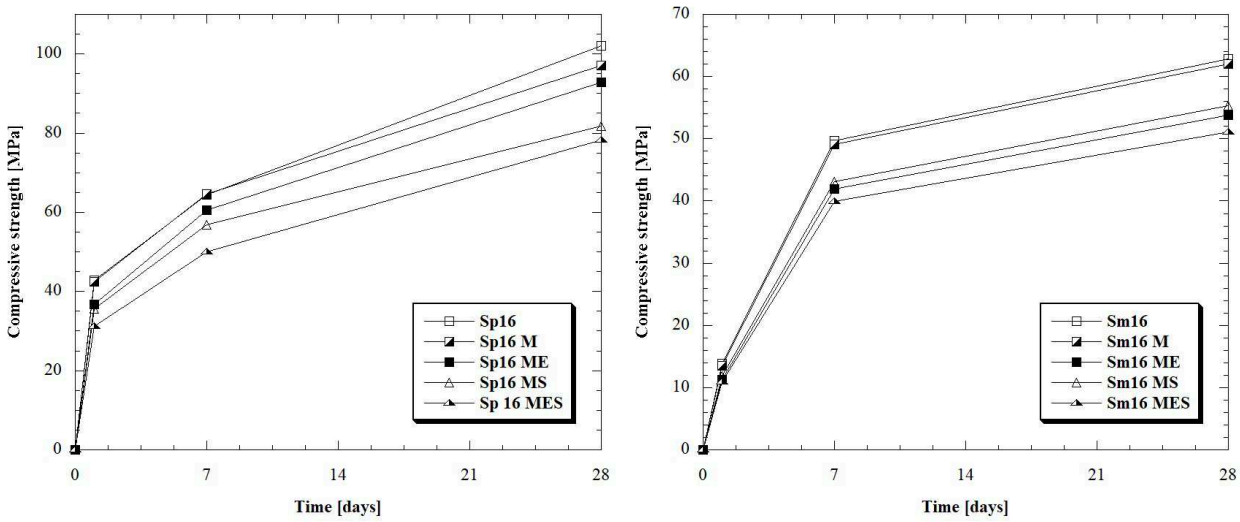

Figure 109 - Compressive strength of AAS pastes (left) and mortars (right) vs time

Figure 110 shows the free shrinkage up to 150 days of AAS mortars manufactured with different admixtures. The MC and MS admixtures, used to improve the fresh properties of mortars, have no effect on the free shrinkage. On the contrary, both the CaO-based EA and ethylene glycol-based SRA admixtures reduce shrinkage by 50% and 40% with respect of Sm16, respectively.

Finally, as already observed by Corinaldesi [152] in Portland-based mixtures, the combined use of expansive agents and SRA further reduces shrinkage, reaching values close to 1000 μm/m, typical of mortars manufactured with OPC. Palacios et al. [239] explains that this beneficial effect of the SRA is due primarily to two developments:

- The decrease in the surface tension of water in the porous system and the concomitantly smaller internal stress when the water evaporates;
- The redistribution of the porous structure, because the admixture increases the percentage of pores with diameters ranging from 1.0 to 0.1 μm, which exhibit a capillary stress much lower than the smaller pores that prevail in mortars without admixture. This redistribution of the pores

is due to the decrease of the capillary stress of the water that SRA induces during the mixing process.

Finally, the dynamic modulus of elasticity varies by adding the admixtures. According to Thomas et al. [190], reducing the shrinkage of alkali-activated materials could lead to an increase in the elastic modulus of the AAS pastes due to reduced micro-cracking.

In addition, according to Chen et al. [286], the presence of dispersed inclusions (such as the crystals of portlandite) should further increase the stiffness of the matrix. However, from the data shown in Figure 110 it seems evident that the variation of elastic modulus measured, even if modest, are to be correlated to the variation of compressive strength and not to a reduction of shrinkage or presence of portlandite.

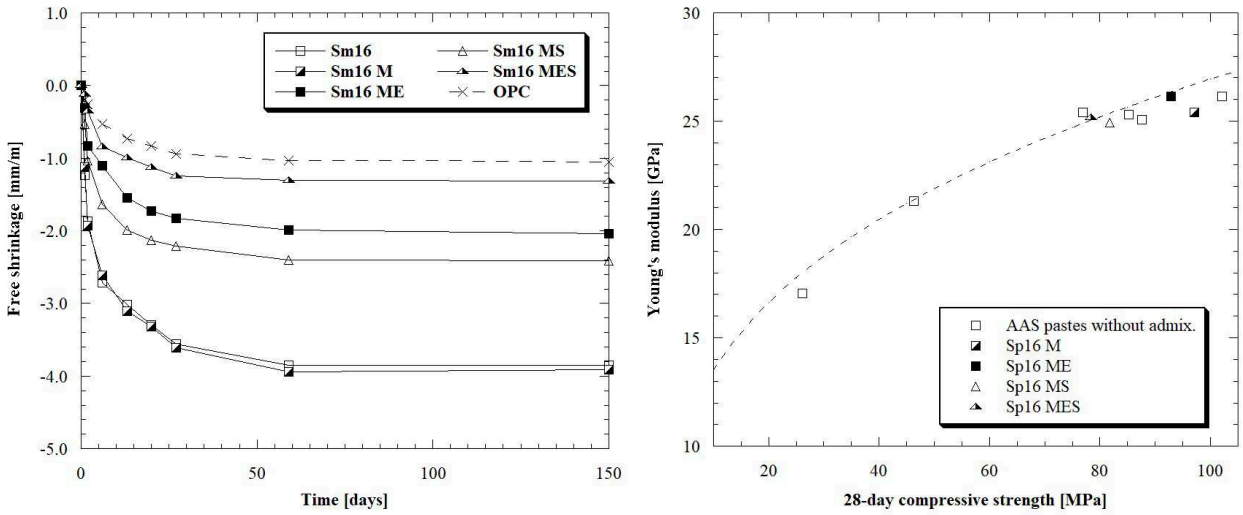

Figure 110 - Compressive strength of AAS pastes (left) and mortars (right) vs time

7.3 Conclusions

In this chapter, the effect of addition of several admixture (methylcellulose, modified starch, shrinkage reducing admixture and CaO-based expansive agent) devoted to the reduction of the shrinkage of AAS materials was evaluated. In accordance with the experimental results, it is possible to conclude that:

- The addition of expansive agent reduces the workability of AAS pastes and mortars. On the other hand, no variations on consistency were detected when MS, MC and SRA are used;
- The use of admixtures limits the development of the mechanical strength of both AAS pastes and mortars. The reduction of 28-day compressive strength is lower than 20% respect to reference mixture manufactured without admixtures;

- Both the CaO-based EA and ethylene glycol-based SRA admixtures reduce shrinkage by 50% and 40% with respect of Sm16, respectively. Moreover, the combined use of expansive agents and SRA further reduces shrinkage, reaching values close to 1000 μm/m, typical of mortars manufactured with OPC;
- No correlation has been highlighted between the reduction of the shrinkage (and therefore of the micro-cracking) and the variation of the elastic modulus.

8. An application: lightweight AAS plaster

The growing attention to the preservation of the historical heritage has remarkably boosted research in the field of the structural rehabilitation, drawing the scientific community toward the investigation of the conservation state and the mechanical properties of the materials [293–295], the modelling and the analysis of the structural response of unreinforced and reinforced masonry constructions [296–299], as well as toward the conceptual design of effective and targeted strengthening techniques [300–303].

The vulnerability of the existing historical masonry constructions under static and dynamic loads was repeatedly observed, particularly in the aftermath of recent Italian seismic events [304–307]. Structural conceptual design with respect to static and seismic actions, global layout of the masonry walls, location of the openings, constructive details, material properties, texture of the stone or brickwork, as well as environmental conditions and other parameters were shown to affect the structural response.

Interestingly, the assessment of the quality of the masonry was shown to stand as a prerequisite to any other in-depth study on the existing construction. Quality of the masonry is the result of the quality of the constitutive materials, the effectiveness of the bonding between the elements, the accuracy of the arrangement of the stonework and structural details, level and extension of material decay [294].

The most relevant evidence of poor quality of the stonework is the absence of mutual-interlocking of the leaves, resulting in three-leaf walls (Figure 111). Conglomerate-like and random rubble stonework, particularly those with rounded pebbles are also acknowledged as poor-quality masonry typologies. Other evidences of poor quality are: stacked rather than staggered head joints, irregular and discontinuous bed joints, thick joints, very weak or dusty mortar with no cohesion or no mortar in rubble or pebble stonework, porous stones or bricks with weak bonding to mortar, extended crack patterns, etc. [294].

Quality of the masonry plays a major role on both the static and seismic response of the construction. The load bearing capacity under static loads strictly depends on the constructive details of the walls, quality of the materials and their interaction. Poor quality masonry typologies may fail for the onset of local failure mechanisms, such as local detachment and buckling of the masonry leaves, substantially reducing the compressive, shear and flexural strength of the wall [308].

Figure 111 - Examples of poor-quality masonry stonework: a) concrete-like masonry wall earthen-based mortar and b) three-leaf wall cross section

As for the seismic behavior, poor quality of the masonry, particularly in the case of three leaf walls, may dramatically anticipate the failure of the wall, which may be triggered by the out-of-plane overturning of the lee-ward leaf (Figure 112). In the worst cases, the walls may crumble prior to the onset of the typical local mechanisms under the dynamic excitation induced by the earthquake [302,304]. The crumbling effect exhibited by poor quality masonry under seismic conditions is emphasized in the case of those superficial earthquakes (typical in the Italian territory) introducing large vertical vibrations, which further weaken the mutual bond between the units, reducing internal compaction of the masonry by extending possible internal micro cracks and spreading local disruption.

Furthermore, quality of the masonry also influences the effectiveness of the most common seismic mitigation measures, such as perimeter ties or floor and roof diaphragms. Perimeter ties rely on the onset of a tied-arch mechanism, with the compressed arch-strut developing within the masonry wall thickness. Poor quality may inhibit the onset of the resisting compressed arch within the masonry wall, and may jeopardize the effectiveness of the tie anchorages by the arch supports [309]. Floor and roof diaphragms require effective connections to the masonry walls; whose envisioned performance can only be attained if the connectors are embedded within good quality masonry walls [310]. Neither techniques can be therefore addressed until the quality of the masonry has been restored or improved. Different technical solutions have been proposed to consolidate poor quality masonry walls, such as random rubble stonework or three-leaf stone masonry walls. To date, the upgrade of their static and seismic performances can be pursuit by repointing or deep repointing, grout injections, jacketing and transversal tying of the external leaves, or by partial replacement of masonry wall portions [80].

Figure 112 - a) Collapse or partial failure induced by poor-quality of the stonework; b) ineffectiveness of perimeter ties and c) of the connection of roof diaphragms in the case of poor-quality masonry stonework

Repointing and deep repointing of the bed-joints consists in the partial replacement of the mortar joints with a new lime-based mortar of improved compactness and durability [311,312].

The mechanical properties of the repointing material should be similar to those of the original wall to avoid abrupt changes in the wall stiffness. In the case of continuous bed joints, the repointing can be strengthened through the insertion of steel or fiber reinforced polymer bars along the bed joints. The effectiveness of this technique may be limited, particularly in the case of very thick walls, provided that the repointing penetration depth is limited. Continuous grid of high strength steel cords placed into the mortar joints, having the nodes secured by means of metal through-rods, may improve the capacity of the wall by also improving the transverse connection of the leaves [313,314].

Injections of low-pressure hydraulic lime-based grouts is a widespread consolidation technique, often suitable for multi-leaf masonries. Injections are aimed at increasing the compactness and consistency of the masonry by filling the internal cracks, voids, collar joints and cavities, thereby improving the bond between the units [315]. Chemical, physical and mechanical compatibility of the grout with the original materials, as well as specific injection protocols are necessary to ensure the efficiency and durability of the intervention. The grout mix-design must be calibrated for each treated wall. Actual injectability of the masonry wall should also be assessed. Injectability depends on the network and percentage of the voids of the inner leaf, which must be sufficiently large as to enable the penetration and diffusion of the grout, but not too large to avoid its percolation and dispersion through the

interstices. Also, when the binding of the stone elements is provided by very weak mortar or earthen-based mortars (Figure 110), injections may be ineffective, given that bonding of the injected material to the surface of the stones is unreliable.

Particularly in the latter case, the injected grout could hardly adhere to the dirty stone elements, which would not be washed even with extended flushing of clean water. For all these reasons the envisioned strengthening of the masonry wall could not be attained and the effectiveness of the injections must be attentively verified through in-situ testing [316].

Transversal tying of the external leaves significantly improves the interlocking of the leaves and introduces a beneficial confining action, which can be further increased through slight pretension of the ties. The technique inhibits the local buckling of the single leaf, thus increasing the load bearing capacity, and substantially increases the ductility of the masonry walls [294]. To be effective, the tie spacing must be sufficiently small, and shorter than the thickness of the wall; only in these conditions the confined masonry core is sufficiently extended to improve the behavior of the masonry wall.

Jacketing with structural plaster and transversal tying of the external leaves is often proposed to improve the in-plane capacity of the unreinforced stone walls against seismic actions [317]. The existing plaster is removed and the exposed masonry is finished with a new plaster layer. Two different layouts can be adopted: single-side or double-side strengthening. The latter represents the best option as it maintains symmetry along the wall. The technique remarkably increases the in-plane resistance to shear sliding, diagonal tensile cracking, and flexure, depending on the material properties and thickness of the coating layer, as well as on the height-to-thickness ratio of the masonry wall. The beneficial effect is triggered by the additional layers, which can withstand large in-plane actions. Tying rods avoid instability or detachment of the coating layer from the support.

The same technique can also be adopted to increase the load bearing capacity with respect to both vertical and horizontal actions of random rubble and concrete-like stone masonry, whose capacity depends on the internal cohesion, the aggregate interlocking between the elements, and residual tensile strength after cracking, as well as on the possible confinement stress level [308]. In this application, the thin coating, together with the tying steel rods, provides a beneficial restraining confinement action to the masonry cross section, introducing a triaxial stress state, improving ductility and resistance of the existing stonework against both vertical and horizontal actions (Figure 111). To this end, lime-based plasters strengthened with GFRP mesh may be adopted [314]. Cement based plaster should be discarded for incompatibility in the case of existing masonry with binding lime mortars. Alternatively, the effectiveness of GFRP mesh inserted into a thin layer made of an inorganic matrix was ascertained by many researchers [318,319]. The technique is quite invasive and does not apply in the presence of valuable plasters or frescoes, nor to listed buildings of historical value or to

exposed stonework. However, it is worth noting that in the case of random rabble stone masonry of lower artistic value the technique substantially improves the mechanical properties of the buildings and represents a quite effective retrofit solution. Furthermore, by adopting a thermal-insulating plaster, the same technique can be conveniently enhanced to improve the energy efficiency of the construction, thus generating a tangible benefit that can partly pay for the integrated renovation.

In this scenario, in this chapter a new material is conceived to serve both as structural plaster and as thermo-insulating layer to improve the structural performance and the energy efficiency of poor-quality masonry typologies. The material is designed to be mechanically and chemically compatible with historic walls and to be fully sustainable. These major goals are achieved by adopting a lightweight eco-compatible Portland-free binder based on alkali-activated slag having the compressive strength of a good quality masonry (28-day compressive strength of about 8 MPa) and a reduced specific mass (lower than 1000 kg/m^3) in order to reduce the coating layer transmittance.

8.1 Experimental program

The campaign was planned in two phases. The purpose of the first one was to perform tests in order to evaluate the essential characteristics of the mortars at different lightweight aggregate content and to identify the ideal mix proportioning that meets the general requirements in terms of strength and specific mass. In the second stage, several tests were carried out on the previously selected mortar to obtain a more detailed characterization of its behavior. Finally, the compatibility between the mortar and the glass fiber reinforced polymer (GFRP) mesh was investigated by means of mechanical tests and optical microscope observations.

8.1.1 Materials

Three different series of lightweight plasters were manufactured: a traditional Portland-free mortar (TP) manufactured with hydrated lime (CH) CL90-S (according to EN 459-1) and ground granulated blast furnace slag with 28-day pozzolanic activity index equal to 0.76 (GGBFS: according to EN 15167-1 and EN 196-5) and two innovative alkali-activated slag-based mixtures (IP) with different activator/precursor ratio. According to the previous chapter, a blend of activator in powder form (sodium metasilicate pentahydrate : potassium hydroxide : sodium carbonate = 7 : 3 : 1) was used to produce the innovative plasters with the dosage of the activator equal to 20% and 24% by binder mass. The physical properties, the chemical composition and the laser granulometry and XRD pattern of GGBFS were reported in Table 6, Table 24, Figure 93, respectively. Furthermore, the physical properties of CH (CaO content equal to 94 wt.%) was reported in Table 6.

The water was adjusted in order to attain the same workability at the end of mixing, equal to 160 mm ± 10 mm by means of a flow table. An air-entraining agent (AEA, specific mass of 0.99 g/cm^3) based on cocamide diethanomaline (according to EN 934-2 and EN 480-2) was added to the mix at 2 kg/m^3

to lighten the mortars, reducing, at the same time, the tendency to bleeding and segregation [100]. In addition, the natural siliceous aggregates (NA) were replaced by expanded recycled glass aggregates (EGA), properly combined to meet the Bolomey curve (Figure 113 and Table 43).

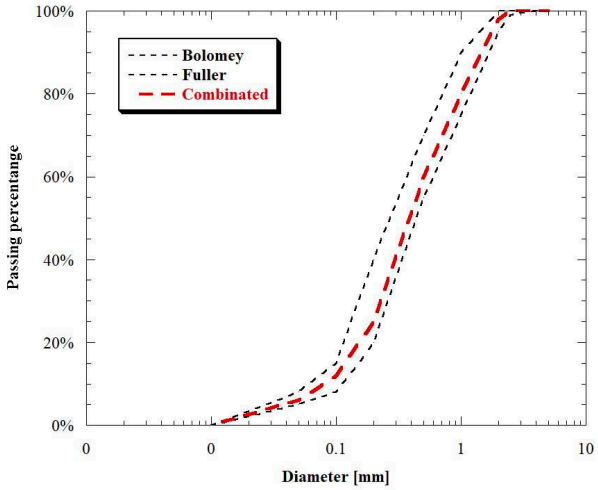

Figure 113 - Granulometry of aggregates

	Specific mass [kg/m^3]	Water absorption [%]
NA 0 – 2.5	2640	0.20
NA 0.25 – 0.50	2700	0.76
NA 0.50 – 1.00	2580	0.77
NA 1.00 – 2.00	2610	0.89
NA 2.00 – 2.50	2620	1.02
EGA 0 – 0.50	700	0.86
EGA 0.50 – 1.00	500	0.92
EGA 1.00 – 2.00	400	1.18

Table 43 – Physical properties of aggregates

On the second stage, due to the high shrinkage of alkali-activated slag-based materials [195], methylcellulose (MC), modified starch (MS), polypropylene fibers (length 6.5 mm, aspect ratio 200) and shrinkage reducing admixture (SRA) were added to the mortar in order to minimize the risk of cracking and detachments of plaster (Table 36). Lastly, the properties of the GFRP mesh (epoxy-vinylester resin and glass fiber) was reported in Table 44.

Property	Value	Standard
Mesh size	33 x 33 mm	CNR-DT 203/2006
Average thickness	3 mm	CNR-DT 203/2006
Weight	1000 g/m^2	-
Glass fiber	Glass AR – ZrO_2 16%	ASTM C1666M-07
Polymer	Epoxy-vinylester resin	-
Fiber/resin ratio	65/35 by weight	-

Table 44 – Properties of the GFRP mesh (provided by the supplier)

8.1.2 First phase

Three different series of plaster were manufactured by varying the EGA/NA ratio according to the composition reported in Table 45. Workability was measured by means of flow table according to EN 1015-3. Specific mass at fresh state and entrapped air were detected in accordance with EN 1015-6 and EN 1015-7, respectively. Specimens 40 x 40 x 160 mm^3 were produced, cured for 24 hours in mold and then stored in a climatic chamber at 20°C and R.H. 60%. Specific mass at hardened state, compressive and flexural strength were also determined on three specimens for each age and composition (EN 1015-11).

8.1.3 Second phase

During the second stage, several tests were carried out on the mortar that reached the "target" performances (IP24-100) and on the same mixture manufacturing by adding MC, MS, SRA and fibers (Tables 46 and 47). In addition to the tests conducted on the first phase, setting time was measured by means of Vicat apparatus (EN 196-3). Secant modulus of elasticity (E_s, in accordance with method B, EN 12390-13) on 28-day cured cylindrical specimens was evaluated by means of compression testing machine (BRT1000) and linear variable displacement transducers applied on the mortar samples. Furthermore, three specimens 40 x 40 x 160 mm^3 were used to estimate the 28-day dynamic modulus of elasticity (Ed) in accordance with EN 12504-4 (direct transmission). A thin layer of glycerol paste was interposed between the mortar surface and the transducers of the ultrasonic digital indicator tester (UDIT) in order to ensure an adequate acoustical coupling between the specimen and the transducers. The UDIT measures the transmission time of ultrasonic pulse, allowing to calculate the velocity of ultrasonic pulse, note the length of the specimen (160 mm). Ed can be calculated through the equation (29).

In addition, bond strength by pull-off was determined on mortars applied with different thicknesses (20 mm and 45 mm) on a brick wall after 28 days from casting according to the procedure proposed by EN 1542. Drying shrinkage was also measured over time on prismatic specimens stored 24 hours

after the mixing in a climatic chamber at a controlled temperature and humidity (T = 20°C, R.H. = 60%). Moreover, capillary water absorption coefficient of plasters was investigated according to EN 13057.

Composition [kg/m^3]	GGBFS	CH	Activator	NA	EGA	Water	AEA
TP-0	290	70	-	1080	-	215	2
TP-10	290	70	-	970	25	215	2
TP-20	290	70	-	865	55	215	2
TP-30	290	70	-	755	80	215	2
TP-60	290	70	-	430	160	215	2
TP-80	290	70	-	215	210	215	2
TP-100	290	70	-	-	265	215	2
IP20-0	275	-	55	990	-	165	2
IP20-10	275	-	55	890	25	165	2
IP20-20	275	-	55	790	50	165	2
IP20-30	275	-	55	690	75	165	2
IP20-60	275	-	55	395	145	165	2
IP20-80	275	-	55	200	195	165	2
IP20-100	275	-	55	-	245	165	2
IP24-0	270	-	65	1005	-	155	2
IP24-10	270	-	65	905	25	155	2
IP24-20	270	-	65	805	50	155	2
IP24-30	270	-	65	705	75	155	2
IP24-60	270	-	65	400	150	155	2
IP24-80	270	-	65	205	200	155	2
IP24-100	270	-	65	-	250	155	2

Table 45 – Composition of mortars

The thermal conductivity of plaster was determined by hot box method using a heat flow meter according to EN 1934 (Figure 114). The mortar was applied on a panel (120 cm x 80 cm) manufactured with lightweight bricks (30 cm x 24.5 cm x 19.5 cm) and traditional Portland cement-based mortar. The thickness of the plaster (applied on both surfaces) was 35 mm. The surface temperatures and the heat flow were measured for 168 hours by setting an internal temperature of 0°C and an external temperature of 20°C.

Finally, GFRP mesh was embedded in 400 x 400 x 40 mm^3 mortar specimen and GFRP samples were immersed in 1M $Na(OH)_2$ solution in order to evaluate the degradation promoted by the alkaline environment on the epoxy-vinylester resin. The damage degree of GFRP mesh was evaluated through optical microscope observations and measuring the tensile strength loss (ISO 527-4) after 40 days in alkaline environments at 20°C.

Composition [kg/m^3]	IP24-100	IP24-100LS
GGBFS	270	270
Activator	65	65
EGA	250	250
Water	155	155
AEA	2	2
MC	-	0.40
MS	-	0.15
SRA	-	5.00
Fibers	-	2.70

Table 46 – Composition of mortars IP24-100 and IP24-100LS

Figure 114 - Thermal characterization of the innovative plaster

Test	Ages	Format	Number
Flexural and compressive strength	1-7-28 d	Beam 40x40x160 mm^3	9
E_d and specific mass	28 d	Beam 40x40x160 mm^3	3
Free shrinkage	Up to 100 d	Beam 40x40x160 mm^3	3
Bond strength	28 d	Thickness: 20 and 45 mm	16 pull-off
Water absorption	28 d	Beam 40x40x160 mm^3	3
Thermal conductivity	28 d	Thickness: 35 mm	2 tests

Table 47 – Mortar's specimens manufactured for each test

8.2 Results of first phase

The water dosage to attain the target workability varies by varying the type of mortars. In fact, in alkali-activated slag based plasters, the amount of water to achieve 160 mm spreading decreases as the activators dosage increases due to the plasticizing and deflocculating effects of sodium silicate explained by Kashani et al. [276]. On the contrary, traditional mortars TP require higher mixing water dosages, generally greater than 30-35% compared to the innovative mixtures. Furthermore, the water content is not affected by the EGA/NA ratio due to the similar water absorption of the aggregates used (Table 43).

The air content of mortars at fresh state does not change as the lightweight aggregate dosage varies (Table 48). On the other hand, the air-entraining agent efficiency seems to be influenced by the nature of binder used (alkali-activated slag or slag/hydrated lime). Indeed, the innovative plasters IP show an entrapped air equal to 35% while the traditional plasters TP are limited to 25%.

The specific mass both at fresh and hardened state decrease with the increase of the EGA/NA ratio, independently of binder used (Figure 115 and 116). In particular, by manufacturing traditional mortars containing only expanded glass aggregates EGA, it is possible to reach density close to 930 kg/m^3 at fresh state and 870 kg/m^3 at hardened state, while innovative plasters exhibit lower densities of about 150 kg/m^3 both at fresh and hardened state due to the higher air content respect to TP.

Figure 116 and 117 show that the mechanical strength of GGBFS/lime-based mortars are not influenced by the EGA/NA ratio. In fact, regardless of the aggregate used, the compressive strength is small (about 2.5 MPa at 28 days) and not compatible for use in seismic improvement of existing masonry buildings. On the contrary, the innovative mortars based on alkali-activated slag show much higher strength than those measured in traditional plasters TP. Moreover, the compressive strength decreases with the increase of EGA/NA ratio similarly to the specific mass. In detail, the innovative plasters IP manufactured only with expanded glass aggregates guarantee strength between 5.5 MPa (IP20-100) and 8 MPa (IP24-100) with a density close to 750 kg/m^3.

	Air content [%]	Specific mass		Compressive strength [MPa]		
		Fresh	Hardened	1 d	7 d	28 d
TP-0	25	1620	1540	0.51	2.41	2.57
TP-10	25	1590	1480	0.45	2.31	2.54
TP-20	25	1470	1420	0.45	2.18	2.54
TP-30	25	1390	1380	0.44	1.99	2.40
TP-60	25	1170	1080	0.39	1.89	2.31
TP-80	25	1050	990	0.41	1.60	2.18
TP-100	25	930	870	0.40	1.39	2.03
IP20-0	35	1510	1450	6.50	11.03	13.18
IP20-10	35	1480	1400	5.96	10.40	11.26
IP20-20	35	1295	1230	5.68	9.88	10.34
IP20-30	35	1250	1190	4.47	7.20	8.31
IP20-60	35	1050	990	3.94	6.72	7.89
IP20-80	35	900	830	3.12	5.46	6.18
IP20-100	35	710	690	2.85	4.89	5.51
IP24-0	35	1550	1520	7.85	12.53	15.03
IP24-10	35	1500	1460	6.75	11.52	13.28
IP24-20	35	1360	1330	6.87	11.02	11.95
IP24-30	35	1290	1250	6.29	10.36	10.88
IP24-60	35	1100	1070	5.67	9.89	10.23
IP24-80	35	970	920	3.49	9.03	9.86
IP24-100	35	760	720	2.85	7.17	8.26
IP24-100LS	35	770	725	2.91	7.24	8.19

Table 48 – Properties of mortars at fresh and hardened state

Furthermore, in Figure 117 it is possible to notice that, for the innovative mixtures, the compressive strength at 28 days from casting is inversely proportional to the specific mass. As a matter of fact, the use of an aggregate of poor mechanical properties strongly penalizes the performance of the mortars. On the other hand, according to Neville [100] and Dzturan et al. [320], in presence of a very weak matrix like that of traditional plasters TP, this effect is negligible.

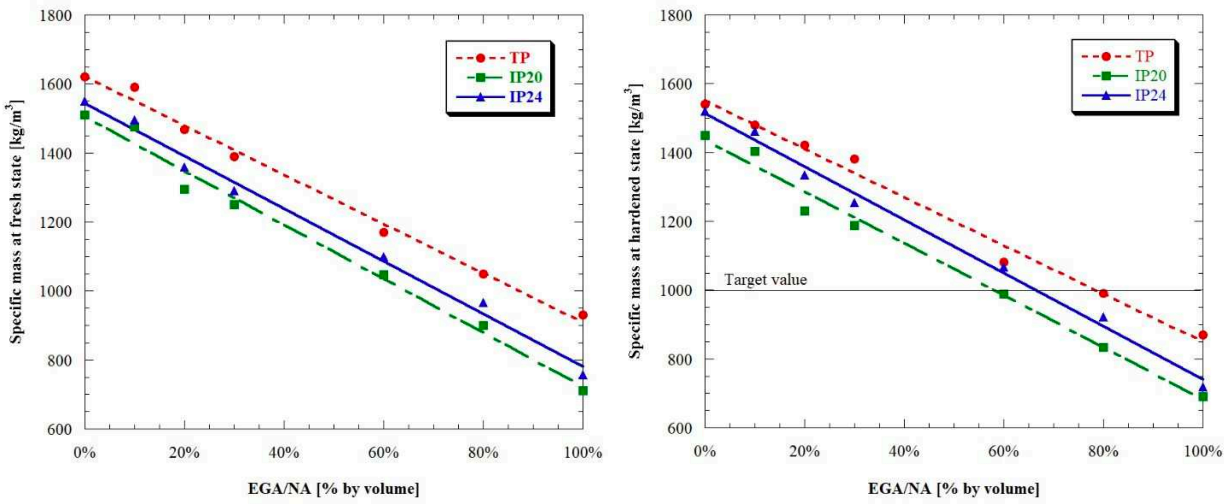

Figure 115 - Specific mass at fresh (left) and hardened (right) state at different EGA content

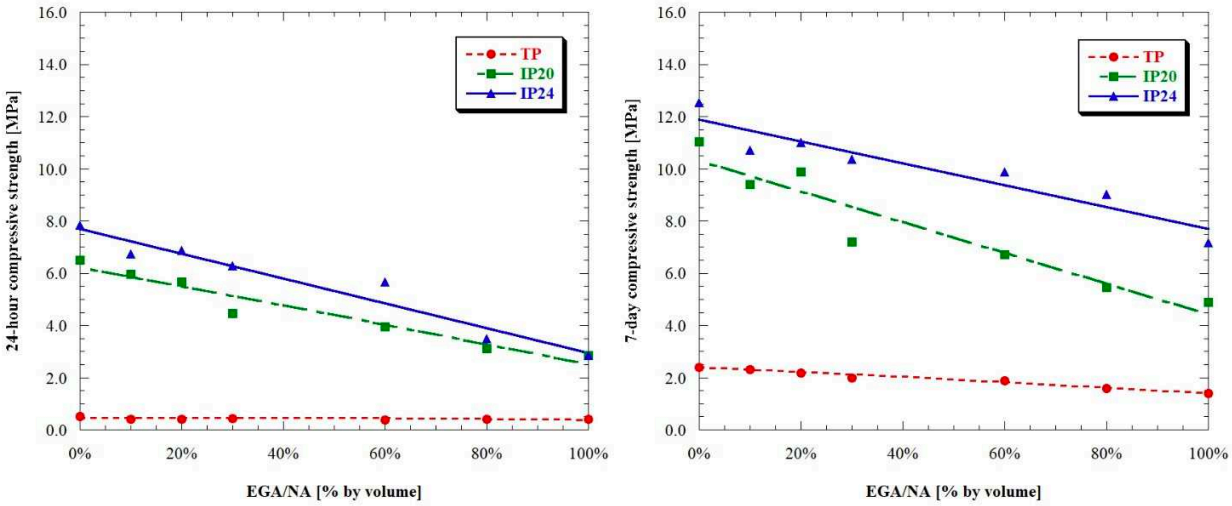

Figure 116 - Compressive strength at 24 h (left) and 7 days (right) at different EGA content

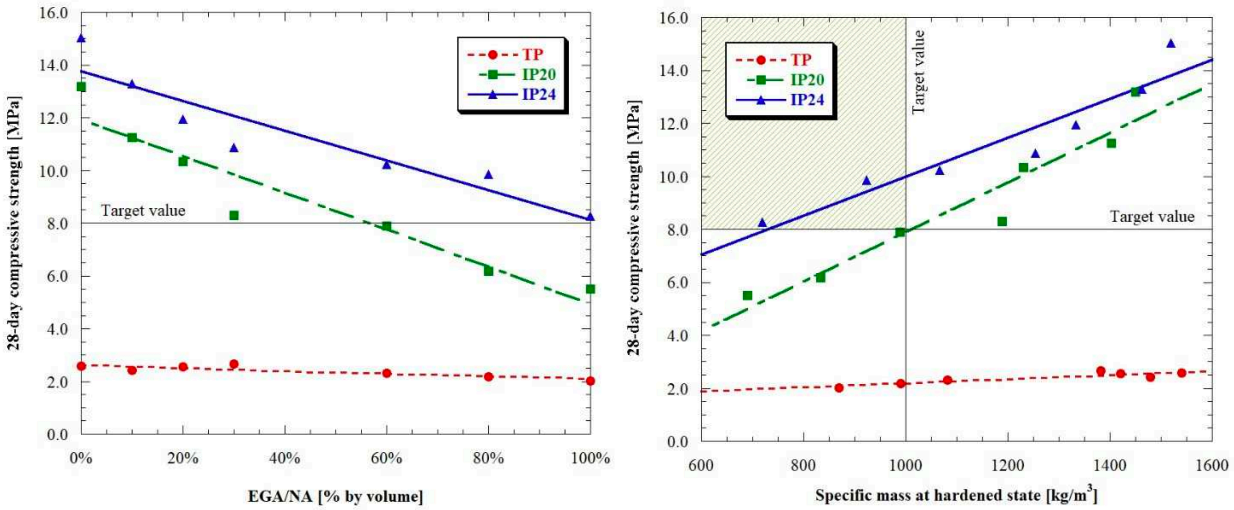

Figure 117 - Compressive strength at 28 days at different EGA content (left) and correlation between strength and density of mortars

In conclusion, the alkali-activated slag-based plaster manufactured with only expanded glass aggregate IP24-100 combines an extreme lightness (density close to 750 kg/m^3) with mechanical strength (28-day compressive strength equal to 8 MPa), which may be considered the upper bound for the use as a thermal reinforced plaster for upgrade of existing poor-quality masonry. Depending on the masonry the strengthening is proposed for, mechanical properties as well thermal properties can be modified by appropriately modifying the mix design.

8.3 Results of second phase

In this stage, the results of the tests carried out on the mortar that reached the "target" performances will be presented. In particular, were analyzed the properties of mortars manufactured with (IP24-100LS) and without (IP24-100) the addition of MC, MS, SRA and fibers. Finally, the results of the test carried out on the GFRP mesh will be presented. In particular, the properties of GFRP mesh embedded in 400 x 400 x 40 mm^3 mortar specimen and GFRP samples immersed in 1M $Na(OH)_2$ solution were analyzed in order to evaluate the degradation promoted by the alkaline environment on the epoxy-vinylester resin.

8.3.1 Rheological properties

The addition of admixtures able to reduce the shrinkage-induced cracking does not change the amount of water at equal workability, specific mass and air content. Furthermore, the initial and final set measured by needle of Vicat (50 minutes initial set, 140 minutes final set) are similar to those of traditional plasters based on Portland cement and lime [321], resulting perfectly compatible with the construction needs.

8.3.2 Elasto-mechanical properties

There are no changes in the mechanical strength between the mortar IP24-100 and IP24-100LS (Table 48). The addition of ethylene glycol, unlike on traditional Portland mixture [152] or on normal-weight AAS-mortars [239,241], does not appear to affect negatively the development of elasto-mechanical properties of alkali-activated slag-based plaster manufactured with only expanded glass aggregate.

The elastic modulus of IP mortars is very low, close to 1.5 GPa for the E_s and 2.5 GPa for the E_d (Table 49). The Young's modulus of the IP is so low because this property depends strongly on the rigidity of the aggregate and on the characteristics of the binder paste [100]. The EGA have poor elasto-mechanical properties that minimize the stiffness of the mortar. Moreover, at the same strength class, Thomas et al. [190] have shown that AAM mortars are characterized by lower elastic modulus than those Portland cement mortars. The reduction of E_d and E_s in IP respect to TP is a consequence of the high shrinkage of AAM mortars which caused microcrack formation.

	IP24-100	IP24-100LS
E_s [GPa]	1.5	1.5
ρ [kg/m^3]	870	875
ν [km/s]	1.85	1.85
E_d [GPa]	2.5	2.5

Table 49 – Elastic modulus of mortars IP24-100 and IP24-100LS

8.3.3 Shrinkage

Dry shrinkage of innovative plaster is given in Figure 118 that shows very high free shrinkage of AAMs compared to mixtures manufactured with traditional binders, as widely reported in the scientific literature [195,242,243].

The addition of admixtures and fiber reduced shrinkage in alkali-activated slag mortars by up to 50%. Palacios et al. [239] explains that this beneficial effect of the SRA is due primarily to two reasons: firstly, the decrease in the surface tension of water in the porous system and the concomitantly smaller internal stress when the water evaporates; secondly, and most importantly, the redistribution of the porous structure, because the admixture increases the percentage of pores with diameters ranging from 1.0 to 0.1 μm, which exhibit a capillary stress much lower than the smaller pores that prevail in mortars without admixture. This redistribution of the pores is due to the decrease of the capillary stress of the water that SRA induces during the mixing process.

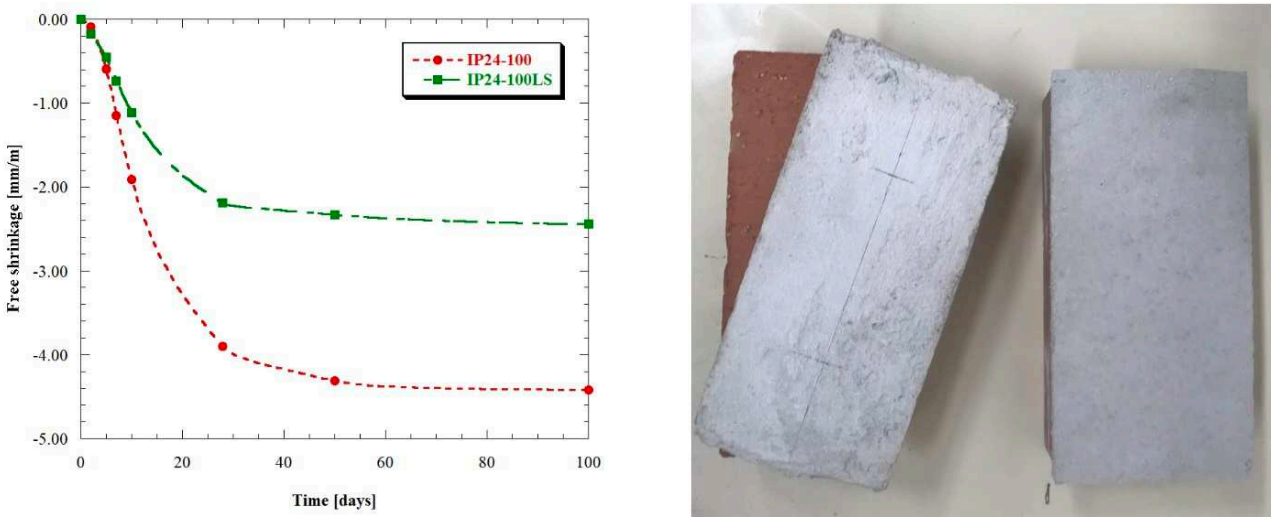

Figure 118 - Free shrinkage of mortars up to 100 d (left) and test on a brick (right): IP24-100 detached and IP24-100LS adherent

Furthermore, due to the low elastic modulus and the limited shrinkage of innovative plaster, tensile stress induced by restrained shrinkage still be low, preventing the mortars from cracks and

detachments. This behavior was verified through the application of thin layers of plaster on brick stored in extra-dry conditions (R.H. < 30%) to emphasize the risk of cracking and detachment (Figure 118). In particular, a 2 cm-thick layer of IP24-100 after a few days was totally detached from the support, while the plaster manufactured with the addition of admixtures and fibers showed no detachments or cracking up to 1 year. Moreover, no cracks were observed on the panels used for thermal conductivity and adhesion tests (Figure 114).

8.3.4 Bond strength

The bond strength between AAM binder and substrate is one of the key engineering properties. In particular, it requires the coating layer to be strongly adhesive to the substrate after final setting to resist after the restauration. As it can be seen from Table 50, the bond strength values are higher when the mortar has been applied with a lower thickness.

In the case with s = 45 mm a 100% cohesive failure was observed in the alkali activated mortar layer, indicating that the repair material is the weakest part of the system. This behavior is probable due to the greater probability of finding faults that strongly influence the tensile strength of the material. On the other hand, the failure type was more variable in the case s = 20 mm, where the observed failures were both cohesive failure in the mortar layer and adhesive failure along the interface surface. Moreover, it can be noted that the adhesion strength is always higher than that required (0,2 MPa).

Test	**Bond strength [MPa] and failure type**			
	t = 20 mm		**t = 45 mm**	
1	1.05	Cohesive	0.17	Cohesive
2	0.68	Cohesive	0.23	Cohesive
3	0.59	Cohesive	0.50	Cohesive
4	0.93	Interface	0.31	Cohesive
5	1.16	Interface	0.41	Cohesive
6	1.01	Interface	0.44	Cohesive
7	1.04	Interface	0.20	Cohesive
8	0.64	Interface	0.38	Cohesive

Table 50 – Bond strength of mortars

8.3.5 Thermal properties and energy saving

The conductivity of ordinary concrete strongly depends on its composition. In general, density does not appreciably affect the conductivity of ordinary concrete, however, due to the low conductivity of air, the thermal conductivity of lightweight concrete varies with its density.

The method for determined the thermal resistance of plaster requires the measurement of surface temperatures and heat-flux through the test wall by the use of heat-flux meters. The thermal resistance R is given by:

$$R_{tot} = \frac{\sum_{j=1}^{n} T_{swj} - T_{scj}}{\sum_{j=1}^{n} q_j} \quad (33)$$

with: T_{sw} = surface temperature on the test wall warm side [K], T_{sc} = surface temperature on the test wall cold side [K], q = transmission heat loss through a wall per unit area [W/m^2].

Note the thermal resistance of the brick wall R_{bw}, the thermal resistance of the plaster R_p can be obtained according to the following relationship:

$$R_p = R_{tot} - R_{bw} \quad (34)$$

The thermal conductivity ¸ of the plaster is obtained from the ratio between the thickness t of the plaster layer during the test and the thermal resistance of the product.

The value of the thermal conductivity of the lightweight plaster (0.35 W/mK) is lower by about 75% compared to a traditional mortar based on Portland cement and lime (about 1.30 W/mK) [100]. On the other hand, comparing the thermal conductivity of IP24-100LS with those of lime plaster (LP) [322], the difference between the conductivity values is around 55% at equal strength class (Table 51). This behavior is due to the replacement of traditional aggregates with expanded recycled glass aggregates [100].

	IP24-100LS	**LP**
Thermal resistance R_p [m^{2}K/W]	0.101	-
Thickness t [mm]	35	-
Thermal conductivity λ [W/mK]	0.35	0.80

Table 51 – Thermal properties of plasters

Furthermore, by using a building thermal modeling computer program [323], the energy consumption of a 100 m^2-detached house in central Apennine mountains (L'Aquila, Italy) was evaluated by varying the thermal properties of reinforced plaster used. In particular, the simulation was carried out with two reinforced plasters (IP24-100LS and LP) applied with a thickness of 6 cm on a stone masonry. As reported in Table 52, the use of lightweight mortar instead of traditional reinforced plaster on a stone masonry building leads to a reduction in energy consumption up to 31 kWh/m^2 year (-20%).

	IP24-100LS	IP24-100LS/LP	LP
Stratigraphy	IP-masonry-IP	IP-masonry-LP	LP-masonry-LP
Thickness [cm]	6 + 60 + 6	6 + 60 + 6	6 + 60 + 6
Wall thermal transmittance [W/m^{2}K]	1.277	1.458	1.712
Building energy consumption [kWh/m^{2}y]	134	146	165
Energy saving vs LP [%]	20%	12%	-

Table 52 – Thermal properties of a detached house in L'Aquila

8.3.6 Water absorption

The absorption coefficient of the lightweight plaster (2.78 kg/m^{2}h$^{0.5}$) is higher compared to a traditional mortar based on Portland cement and lime (1.63 kg/m^{2}h$^{0.5}$) [100]. A higher value of absorption coefficient could cause a reduction in thermal resistance of plaster on site, due to the water saturation of external layer during the raining periods. For this reason, an alchilalcoxisilane-based coating was applied on IP24-100LS surface in order to reduce the water absorption of mortar. As reported in Figure 119, applying a waterproofing material, is possible to reduce the absorption coefficient up to 80%, reducing the risk of saturation of the plaster and, hence, preserving the thermal resistance of the external plaster.

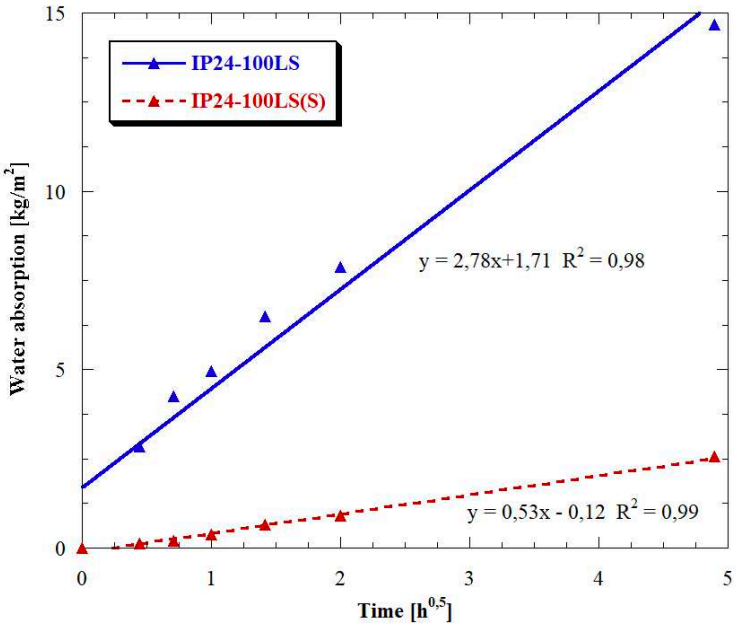

Figure 119 - Capillary water absorption of mortars with (IP24-100LS(S)) and without (IP24-100LS) coating

8.3.7 Characterization of GFRP

The mesh consists of two types of fiber (twist and flat). The tensile ultimate load of fibers was evaluated (ISO 527-4) at 20°C and values similar those shown in the technical data sheet were obtained. In particular, the fiber failure occurred for tensile loads close to 2.05 kN for twist fibers and 3.37 kN for flat fibers.

The same tests were carried out after 40 days of embedding in the lightweight plaster or after 7 days in $Na(OH)_2$ solution. However, strength losses were not observed following exposure to strongly alkaline environments. In addition to the tensile test, optical microscope observations were also carried out. Figure 120 shows the GFRP mesh exposed to different environments: reference fibers (left), fibers after 40 days embedded in lightweight plaster (center), fibers after 7 days in 1M $Na(OH)_2$ solution (right). It is possible to observe that the GFRP mesh, especially the resin surface, did not suffer any degradation.

Figure 120 - Optical microscope observation: reference fibers (left), fibers after 40 d embedded in lightweight plaster (center), fibers after 7 d in 1M $Na(OH)_2$ solution (right)

8.4 Conclusions

In this chapter, a lightweight cement-free reinforced plaster for restoration and seismic retrofitting of stone masonry buildings was developed.

Analyzing the experimental data, it is possible to conclude that:

- The use of expanded recycled glass aggregates (EGA) instead of natural siliceous aggregates (NA) and the addition of air-entraining agent (AEA) reduce the specific mass at fresh and hardened state of mortars up to 750 kg/m^3;
- The traditional plaster TP provides mechanical strength lower than 3 MPa which is not suitable for seismic upgrade of masonry buildings;
- The Portland-free plaster IP24-100LS is able to provide a structural reinforcement (28-day compressive strength equal to 8 MPa) with an improvement of the energy performance of the masonry (thermal conductivity 0.35 W/mK due to density close to 750 kg/m^3);

- The high free-shrinkage of alkali-activated slag based-plaster was strongly reduced by using a blend of admixtures that are able to reduce the shrinkage to values close to those of Portland-based mortars;
- The reduced shrinkage and the low elastic modulus ensure an excellent adhesion to the substrate (up to 1.16 MPa) and the absence of micro-cracks and detachments;
- By using an alchil-alcoxisilane-based coating is possible to reduce the water absorption of mortar up to 80%, avoiding the saturation of plaster on site during raining periods;
- The GFRP mesh showed a high resistance to alkaline environments and is therefore perfectly suitable for this type of application.

9. Sustainability index

The issue of sustainability in the cement and concrete industry has been widely discussed since the 2000s when the world has entered into an era of sustainable development. Damtoft et al. [7] have shown how the reduction of the environmental footprint of concrete structures can be achieved by reducing the CO_2 emissions from cement production, favoring the use of cements with a low clinker factor but also using cementitious mixtures with high mechanical performance (i.e. UHPC) or self-compacting concrete (i.e. SCC). Moreover, they offer an interesting insight into the ability of cement-based materials to permanently absorb (i.e. sequester) CO_2 from the atmosphere, clarifying the difficulties of computation that this approach involves. The same concepts are also reported in the article by Schneider et al. [5] which also includes the concept of education for sustainability, i.e. the need to train all the concrete sector players on the issue of environmental protection.

Gartner and Macphee [288] also dealt with the topic of sustainability of concrete structures. The authors underlined the complexity of the concept of sustainable development in the concrete industry, specifying that currently there are no models capable of assessing the environmental footprint of cement-based materials.

An interesting article by Barcelo et al. [3] focuses on reducing greenhouse gases (GHG) emission and show how, in the future, the most promising path towards a reduced environmental impact is the use of carbon capture and storage (CCS) technologies. However, the authors specify that current technologies are not able to achieve a satisfactory reduction in CO_2 emissions.

Finally, in a recent review by Gartner and Hirao [10], several technologies aimed at reducing the GHG emissions associated with the manufacture of the binder phase in concrete are presented.

From the analysis of the aforementioned literature, it appears evident that the sustainability of concrete structures is a very complex subject, because there is an enormous range of possible concrete compositions potentially available mixing binders, aggregates, water and admixtures. It thus makes little sense to talk about the sustainability of the binder itself.

The goal of this chapter is to evaluate the environmental impact of the whole mixture, taking into account the main sustainability parameters (e.g. CO_2 emissions, primary energy consumption, natural resources consumption), without neglecting the durability of the concretes and its engineering properties.

9.1 Sustainability indicators of first generation

Several authors have proposed methods for assessing the environmental impact of mortars and concretes. In a pioneer paper, Popovics [324] presents the f_{eco} which is defined as the strength developed by one unit of mass of cement. On the other hand, the economic efficiency of a concrete

mix design was defined by Aitcin [325] as the cost of 1 MPa or 1 year of service life of the concrete structure.

In a more general approach, Damineli et al. [81] proposed two simplified indexes to evaluate the environmental footprint of mortars and concretes (Figure 121). The first one is the binder intensity (bi) which measures the total amount of binder necessary to deliver one unit of a given performance indicator e.g. 1 MPa of strength.

$$bi = \frac{b}{p} \tag{35}$$

where b is the total consumption of binder materials (kg/m^3) and p is the performance requirement. In most cases, p is the compressive strength (MPa) at 28 days, but the performance indicator and the age will depend on the application of the concrete. The bi index expressed in terms of units of compressive strength is the inverse of Popovics' index and gives number greater than 1 and seems easier to handle. The second indicator is the CO_2 intensity (ci) defined as the amount of carbon dioxide emitted to deliver one unit of performance.

$$ci = \frac{c}{p} \tag{36}$$

where c is the total CO_2 (kg/m^3) emitted to produce and transport all concrete raw materials. Using the same approach, two other sustainability indexes have also been proposed – the clinker intensity index (cli) and the energy intensity index (ei) – in accordance with the following equations:

$$cli = \frac{cl}{p} \tag{37}$$

$$ei = \frac{e}{p} \tag{38}$$

where cl is the clinker content of Portland cement used to manufacture the concrete (kg/m^3) and the e is the total energy consumed in the fabrication of the concrete (MJ).

The indexes are very simple and understandable and allow to take into account the different performances required for mixtures. However, they overlook fundamental aspects such as the durability, the use of industrial by-products as raw materials and the energy requirements to manufacture concrete.

Yang et al. [257] used the Damineli et al. indexes to assess the sustainability of alkali-activated concretes. However, in the determination of CO_2 emissions, they used the following holistic model:

$$c = C_M + C_T + C_P + C_C \tag{39}$$

where C_M is the carbon dioxide emissions related to the production of raw materials, C_T is the carbon dioxide emissions during the transportation phase (transportation of the material to the concrete plant

and the transportation of the produced concrete to the building yard), C_P and C_C is the CO_2 emission linked to the mixing and curing of concrete, respectively.

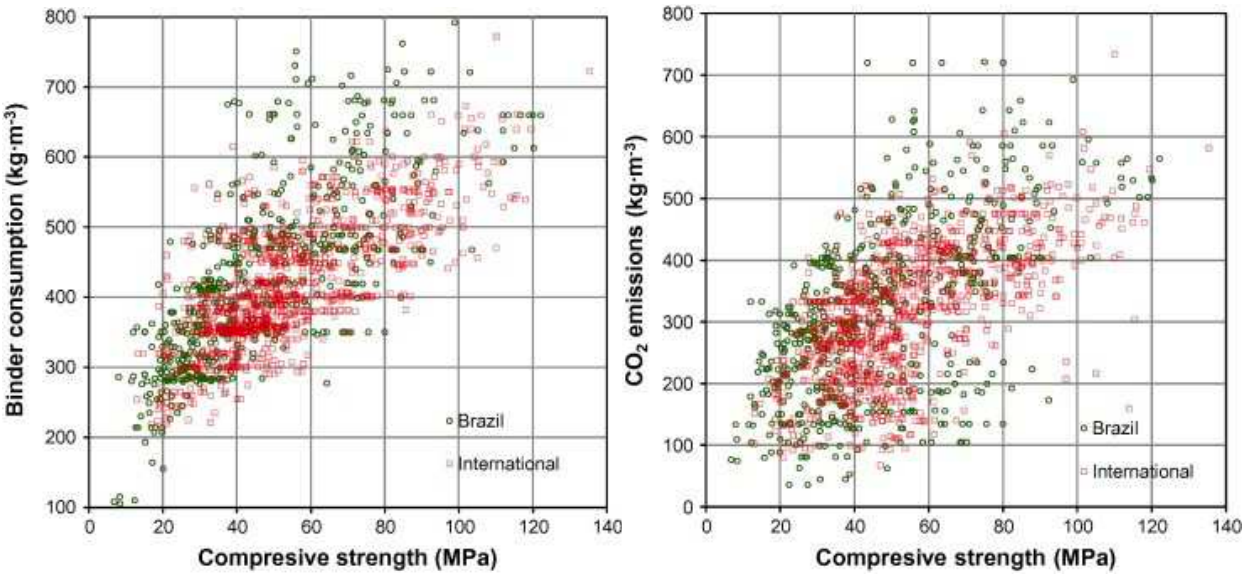

Figure 121 - Correlation between binder consumption (left) or CO_2 emission (right) vs compressive strength [81]

9.2 Sustainability indicators of second generation

All the indicators abovementioned are referenced in terms of the compressive strength considering it as the primary performance parameter for structural concrete. However, there is a great necessity to consider durability as the reference in response to the push for service life design of structures.

In a recent paper, Gettu et al. [326] introduced the A-index (so call apathy index) in order to evaluate the eco-compatibility of concrete structures considering both the environmental impact and the service life. In particular, the numerator for the A-index reflect the environmental impact (e.g. the carbon footprint) while the denominator is a parameter related to the durability of cement-based material (e.g. the chloride migration factor, the carbonation rate). However, no performance parameter is considered.

The building material sustainability potential (BMSP) is an index proposed by Muller et al. [327] that evaluates the sustainability of a concrete in relation to its mechanical performance (P), durability (Service life, SL) and GHG emissions (E).

$$BMSP = \frac{S_L \cdot P}{E} \qquad (40)$$

This index is the most complex and structured reported in the literature (Figure 122). Nevertheless, the denominator overlooks important issues such as the energy requirements and the natural resources consumption. Consider as example two Portland cement concretes manufactured with the same raw

materials, with the exception of aggregates. Concrete A is made of natural aggregates while concrete B is composed by recycled aggregates. By producing concrete with artificial aggregates, substantial changes in CO_2 emissions are not achieved, but the use of non-renewable raw materials is greatly reduced. However, this increase in the sustainability of the mixture cannot be expressed by BMSP, which has to be improved.

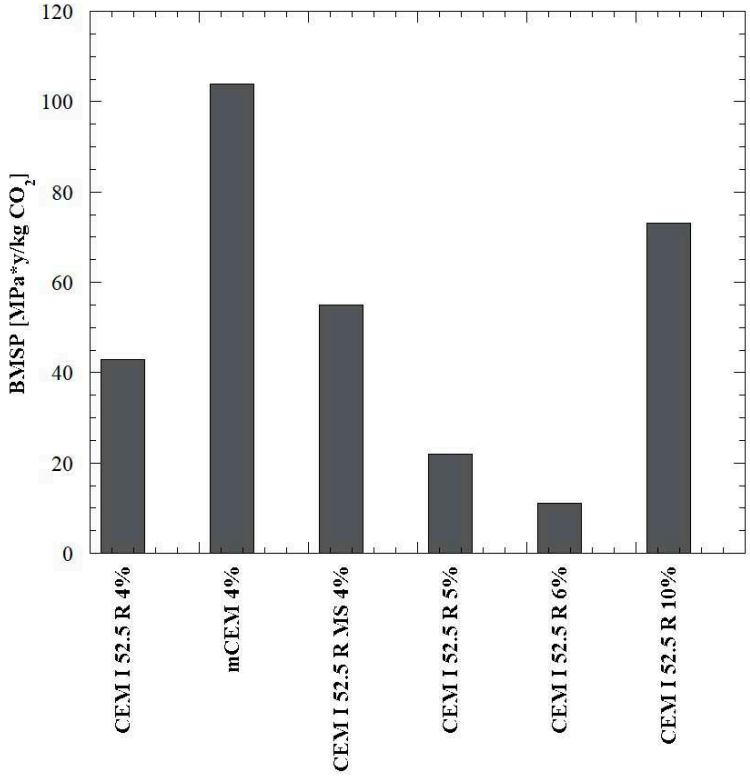

Figure 122 - BSMP of different concretes. Data from [327]

9.3 Sustainability index

Starting from the BMSP [327], a new index of sustainability, called Empathetic Added Sustainability Index (EASI), has been developed that takes into account both the environmental impact (EI) of mixtures but also the durability (Service life, SL) and the specific engineering properties (Performances, P) required by the structure.

The index EASI is expressed through the following expression:

$$EASI = \frac{n \cdot \prod_1^j P \cdot \prod_1^k S_L}{\sum_1^n EI} \qquad (41)$$

Within the environmental impact are considered the main factors related to the eco-compatibility of the materials such as:

- The CO_2 emissions estimated using the Global Warming Potential (GWP) parameter;
- The production energy calculated through the Gross Energy Requirement (GER) parameter;

- The consumption of non-renewable natural resources, including natural aggregates and drinking water, estimated using the Natural Raw Materials Consumption (NRMC) parameter.

The engineering properties considered in the index derive from the design parameters that guide the mix design. The Table 53 shows a non-exhaustive example list of the engineering properties considered under "Performance". Similarly, the environmental exposure of the structure guides the choice of durability parameters to be considered in the index EASI (Table 54).

Application	Performance
Structural concrete	28-day compressive strength
Concrete for slabs on ground	Flexural strength, shrinkage, elastic modulus
Concrete for massive structures	Long-term compressive strength, heat hydration
Mortar for retrofitting	Shrinkage, elastic modulus, tensile strength
Concrete for prefabricated elements	Early-ages compressive strength
Masonry mortars	28-day compressive strength
Plasters and renders	Shrinkage, elastic modulus, tensile strength
Thermal plaster	Shrinkage, elastic modulus, tensile strength, thermal resistance
Grouting mortar	Setting time, tensile strength

Table 53 – Performance taking into account for different applications

Application	Performance
Reinforced concrete exposed to air	Carbonation rate
Reinforced concrete exposed to deicing salts	Chloride migration coefficient
Reinforced concrete exposed to seawater	Chloride migration coefficient, sulfate resistance
Reinforced concrete exposed to freeze/thaw cycles	Freeze/thaw resistance
Reinforced concrete exposed to acid environments	Chemical attack resistance

Table 54 – Durability taking into account for different environments

According to Empathetic Added Sustainability Index EASI, three basic approaches to a sustainable use of concrete exists:

- The optimization of the composition of concrete regarding its environmental impact while maintaining an equal or better performance and service life;
- The improvement of the concrete's performance at equal environmental impact and service life;

- The optimization of service life of the building material and the building structure at equal impact and performance.

A combination of the above-named approaches appears reasonable.

9.4 Applications of EASI

For a structural concrete totally immersed in chloride-rich solution, the EASI can be calculated as

$$EASI_{Cl} = \frac{3 \cdot Rc_{28} \cdot \frac{1}{C_{cl}}}{NRMC + GER + GWP} \quad (42)$$

where Rc_{28} is the 28-day compressive strength and C_{cl} is the thickness of concrete penetrated by chloride in 50 years of service life. On the contrary, for the same concrete exposed to air, the C_{CO2} is used instead of C_{cl} according to the following equation

$$EASI_{CO2} = \frac{3 \cdot Rc_{28} \cdot \frac{1}{C_{CO_2}}}{NRMC + GER + GWP} \quad (43)$$

All the factors are normalized respect to reference Portland cement-based concrete.

Starting from the data reported in the scientific literature, it is possible to calculate the SI for:

- A traditional OPC concrete (OPC);
- A high-volume fly ash concrete (HVFA);
- An alkali-activated slag concrete (AAS);
- A CSA-based binary binder concrete (CSA);
- An OPC concrete manufactured with EAF slag aggregates instead of natural aggregates (EAF).

The analysis of EASI values shows how durability strongly influences the sustainability of concretes and mortars. In fact, in chloride-rich environments, the AAS and HVFA mixtures shows a sustainability index higher than that of all other investigated mixtures. On the contrary, CSA-based mixtures show a SI lower than that of OPC concrete due to its lower resistance in chloride-rich environments. Furthermore, for structures exposed to CO_2, the most sustainable solution among those shown in Table 55 seems to be based on the use of HVFA concrete (Figure 123).

	OPC	HVFA	AAS	CSA	EAF
Reference	[328]	[328]	[329]	[330]	[331]
CEM I [kg/m^3]	347	154	-	-	400
FA [kg/m^3]	-	195	-	-	-
GGBFS [kg/m^3]	-	-	400	-	-
CSA [kg/m^3]	-	-	-	264	-
CŜ [kg/m^3]	-	-	-	66	-
Activator [kg/m^3]	-	-	60	-	-
Water [kg/m^3]	132	123	160	131	200
Nat. aggr. [kg/m^3]	1903	1897	1790	1854	965
EAF aggr. [kg/m^3]	-	-	-	-	1190
Rc_{28} [MPa]	59	52	58	52	56
NRMC [kg/m^3]	2382	2174	2010	2184	1565
GER [MJ/m^3]	2156	1113	1230	1040	2480
GWP [kg CO_2/m^3]	345	157	102	216	397
C_{cl} [mm]	59	32	34	131	62
$EASI_{cl}$	-	2.91	3.36	0.66	1.03
C_{CO2} [m/y$^{0.5}$]	0.53	0.70	1.03	1.92	0.55
$EASI_{CO2}$	-	1.20	1.00	0.41	1.04

Table 55 – Composition, mechanical strength, durability and environmental parameters of concretes

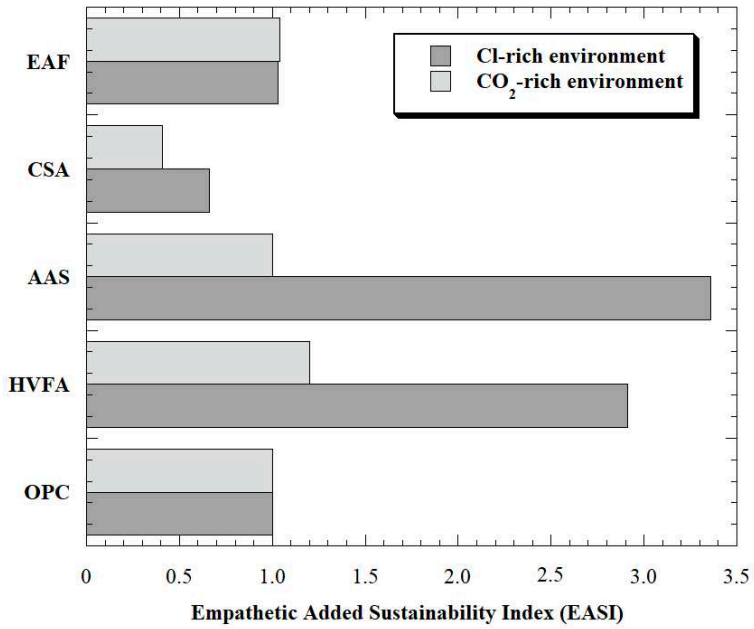

Figure 123 - EASI of concretes in Cl^--rich and CO_2-rich environments

Conversely, for a thermal plaster exposed to freeze and thaw cycles, the EASI can be calculated as

$$EASI_{plaster} = \frac{3 \cdot f_t \cdot \frac{1}{K} \cdot \frac{1}{\sigma_{cs}} \cdot \frac{1}{N_{50\%}}}{NRMC + GER + GWP} \quad (44)$$

where K is the thermal conductivity of plaster, $\sigma_{cs} = E \cdot \varepsilon_{cs}$ is the tensile stress induced by restrained shrinkage, f_t is the tensile strength and $N_{50\%}$ is the number of cycles needed to reduce by half the compressive strength of plaster subjected to freeze/thaw cycles. All the factors are normalized respect to reference NHL-based render. Starting from the data reported in the previous chapters and in the scientific literature, it is possible to calculate the SI for (Table 56):

- A traditional plaster manufactured with natural hydraulic lime (NHL);
- A traditional render based on hydrated lime (HL);
- A lightweight alkali-activated slag mortar (lw-AAS);
- A lightweight gypsum-hydrated lime plaster (lw-Gy/HL).

Results (Figure 124) indicated that the lightweight plasters have a SI about 7 times higher than that of normal-weight NHL mixtures due to the better durability in cold climate and the lower thermal conductivity that ensure a better thermal insulation. Moreover, the total substitution of binder based on natural raw materials such as HL and gypsum with industrial by-products such as GGBFS determine a sharp reduction of NRMC and, subsequently, an increase in Empathetic Added Sustainability Index.

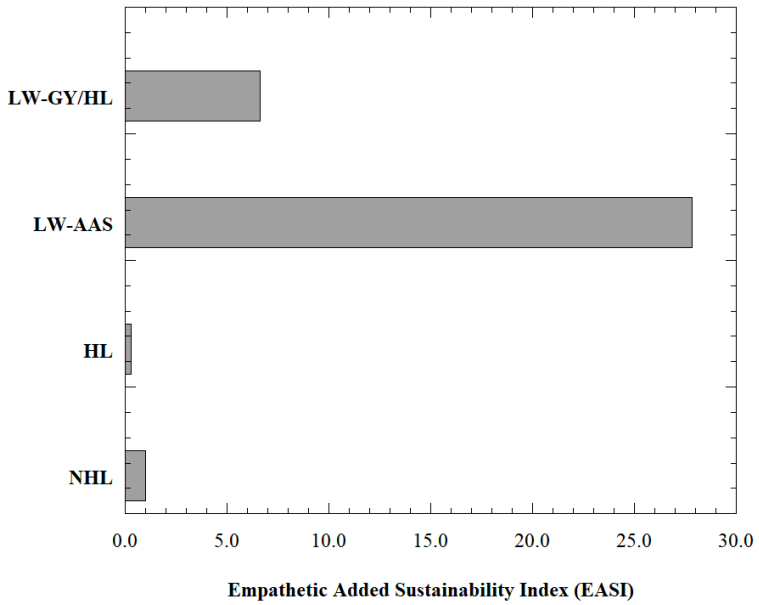

Figure 124 - EASI of thermal plaster

	NHL	HL	Lw-AAS	Lw-Gy/HL
Reference	[332]	[333]	Prev. chapter	[334]
NHL [kg/m^3]	400	-	-	-
HL [kg/m^3]	-	342	-	120
GGBFS [kg/m^3]	-	-	270	-
Gypsum [kg/m^3]	-	-	-	250
Activator [kg/m^3]	-	-	65	-
Nat. Aggr. [kg/m^3]	1200	1286	-	-
Light. Aggr. [kg/m^3]	-	-	250	500
Water [kg/m^3]	300	410	155	200
Density [kg/m^3]	1660	1670	760	930
E [GPa]	0.8	1.0*	1.5	2.5
ε_{cs} [mm/m]	4.5	13.0	2.2	5.8
Tensile strength [MPa]	0.5*	0.65*	1.95	1.1*
K [W/mK]	0.73	0.60	0.35	0.20
$N_{50\%}$	15*	12*	30*	32
NRMC [kg/m^3]	1900	2038	470	1070
GER [MJ/m^3]	1356	1706	1052	750
GWP [kg CO_2/m^3]	123	147	109	97
$EASI_{plaster}$	-	0.30	27.82	6.62

*estimated data based on the curves shown in [100]

Table 56 – Composition, mechanical strength, durability and environmental parameters of plasters

10. Conclusions

This thesis is focused on the alternative binders to Portland cement in order to manufacture sustainable mixtures for special applications such as repair mortars, lightweight reinforced plasters and concretes for slabs on ground. In particular, alkali-activated slag cements and calcium sulphoaluminate-based binders were used to produce Portland-free concretes and mortars.

The main specific conclusions arisen from this PhD thesis are listed below:

- The feasibility of manufacturing EN 1504-3 R3 class CSA-based mortars with supplementary cementitious materials (fly ash, ground granulated blast furnace slag) and hydrated lime instead of Portland cement was confirmed. In particular, the total replacement of OPC with SCMs and lime determines a sharp reduction in terms of elasto-mechanical properties approximately equal to 30%. Moreover, the effectiveness of tartaric acid-set retarding admixture on setting time control was also confirmed. In addition, a "zero shrinkage" behavior of CSA:SCMs:CH:CŜ mortars was also found when mixtures were cured in dry environment. Finally, OPC-free CSA-based mortars are characterized by a reduction both in energy requirement (GER) and greenhouse gases emissions (GWP) close to 60% and 45% respect to traditional OPC-based and CSA:OPC:CŜ mortars at equal strength class, respectively;
- Portland-free CSA-based concretes can be used to manufacture jointless slabs on ground due to their low shrinkage and adequate elasto-mechanical properties. In general, by using Abram's model, it is possible to note that Portland-free concretes have mechanical behavior close to that shown by traditional concretes manufactured with Portland cement or limestone Portland cement. Compressive strength values of reference mixtures CSA:OPC:CŜ are more affected by water/binder ratio than those of CSA:SCMs:CH:CŜ concretes. However, reference concretes, independently of w/b, exhibited compressive strength values higher than those obtained for CEM I 52.5 R based mixtures;
- Alkali-activated mortars and concretes seem to be a reasonable alternative to natural hydraulic lime-based and/or traditional Portland cement-based mixtures for rehabilitation or restoration of ancient masonry buildings and existing concretes structures;
- The key parameter that governed most of the properties both in fresh and hardened state of alkali-activated compounds is the alkali content. In particular, the main reaction product is a calcium silicate hydrate (C-S-H) and its concentration increase by increasing the alkali content. Moreover, the higher the alkali content, the lower is the water demand at equal workability class, the shorter is the setting time and the higher are the mechanical strength at early and long ages. However, shrinkage values are significantly higher (up to 4 times higher respect to OPC mortars)

and strictly related to the alkali content. Similarly to calcium sulphoaluminate cement-based mixtures, slag cement-based mortars evidence 80 – 90% and 70 – 80% reduction in greenhouse gas emission and energy production, respectively, compared to mortars produced with Portland cement;

- Both the CaO-based EA and ethylene glycol-based SRA admixtures reduce shrinkage by 50% and 40% with respect of no-admixed alkali activated mortar, respectively. Moreover, the combined use of expansive agents and SRA further reduces shrinkage, reaching values close to 1000 μm/m, typical of mortars manufactured with OPC;
- An alkali-activated slag-based plaster manufactured with expanded glass aggregates and air entraining admixture is able to provide a structural reinforcement of stone masonry buildings (28-day compressive strength equal to 8 MPa) with an improvement of the energy performance of the masonry (thermal conductivity 0.35 W/mK due to a density close to 800 kg/m^3). Moreover, thanks to the use of proper admixtures, shrinkage could be reduced to values close to those of Portland-based mortars, thus guaranteeing an excellent adhesion to the substrate (up to1.16 MPa) and the absence of micro-cracks;
- A new sustainability index was developed taking into account the environmental impact, the performances and the durability of mixtures. In particular, in the environmental impact section, the natural raw materials consumption, the greenhouse gas emissions and the energy consumption have been considered. Furthermore, depending on the applications and the environments, design parameters and properties related to durability have been assigned to each mixture.

References

1. U.S., G.S.; U.S., D. of I. *Mineral commodity summaries 2017*; 2017; Vol. 1; ISBN 978-1-4113-3548-6.
2. Ighalo, J.O.; Adeniyi, A.G. A perspective on environmental sustainability in the cement industry. *Waste Dispos. Sustain. Energy* **2020**, *2*, 161–164, doi:10.1007/s42768-020-00043-y.
3. Barcelo, L.; Kline, J.; Walenta, G.; Gartner, E. Cement and carbon emissions. *Mater. Struct.* **2014**, *47*, 1055–1065, doi:10.1617/s11527-013-0114-5.
4. Habert, G.; D'Espinose De Lacaillerie, J.B.; Roussel, N. An environmental evaluation of geopolymer based concrete production: Reviewing current research trends. *J. Clean. Prod.* **2011**, *19*, 1229–1238.
5. Schneider, M.; Romer, M.; Tschudin, M.; Bolio, H. Sustainable cement production-present and future. *Cem. Concr. Res.* **2011**, *41*, 642–650, doi:10.1016/j.cemconres.2011.03.019.
6. Chen, C.; Habert, G.; Bouzidi, Y.; Jullien, A. Environmental impact of cement production: detail of the different processes and cement plant variability evaluation. *J. Clean. Prod.* **2010**, *18*, 478–485, doi:10.1016/j.jclepro.2009.12.014.
7. Damtoft, J.S.; Lukasik, J.; Herfort, D.; Sorrentino, D.; Gartner, E.M. Sustainable development and climate change initiatives. *Cem. Concr. Res.* **2008**, *38*, 115–127, doi:10.1016/J.CEMCONRES.2007.09.008.
8. Puertas, F.; García-Díaz, I.; Barba, A.; Gazulla, M.F.; Palacios, M.; Gómez, M.P.; Martínez-Ramírez, S. Ceramic wastes as alternative raw materials for Portland cement clinker production. *Cem. Concr. Compos.* **2008**, *30*, 798–805, doi:10.1016/j.cemconcomp.2008.06.003.
9. Nidheesh, P. V; Kumar, M.S. An overview of environmental sustainability in cement and steel production. *J. Clean. Prod.* **2019**, *231*, 856–871, doi:https://doi.org/10.1016/j.jclepro.2019.05.251.
10. Gartner, E.; Hirao, H. A review of alternative approaches to the reduction of CO2 emissions associated with the manufacture of the binder phase in concrete. *Cem. Concr. Res.* **2015**, *78*, 126–142, doi:10.1016/j.cemconres.2015.04.012.
11. Pan, J.R.; Huang, C.; Kuo, J.-J.; Lin, S.-H. Recycling MSWI bottom and fly ash as raw materials for Portland cement. *Waste Manag.* **2008**, *28*, 1113–1118, doi:10.1016/J.WASMAN.2007.04.009.
12. Rahman, A.; Rasul, M.G.; Khan, M.M.K.; Sharma, S. Recent development on the uses of alternative fuels in cement manufacturing process. *Fuel* **2015**, *145*, 84–99,

doi:10.1016/j.fuel.2014.12.029.

13. Aranda Usón, A.; López-Sabirón, A.M.; Ferreira, G.; Llera Sastresa, E. Uses of alternative fuels and raw materials in the cement industry as sustainable waste management options. *Renew. Sustain. Energy Rev.* **2013**, *23*, 242–260, doi:10.1016/j.rser.2013.02.024.
14. Horsley, C.; Emmert, M.H.; Sakulich, A. Influence of alternative fuels on trace element content of ordinary portland cement. *Fuel* **2016**, *184*, 481–489, doi:10.1016/j.fuel.2016.07.038.
15. Rodrigues, F.A.; Joekes, I. Cement industry: Sustainability, challenges and perspectives. *Environ. Chem. Lett.* 2011, *9*, 151–166.
16. Ahmaruzzaman, M. A review on the utilization of fly ash. *Prog. Energy Combust. Sci.* **2010**, *36*, 327–363, doi:10.1016/j.pecs.2009.11.003.
17. Siddique, R. Performance characteristics of high-volume Class F fly ash concrete. *Cem. Concr. Res.* **2004**, *34*, 487–493, doi:10.1016/j.cemconres.2003.09.002.
18. Özbay, E.; Erdemir, M.; Durmuş, H.I. Utilization and efficiency of ground granulated blast furnace slag on concrete properties - A review. *Constr. Build. Mater.* **2016**, *105*, 423–434.
19. Ding, J.T.; Li, Z. Effects of metakaolin and silica fume on properties of concrete. *ACI Mater. J.* **2002**, *99*, 393–398, doi:10.14359/12222.
20. Uzal, B.; Turanli, L.; Mehta, P.K. High-Volume Natural Pozzolan Concrete for Structural Applications. *Mater. J. 104*, doi:10.14359/18910.
21. Rahla, K.M.; Mateus, R.; Bragança, L. Comparative sustainability assessment of binary blended concretes using Supplementary Cementitious Materials (SCMs) and Ordinary Portland Cement (OPC). *J. Clean. Prod.* **2019**, *220*, 445–459, doi:https://doi.org/10.1016/j.jclepro.2019.02.010.
22. American Road & Transportation Builders Association *Global Fly Ash Market 2024, 2016*; 2015;
23. *Global Fly Ash Market 2024: Outlook, Insights, Forecast, Trends, Demand Analysis Reports 2016-2024, Published on 2017-09-15, Reported page:210*;
24. Hirt, G. Process Technology of Cement Manufacturing. In Proceedings of the Proceedings of 7th VDZ Congress; 2014.
25. Duxson, P.; Provis, J.L.; Lukey, G.C.; van Deventer, J.S.J. The role of inorganic polymer technology in the development of "green concrete." *Cem. Concr. Res.* **2007**, *37*, 1590–1597, doi:10.1016/j.cemconres.2007.08.018.
26. Juenger, M.C.G.; Winnefeld, F.; Provis, J.L.; Ideker, J.H. Advances in alternative cementitious binders. *Cem. Concr. Res.* **2011**, *41*, 1232–1243, doi:10.1016/j.cemconres.2010.11.012.
27. Provis, J.L. Geopolymers and other alkali activated materials: why, how, and what? *Mater.*

Struct. **2014**, *47*, 11–25, doi:10.1617/s11527-013-0211-5.

28. Yuan, B.; Yu, Q.L.; Brouwers, H.J.H. Evaluation of slag characteristics on the reaction kinetics and mechanical properties of Na2CO3 activated slag. *Constr. Build. Mater.* **2017**, *131*, 334–346, doi:10.1016/J.CONBUILDMAT.2016.11.074.
29. Bernal, S.A.; Provis, J.L. Durability of Alkali-Activated Materials: Progress and Perspectives. *J. Am. Ceram. Soc.* **2014**, *97*, 997–1008, doi:10.1111/jace.12831.
30. Pacheco-Torgal, F.; Abdollahnejad, Z.; Camões, A.F.; Jamshidi, M.; Ding, Y. Durability of alkali-activated binders: A clear advantage over Portland cement or an unproven issue? *Constr. Build. Mater.* **2012**, *30*, 400–405, doi:10.1016/J.CONBUILDMAT.2011.12.017.
31. Provis, J.L.; Palomo, A.; Shi, C. Advances in understanding alkali-activated materials. *Cem. Concr. Res.* **2015**, *78*, 110–125, doi:10.1016/j.cemconres.2015.04.013.
32. da Costa, E.B.; Rodríguez, E.D.; Bernal, S.A.; Provis, J.L.; Gobbo, L.A.; Kirchheim, A.P. Production and hydration of calcium sulfoaluminate-belite cements derived from aluminium anodising sludge. *Constr. Build. Mater.* **2016**, *122*, 373–383, doi:10.1016/j.conbuildmat.2016.06.022.
33. El-Alfi, E.A.; Gado, R.A. Preparation of calcium sulfoaluminate-belite cement from marble sludge waste. *Constr. Build. Mater.* **2016**, *113*, 764–772, doi:10.1016/J.CONBUILDMAT.2016.03.103.
34. Gastaldi, D.; Canonico, F.; Boccaleri, E. Ettringite and calcium sulfoaluminate cement: investigation of water content by near-infrared spectroscopy. *J. Mater. Sci.* **2009**, *44*, 5788–5794, doi:10.1007/s10853-009-3812-1.
35. Trauchessec, R.; Mechling, J.M.; Lecomte, A.; Roux, A.; Le Rolland, B. Hydration of ordinary Portland cement and calcium sulfoaluminate cement blends. *Cem. Concr. Compos.* **2015**, *56*, 106–114, doi:10.1016/j.cemconcomp.2014.11.005.
36. Winnefeld, F.; Lothenbach, B. Hydration of calcium sulfoaluminate cements — Experimental findings and thermodynamic modelling. *Cem. Concr. Res.* **2010**, *40*, 1239–1247, doi:10.1016/j.cemconres.2009.08.014.
37. Martin, L.H.J.; Winnefeld, F.; Tschopp, E.; Müller, C.J.; Lothenbach, B. Influence of fly ash on the hydration of calcium sulfoaluminate cement. *Cem. Concr. Res.* **2017**, *95*, 152–163, doi:10.1016/J.CEMCONRES.2017.02.030.
38. García-Maté, M.; De La Torre, A.G.; León-Reina, L.; Aranda, M.A.G.; Santacruz, I. Hydration studies of calcium sulfoaluminate cements blended with fly ash. *Cem. Concr. Res.* **2013**, *54*, 12–20, doi:10.1016/j.cemconres.2013.07.010.
39. Cau Dit Coumes, C.; Dhoury, M.; Champenois, J.B.; Mercier, C.; Damidot, D. Physico-

chemical mechanisms involved in the acceleration of the hydration of calcium sulfoaluminate cement by lithium ions. *Cem. Concr. Res.* **2017**, *96*, 42–51, doi:10.1016/j.cemconres.2017.03.004.

40. Cau Dit Coumes, C.; Dhoury, M.; Champenois, J.-B.; Mercier, C.; Damidot, D. Combined effects of lithium and borate ions on the hydration of calcium sulfoaluminate cement. *Cem. Concr. Res.* **2017**, *97*, 50–60, doi:10.1016/J.CEMCONRES.2017.03.006.
41. Champenois, J.-B.; Dhoury, M.; Cau Dit Coumes, C.; Mercier, C.; Revel, B.; Le Bescop, P.; Damidot, D. Influence of sodium borate on the early age hydration of calcium sulfoaluminate cement. *Cem. Concr. Res.* **2015**, *70*, 83–93, doi:10.1016/J.CEMCONRES.2014.12.010.
42. Yuan, X.; Chen, W.; Yang, M. Effect of superplasticizers on the early age hydration of sulfoaluminate cement. *J. Wuhan Univ. Technol. Mater. Sci. Ed.* **2014**, *29*, 757–762, doi:10.1007/s11595-014-0992-6.
43. Pelletier-Chaignat, L.; Winnefeld, F.; Lothenbach, B.; Saout, G. Le; Müller, C.J.; Famy, C. Influence of the calcium sulphate source on the hydration mechanism of Portland cement-calcium sulphoaluminate clinker-calcium sulphate binders. *Cem. Concr. Compos.* **2011**, *33*, 551–561, doi:10.1016/j.cemconcomp.2011.03.005.
44. Batayneh, M.; Marie, I.; Asi, I. Use of selected waste materials in concrete mixes. *Waste Manag.* **2007**, *27*, 1870–1876, doi:10.1016/j.wasman.2006.07.026.
45. Aydin, E.; Arel, H.Ş. High-volume marble substitution in cement-paste: Towards a better sustainability. *J. Clean. Prod.* **2019**, *237*, 117801, doi:https://doi.org/10.1016/j.jclepro.2019.117801.
46. Behera, M.; Bhattacharyya, S.K.; Minocha, A.K.; Deoliya, R.; Maiti, S. Recycled aggregate from C&D waste & its use in concrete - A breakthrough towards sustainability in construction sector: A review. *Constr. Build. Mater.* **2014**, *68*, 501–516, doi:10.1016/j.conbuildmat.2014.07.003.
47. Carsana, M.; Frassoni, M.; Bertolini, L. Comparison of ground waste glass with other supplementary cementitious materials. *Cem. Concr. Compos.* **2014**, *45*, doi:10.1016/j.cemconcomp.2013.09.005.
48. Colangelo, F.; Cioffi, R. Mechanical properties and durability of mortar containing fine fraction of demolition wastes produced by selective demolition in South Italy. *Compos. Part B Eng.* **2017**, *115*, 43–50, doi:10.1016/J.COMPOSITESB.2016.10.045.
49. Foti, D. Use of recycled waste pet bottles fibers for the reinforcement of concrete. *Compos. Struct.* **2013**, *96*, 396–404, doi:10.1016/j.compstruct.2012.09.019.
50. Siddique, R.; Schutter, G. de; Noumowe, A. Effect of used-foundry sand on the mechanical

properties of concrete. *Constr. Build. Mater.* **2009**, *23*, 976–980.

51. Coppola, L.; Kara, P.; Lorenzi, S. Concrete manufactured with crushed asphalt as partial replacement of natural aggregates. *Mater. Constr.* **2016**, *66*, doi:10.3989/mc.2016.06515.
52. Coppola, L.; Buoso, A.; Coffetti, D.; Kara, P.; Lorenzi, S. Electric arc furnace granulated slag for sustainable concrete. *Constr. Build. Mater.* **2016**, *123*, doi:10.1016/j.conbuildmat.2016.06.142.
53. Shi, C.; Zheng, K. A review on the use of waste glasses in the production of cement and concrete. *Resour. Conserv. Recycl.* **2007**, *52*, 234–247, doi:10.1016/j.resconrec.2007.01.013.
54. Ecorsy *EU Construction and demolition waste management protocol*; 2016;
55. Coppola, L.; Cerulli, T.; Salvioni, D. Sustainable development and durability of self-compacting concretes. In Proceedings of the 11th International Conference on Fracture 2005, ICF11; 2005; Vol. 3.
56. Ponikiewski, T.; Gołaszewski, J. The Rheological and Mechanical Properties of High-performance Self-compacting Concrete with High-calcium Fly Ash. *Procedia Eng.* **2013**, *65*, 33–38, doi:10.1016/J.PROENG.2013.09.007.
57. Janotka, I.; Krajči, L. An experimental study on the upgrade of sulfoaluminate—belite cement systems by blending with Portland cement. *Adv. Cem. Res.* **1999**, *11*, 35–41.
58. Sharp, J.H.; Lawrence, C.D.; Yang, R. Calcium sulfoaluminate cements—low-energy cements, special cements or what? *Adv. Cem. Res.* **1999**, *11*, 3–13, doi:10.1680/adcr.1999.11.1.3.
59. Kasselouri, V.; Tsakiridis, P.; Malami, C.; Georgali, B.; Alexandridou, C. A study on the hydration products of a non-expansive sulfoaluminate cement. *Cem. Concr. Res.* **1995**, *25*, 1726–1736, doi:10.1016/0008-8846(95)00168-9.
60. Hanic, F.; Kaprálik, I.; Gabrisová, A. Mechanism of hydration reactions in the system C4A3SCSCaOH2O referred to hydration of sulphoaluminate cements. *Cem. Concr. Res.* **1989**, *19*, 671–682, doi:10.1016/0008-8846(89)90038-0.
61. Zhang, L.; Su, M.; Wang, Y. Development of the use of sulfo- and ferroaluminate cements in China. *Adv. Cem. Res.* **1999**, *11*, 15–21, doi:10.1680/adcr.1999.11.1.15.
62. Mehta, P.K. Investigations on energy-saving cements. *World Cem. Technol.* **1980**, *May*, 166–177.
63. Lan, W.; Glasser, F.P. Hydration of calcium sulphoaluminate cements. *Adv. Cem. Res.* **1996**, *8*, 127–134, doi:10.1680/adcr.1996.8.31.127.
64. Beretka, J.; de Vito, B.; Santoro, L.; Sherman, N.; Valenti, G.L. Hydraulic behaviour of calcium sulfoaluminate-based cements derived from industrial process wastes. *Cem. Concr.*

Res. **1993**, *23*, 1205–1214, doi:10.1016/0008-8846(93)90181-8.

65. Glasser, F.P.; Zhang, L. High-performance cement matrices based on calcium sulfoaluminate-belite compositions. *Cem. Concr. Res.* **2001**, *31*, 1881–1886, doi:10.1016/S0008-8846(01)00649-4.
66. Quillin, K. Performance of belite–sulfoaluminate cements. *Cem. Concr. Res.* **2001**, *31*, 1341–1349.
67. Péra, J.; Ambroise, J. New applications of calcium sulfoaluminate cement. *Cem. Concr. Res.* **2004**, *34*, 671–676, doi:10.1016/j.cemconres.2003.10.019.
68. Gartner, E. Industrially interesting approaches to "low-CO2" cements. *Cem. Concr. Res.* **2004**, *34*, 1489–1498, doi:10.1016/j.cemconres.2004.01.021.
69. Julphunthong, P. Synthesizing of calcium sulfoaluminate-belite (CSAB) cements from industrial waste materials. *Mater. Today Proc.* **2018**, *5*, 14933–14938, doi:10.1016/j.matpr.2018.04.033.
70. Telesca, A.; Marroccoli, M.; Tomasulo, M.; Valenti, G.L.; Dieter, H.; Montagnaro, F. Calcium looping spent sorbent as a limestone replacement in the manufacture of portland and calcium sulfoaluminate cements. *Environ. Sci. Technol.* **2015**, *49*, 6865–6871.
71. Guo, X.; Shi, H.; Hu, W.; Wu, K. Durability and microstructure of CSA cement-based materials from MSWI fly ash. **2014**, doi:10.1016/j.cemconcomp.2013.10.015.
72. Wu, K.; Shi, H.; Guo, X. Utilization of municipal solid waste incineration fly ash for sulfoaluminate cement clinker production. *Waste Manag.* **2011**, *31*, 2001–2008.
73. Marroccoli, M.; Pace, M.L.; Telesca, A.; Valenti, G.L.; Montagnaro, F. Utilization of coal combustion ashes for the synthesis of ordinary and special cements. *Combust. Sci. Technol.* **2010**, *182*, 588–599.
74. Shen, Y.; Qian, J.; Chai, J.; Fan, Y. Calcium sulphoaluminate cements made with phosphogypsum: Production issues and material properties. *Cem. Concr. Compos.* **2014**, *48*, 67–74, doi:10.1016/j.cemconcomp.2014.01.009.
75. Zhang, L. Microstructure and performance of calcium sulfoaluminate cements, 2000.
76. Pelletier, L.; Winnefeld, F.; Lothenbach, B. The ternary system Portland cement-calcium sulphoaluminate clinker-anhydrite: Hydration mechanism and mortar properties. *Cem. Concr. Compos.* **2010**, *32*, 497–507, doi:10.1016/j.cemconcomp.2010.03.010.
77. Álvarez-Pinazo, G.; Cuesta, A.; García-Maté, M.; Santacruz, I.; Losilla, E.R.; La Torre, A.G.D.; León-Reina, L.; Aranda, M.A.G. Rietveld quantitative phase analysis of Yeelimite-containing cements. *Cem. Concr. Res.* **2012**, *42*, 960–971, doi:10.1016/j.cemconres.2012.03.018.

78. Duan, P.; Chen, W.; Ma, J.; Shui, Z. Influence of layered double hydroxides on microstructure and carbonation resistance of sulphoaluminate cement concrete. **2013**, doi:10.1016/j.conbuildmat.2013.07.049.
79. Bernardo, G.; Telesca, A.; Valenti, G.L. A porosimetric study of calcium sulfoaluminate cement pastes cured at early ages. *Cem. Concr. Res.* **2006**, *36*, 1042–1047, doi:10.1016/j.cemconres.2006.02.014.
80. Binda, L.; Modena, C.; Baronio, G.; Abbaneo, S. Repair and investigation techniques for stone masonry walls. *Constr. Build. Mater.* **1997**, *11*, 133–142, doi:10.1016/S0950-0618(97)00031-7.
81. Damineli, B.L.; Kemeid, F.M.; Aguiar, P.S.; John, V.M. Measuring the eco-efficiency of cement use. *Cem. Concr. Compos.* **2010**, *32*, 555–562, doi:10.1016/j.cemconcomp.2010.07.009.
82. Gastaldi, D.; Paul, G.; Marchese, L.; Irico, S.; Boccaleri, E.; Mutke, S.; Buzzi, L.; Canonico, F. Hydration products in sulfoaluminate cements: Evaluation of amorphous phases by XRD/solid-state NMR. *Cem. Concr. Res.* **2016**, *90*, 162–173, doi:10.1016/J.CEMCONRES.2016.05.014.
83. Hanein, T.; Imbabi, M.; Glasser, F.P.; Bannerman, M. Lowering the carbon footprint and energy consumption of cement production: a novel Calcium SulfoAluminate cement production process. In Proceedings of the 1st International conference on Grand Challenges in Construction Materials; 2016.
84. García-Maté, M. Processing and characterization of calcium sulphoaluminate (CSA) eco-cements with tailored performances, 2014.
85. Phair, J.W. Green chemistry for sustainable cement production and use. *Green Chem.* 2006, *8*, 763–780.
86. McCaffrey, R. Climate change and the cement industry. *Environ. Overv.* **2002**.
87. Tang, S.W.; Zhu, H.G.; Li, Z.J.; Chen, E.; Shao, H.Y. Hydration stage identification and phase transformation of calcium sulfoaluminate cement at early age. *Constr. Build. Mater.* **2015**, *75*, 11–18, doi:10.1016/j.conbuildmat.2014.11.006.
88. Álvarez-Pinazo, G.; Cuesta, A.; García-Maté, M.; Santacruz, I.; Losilla, E.R.; Sanfélix, S.G.; Fauth, F.; Aranda, M.A.G.; De La Torre, A.G. In-situ early-age hydration study of sulfobelite cements by synchrotron powder diffraction. *Cem. Concr. Res.* **2014**, *56*, 12–19, doi:10.1016/j.cemconres.2013.10.009.
89. Meller, N.; Hall, C.; Jupe, A.C.; Colston, S.L.; Jacques, S.D.M.; Barnes, P.; Phipps, J. The paste hydration of brownmillerite with and without gypsum: A time resolved synchrotron

diffraction study at 30, 70, 100 and 150 °C. *J. Mater. Chem.* **2004**, *14*, 428–435, doi:10.1039/b313215c.

90. Meredith, P.; Donald, A.M.; Meller, N.; Hall, C. Tricalcium aluminate hydration: Microstructural observations by in-situ electron microscopy. In Proceedings of the Journal of Materials Science; Kluwer Academic Publishers, 2004; Vol. 39, pp. 997–1005.
91. Han, S.; Yan, P.Y.; Liu, R.G. Study on the hydration product of cement in early age using TEM. *Sci. China Technol. Sci.* **2012**, *55*, 2284–2290, doi:10.1007/s11431-012-4860-3.
92. Telesca, A.; Marroccoli, M.; Pace, M.L.; Tomasulo, M.; Valenti, G.L.; Monteiro, P.J.M. A hydration study of various calcium sulfoaluminate cements. *Cem. Concr. Compos.* **2014**, *53*, 224–232, doi:10.1016/j.cemconcomp.2014.07.002.
93. Telesca, A.; Marroccoli, M.; Tomasulo, M.; Valenti, G.L. Hydration Properties and Technical Behavior of Calcium Sulfoaluminate Cements. *Spec. Publ.* **2015**, *303*, 237–254.
94. Marchi, M.; Costa, U. Influence of the calcium sulphate and w/c ratio on the hydration of calcium sulfoaluminate cement. In Proceedings of the Proceedings of 13th International conference on the chemistry of cement; 2011.
95. Moncea, A.; Georgescu, M. Influence of the calcium sulphate type on the hydration and hardening processes of some ternary binders silicate-aluminate-sulphate. *U.P.B. Sci. Bull., Ser. B* **2013**, *75*.
96. Telesca, A.; Marroccoli, M.; Pace, M.L.; Tomasulo, M.; Valenti, G.L.; Naik, T.R. Expansive and non-expansive calcium sulfoaluminate-based cements. *3rd Int. Conf. Sustain. Constr. Mater. Technol.* **2013**, *3*.
97. Winnefeld, F.; Barlag, S. Influence of calcium sulfate and calcium hydroxide on the hydration of calcium sulfoaluminate clinker. In Proceedings of the ZKG International; 2009.
98. Winnefeld, F.; Barlag, S. Calorimetric and thermogravimetric study on the influence of calcium sulfate on the hydration of ye'elimite., doi:10.1007/s10973-009-0582-6.
99. Taczuk, L.; Bayoux, J.; Sorrentino, F.; Capmas, A. Understanding of the hydration mechanism of C4A3S-Portland clinker-CaSO4 mixes. In Proceedings of the Proceedings of 9th ICCC - New Delhi: National council for cement and buildings materials; 1992; pp. 278–284.
100. Neville, A. *Properties of Concrete*; Prentice Hall, Ed.; 2011; ISBN 9780273786320.
101. Collepardi, M. A state-of-the-art review on delayed ettringite attack on concrete. *Cem. Concr. Compos.* 2003, *25*, 401–407.
102. Beretka, J.; Marroccoli, M.; Sherman, N.; Valenti, G.L. The influence of C4A3$\bar{S}$ content and WS ratio on the performance of calcium sulfoaluminate-based cements. *Cem. Concr. Res.* **1996**, *26*, 1673–1681, doi:10.1016/S0008-8846(96)00164-0.

103. Chen, I.A.; Hargis, C.W.; Juenger, M.C.G. Understanding expansion in calcium sulfoaluminate-belite cements. *Cem. Concr. Res.* **2012**, *42*, 51–60, doi:10.1016/j.cemconres.2011.07.010.
104. Sahu, S.; Havlica, J.; Tomková, V.; Majling, J. Hydration behaviour of sulphoaluminate belite cement in the presence of various calcium sulphates. *Thermochim. Acta* **1991**, *175*, 45–52, doi:10.1016/0040-6031(91)80244-D.
105. Hargis, C.W.; Telesca, A.; Monteiro, P.J.M. Calcium sulfoaluminate (Ye'elimite) hydration in the presence of gypsum, calcite, and vaterite. *Cem. Concr. Res.* **2014**, *65*, 15–20, doi:10.1016/j.cemconres.2014.07.004.
106. Ioannou, S. An assessment of the performance of calcium sulfoaluminate and supersulfated cements for use in concrete, 2013.
107. Ioannou, S.; Paine, K.; Reig, L.; Quillin, K. Performance characteristics of concrete based on a ternary calcium sulfoaluminate-anhydrite-fly ash cement. *Cem. Concr. Compos.* **2015**, *55*, 196–204, doi:10.1016/j.cemconcomp.2014.08.009.
108. Li, G.; Zhang, J.; Song, Z.; Shi, C.; Zhang, A. Improvement of workability and early strength of calcium sulphoaluminate cement at various temperature by chemical admixtures. *Constr. Build. Mater.* **2018**, *160*, 427–439, doi:10.1016/j.conbuildmat.2017.11.076.
109. Sherman, N.; Beretka, J.; Santoro, L.; Valenti, G.L. Long-term behaviour of hydraulic binders based on calcium sulfoaluminate and calcium sulfosilicate. *Cem. Concr. Res.* **1995**, *25*, 113–126, doi:10.1016/0008-8846(94)00119-J.
110. Sirtoli, D. Mechanical performance of sulfo-based rapid hardening concrete systems focusing on blends with Portland cement, University of Bergamo, 2018.
111. Valenti, G.L.; Marroccoli, M.; Pace, M.L.; Telesca, A. Discussion of the paper Understanding expansion in calcium sulfoaluminate-belite cements by I.A. Chen et al., Cem. Concr. Res. 42 (2012) 51-60. *Cem. Concr. Res.* 2012, *42*, 1555–1559.
112. Chen, I.A.; Hargis, C.W.; Juenger, M.C.G. Reply to the discussion of the paper Understanding expansion in calcium sulfoaluminate-belite cements by G.L. Valenti, M. Marroccoli, M.L. Pace, A. Telesca. *Cem. Concr. Res.* **2012**, *42*, 1560–1562, doi:10.1016/j.cemconres.2012.08.001.
113. Wang, S.; Ji, X.S.; Liu, Y.; Hu, K. Effect of alkali on the expansive properties of sulfoaluminate cement pastes. In Proceedings of the Proceedings of 8th international congress of chemistry of cement; 1986; pp. 301–305.
114. Gu, P.; Beaudoin, J.J.; Quinn, E.G.; Myers, R.E. Early strength development and hydration of ordinary portland cement/calcium aluminate cement pastes. *Adv. Cem. Based Mater.* **1997**, *6*,

53–58, doi:10.1016/S1065-7355(97)00008-4.

115. Glasser, F. Advances in sulfoaluminate cements. Proc. 5th Int. Symp. Cem. Concr.; Shanghai (China), 2002; pp. 1: 14-24.
116. Sirtoli, D.; Tortelli, S.; Riva, P.; Marchi, M.; Cucitore, R.; Rose, M.N. Mechanical and environmental performances of sulpho-based rapid hardening concrete. In Proceedings of the American Concrete Institute, ACI Special Publication; 2015; Vol. 2015-Janua.
117. Živica, V. Properties of blended sulfoaluminate belite cement. *Constr. Build. Mater.* **2000**, *14*, 433–437, doi:10.1016/S0950-0618(00)00050-7.
118. Ioannou, S.; Reig, L.; Paine, K.; Quillin, K. Properties of a ternary calcium sulfoaluminate-calcium sulfate-fly ash cement. *Cem. Concr. Res.* **2014**, *56*, 75–83, doi:10.1016/j.cemconres.2013.09.015.
119. Burris, L.E.; Kurtis, K.E. Influence of set retarding admixtures on calcium sulfoaluminate cement hydration and property development. *Cem. Concr. Res.* **2017**, *104*, 105–113, doi:10.1016/j.cemconres.2017.11.005.
120. Velazco, G.; Almanza, J.M.; Cortés, D.A.; Escobedo, J.C. Effect of citric acid and the hemihydrate amount on the properties of a calcium sulphoaluminate cement. *Mater. Constr.* **2014**, *64*, 1–8.
121. Zhang, G.; Li, G.; Li, Y. Effects of superplasticizers and retarders on the fluidity and strength of sulphoaluminate cement. *Constr. Build. Mater.* **2016**, *126*, 44–54, doi:10.1016/j.conbuildmat.2016.09.019.
122. Guo, W.; Sun, N.; Qin, J.; Zhang, J.; Pei, M.; Wang, Y.; Wang, S. Synthesis and properties of an amphoteric polycarboxylic acid-based superplasticizer used in sulfoaluminate cement. *J. Appl. Polym. Sci.* **2012**, *125*, 283–290, doi:10.1002/app.35565.
123. Maltese, C.; Pistolesi, C.; Lolli, A.; Bravo, A.; Cerulli, T.; Salvioni, D. Combined effect of expansive and shrinkage reducing admixtures to obtain stable and durable mortars. *Cem. Concr. Res.* **2005**, *35*, 2244–2251, doi:10.1016/j.cemconres.2004.11.021.
124. Collepardi, M.; Borsoi, A.; Collepardi, S.; Ogoumah Olagot, J.J.; Troli, R. Effects of shrinkage reducing admixture in shrinkage compensating concrete under non-wet curing conditions. *Cem. Concr. Compos.* **2005**, *27*, 704–708, doi:10.1016/j.cemconcomp.2004.09.020.
125. Ambroise, J.; Georgin, J.F.; Peysson, S.; Péra, J. Influence of polyether polyol on the hydration and engineering properties of calcium sulfoaluminate cement. *Cem. Concr. Compos.* **2009**, *31*, 474–482, doi:10.1016/j.cemconcomp.2009.04.009.
126. Hargis, C.W.; Lothenbach, B.; Müller, C.J.; Winnefeld, F. Carbonation of calcium sulfoaluminate mortars. *Cem. Concr. Compos.* **2017**, *80*, 123–134,

doi:10.1016/j.cemconcomp.2017.03.003.

127. Su, M.; Wang, Y.; Zhang, L.; Li, D. Preliminary study on the durability of sulfo/ferro-aluminate cements. In Proceedings of the Proceedings of 10th International Congress on the Chemistry of Cement; 1997; p. paper 4iv029.
128. Zhang, L.; Glasser, F.P. Investigation of the microstructure and carbonation of C$\bar{S}$A-based concretes removed from service. *Cem. Concr. Res.* **2005**, *35*, 2252–2260, doi:10.1016/j.cemconres.2004.08.007.
129. Zhang, D.; Xu, D.; Cheng, X.; Chen, W. Carbonation resistance of sulphoaluminate cement-based high performance concrete. *J. Wuhan Univ. Technol. Mater. Sci. Ed.* **2009**, *24*, 663–666, doi:10.1007/s11595-009-4663-y.
130. Hajimohammadi, A.; Ngo, T.; Mendis, P.; Kashani, A.; van Deventer, J.S.J. Alkali activated slag foams: The effect of the alkali reaction on foam characteristics. *J. Clean. Prod.* **2017**, *147*, 330–339, doi:https://doi.org/10.1016/j.jclepro.2017.01.134.
131. Rai, S.; Singh, N.B.; Singh, N.P. Interaction of tartaric acid during hydration of Portland cement. *Indian J. Chem. Technol.* **2006**, *13*, 255–261.
132. Bishop, M.; Barron, A.R. Cement hydration inhibition with sucrose, tartaric acid, and lignosulfonate: Analytical and spectroscopic study. *Ind. Eng. Chem. Res.* **2006**, *45*, 7042–7049, doi:10.1021/ie060806t.
133. Mehta, P.K. *High Performance, High Volume Fly Ash Concrete For Sustainable Development*; 2004; ISBN 0965231070.
134. Marroccoli, M.; Montagnaro, F.; Telesca, A.; Valenti, G.L. Environmental implications of the manufacture of calcium sulfoaluminate-based cements. In Proceedings of the Proceedings of the 2nd International Conference on Sustainable Construction Materials and Technologies; Ancona, Italy, 2010; Vol. 1, pp. 625–635.
135. Gastaldi, D.; Bertola, F.; Canonico, F.; Buzzi, L.; Mutke, S.; Irico, S.; Paul, G.; Marchese, L.; Boccaleri, E. A chemical/mineralogical investigation of the behavior of sulfoaluminate binders submitted to accelerated carbonation. *Cem. Concr. Res.* **2018**, *109*, 30–41, doi:10.1016/j.cemconres.2018.04.006.
136. Leemann, A.; Pahlke, H.; Loser, R.; Winnefeld, F. Carbonation resistance of mortar produced with alternative cements. *Mater. Struct. Constr.* **2018**, *51*, 114, doi:10.1617/s11527-018-1239-3.
137. Carsana, M.; Canonico, F.; Bertolini, L. Corrosion resistance of steel embedded in sulfoaluminate-based binders. *Cem. Concr. Compos.* **2018**, *88*, 211–219, doi:10.1016/j.cemconcomp.2018.01.014.

138. Venkateswara Reddy, V.; Sudarsana Rao, H.; Jayaveera, K.N. Influence of strong alkaline substances (sodium carbonate and sodium bicarbonate) in mixing water on strength and setting properties of concrete. *Indian J. Eng. Mater. Sci.* **2006**, *13*, 123–128.
139. Zhang, Y.; Wang, Y.; Li, T.; Xiong, Z.; Sun, Y. Effects of lithium carbonate on performances of sulphoaluminate cement-based dual liquid high water material and its mechanisms. *Constr. Build. Mater.* **2018**, *161*, 374–380, doi:10.1016/J.CONBUILDMAT.2017.11.130.
140. Mynarcik, P. Technology and trends of concrete industrial floors. In Proceedings of the Procedia Engineering; 2013; Vol. 65, pp. 107–112.
141. Bissonnette, B.; Miltenberger, M.A.; Fortin, C.; Attiogbe, E.K. Drying Shrinkage, Curling, and Joint Opening of Slabs-on-Ground. *Mater. J. 104*, doi:10.14359/18671.
142. Ababneh, A.N.; Al-Rousan, R.Z.; Alhassan, M.A.; Sheban, M.A. Assessment of shrinkage-induced cracks in restrained and unrestrained cement-based slabs. **2017**, doi:10.1016/j.conbuildmat.2016.11.036.
143. Shadravan, S.; Ramseyer, C.; Kang, T.H.-K. A long term restrained shrinkage study of concrete slabs on ground. *Eng. Struct.* **2015**, *102*, 258–265, doi:10.1016/j.engstruct.2015.08.018.
144. Zhang, Y.; Collepardi, M.; Coppola, L.; Guan, W.L.; Zaffaroni, P. *Industria Italiana del Cemento*. 2003,.
145. García Calvo, J.L.; Revuelta, D.; Carballosa, P.; Gutiérrez, J.P. Comparison between the performance of expansive SCC and expansive conventional concretes in different expansion and curing conditions. *Constr. Build. Mater.* **2017**, *136*, 277–285, doi:10.1016/j.conbuildmat.2017.01.039.
146. Coppola, L.; Buoso, A.; Coffetti, D.; Kara, P.; Lorenzi, S. Electric arc furnace granulated slag for sustainable concrete. *Constr. Build. Mater.* **2016**, *123*, 115–119, doi:10.1016/j.conbuildmat.2016.06.142.
147. Han, J.; Jia, D.; Yan, P. Understanding the shrinkage compensating ability of type K expansive agent in concrete. *Constr. Build. Mater.* **2016**, *116*, 36–44, doi:10.1016/j.conbuildmat.2016.04.092.
148. Liu, F.; Shen, S.-L.; Hou, D.-W.; Arulrajah, A.; Horpibulsuk, S. Enhancing behavior of large volume underground concrete structure using expansive agents. *Constr. Build. Mater.* **2016**, *114*, 49–55, doi:10.1016/J.CONBUILDMAT.2016.03.075.
149. Monosi, S.; Troli, R.; Favoni, O.; Tittarelli, F. Effect of SRA on the expansive behaviour of mortars based on sulphoaluminate agent. *Cem. Concr. Compos.* **2011**, *33*, 485–489, doi:10.1016/j.cemconcomp.2011.01.001.

150. Sant, G.; Lothenbach, B.; Juilland, P.; Saout, G. Le; Weiss, J.; Scrivener, K. The origin of early age expansions induced in cementitious materials containing shrinkage reducing admixtures. *Cem. Concr. Res.* **2011**, *41*, 218–229, doi:10.1016/j.cemconres.2010.12.004.
151. Collepardi, M.; Troli, R.; Bressan, M.; Liberatore, F.; Sforza, G. Crack-free concrete for outside industrial floors in the absence of wet curing and contraction joints. *Cem. Concr. Compos.* **2008**, *30*, 887–891, doi:10.1016/j.cemconcomp.2008.07.002.
152. Corinaldesi, V. Combined effect of expansive, shrinkage reducing and hydrophobic admixtures for durable self compacting concrete. *Constr. Build. Mater.* **2012**, *36*, 758–764, doi:10.1016/j.conbuildmat.2012.04.129.
153. Coppola, L.; Coffetti, D.; Crotti, E. Plain and ultrafine fly ashes mortars for environmentally friendly construction materials. *Sustain.* **2018**, *10*, doi:10.3390/su10030874.
154. Yeh, I.C. Generalization of strength versus water-cementitious ratio relationship to age. *Cem. Concr. Res.* **2006**, *36*, 1865–1873, doi:10.1016/j.cemconres.2006.05.013.
155. Abd elaty, M. abd allah Compressive strength prediction of Portland cement concrete with age using a new model. *HBRC J.* **2014**, *10*, 145–155, doi:10.1016/j.hbrcj.2013.09.005.
156. Kuhl, H. Slag cement and process of making the same 1908, 900,939.
157. Purdon, A.O. The action of alkalis on blast-furnace slag. *J. Soc. Chem. Ind.* **1940**, *59*, 191–202.
158. Wang, S.-D.; Pu, X.-C.; Scrivener, K.L.; Pratt, P.L. Alkali-activated slag cement and concrete: a review of properties and problems. *Adv. Cem. Res.* **1995**, *7*, 93–102.
159. Glukhovsky, V.D. Gruntosilikaty (Soil Silicates). *Gosstroyizdat* **1959**.
160. Wang, S.D.; Scrivener, K.L.; Pratt, P.L. Factors affecting the strength of alkali-activated slag. *Cem. Concr. Res.* **1994**, *24*, 1033–1043, doi:10.1016/0008-8846(94)90026-4.
161. Provis, J.L.; Van Deventer, J.S.J. *Geopolymers: structures, processing, properties and industrial applications*; Woodhead Publishing Limited, 2009;
162. Pal, S.C.; Mukherjee, A.; Pathak, S.R. Investigation of hydraulic activity of ground granulated blast furnace slag in concrete. *Cem. Concr. Res.* **2003**, *33*, 1481–1486.
163. Puligilla, S.; Mondal, P. Role of slag in microstructural development and hardening of fly ash-slag geopolymer. *Cem. Concr. Res.* **2013**, *43*, 70–80, doi:10.1016/j.cemconres.2012.10.004.
164. Provis, J.L.; Duxson, P.; van Deventer, J.S.J. The role of particle technology in developing sustainable construction materials. *Adv. Powder Technol.* **2010**, *21*, 2–7, doi:10.1016/j.apt.2009.10.006.
165. Puertas, F. Cementos de escorias activadas alcalinamente: Situación actual y perspectivas de futuro. *Mater. Construcción* **1995**, *45*, 53–64.

166. Provis, J.; van Deventer, J. Alkali Activated Materials State-of-the-Art Report. In Proceedings of the RILEM TC 224-AAM; Springer, London, UK, 2014; pp. 59–85.
167. Brough, A.R.; Atkinson, A. Sodium silicate-based, alkali-activated slag mortars - Part I. Strength, hydration and microstructure. *Cem. Concr. Res.* **2002**, *32*, 865–879.
168. Escalante-García, J.I.; Fuentes, A.F.; Gorokhovsky, A.; Fraire-Luna, P.E.; Mendoza-Suarez, G. Hydration products and reactivity of blast-furnace slag activated by various alkalis. *J. Am. Ceram. Soc.* **2003**, *86*, 2148–2153, doi:10.1111/j.1151-2916.2003.tb03623.x.
169. Huanhai, Z.; Xuequan, W.; Zhongzi, X.; Mingshu, T. Kinetic study on hydration of alkali-activated slag. *Cem. Concr. Res.* **1993**, *23*, 1253–1258, doi:10.1016/0008-8846(93)90062-E.
170. Lothenbach, B.; Gruskovnjak, A. Hydration of alkali-activated slag: thermodynamic modelling. *Adv. Cem. Res.* **2007**, *19*, 81–92.
171. Bernal, S.A.; de Gutierrez, R.M.; Provis, J.L.; Rose, V. Effect of silicate modulus and metakaolin incorporation on the carbonation of alkali silicate-activated slags. *Cem. Concr. Res.* **2010**, *40*, 898–907, doi:10.1016/j.cemconres.2010.02.003.
172. Chen, W.; Brouwers, H.J.H. The hydration of slag, part 1: Reaction models for alkali-activated slag. *J. Mater. Sci.* **2007**, *42*, 428–443, doi:10.1007/s10853-006-0873-2.
173. Haha, M. Ben; Lothenbach, B.; Le Saout, G.; Winnefeld, F. Influence of slag chemistry on the hydration of alkali-activated blast-furnace slag - Part II: Effect of Al2O3. *Cem. Concr. Res.* **2012**, *42*, 74–83.
174. Myers, R.J.; Bernal, S.A.; San Nicolas, R.; Provis, J.L. Generalized structural description of calcium-sodium aluminosilicate hydrate gels: The cross-linked substituted tobermorite model. *Langmuir* **2013**, *29*, 5294–5306, doi:10.1021/la4000473.
175. Zhang, Y.J.; Zhao, Y.L.; Li, H.H.; Xu, D.L. Structure characterization of hydration products generated by alkaline activation of granulated blast furnace slag. *J. Mater. Sci.* **2008**, *43*, 7141–7147, doi:10.1007/s10853-008-3028-9.
176. Komljenovic, M.; Bascarevic, Z.; Marjanovic, N.; Nikolic, V. External sulfate attack on alkali-activated slag. *Constr. Build. Mater.* **2013**, *49*, 31–39, doi:10.1016/j.conbuildmat.2013.08.013.
177. Fernandez-Jimenez, A.; Puertas, F. Effect of activator mix on the hydration and strength behaviour of alkali-activated slag cements. *Adv. Cem. Res.* **2003**, *15*, 129–136.
178. Taylor, H.F.W. *Cement chemistry*; Thomas Telford, 1997; ISBN 0727725920.
179. Najafi Kani, E.; Allahverdi, A.; Provis, J.L. Efflorescence control in geopolymer binders based on natural pozzolan. *J. Therm. Anal. Calorim.* **2012**, *34*, 25–33.
180. Weldes, H.H.; Lange, K.R. Properties of soluble silicates. *Ind. Eng. Chem.* **1969**, *61*, 29–44.
181. Wills, J.H. The A Review of the System Na2O—SiO2—H2O. *J. Phys. Chem.* **1950**, *54*, 304–

310.

182. Acocella, J.; Tomozawa, M.; Watson, E.B. The nature of dissolved water in sodium silicate glasses and its effect on various properties. *J. Non. Cryst. Solids* **1984**, *65*, 355–372.
183. Fernández-Jiménez, A.; Puertas, F. Setting of alkali-activated slag cement. Influence of activator nature. *Adv. Cem. Res.* **2001**, *13*, 115–121.
184. Pacheco-Torgal, F.; Castro-Gomes, J.; Jalali, S. Alkali-activated binders: A review. Part 2. About materials and binders manufacture. **2007**, doi:10.1016/j.conbuildmat.2007.03.019.
185. Chang, J.J. A study on the setting characteristics of sodium silicate-activated slag pastes. *Cem. Concr. Res.* **2003**, *33*, 1005–1011, doi:10.1016/S0008-8846(02)01096-7.
186. Collins, F.G.; Sanjayan, J.G. Workability and mechanical properties of alkali activated slag concrete. *Cem. Concr. Res.* **1999**, *29*, 455–458, doi:10.1016/S0008-8846(98)00236-1.
187. Bernal, S.; San Nicolas, R.; Provis, J.; van Deventer, J.S.J. Alkali-activated slag cements produced with a blended sodium carbonate / sodium silicate activator. *Adv. Cem. Res.* **2015**, *28*, 1–12.
188. Fernández-Jiménez, A.; Palomo, J.G.; Puertas, F. Alkali-activated slag mortars: Mechanical strength behaviour. *Cem. Concr. Res.* **1999**, *29*, 1313–1321, doi:10.1016/S0008-8846(99)00154-4.
189. Chi, M. Effects of dosage of alkali-activated solution and curing conditions on the properties and durability of alkali-activated slag concrete. *Constr. Build. Mater.* **2012**, *35*, 240–245, doi:10.1016/j.conbuildmat.2012.04.005.
190. Thomas, R.J.; Peethamparan, S. Alkali-activated concrete: Engineering properties and stress–strain behavior. *Constr. Build. Mater.* **2015**, *93*, 49–56.
191. Ding, Y.; Dai, J.G.; Shi, C.J. Fracture properties of alkali-activated slag and ordinary Portland cement concrete and mortar. *Constr. Build. Mater.* **2018**, *165*, 310–320, doi:10.1016/j.conbuildmat.2017.12.202.
192. Duran Atiş, C.; Bilim, C.; Çelik, Ö.; Karahan, O. Influence of activator on the strength and drying shrinkage of alkali-activated slag mortar. *Constr. Build. Mater.* **2009**, *23*, 548–555, doi:10.1016/J.CONBUILDMAT.2007.10.011.
193. Melo Neto, A.A.; Cincotto, M.A.; Repette, W. Drying and autogenous shrinkage of pastes and mortars with activated slag cement. *Cem. Concr. Res.* **2008**, *38*, 565–574, doi:10.1016/J.CEMCONRES.2007.11.002.
194. Cartwright, C.; Rajabipour, F.; Radlińska, A. Shrinkage Characteristics of Alkali-Activated Slag Cements. *J. Mater. Civ. Eng.* **2015**, *27*, B4014007, doi:10.1061/(ASCE)MT.1943-5533.0001058.

195. Ye, H.; Radlińska, A. Shrinkage mechanisms of alkali-activated slag. *Cem. Concr. Res.* **2016**, *88*, 126–135.
196. Collins, F.; Sanjayan, J.. Effect of pore size distribution on drying shrinking of alkali-activated slag concrete. *Cem. Concr. Res.* **2000**, *30*, 1401–1406.
197. Sajedi, F.; Razak, H.A. The effect of chemical activators on early strength of ordinary Portland cement-slag mortars. *Constr. Build. Mater.* **2010**, *24*, 1944–1951, doi:https://doi.org/10.1016/j.conbuildmat.2010.04.006.
198. Bakharev, T.; Sanjayan, J.G.; Cheng, Y.B. Effect of elevated temperature curing on properties of alkali-activated slag concrete. *Cem. Concr. Res.* **1999**, *29*, 1619–1625, doi:10.1016/S0008-8846(99)00143-X.
199. Rodríguez, E.; Bernal, S.; Mejía de Gutiérrez, R.; Puertas, F. Alternative concrete based on alkali-activated slag. *Mater. Construcción* **2008**, *58*, 53–67, doi:10.3989/mc.2008.v58.i291.104.
200. Fernández Bertos, M.; Simons, S.J.R.; Hills, C.D.; Carey, P.J. A review of accelerated carbonation technology in the treatment of cement-based materials and sequestration of CO2. *J. Hazard. Mater.* **2004**, *112*, 193–205, doi:10.1016/j.jhazmat.2004.04.019.
201. Bernal, S.A.; San Nicolas, R.; Provis, J.L.; Mejía De Gutiérrez, R.; Van Deventer, J.S.J. Natural carbonation of aged alkali-activated slag concretes. *Mater. Struct. Constr.* **2014**, *47*, 693–707, doi:10.1617/s11527-013-0089-2.
202. Palacios, M.; Puertas, F. Effect of carbonation on alkali-activated slag paste. *J. Am. Ceram. Soc.* **2006**, *89*, 3211–3221, doi:10.1111/j.1551-2916.2006.01214.x.
203. Bernal, S.A.; San Nicolas, R.; Myers, R.J.; Mejía De Gutiérrez, R.; Puertas, F.; Van Deventer, J.S.J.; Provis, J.L. MgO content of slag controls phase evolution and structural changes induced by accelerated carbonation in alkali-activated binders. *Cem. Concr. Res.* **2014**, *57*, 33–43, doi:10.1016/j.cemconres.2013.12.003.
204. Bernal, S.A.; Mejía de Gutiérrez, R.; Pedraza, A.L.; Provis, J.L.; Rodriguez, E.D.; Delvasto, S. Effect of binder content on the performance of alkali-activated slag concretes. *Cem. Concr. Res.* **2011**, *41*, 1–8.
205. Puertas, F.; Palacios, M.; Vázquez, T. Carbonation process of alkali-activated slag mortars. *J. Mater. Sci.* **2006**, *41*, 3071–3082, doi:10.1007/s10853-005-1821-2.
206. Hua, X.; Provis, J.L.; Van Deventer, J.S.J.; Krivenko, P. V. Characterization of Aged Slag Concretes. *ACI Mater. J.* **2008**, *105*, 131–139, doi:10.14359/19753.
207. Ismail, I.; Bernal, S.A.; Provis, J.L.; San Nicolas, R.; Brice, D.G.; Kilcullen, A.R.; Hamdan, S.; Van Deventer, J.S.J. Influence of fly ash on the water and chloride permeability of alkali-

activated slag mortars and concretes. *Constr. Build. Mater.* **2013**, *48*, 1187–1201, doi:10.1016/j.conbuildmat.2013.07.106.

208. Bernal, S.A.; Mejía De Gutiérrez, R.; Provis, J.L. Engineering and durability properties of concretes based on alkali-activated granulated blast furnace slag/metakaolin blends. *Constr. Build. Mater.* **2012**, *33*, 99–108, doi:10.1016/j.conbuildmat.2012.01.017.
209. Law, D.W.; Adam, A.A.; Molyneaux, T.K.; Patnaikuni, I. Durability assessment of alkali activated slag (AAS) concrete. *Mater. Struct.* **2012**, *45*, 1425–1437, doi:10.1617/s11527-012-9842-1.
210. Ravikumar, D.; Neithalath, N. An electrical impedance investigation into the chloride ion transport resistance of alkali silicate powder activated slag concretes. *Cem. Concr. Compos.* **2013**, *44*, 58–68, doi:10.1016/j.cemconcomp.2013.06.002.
211. Ravikumar, D.; Neithalath, N. Electrically induced chloride ion transport in alkali activated slag concretes and the influence of microstructure. *Cem. Concr. Res.* **2013**, *47*, 31–42, doi:10.1016/j.cemconres.2013.01.007.
212. Roa-Rodriguez, G.; Aperador, W.; Delgado, A. Resistance to chlorides of the alkali-activated slag concrete. *Int. J. Electrochem. Sci.* **2014**, *9*, 282–291.
213. Roy, D.M.; Jiang, W.; Silsbee, M.R. Chloride diffusion in ordinary, blended, and alkali-activated cement pastes and its relation to other properties. *Cem. Concr. Res.* **2000**, *30*, 1879–1884, doi:10.1016/S0008-8846(00)00406-3.
214. Bakharev, T.; Sanjayan, J.G.; Cheng, Y.B. Sulfate attack on alkali-activated slag concrete. *Cem. Concr. Res.* **2002**, *32*, 211–216, doi:10.1016/S0008-8846(01)00659-7.
215. Ismail, I.; Bernal, S.A.; Provis, J.L.; Hamdan, S.; Van Deventer, J.S.J. Microstructural changes in alkali activated fly ash/slag geopolymers with sulfate exposure. *Mater. Struct. Constr.* **2013**, *46*, 361–373, doi:10.1617/s11527-012-9906-2.
216. Shi, C.; Stegemann, J.A. Acid corrosion resistance of different cementing materials. *Cem. Concr. Res.* **2000**, *30*, 803–808, doi:10.1016/S0008-8846(00)00234-9.
217. Scrivener, K.L.; Young, J.F. *Mechanisms of chemical degradation of cement-based systems: proceedings of the Material Research Society's Symposium on Mechanisms of Chemical Degradation of Cement-based Systems, Boston, USA, 27-30 November 1995*; E & FN Spon, 1997; ISBN 0419215700.
218. Joseph Davidovits John H. Paterson, Douglas J. Ritcey, D.C.C. Geopolymeric concretes For Environmental Protection. *Concr. Int. 12*.
219. Bakharev, T.; Sanjayan, J.G.; Cheng, Y.B. Resistance of alkali-activated slag concrete to acid attack. *Cem. Concr. Res.* **2003**, *33*, 1607–1611, doi:10.1016/S0008-8846(03)00125-X.

220. Davidovits, J. Geopolymers: Inorganic polymeric new materials. *J. Therm. Anal.* **1991**, *37*, 1633–1634.
221. Bakharev, T.; Sanjayan, J.G.; Cheng, Y.B. Resistance of alkali-activated slag concrete to alkali-aggregate reaction. *Cem. Concr. Res.* **2001**, *31*, 331–334, doi:10.1016/S0008-8846(00)00483-X.
222. Fu, Y.; Cai, L.; Yonggen, W. Freeze-thaw cycle test and damage mechanics models of alkali-activated slag concrete. *Constr. Build. Mater.* **2011**, doi:10.1016/j.conbuildmat.2010.12.006.
223. Cai, L.; Wang, H.; Fu, Y. Freeze-thaw resistance of alkali-slag concrete based on response surface methodology. *Constr. Build. Mater.* **2013**, *49*, 70–76, doi:10.1016/j.conbuildmat.2013.07.045.
224. Li, Q.; Cai, L.; Fu, Y.; Wang, H.; Zou, Y. Fracture properties and response surface methodology model of alkali-slag concrete under freeze-thaw cycles. *Constr. Build. Mater.* **2015**, *93*, 620–626, doi:10.1016/j.conbuildmat.2015.06.037.
225. Shahrajabian, F.; Behfarnia, K. The effects of nano particles on freeze and thaw resistance of alkali-activated slag concrete. *Constr. Build. Mater.* **2018**, *176*, 172–178, doi:10.1016/j.conbuildmat.2018.05.033.
226. Zuda, L.; Pavlík, Z.; Rovnaníková, P.; Bayer, P.; Černý, R. Properties of alkali activated aluminosilicate material after thermal load. *Int. J. Thermophys.* **2006**, *27*, 1250–1263, doi:10.1007/s10765-006-0077-7.
227. Zuda, L.; Rovnaník, P.; Bayer, P.; Černý, R. Thermal properties of alkali-activated slag subjected to high temperatures. *J. Build. Phys.* **2007**, *30*, 337–350, doi:10.1177/1744259106075234.
228. Mejía de Gutiérrez, R.; Maldonado, J.; Gutiérrez, C. Resistencia a temperaturas elevadas de escorias activadas alcalinamente. *Mater. Construcción* **2004**, *54*, 87–92, doi:10.3989/mc.2004.v54.i276.257.
229. Guerrieri, M.; Sanjayan, J.; Collins, F. Residual strength properties of sodium silicate alkali activated slag paste exposed to elevated temperatures. *Mater. Struct.* **2010**, *43*, 765–773, doi:10.1617/s11527-009-9546-3.
230. Rashad, A.M.; Khalil, M.H. A preliminary study of alkali-activated slag blended with silica fume under the effect of thermal loads and thermal shock cycles. *Constr. Build. Mater.* **2013**, *40*, 522–532, doi:10.1016/J.CONBUILDMAT.2012.10.014.
231. Rashad, A.M.; Bai, Y.; Basheer, P.A.M.; Collier, N.C.; Milestone, N.B. Chemical and mechanical stability of sodium sulfate activated slag after exposure to elevated temperature. *Cem. Concr. Res.* **2012**, *42*, 333–343, doi:10.1016/J.CEMCONRES.2011.10.007.

232. Bakharev, T.; Sanjayan, J.G.; Cheng, Y.B. Effect of admixtures on properties of alkali-activated slag concrete. *Cem. Concr. Res.* **2000**, *30*, 1367–1374.
233. Douglas, E.; Brandstetr, J. A preliminary study on the alkali activation of ground granulated blast-furnace slag. *Cem. Concr. Res.* **1990**, *20*, 746–756, doi:10.1016/0008-8846(90)90008-L.
234. Palacios, M.; Puertas, F. Effect of superplasticizer and shrinkage-reducing admixtures on alkali-activated slag pastes and mortars. *Cem. Concr. Res.* **2005**, *35*, 1358–1367, doi:10.1016/j.cemconres.2004.10.014.
235. Jang, J.G.; Lee, N.K.; Lee, H.K. Fresh and hardened properties of alkali-activated fly ash/slag pastes with superplasticizers. *Constr. Build. Mater.* **2014**, *50*, 169–176, doi:10.1016/J.CONBUILDMAT.2013.09.048.
236. Palacios, M.; Houst, Y.F.; Bowen, P.; Puertas, F. Adsorption of superplasticizer admixtures on alkali-activated slag pastes. *Cem. Concr. Res.* **2009**, *39*, 670–677, doi:10.1016/J.CEMCONRES.2009.05.005.
237. Marta Palacios and Francisca Puertas, P.F.G.B. Rheology and Setting of Alkali-Activated Slag Pastes and Mortars: Effect of Organic Admixture. *Mater. J. 105*, doi:10.14359/19754.
238. Rashad, A.M. A comprehensive overview about the influence of different additives on the properties of alkali-activated slag - A guide for Civil Engineer. *Constr. Build. Mater.* **2013**, *47*, 29–55, doi:10.1016/j.conbuildmat.2013.04.011.
239. Palacios, M.; Puertas, F. Effect of shrinkage-reducing admixtures on the properties of alkali-activated slag mortars and pastes. *Cem. Concr. Res.* **2007**, *37*, 691–702, doi:10.1016/j.cemconres.2006.11.021.
240. Bilim, C.; Karahan, O.; Atiş, C.D.; Ilkentapar, S. Influence of admixtures on the properties of alkali-activated slag mortars subjected to different curing conditions. *Mater. Des.* **2013**, *44*, 540–547.
241. Bílek, V.; Kalina, L.; Novotný, R.; Tkacz, J.; Pařízek, L. Some Issues of Shrinkage-Reducing Admixtures Application in Alkali-Activated Slag Systems. *Materials (Basel).* **2016**, *9*, 462, doi:10.3390/ma9060462.
242. Yuan, X.H.; Chen, W.; Lu, Z.A.; Chen, H. Shrinkage compensation of alkali-activated slag concrete and microstructural analysis. *Constr. Build. Mater.* **2014**, *66*, 422–428, doi:10.1016/j.conbuildmat.2014.05.085.
243. Ye, H.; Radlińska, A. Shrinkage mitigation strategies in alkali-activated slag. *Cem. Concr. Res.* **2017**, *101*, 131–143, doi:10.1016/j.cemconres.2017.08.025.
244. Yang, K.H.; Lee, K.H.; Song, J.K.; Gong, M.H. Properties and sustainability of alkali-activated slag foamed concrete. *J. Clean. Prod.* **2014**, *68*, 226–233, doi:10.1016/j.jclepro.2013.12.068.

245. Zhang, H.Y.; Kodur, V.; Cao, L.; Qi, S.L. Fiber reinforced geopolymers for fire resistance applications. In Proceedings of the Procedia Engineering; Elsevier, 2014; Vol. 71, pp. 153–158.

246. Rovnaník, P.; Bayer, P.; Rovnaníková, P. Characterization of alkali activated slag paste after exposure to high temperatures. *Constr. Build. Mater.* **2013**, *47*, 1479–1487, doi:https://doi.org/10.1016/j.conbuildmat.2013.06.070.

247. Cheng, T.W.; Chiu, J.P. Fire-resistant geopolymer produced by granulated blast furnace slag. *Miner. Eng.* **2003**, *16*, 205–210, doi:https://doi.org/10.1016/S0892-6875(03)00008-6.

248. Roy, D.M. Alkali-activated cements: Opportunities and challenges. *Cem. Concr. Res.* **1999**, *29*, 249–254.

249. Hughes, P.; Glendinning, S. Deep dry mix ground improvement of a soft peaty clay using blast furnace slag and red gypsum. *Q. J. Eng. Geol. Hydrogeol.* **2004**, *37*, 205–216, doi:10.1144/1470-9236/04-003.

250. Guangren, Q.; Yuxiang, L.; Facheng, Y.; Rongming, S. Improvement of metakaolin on radioactive Sr and Cs immobilization of alkali-activated slag matrix. *J. Hazard. Mater.* **2002**, *92*, 289–300, doi:https://doi.org/10.1016/S0304-3894(02)00022-5.

251. Xuequan, W.; Sheng, Y.; Xiaodong, S.; Mingshu, T.; Liji, Y. Alkali-activated slag cement based radioactive waste forms. *Cem. Concr. Res.* **1991**, *21*, 16–20, doi:https://doi.org/10.1016/0008-8846(91)90026-E.

252. Yunsheng, Z.; Wei, S.; Qianli, C.; Lin, C. Synthesis and heavy metal immobilization behaviors of slag based geopolymer. *J. Hazard. Mater.* **2007**, *143*, 206–213, doi:https://doi.org/10.1016/j.jhazmat.2006.09.033.

253. Weil, M.; Dombrowski, K.; Buchwald, A. 10 - Life-cycle analysis of geopolymers. In *Geopolymers*; Provis, J.L., van Deventer, J.S.J., Eds.; Woodhead Publishing Series in Civil and Structural Engineering; Woodhead Publishing, 2009; pp. 194–210 ISBN 978-1-84569-449-4.

254. Habert, G.; D'Espinose De Lacaillerie, J.B.; Roussel, N. An environmental evaluation of geopolymer based concrete production: Reviewing current research trends. *J. Clean. Prod.* **2011**, *19*, 1229–1238, doi:10.1016/j.jclepro.2011.03.012.

255. McLellan, B.C.; Williams, R.P.; Lay, J.; Van Riessen, A.; Corder, G.D. Costs and carbon emissions for geopolymer pastes in comparison to ordinary portland cement. *J. Clean. Prod.* **2011**, *19*, 1080–1090, doi:10.1016/j.jclepro.2011.02.010.

256. Turner, L.K.; Collins, F.G. Carbon dioxide equivalent (CO2-e) emissions: A comparison between geopolymer and OPC cement concrete. *Constr. Build. Mater.* **2013**, *43*, 125–130,

doi:10.1016/j.conbuildmat.2013.01.023.

257. Yang, K.H.; Song, J.K.; Song, K. Il Assessment of CO 2 reduction of alkali-activated concrete. *J. Clean. Prod.* **2013**, *39*, 265–272, doi:10.1016/j.jclepro.2012.08.001.

258. Duxson, P.; Provis, J.L.; Lukey, G.C.; Van Deventer, J.S.J.; Separovic, F.; Gan, Z.H. 39K NMR of free potassium in geopolymers. *Ind. Eng. Chem. Res.* **2006**, *45*, 9208–9210, doi:10.1021/ie060838g.

259. Wang, S.-D.; Scrivener, K.L. Hydration products of alkali activated slag cement. *Cem. Concr. Res.* **1995**, *25*, 561–571.

260. Bayuaji, R.; Yasin, A.K.; Susanto, T.E.; Darmawan, M.S.; Darmawan, S. A review in geopolymer binder with dry mixing method (geopolymer cement). *AIP Conf. Proc.* **2017**, *1887*, 20042, doi:10.1063/1.5003513.

261. Criado, M.; Aperador, W.; Sobrados, I. Microstructural and mechanical properties of alkali activated Colombian raw materials. *Materials (Basel).* **2016**, *9*, doi:10.3390/ma9030158.

262. Burciaga-Díaz, O.; Escalante-García, J.I. Structure, mechanisms of reaction, and strength of an alkali-activated blast-furnace slag. *J. Am. Ceram. Soc.* **2013**, *96*, 3939–3948, doi:10.1111/jace.12620.

263. Zhang, Y.J.; Zhao, Y.L.; Li, H.H.; Xu, D.L. Structure characterization of hydration products generated by alkaline activation of granulated blast furnace slag. *J. Mater. Sci.* **2008**, *43*, 7141–7147.

264. Grangeon, S.; Claret, F.; Linard, Y.; Chiaberge, C. X-ray diffraction: A powerful tool to probe and understand the structure of nanocrystalline calcium silicate hydrates. *Acta Crystallogr. Sect. B Struct. Sci. Cryst. Eng. Mater.* **2013**, *69*, 465–473, doi:10.1107/S2052519213021155.

265. Matsui, K.; Kikuma, J.; Tsunashima, M.; Ishikawa, T.; Matsuno, S.Y.; Ogawa, A.; Sato, M. In situ time-resolved X-ray diffraction of tobermorite formation in autoclaved aerated concrete: Influence of silica source reactivity and Al addition. *Cem. Concr. Res.* **2011**, *41*, 510–519, doi:10.1016/j.cemconres.2011.01.022.

266. Wiyantoko, B.; Kurniawati, P.; Purbaningtias, T.E.; Fatimah, I. Synthesis and Characterization of Hydrotalcite at Different Mg/Al Molar Ratios. *Procedia Chem.* **2015**, *17*, 21–26, doi:10.1016/j.proche.2015.12.115.

267. Marincea, Ş.; Dumitraş, D.G.; Ghineţ, C.; Fransolet, A.M.; Hatert, F.; Rondeaux, M. Gehlenite from three occurrences of high-temperature skarns, Romania: New mineralogical data. *Can. Mineral.* **2011**, *49*, 1001–1014, doi:10.3749/canmin.49.4.1001.

268. Haha, M. Ben; Lothenbach, B.; Saout, G. Le; Winnefeld, F. Cement and Concrete Research In fl uence of slag chemistry on the hydration of alkali-activated blast-furnace slag — Part I :

Effect of MgO. *Cem. Concr. Res.* **2011**, *41*, 955–963, doi:10.1016/j.cemconres.2011.05.002.

269. A. Allahverdi; E. Najafi Kani; S. Esmaeilpoor Effects of Silica Modulus and Alkali Concentration on Activation of Blast-Furnace Slag. *Iran. J. Mater. Sci. Eng.* **2008**, *5*, 32–35.
270. Song, S.; Jennings, H.M. Pore solution chemistry of alkali-activated ground granulated blast-furnace slag. *Cem. Concr. Res.* **1999**, *29*, 159–170, doi:10.1016/S0008-8846(98)00212-9.
271. Park, H.; Jeong, Y.; Jeong, J.H.; Oh, J.E. Strength development and hydration behavior of self-activation of commercial ground granulated blast-furnace slag mixed with purified water. *Materials (Basel).* **2016**, *9*, doi:10.3390/ma9030185.
272. Escalante, J.I.; Gómez, L.Y.; Johal, K.K.; Mendoza, G.; Mancha, H.; Méndez, J. Reactivity of blast-furnace slag in Portland cement blends hydrated under different conditions. *Cem. Concr. Res.* **2001**, *31*, 1403–1409, doi:10.1016/S0008-8846(01)00587-7.
273. Tajuelo Rodriguez, E.; Garbev, K.; Merz, D.; Black, L.; Richardson, I.G. Thermal stability of C-S-H phases and applicability of Richardson and Groves' and Richardson C-(A)-S-H(I) models to synthetic C-S-H. *Cem. Concr. Res.* **2017**, *93*, 45–56, doi:10.1016/j.cemconres.2016.12.005.
274. Bellotto, M.; Rebours, B.; Clause, O.; Lynch, J.; Bazin, D.; Elkaïm, E. Hydrotalcite decomposition mechanism: A clue to the structure and reactivity of spinel-like mixed oxides. *J. Phys. Chem.* **1996**, *100*, 8535–8542, doi:10.1021/jp960040i.
275. Frost, R.L.; Martens, W.; Ding, Z.; Kloprogge, J.T. DSC and high-resolution TG of synthesized hydrotalcites Mg and Zn. *J. Therm. Anal. Calorim.* **2003**, *71*, 429–438, doi:10.1023/A:1022835305846.
276. Kashani, A.; Provis, J.L.; Qiao, G.G.; Van Deventer, J.S.J. The interrelationship between surface chemistry and rheology in alkali activated slag paste. *Constr. Build. Mater.* **2014**, *65*, 583–591, doi:10.1016/j.conbuildmat.2014.04.127.
277. Živica, V. Effects of type and dosage of alkaline activator and temperature on the properties of alkali-activated slag mixtures. *Constr. Build. Mater.* **2007**, *21*, 1463–1469, doi:10.1016/j.conbuildmat.2006.07.002.
278. Pacheco-Torgal, F.; Labrincha, J.; Leonelli, C.; Palomo, A.; Chindaprasirt, P. *Handbook of alkali-activated cements, mortars and concretes*; 2014; ISBN 9781782422884.
279. Tang, M.S.; Su-Fen, H. Effect of Ca(OH)2 on alkali-silica reaction. In Proceedings of the Proceedings of the 8th international Congress of Cement Chemistry; 1980; pp. 94–99.
280. Lecomte, I.; Henrist, C.; Liégeois, M.; Maseri, F.; Rulmont, A.; Cloots, R. (Micro)-structural comparison between geopolymers, alkali-activated slag cement and Portland cement. *J. Eur. Ceram. Soc.* **2006**, *26*, 3789–3797, doi:10.1016/j.jeurceramsoc.2005.12.021.

281. Xu, H.; Provis, J.L.; van Deventer, J.S.J.; Krivenko, P. V Characterization of aged slag concretes. *ACI Mater. J.* **2008**, *105*, 131.
282. Li, Z.; Zhao, X.; He, T.; Zhao, S.; Liu, Y.; Qu, X. A study of high-performance slag-based composite admixtures. *Constr. Build. Mater.* **2017**, *155*, 126–136.
283. Alderete, N.; Villagrán, Y.; Mignon, A.; Snoeck, D.; De Belie, N. Pore structure description of mortars containing ground granulated blast-furnace slag by mercury intrusion porosimetry and dynamic vapour sorption. *Constr. Build. Mater.* **2017**, *145*, 157–165.
284. Jennings, H.M. Refinements to colloid model of C-S-H in cement: CM-II. *Cem. Concr. Res.* **2008**, *38*, 275–289, doi:10.1016/j.cemconres.2007.10.006.
285. Ye, H. Creep Mechanisms of Calcium–Silicate–Hydrate: An Overview of Recent Advances and Challenges. *Int. J. Concr. Struct. Mater.* **2015**, *9*, 453–462, doi:10.1007/s40069-015-0114-7.
286. Chen, J.J.; Sorelli, L.; Vandamme, M.; Ulm, F.; Chanvillard, G. A Coupled nanoindentation/SEM-EDS study on low water/cement ratio Portland cement paste: evidence for C–S–H/Ca (OH) 2 nanocomposites. *J. Am. Ceram. Soc.* **2010**, *93*, 1484–1493.
287. Ye, H.; Cartwright, C.; Rajabipour, F.; Radli?ska, A. Understanding the drying shrinkage performance of alkali-activated slag mortars. *Cem. Concr. Compos.* **2017**, *76*, 13–24.
288. Gartner, E.M.; MacPhee, D.E. A physico-chemical basis for novel cementitious binders. *Cem. Concr. Res.* **2011**, *41*, 736–749.
289. Shi, C.; Jiménez, A.F.; Palomo, A. New cements for the 21st century: The pursuit of an alternative to Portland cement. *Cem. Concr. Res.* **2011**, *41*, 750–763, doi:10.1016/j.cemconres.2011.03.016.
290. Angulo-Ramírez, D.E.; Mejía de Gutiérrez, R.; Puertas, F. Alkali-activated Portland blast-furnace slag cement: Mechanical properties and hydration. *Constr. Build. Mater.* **2017**, *140*, 119–128.
291. Jin, F.; Gu, K.; Al-Tabbaa, A. Strength and drying shrinkage of reactive MgO modified alkali-activated slag paste. *Constr. Build. Mater.* **2014**, *51*, 395–404, doi:10.1016/j.conbuildmat.2013.10.081.
292. Iizuka, R.; Yagi, T.; Tsuchiya, T.; Kusaba, K.; Kagi, H. Crystal structure of the high-pressure phase of calcium hydroxide, portlandite: In situ powder and single-crystal X-ray diffraction study. *Am. Mineral.* **2013**, *98*, 1421–1428, doi:10.2138/am.2013.4386.
293. Binda, L.; Saisi, A.; Tiraboschi, C. Investigation procedures for the diagnosis of historic masonries. *Constr. Build. Mater.* **2000**, *14*, 199–233, doi:10.1016/S0950-0618(00)00018-0.
294. Borri, A.; Corradi, M.; Castori, G.; De Maria, A. A method for the analysis and classification

of historic masonry. *Bull. Earthq. Eng.* **2015**, *13*, 2647–2665, doi:10.1007/s10518-015-9731-4.

295. Shuller, M.; Atkinson, R.; Noland, J. Structural evaluation of historic masonry buildings. *APT Bull. J. Preserv. Technol.* **1995**, *26*, 51–61.
296. Lourenço, P.B.; Mendes, N.; Ramos, L.F.; Oliveira, D. V. Analysis of masonry structures without box behavior. *Int. J. Archit. Herit.* **2011**, *5*, 369–382, doi:10.1080/15583058.2010.528824.
297. Rota, M.; Penna, A.; Magenes, G. A framework for the seismic assessment of existing masonry buildings accounting for different sources of uncertainty. *Earthq. Eng. Struct. Dyn.* **2014**, *43*, 1045–1066, doi:10.1002/eqe.2386.
298. Silva, R. V.; De Brito, J.; Dhir, R.K. Properties and composition of recycled aggregates from construction and demolition waste suitable for concrete production. *Constr. Build. Mater.* **2014**, *65*, 201–217, doi:10.1016/j.conbuildmat.2014.04.117.
299. Valluzzi, M.R.; Da Porto, F.; Modena, C. Behavior and modeling of strengthened three-leaf stone masonry walls. *Mater. Struct. Constr.* **2004**, *37*, 184–192, doi:10.1617/13977.
300. Avorio, A.; Borri, A.; Cangi, G. Riparazione e consolidamento degli edifici in muratura. In *Manuale per la riabilitazione e la ricostruzione post sismica degli edifici*; Rome, 1999.
301. Ferrario, L.; Marini, A.; Riva, P.; Giuriani, E. Traditional and innovative techniques for the seismic strengthening of barrel vaulted structures subjected to rocking of the abutments. In Proceedings of the Proceedings of ATC-SEI conference on Improving the Seismic Performance of Existing Buildings and Other Structures - San Francisco (California); American Society of Civil Engineers: Reston, VA, 2009.
302. Giuriani, E.; Marini, A. Experiences from the Northern Italy 2004 earthquake: vulnerability assessment and strengthening of historic churches. In Proceedings of the Proceedings of VI International Conference on Structural Analysis of Historical Constructions SAHC - Bath (England); 2008; pp. 13–24.
303. Giuriani, E.P.; Marini, A.; Preti, M. Thin-folded Shell for the Renewal of Existing Wooden Roofs. *Int. J. Archit. Herit.* **2016**, *10*, 797–816, doi:10.1080/15583058.2015.1075626.
304. D'Ayala, D.F.; Paganoni, S. Assessment and analysis of damage in L'Aquila historic city centre after 6th April 2009. *Bull. Earthq. Eng.* **2011**, *9*, 81–104, doi:10.1007/s10518-010-9224-4.
305. Giuriani, E.; Marini, A.; Porteri, C.; Preti, M. Seismic vulnerability for churches in association with transverse arch rocking. *Int. J. Archit. Herit.* **2009**, *3*, 212–234, doi:10.1080/15583050802400240.

306. Lagomarsino, S.; Podestà, S. Seismic vulnerability of ancient churches: II. Statistical analysis of surveyed data and methods for risk analysis. *Earthq. Spectra* **2004**, *20*, 395–412, doi:10.1193/1.1737736.
307. Senaldi, I.; Magenes, G.; Ingham, J. Performance of unreinforced stone masonry buildings during the 2010/2011 Canterbury earthquake swarm and retrofit techniques for their seismic improvement. *SESOC J.* **2011**, *24*, 44.
308. Cominelli, S.; Giuriani, E.; Marini, A. Mechanisms governing the compressive strength of unconfined and confined rubble stone masonry. *Mater. Struct. Constr.* **2017**, *50*, 10, doi:10.1617/s11527-016-0905-6.
309. Marini, A.; Giuriani, E.; Belleri, A.; Cominelli, S. Dowel connections securing roof-diaphragms to perimeter walls in historic masonry buildings and in-field testing for capacity assessment. *Bull. Earthq. Eng.* **2018**, *16*, 4001–4025, doi:10.1007/s10518-018-0333-9.
310. Giuriani, E.; Marini, A. Wooden roof box structure for the anti-seismic strengthening of historic buildings. *Int. J. Archit. Herit.* **2008**, *2*, 226–246, doi:10.1080/15583050802063733.
311. Garbin, E.; Valluzzi, M.R.; Modena, C. Testing and numerical modelling of the structural behaviour of brick masonry strengthened by the bed joints reinforcement technique. In Proceedings of the Proceedings of 1st WTA International PhD symposium - building materials and building technology to preserve the built heritage - Leuven (Belgium); 2009; pp. 489–516.
312. Valluzzi, M.R.; Binda, L.; Modena, C. Mechanical behaviour of historic masonry structures strengthened by bed joints structural repointing. *Constr. Build. Mater.* **2005**, *19*, 63–73, doi:10.1016/j.conbuildmat.2004.04.036.
313. Corradi, M.; Borri, A.; Castori, G.; Sisti, R. The Reticulatus method for shear strengthening of fair-faced masonry. *Bull. Earthq. Eng.* **2016**, *14*, 3547–3571, doi:10.1007/s10518-016-0006-5.
314. Borri, A.; Corradi, M.; Sisti, R.; Buratti, C.; Belloni, E.; Moretti, E. Masonry wall panels retrofitted with thermal-insulating GFRP-reinforced jacketing. *Mater. Struct. Constr.* **2016**, *49*, 3957–3968, doi:10.1617/s11527-015-0766-4.
315. Oliveira, D. V.; Silva, R.A.; Garbin, E.; Lourenĉo, P.B. Strengthening of three-leaf stone masonry walls: An experimental research. *Mater. Struct. Constr.* **2012**, *45*, 1259–1276, doi:10.1617/s11527-012-9832-3.
316. Valluzzi, M.R.; Cescatti, E.; Cardani, G.; Cantini, L.; Zanzi, L.; Colla, C.; Casarin, F. Calibration of sonic pulse velocity tests for detection of variable conditions in masonry walls. *Constr. Build. Mater.* **2018**, *192*, 272–286, doi:https://doi.org/10.1016/j.conbuildmat.2018.10.073.

317. Corradi, M.; Borri, A.; Castori, G.; Sisti, R. Shear strengthening of wall panels through jacketing with cement mortar reinforced by GFRP grids. *Compos. Part B Eng.* **2014**, *64*, 33–42, doi:10.1016/j.compositesb.2014.03.022.
318. Gattesco, N.; Dudine, A. Effectiveness of masonry strengthening technique made with plaster reinforced with a GFRP net. In Proceedings of the Proceedings of 8th International Masonry Conference - Dresden (Germany); 2010.
319. Parisi, F.; Iovinella, I.; Balsamo, A.; Augenti, N.; Prota, A. In-plane behaviour of tuff masonry strengthened with inorganic matrix-grid composites. *Compos. Part B Eng.* **2013**, *45*, 1657–1666, doi:10.1016/j.compositesb.2012.09.068.
320. Dzturan, T.; Ceqen, C. Effect of coarse aggregate type on mechanical properties of concretes with different strengths. *Cem. Concr. Res.* **1997**, *27*, 165–170.
321. Silva, B.A.; Ferreira Pinto, A.P.; Gomes, A. Natural hydraulic lime versus cement for blended lime mortars for restoration works. *Constr. Build. Mater.* **2015**, *94*, 346–360, doi:10.1016/j.conbuildmat.2015.06.058.
322. Walker, R.; Pavia, S. Thermal and hygric properties of insulation materials suitable for historic fabrics. In Proceedings of the Proceedings of III international congress on Construction and Buildings Research; 2015.
323. Crawley, D.B.; Lawrie, L.K.; Pedersen, C.O.; Winkelmann, F.C. Energy plus: energy simulation program. *ASHRAE J.* **2000**, *42*, 49–56.
324. Popovics, S. Analysis of concrete strength versus water-cement ratio relationship. *Mater. J.* **1990**, *87*, 517–529.
325. Aïtcin, P.C. Cements of yesterday and today - concrete of tomorrow. *Cem. Concr. Res.* **2000**, *30*, 1349–1359, doi:10.1016/S0008-8846(00)00365-3.
326. Gettu, R.; Pillai, R.G.; Meena, J.; Basavaraj, A.S.; Santhanam, M.; Dhanya, B.S. Considerations of sustainability in the mixture proportioning of concrete for strength and durability. In Proceedings of the Proceedings of 2nd International Workshop on Durability and Sustainability of Concrete Structures. Moscow; 2018.
327. Muller, H.S.; Haist, M.; Vogel, M.; Moffatt, J.S. Design approach and properties of a new generation of sustainable stuctural concretes. In Proceedings of the Proceedings of 2nd International Workshop on Durability and Sustainability of Concrete Structures. Moscow; 2018.
328. Moffatt, E.G.; Thomas, M.D.A.; Fahim, A. Performance of high-volume fly ash concrete in marine environment. *Cem. Concr. Res.* **2017**, *102*, 127–135, doi:10.1016/J.CEMCONRES.2017.09.008.

329. Ramezanianpour, A.A.; Zadeh, F.B.; Zolfagharnasab, A.; Ramezanianpour, A.M. Mechanical properties and chloride ion penetration of alkali activated slag concrete. In Proceedings of the High Tech Concrete: Where Technology and Engineering Meet - Proceedings of the 2017 fib Symposium; Springer International Publishing: Cham, 2017; pp. 2203–2212.
330. Ann, K.Y.; Cho, C.-G. Corrosion Resistance of Calcium Aluminate Cement Concrete Exposed to a Chloride Environment. *Mater. (Basel, Switzerland)* **2014**, *7*, 887–898, doi:10.3390/ma7020887.
331. Faleschini, F.; Alejandro Fernández-Ruíz, M.; Zanini, M.A.; Brunelli, K.; Pellegrino, C.; Hernández-Montes, E. High performance concrete with electric arc furnace slag as aggregate: Mechanical and durability properties. *Constr. Build. Mater.* **2015**, *101*, 113–121, doi:10.1016/J.CONBUILDMAT.2015.10.022.
332. Černý, R.; Kunca, A.; Tydlitát, V.; Drchalová, J.; Rovnaníková, P. Effect of pozzolanic admixtures on mechanical, thermal and hygric properties of lime plasters. *Constr. Build. Mater.* **2006**, *20*, 849–857, doi:10.1016/j.conbuildmat.2005.07.002.
333. Izaguirre, A.; Lanas, J.; Álvarez, J.I. Cement and Concrete Research Effect of water-repellent admixtures on the behaviour of aerial lime-based mortars. *Cem. Concr. Res.* **2009**, *39*, 1095–1104, doi:10.1016/j.cemconres.2009.07.026.
334. Vimmrová, A.; Keppert, M.; Michalko, O.; Černý, R. Calcined gypsum-lime-metakaolin binders: Design of optimal composition. *Cem. Concr. Compos.* **2014**, *52*, 91–96, doi:10.1016/j.cemconcomp.2014.05.011.

List of figures

List of tables

Appendix 1

The results reported in this PhD thesis were published in the following papers (from newest to oldest):

- Telesca, A.; Marroccoli, M.; Coppola, L.; Coffetti, D.; Candamano, S. Tartaric acid effects on hydration development and physico-mechanical properties of blended calcium sulphoaluminate cements. *Cem.Con.Comp.*, under review.
- Coppola, L.; Coffetti, D.; Crotti, E.; Candamano, S.; Crea, F., Pastore, T. The combined use of admixtures for shrinkage reduction in one-part alkali activated slag-based mortars and pastes. *Con.Build.Mat* **2020**, 248, 118682
- Coppola, L.; Coffetti, D.; Crotti, E.; Dell'Aversano, R.; Gazzaniga, G., Pastore, T. Influence of lithium carbonate and sodium carbonate on physical and elastic properties and carbonation resistance of calcium sulphoaluminate-based mortars. *App. Scie.* **2020**, 10(1), 176
- Coppola, L.; Coffetti, D.; Crotti, E.; Marini, A.; Passoni, C.; Pastore, T. Lightweight cement-free alkali-activated slag plaster for the structural retrofit and energy upgrading of poor-quality masonry walls. *Cem.Con.Comp.* **2019**, 104, 103341
- Coppola, L.; Coffetti, D.; Crotti, E.; Gazzaniga, G.; Pastore, T. An empathetic added sustainability index (EASI) for cementitious based construction materials. *J.Cle.Pro.* **2019**, 220, 475-482
- Coppola, L.; Coffetti, D.; Crotti, E.; Pastore, T. CSA-based Portland-free binders to manufacture sustainable concretes for jointless slabs on ground. *Con.Build.Mat* **2018**, 187, 691-698
- Coppola, L.; Coffetti, D.; Crotti, E. Pre-packed alkali activated cement-free mortars for repair of existing masonry buildings and concrete structures. *Con.Build.Mat* **2018**, 173, 111-117
- Coppola, L.; Coffetti, D.; Crotti, E. Use of tartaric acid for the production of sustainable Portland-free CSA-based mortars. *Con.Build.Mat* **2018**, 171, 243-249
- Coppola, L.; Coffetti, D.; Crotti, E. One-part alkali-activated slag cement for conservation of existing structures. *ACI Spec. Pub.* **2018**, SP 330, 107-121
- Coppola, L.; Coffetti, D.; Crotti, E. CSA-based mortars manufactured with tartaric acid-based retarder. *ACI Spec. Pub.* **2018**, SP 329, 373-388
- Coppola, L.; Coffetti, D.; Crotti, E. Environmentally friendly concretes manufactured with CSA cement. *ACI Spec. Pub.* **2018**, SP 326

Moreover, the following papers were further published by the author in the field of construction materials (from newest to oldest):

- Candamano, S.; De Luca, P.; Coppola, L.; Coffetti, D.; Crea, F. Influence of acrylic latex and pre-treated hemp fibers on cement-based mortar properties. *Con.Build.Mat,* **in press**
- D'Alessandro, A.; Coffetti, D.; Crotti, E.; Coppola, L.; Meoni, A.; Ubertini, F. Self-sensing properties of green alkali-activated binders with carbon-based nanoinclusions. *Sust,* **in press**
- Cabrini, M.; Lorenzi, S.; Coffetti, D.; Coppola, L.; Pastore, T. Inhibition effect of tartrate ions on the localized corrosion of steel in pore solution at different chloride concentrations. *Build.* **2020**, 10(6), 105
- Coppola, L.; Coffetti, D.; Crotti, E.; Gazzaniga, G., Pastore, T. The durability of one-part alkali-activated slag-based mortars in different environments. *Sust.* **2020**, 12(9), 3561
- Coppola, L.; Coffetti, D.; Crotti, E.; Gazzaniga, G., Pastore, T. Chloride diffusion in concrete protected with a silane-based corrosion inhibitor. *Mat.* **2020**, 13(8), 2001
- Coppola, L.; Coffetti, D.; Crotti, E.; Dell'Aversano, R.; Gazzaniga, G. The influence of heat and steam curing on the properties of one-part fly ash/slag alkali activated materials: preliminary results. *AIP Conf. Proc.* **2019**, 2196, 020038
- Coppola, L.; Coffetti, D.; Crotti, E. A holistic approach to a sustainable future in concrete construction. *IOP Conf. Ser: Mat. Sci. Eng.* **2018**, 442(1), 012024
- Coppola, L.; Coffetti, D. et al. Binders alternative to Portland cement and waste management for sustainable construction – part 2. *J. Appl. Bio. Fun. Mat*. **2018**, 16(4), 207-221
- Coppola, L.; Coffetti, D. et al. Binders alternative to Portland cement and waste management for sustainable construction – part 1. *J. Appl. Bio. Fun. Mat*. **2018**, 16(3), 186-202
- Coppola, L.; Coffetti, D.; Crotti, E.; Forni, D.; Cadoni, E. Fiber reinforced mortars based on free Portland – CSA binders under high stress rate. *EPJ Web Conf.* **2018**, 183, 04013
- Coppola, L.; Coffetti, D.; Crotti, E. Innovative carboxylic acid waterproofing admixture for self-sealing watertight concretes. *Con.Build.Mat* **2018**, 171, 817-824
- Coppola, L.; Coffetti, D.; Crotti, E. Plain and ultrafine fly ashes for environmentally friendly construction materials. *Sust.* **2018**, 10(3), 874
- Coppola, L.; Coffetti, D.; Crotti, E. Rheological and physical performances of mortars manufactured with plain and ultrafine fly ashes. *ACI Spec. Pub.* **2018**, SP 326
- Coppola, L.; Buoso, A.; Coffetti, D.; Kara, P.; Lorenzi, S. Electric arc furnace slag for sustainable concrete. *Con.Build.Mat* **2016**, 123, 115-119
- Coppola, L.; Coffetti, D.; Lorenzi, S. Cement-based renders manufactured with phase-change materials: applications and feasibility. *Adv. Mat. Sci. Eng*. **2016**, 7254823

Appendix 2

List of principal chemical notations

Compounds	Notation	
	Chemistry	Cement
Oxides, carbonates and sulphates		
Calcium dioxide (lime)	CaO	C
Silicon oxide	SiO_2	S
Alumina oxide	Al_2O_3	A
Iron oxide	Fe_2O_3	F
Sulphur oxide	SO_3	$\hat{S}$
Water	H_2O	H
Carbon dioxide	CO_2	$\hat{C}$
Calcium carbonate	$CaCO_3$	$C\hat{C}$
Calcium sulphate	$CaSO_4$	$C\hat{S}$
Binder compounds		
Tricalcium silicate (alite)	$3CaO{\cdot}SiO_2$	C_3S
Dicalcium silicate (belite)	$2CaO{\cdot}SiO_2$	C_2S
Tricalcium aluminate	$3CaO{\cdot}Al_2O_3$	C_3A
Gehlenite	$2CaO{\cdot}Al_2O_3{\cdot}SiO_2$	C_2AS
Mayenite	$12CaO{\cdot}7Al_2O_3$	$C_{12}A_7$
Perovskite	$CaO{\cdot}TiO_2$	CT
Tetracalcium aluminoferrite	$4CaO{\cdot}Al_2O_3{\cdot}Fe_2O_3$	C_4AF
Calcium aluminate	$3CaO{\cdot}Al_2O_3$	CA
Fluorellestadite	$10CaO{\cdot}3SiO_2{\cdot}3SO_3{\cdot}F_2$	$C_{10}S_3\hat{S}_3F_2$
Calcium sulphoaluminate	$4CaO{\cdot}3Al_2O_3{\cdot}SO_3$	$C_4A_3\hat{S}$
Anhydrite	$CaSO_4$	$C\hat{S}$
Hydration products		
Calcium silicate hydrate	$3CaO{\cdot}2SiO_2{\cdot}H_2O$	C-S-H
Calcium hydroxide (portlandite)	$Ca(OH)_2$	CH
Ettringite (AFt)	$6CaO{\cdot}Al_2O_3{\cdot}3SO_3{\cdot}32H_2O$	$C_6A\hat{S}_3H_{32}$
Monosulphate (AFm)	$4CaO{\cdot}Al_2O_3{\cdot}SO_3{\cdot}12H_2O$	$C_4A\hat{S}H_{12}$
Aluminate hydroxide (Gibbsite)	$Al(OH)_3$	AH_3
Strätlingite	$2CaO{\cdot}Al_2O_3{\cdot}SiO_2{\cdot}8H_2O$	C_2ASH_8